Thermodynamics and Biological Applications of DNA Nanostructures

by

Xixi Wei

A Dissertation Presented in Partial Fulfillment
of the Requirements for the Degree
Doctor of Philosophy

Approved April 2014 by the
Graduate Supervisory Committee:

Yan Liu, Co-Chair
Hao Yan, Co-Chair
Julian Chen
Ian Gould

ARIZONA STATE UNIVERSITY

May 2014

ABSTRACT

DNA nanotechnology is one of the most flourishing interdisciplinary research fields. Through the features of programmability and predictability, DNA nanostructures can be designed to self-assemble into a variety of periodic or aperiodic patterns of different shapes and length scales, and more importantly, they can be used as scaffolds for organizing other nanoparticles, proteins and chemical groups. By leveraging these molecules, DNA nanostructures can be used to direct the organization of complex bio-inspired materials that may serve as smart drug delivery systems and *in vitro* or *in vivo* bio-molecular computing and diagnostic devices.

In this dissertation I describe a systematic study of the thermodynamic properties of complex DNA nanostructures, including 2D and 3D DNA origami, in order to understand their assembly, stability and functionality and inform future design endeavors. It is conceivable that a more thorough understanding of DNA self-assembly can be used to guide the structural design process and optimize the conditions for assembly, manipulation, and functionalization, thus benefiting both upstream design and downstream applications.

As a biocompatible nanoscale motif, the successful integration, stabilization and separation of DNA nanostructures from cells/cell lysate suggests its potential to serve as a diagnostic platform at the cellular level. Here, DNA origami was used to capture and identify multiple T cell receptor mRNA species from single cells within a mixed cell population. This demonstrates the potential of DNA nanostructure as an ideal nano scale tool for biological applications.

ACKNOWLEDGMENTS

I sincerely appreciate everyone who has ever helped and supported me during the pursuit of my PhD. First, I would like to thank my parents and my boyfriend Guozheng Li who always stood by my side and provided me with a warm family full of love and energy so that I could pursue my dreams overseas.

I am grateful to Dr. Yan Liu and Dr. Hao Yan, the mentors who opened my eyes to the amazing world of DNA nanotechnology and impressed upon me examples of passionate, creative and rigorous scientists. Their tremendous guidance and kind encouragement for my entire graduate career are appreciated. I want to acknowledge my graduate and oral committee members Dr. Julian Chen, Dr. Ian Gould, Dr. Marcia Levitus and Dr. Alexandra Ros for their invaluable advice and support. I also want to thank my collaborators, Dr. Joseph Blattman, Dr. Stuart Lindsay, Dr. Deirdre Meldrum, Dr. Roger Johnson and Dr. Cody Youngbull for their help ensuring the success of my work.

Finally I would like to thank all former and current Yan lab members with whom I have had many great discussions about my research, and were my best friends in daily life, especially Dr. Chenxiang Lin, Dr. Jeanette Nangreave, Dr. Zhe Li, Dr. Xiaowei Liu, Dr. Yang Yang, Dr. Minghui Liu, Dr. Zhao Zhao, Chad Simmons, Anirban Samanta, Wei Li, Fei Zhang, Yuhe Yang, Shuoxing Jiang, Zhilei Ge, Guoliang Ke and Yu Zhou. I also want to thank Dr. Qian Mei, Dr. Fengyu Su and Louis Schoettle for being great collaborators. I appreciate Dr. Jeanette Nangreave for her suggestions about my manuscripts.

TABLE OF CONTENTS

Page

CHAPTER Page

CHAPTER Page

LIST OF TABLES

LIST OF FIGURES

Figure Page

Figure Page

CHAPTER 1

INTRODUCTION

1.1 Introduction of DNA nanotechnology

1.1.1 Overview

DNA nanotechnology is a field in which artificial nucleic acid nanostructures are designed and constructed for a variety of technological purposes[1-6]. With accurate helical dimensions and predictable Watson-Crick hydrogen bond interactions, double helical DNA motifs have been widely utilized as programmable nanometer scale building blocks in this and several other research fields. DNA has a persistence length of 50 nm, and so, is rigid enough to provide structural stability in the nanometer range; meanwhile, single stranded and branched DNA motifs exhibit the flexibility necessary to construct complex, higher order one-, two- and three- dimensional (1D, 2D, 3D) structures[2,7-12]. Due to recent developments in molecular biology, there are of a range of commercially available enzymes and tool kits that can be used to easily manipulate DNA through synthesis, amplification, selective cleavage, digestion, insertion, ligation, labeling and conjugation. The field of DNA nanotechnology has undergone explosive development over the past three decades.[11]

The growth and development of DNA nanotechnology has culminated in a variety of interesting structures and applications: from organizing nanoparticles, proteins, and nucleic acids, to serving as platforms for the assembly of complex biochemical machinery[3-5]. Most of these applications relied only on controlling the initial design parameters and observing the corresponding outcome, without much concern for the thermal features and/or mechanisms of nanostructure assembly.

1.2.1 DNA nanostructures

Bridging the gap between nano- and micro-scale structures, and achieving ever-increasing complexity, is an ongoing challenge in structural DNA nanotechnology. In the early years researchers used a few short single strands of DNA (ssDNA), usually less than 100 nucleotides (nts), to form 10-30 nm DNA building blocks (tiles) with simple geometries.[31, 8, 9] (Figure 1.1A) In 2006, Rothemund employed a 7249-nt single stranded virus genome (M13) and developed a scaffolded assembly method, commonly referred to as DNA origami.[40] By using a large number (~ 200) of short, specifically designed ssDNAs (20-40 nts) that were complementary to various regions of the scaffold strand, he was able to fold the scaffold into relatively complex structures with ~ 100 nm dimensions. Each short ssDNA (staple) strand represented a 6-nm "pixel" that provided a fully addressable surface for patterning DNA and other molecules. This important scaffolding strategy was a breakthrough in nano scale DNA structural design and facilitated larger sized structures, greater complexity and even curvature. (Figure 1.1B) Recently, Yin and co-workers successfully constructed complex 2D and 3D structures of comparable size to scaffolded DNA origami using a scaffold-less strategy.[2] They cleverly designed hundreds of short DNA strands, referred to as single stranded tiles (SST) that self-assembled into more complex patterns. (Figure 1.1C)

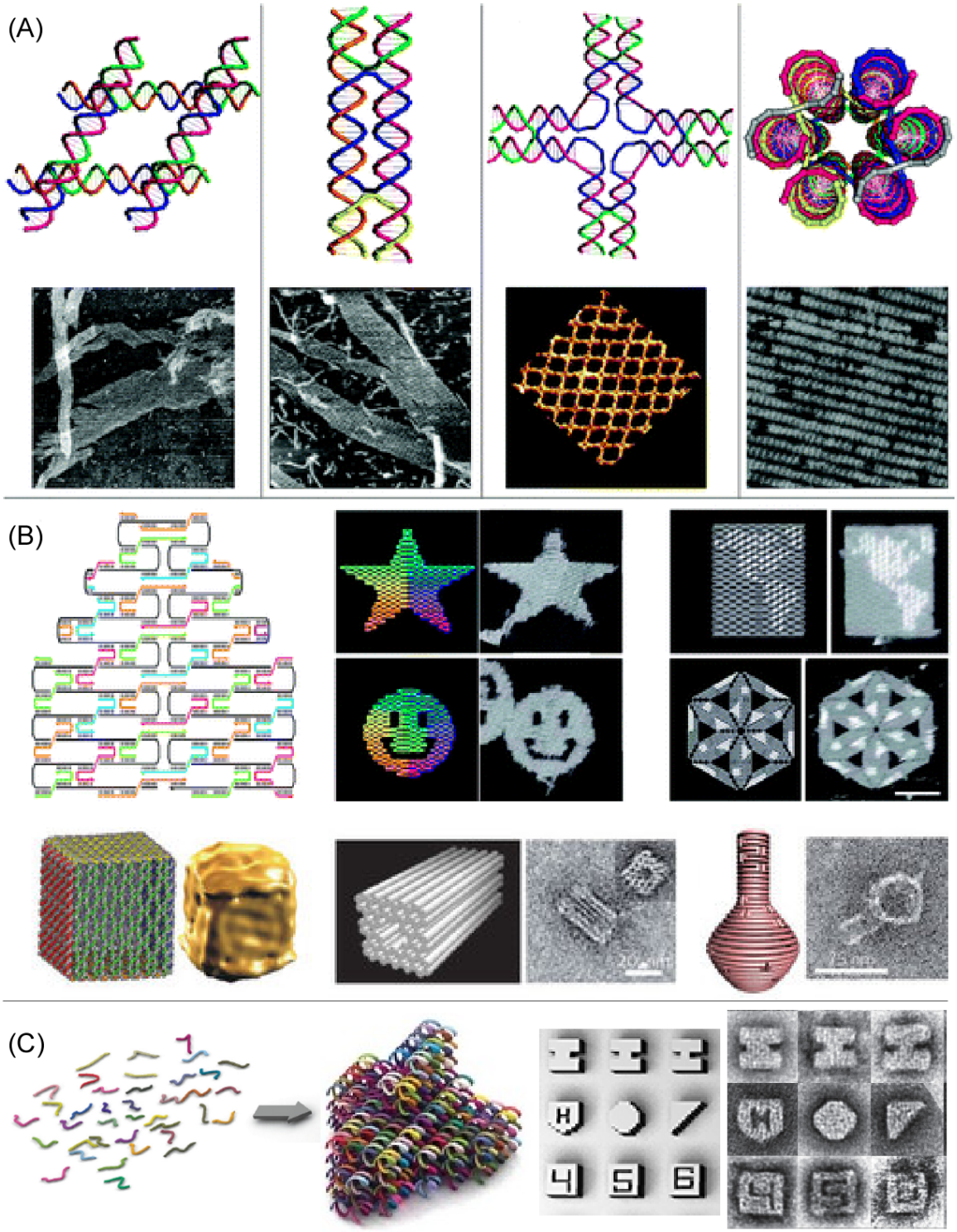

Figure 1.1 Representative structures in DNA nanotechnology. (A) Examples of DNA tiles and assembled periodic arrays.[41] (B) Illustration of scaffolded DNA origami and typical 2D and 3D structures.[40, 42] (C) Illustration of scaffoldless DNA origami and examples.[2] (Adapted with permission from ref 41, 40, 42, 2)

Another route to scale up the size and complexity of DNA nanostructures is to utilize inter-tile association strategies. In these methods complementary single stranded "sticky ends" are displayed from the edges of discrete DNA tiles or origami structures such that the individual tile units are connected together and anchored by hybridization of the sticky ends.[10] The way in which the tiles extend in 1D or 2D and the number of tile units that associate together determine the final scale of the DNA array. (Figure 1.1A)

1.1.3 Challenges of structural DNA nanotechnology

One major challenge in structural DNA nanotechnology is to both increase the size and complexity of DNA assemblies while simultaneously controlling the error rate. The purity and relative stoichiometry of the participating ssDNA, and parameters such as structural constraints, DNA concentration, annealing profile, salt/ion concentration, and pH, should be optimized to reduce errors and improve the final assembly yield. In many cases researchers have to perform tedious and iterative experimental analyses to identify the optimal assembly conditions for a particular design, often based solely on their own previous experience and intuition, which is largely due to a lack of understanding of the underlying mechanisms of assembly and the availability of pertinent thermodynamic and kinetic data.

Although many research directions have been established using either simple or complex DNA structures, most of them are focused on the starting conditions and final assembly outcomes, leaving the thermal behavior and mechanisms of assembly unknown, or "in the black box". Studying the thermodynamic and kinetic properties of complex DNA systems will shed light on the process of DNA nanostructure assembly. DNA nanotechnology actually represents a unique opportunity to gain insight about the

dynamic changes and transition states of polyvalent binding events that accompany the association of DNA strands.[13,14] A few mechanistic studies of the formation of DNA nanostructures have already revealed various physical and chemical aspects of assembly, not only providing valuable predictive power that promotes upstream design efficiency, but also informing the construction of complex systems for downstream applications via purposive modifications for upstream applications. (Figure 1.2)

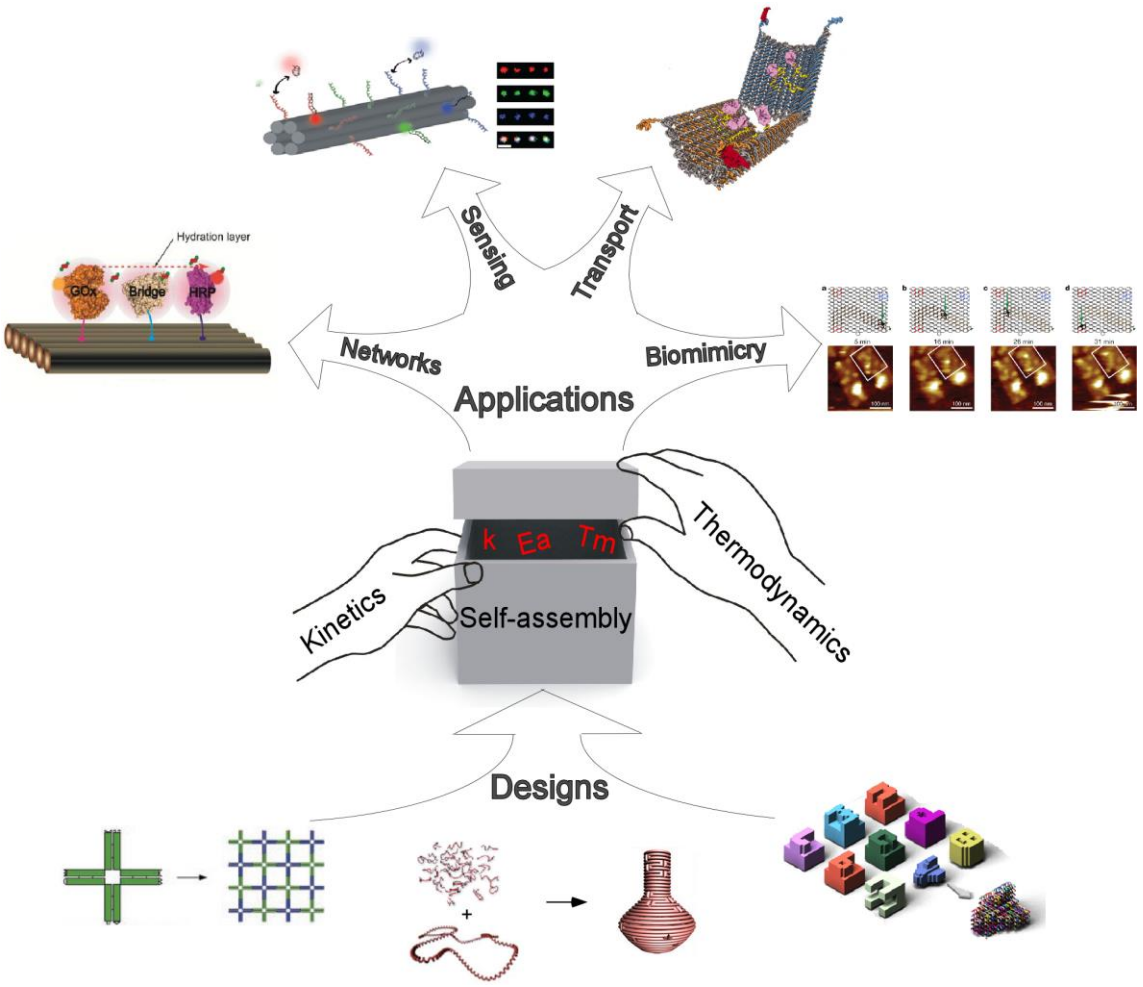

Figure 1.2 Thermodynamics and Kinetics of DNA Nanostructure Self-assembly benefit upstream structural design and downstream applications. [1-5, 9] (Adapted with permission from ref 1-5, 9)

1.2 Thermodynamics of DNA Nanostructures

1.2.1 Overview of the thermodynamics and kinetics

The thermodynamics of DNA structures explains the overall energy changes and transitions between single and double stranded states, reflecting the stability, cooperativity and intrinsic flexibility of assembled structures. When ssDNAs with rationally designed sequences are mixed together, heated to a high temperature to disrupt unwanted base pairing, and then gradually cooled, the DNA strands associate with complementary strands and self-assemble into the designed shapes and patterns. In contrast, the assembled structures dissociate (melt) into the individual ssDNAs in response to increasing temperature. For cases in which the rate of temperature change is sufficiently low, dynamic equilibrium at each temperature is achieved. The association/dissociation processes can be considered reversible and are expected to display overlapping traces. From these thermal association/dissociation curves we can extract the melting temperature (T_m), which is the midpoint of the transition where half of the structure is associated and half is dissociated (Figure 1.3A), and the width of the transitions, reflecting the cooperativity of association/dissociation. Other thermodynamic parameters that can be extracted from van't Hoff analyses include the free energy change (ΔG), enthalpy change (ΔH), and entropy change (ΔS) of association/dissociation. These parameters reflect the overall thermal stability, contribution from intermolecular interactions, and internal rigidity/flexibility of the nanostructures, respectively.

Kinetic analyses describe reaction rates in non-equilibrium states, and provide instructional information about the reaction's transition states and the time required to

reach reaction equilibrium under certain conditions. For example, kinetic studies of DNA nanostructures that focus on the rate of structural formation and underlying mechanisms such as the activation energy (E_a) reveal details that are not accessible through thermodynamics studies. Temperature dependent rate constants (k) can be determined from kinetic curves (Figure 1.3B). The E_a of a reaction reflects the energy barrier required to facilitate a given reaction pathway and can be obtained from temperature dependent kinetic measurements (Arrhenius plots).

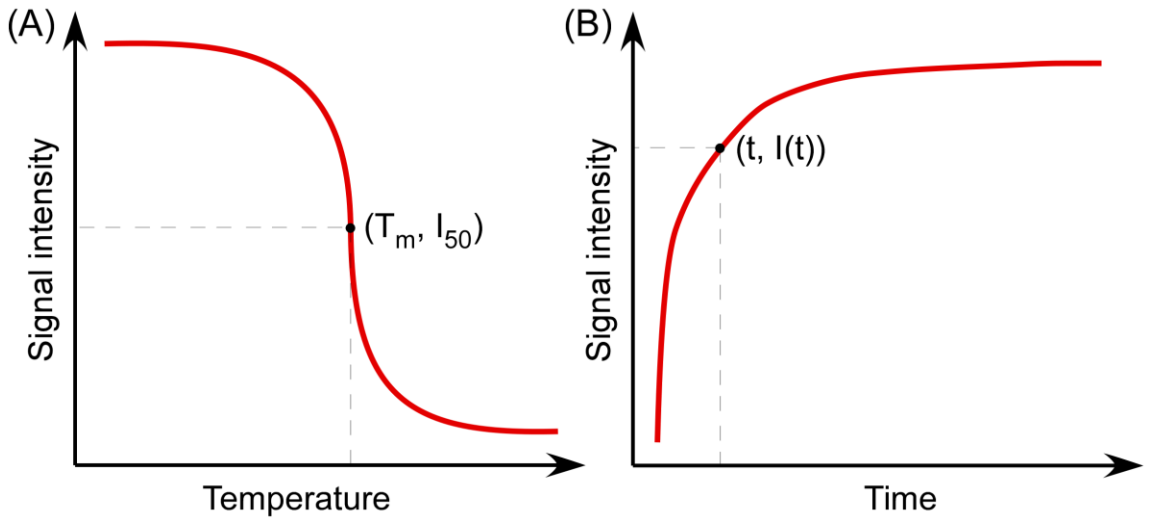

Figure 1.3 Data profiles of thermodynamic and kinetic measurements. (A) A representative thermal curve. The melting temperature (T_m) is the temperature at which 50% of the reaction is complete. (B) A representative kinetic curve.

DNA nanostructure assembly can be evaluated from two perspectives: single-stranded DNA interactions that form structural motifs, and the overall structural stability and flexibility of the final assembly. The main factors that affect the thermodynamic and kinetic behavior of the structural motifs are the length and sequence of the participating ssDNAs and their binding domains; other factors include the overall dimensions of the nanostructure (i.e. its translational and rotational diffusion dynamics), the locations of the

binding domains that may be sterically hindered, the rigidity of the structures before and after assembly, the folding path of the ssDNAs, and the distances between crossover points.

1.2.2 Measurement strategies

Until now, a few methods have been reported for observation of the dynamic assembly of DNA nanostructures, including optical spectroscopy, atomic force microscopy[15], and micro-calorimetry[16]. The latter two are less commonly used due to the slow (delayed) read out, large sample volumes required, and possible interference from environmental factors.

For optical spectroscopy methods, researchers generally utilize the change in UV absorbance at 260 nm that occurs when DNA double helices change from ordered (native) to disordered (denatured) structures, referred to as the hyperchromic effect. The primary drawbacks of this method are the relatively small signal change, especially for DNA origami samples in the presence of large excess of staple strands, and the structural damage to DNA that is caused by prolonged UV exposure.

DNA intercalating dyes, e.g. SYBR Green (or SYBR Gold, YOYO dyes), preferentially bind to double rather than single stranded DNA, exhibiting a concurrent increase in fluorescence quantum yield when intercalated between the DNA base pairs. They have been used for studying the DNA self-assembly process in real time by monitoring the fluorescence intensity change with temperature or time.[16,17] The ratio of dye molecules to DNA base pairs must be carefully controlled to produce a usable signal change while simultaneously minimizing the background. However, the intercalating dyes may induce a change in the helical twist of the DNA, leading to conformational

distortions of the structures[1]. Moreover, the switches between single and double stranded states induce a new equilibrium between the molecules, which may result in a delayed detection of the signal change. Finally, the strong interactions between the intercalating dyes with the DNA bases may cause changes in the thermal stability of the DNA structures to be investigated. Nevertheless, the sensitivity and convenience of this method make it useful in many thermal studies.[17,18]

An alternative optical spectroscopy method for monitoring the thermal or kinetic behavior of DNA nanostructures is through the covalent incorporation of fluorescent dyes, either pairs of Förster Resonance Energy Transfer (FRET) dyes or fluorescence dye-quencher pairs. FRET is a well-established measurement technique commonly used to study distance dependent molecular events. It is well suited for studying dynamic DNA nanostructure assembly/disassembly due to the predictable behavior of the energy transfer process at the nanometer scale. When a strategically placed FRET pair is brought into close proximity during assembly of the DNA nanostructure, resonance energy transfer between the donor and acceptor fluorophores result in a decrease in the intensity of donor emission and a simultaneous increase of acceptor emission, while the opposite occurs during the dissociation process. Thus, the FRET or quenching efficiency reflects the assembly yield of the DNA structures accurately, sensitively and instantly, which have made fluorescence spectroscopy a popular method in DNA thermodynamics and kinetics studies.[19,20]

Fluorescently labeled ssDNA (labeled at the 5’ or 3’ end or internally on the sugar or the base) is commercially available with a variety of dye choices with unique excitation/emission wavelengths. This convenience has made fluorescence spectroscopy

the most popular way to study the thermodynamics and kinetics of DNA nanostructures.[19, 20] Since only one or two labeled strands are required for experiments, there is minimal background interference. For multi-molecular (n>2) reactions, a FRET pair can simplify data analysis by enabling the use of a two-component model to describe the assembly process. However, experiments have shown that the thermal properties that are derived only reflect the portions of the structure that are labeled by the FRET pair, and do not freely extend to reflect that of the whole structure.[19] A recent study demonstrated that that FRET dye pairs can be used as probes to sense the presence or absence of strands surrounding the FRET dye.[21] This suggests that the sensitivity of some reporter dyes to the local environment can not only be used to probe the global structure, but can also distinguish fine structural changes within a larger structure. Some fluorophores display significant signal changes upon hybridization to ssDNA, possibly due to changes in their interaction with neighboring nucleotides (accompanied by a change in quantum yield), which makes it possible to use a single fluorophore to indicate structural changes.[22]

Besides these spectroscopic approaches, a more direct method of analysis was performed by Dong and co-workers.[15] They used atomic force microscopy (AFM) to visualize the conformational transformation of a DNA origami assembly. Although the temperature on a mica surface cannot be well controlled, and the formation of the origami in their study occurred at a solid-liquid interface (and likely exhibits different thermal behavior compared to in solution), it still demonstrates that researchers are pursuing advanced techniques to more broadly study the thermal behavior of DNA nanostructures.

1.2.3 Principles of DNA thermodynamics

To uncover the thermodynamics of DNA self-assembly through optical spectroscopy, the intensity of the absorbent or fluorescent signal (I) should be sampled and recorded at many temperature points during both the annealing (cooling) and denaturing (heating) processes to generate a thermal profile. The rate of temperature change should be slow enough to allow the system to reach thermal equilibrium at each sampling temperature and the background signal should be minimized and subtracted. At temperature points well above and below the transition temperature, a plateau in the thermal curve will be observed, indicating the complete dissociation or assembly of the DNA nanostructure, respectively. The variation of I with temperature reflects temperature dependent structural changes within the nanostructure. Assuming a linear dependence of the signal with concentration, the normalized intensity is expected to be proportional to the concentration of fully formed structures (θ):

$$\theta = \frac{I - I_{min}}{I_{max} - I_{min}}, \quad (1)$$

where I_{min} and I_{max} are minimum and maximum signal intensity, respectively. The value of θ is between 1 and 0, where 1 corresponds to complete assembly of all structures in solution, and 0 corresponds to complete dissociation.

For FRET experiments, typically, the emission of the donor fluorophore is recorded for two samples: one in which both FRET dyes are present, and a reference sample in which only the donor dye is present (Figure 1.4A). Rather than directly comparing the signal levels, the FRET efficiency (E) is calculated using the following

equation to reflect the change in distance between the FRET pair, and thus, the temperature dependent structural changes:

$$E = \frac{I_D - I_{DA}}{I_D}, \quad (2)$$

where I_{DA} and I_D represent the emission signal of the donor dye with and without the acceptor dye present, respectively. Similarly, the proportion of assembled structures (θ) is calculated from the normalized FRET efficiency using the following equation:

$$\theta = \frac{E - E_{min}}{E_{max} - E_{min}}, \quad (3)$$

where E_{min} represents the minimum FRET efficiency that occurs when the nanostructure is completely dissociated, and E_{max} represents the maximum FRET efficiency that occurs when the nanostructure is completely assembled.

After determining the assembled fraction of dimers at each temperature using Equation 3, θ is plotted against temperature and the heating and cooling profiles are superimposed (Figure 1.4B). If the two curves overlap well with each other, it can be concluded that the assembly/disassembly process is reversible and that thermal equilibrium was achieved at each temperature. In order to determine the midpoint of the assembly/disassembly process, the first derivative of θ (dθ/dT) is plotted versus T and a Gaussian function is used to fit the curve. The melting temperature (T_m) corresponds to the point in the curve at which half of the structures are fully assembled, and half are fully denatured. The higher the melting temperature of the DNA structure, the more stable the final assembly is. The Gaussian fit also reflects the width (w) of the transition, indicating if the assembly/disassembly process occurs over a narrow or wide temperature

range; the more narrow the width of the transition, the more cooperative the assembly/disassembly process is (Figure 1.4C).

For a reversible thermal transition in a bi-molecular reaction system, where equilibrium is reached at each temperature, the van't Hoff law can be applied to obtain the enthalpy change (ΔH), entropy change (ΔS) and free energy change (ΔG). The equilibrium constant (Keq) with temperature is a function of θ and is given by the following equation:

$$K_{eq} = \frac{\theta}{C_0(1-\theta)^2}, \quad (4)$$

where C_0 is the initial concentration of individual the ssDNAs and thus, the DNA nanostructure. K_{eq} can also be expressed as a function of temperature by the following equation:

$$\ln K_{eq} = -\frac{\Delta H}{RT} + \frac{\Delta S}{R} \quad (5)$$

ΔH and ΔS can be obtained from a plot of ln K_{eq} versus 1/T in the linear range in which ΔH and ΔS are temperature independent (Figure 1.4D). Finally, ΔG can be calculated from the van 't Hoff enthalpy and entropy changes by the Gibbs equation:

$$\Delta G = \Delta H - T\Delta S, \quad (6)$$

where T is 298 K (25 ℃). The energetic gains and losses of ΔG, ΔH and ΔS should be considered together to describe the stability and flexibility of the DNA structures.

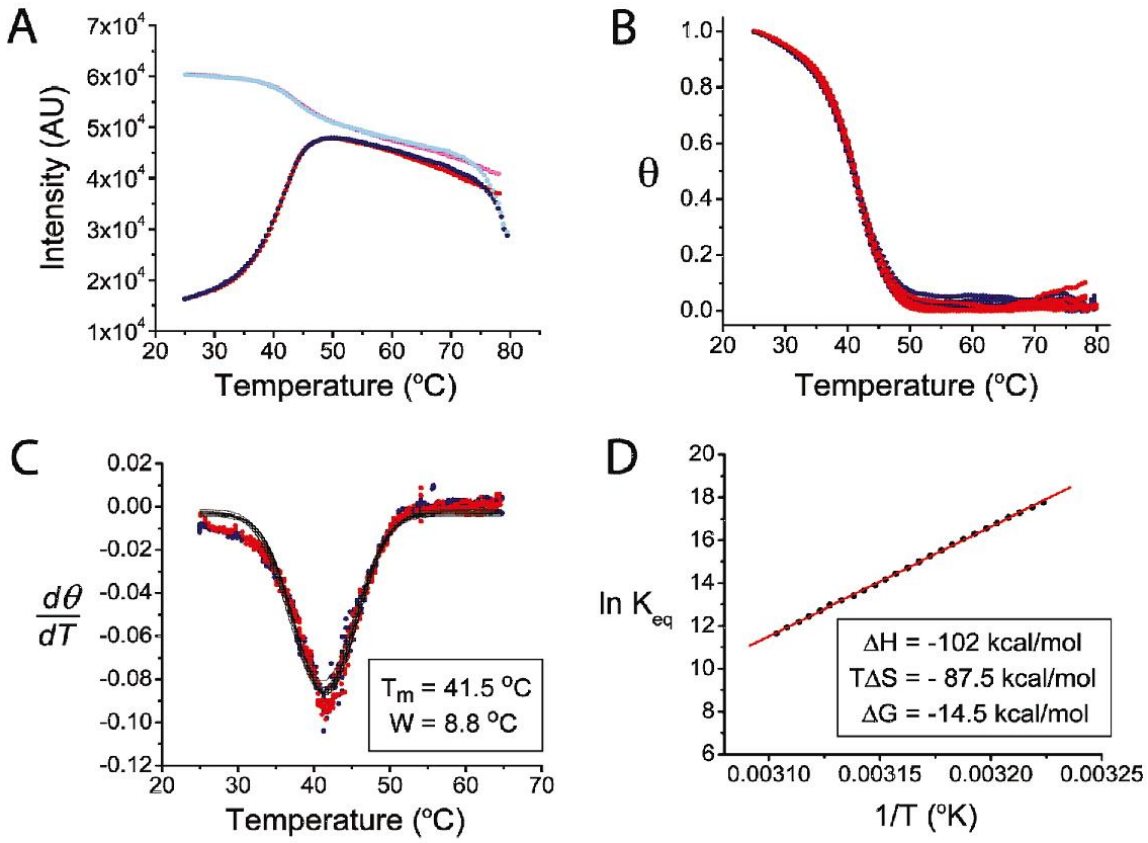

Figure 1.4. An example of thermodynamic data analysis when a FRET pair is used as an indicator.[14] (A) Plot of the raw fluorescent intensity of the donor dye versus temperature. The data was collected during both the cooling/heating processes, shown in dark blue and red for the donor/acceptor sample, and light blue and pink for donor only sample, respectively. (B) Plot of normalized FRET efficiency (θ) as a function of temperature. (C) First derivative of curves shown in B as a function of temperature, fit by a Gaussian function to yield the melting temperature (T_m) and the width of the transition (W). (D) The corresponding van't Hoff plot with a linear fit to obtain the enthalpy (ΔH) entropy (TΔS), and free energy changes (ΔG). (Reprinted with permission from ref 14)

There are several important considerations when applying this type of thermodynamic analysis to DNA nanostructures. First, in some complex structures like 3D origami, the cooling/heating curves that reflect the assembly/disassembly processes do not overlap, regardless of the rate of temperature change.[17, 21] In such structures the long scaffold strand, under the direction of hundreds of staple strands, must overcome a relatively high energy barrier to realize the complicated folding pathway. This is a slow

process and occurs at a lower temperature than the corresponding dissociation of the structure. The assembly likely occurs in steps, as partial double helices are formed in sequence until the final structure is achieved; however, the melting occurs quickly and completely at higher temperatures. Second, there are situations in which more than one transition is observed, indicating the presence of a barrier to homogeneous nucleation and assembly. For example, for the one-pot assembly of a periodic lattice from repeating DNA tiles the individual tiles will first self-assemble at higher temperatures, followed by cohesion of sticky ends between the tiles to form the final lattice structure. Also, if the DNA nanostructure has relatively flexible regions, it is possible to detect the transitions corresponding to the assembly of long, continuous domains versus shorter, more flexible domains or nick points within the same assembly.[30, 32]

1.3 Development of DNA nanostructure thermodynamics

1.3.1 Development of thermodynamic study

As early as 1987, Breslauer and co-workers studied the thermal behavior of DNA junction motifs by UV absorbance and other calorimetry methods[23]. With the development and application of improved measurement approaches, more accurate and thorough analyses of the thermodynamic properties of DNA nanostructures have since been achieved. Estimating the thermal parameters of Watson-Crick base pairing based on the nearest neighbor model, when the salt conditions and sequences are provided, is now common using software such as Mfold.[24,25] The formation of a 9 bp duplex was shown to have ΔH= - 62.1 kcal/mol and ΔS = - 176 cal/K/mol by Howard (Figure 1.5A).[26] Duplexes with bulges or mismatches have lower T_ms, which can be remitted using higher Na^+ or Mg^{2+} concentrations.[27] The thermodynamic properties of 8 bp DNA/DNA,

RNA/RNA and DNA/RNA hybrid duplexes indicated that RNA duplexes are the most stable, with T_ms in the 60-66 ℃ range and ΔG_{37} of -13 kcal/mol, compared to DNA/DNA or hybrid duplexes, both with T_ms between 42-54 ℃ and ΔG_{37} ~ - 9 kcal/mol.[28]

Double (DX) crossover motifs are composed of two duplexes linked side by side at two double crossover points (as in a Holliday junction), and have been used to construct periodic 1D and 2D arrays via sticky end associations.[19,29] The thermal behavior of individual DX tiles show multiple transitions between 45 ℃ to 70 ℃[12,30,31], where the folding of long undisrupted duplexes, and duplexes with a nick point, are distinguishable by two transitions (Figure 1.5B). 4-helix tiles are two DX tiles linked side by side and display similar thermal transitions as DX tiles (Figure 1.5C), while more complex 8- and 12-helix tiles have a single thermal transition indicating the existence of more cooperative assembly processes in larger systems (Figure 1.5D, 1.5E).[8]

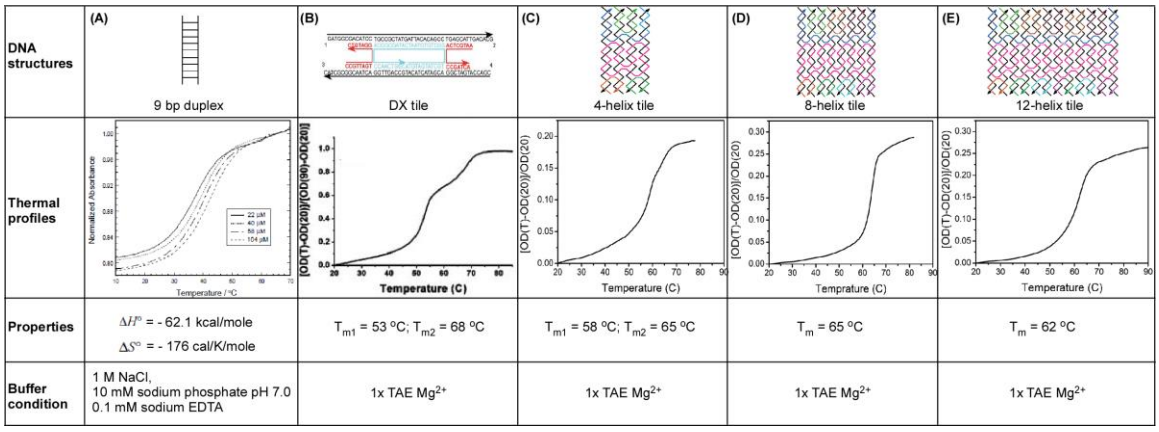

Figure 1.5 Examples of thermodynamic analyses of DNA tile nanostructures. (A) 9 bp duplex[26], (Reprinted with permission from ref 26. Copyright 2000 American Chemical Society.) (B) DX tile[31], (C) 4-helix tile[8], (D) 8-helix tile[8] and (E) 12- helix tile[8] A representative thermodynamic profile, values of T_m (or ΔH and ΔS if reported), and conditions are listed.

More complicated junction tiles, including triple crossover (TX) and parallel crossover (PX) tiles were investigated by the Seeman group.[7,32-34] When they compared

DX and TX tiles of the same length and similar GC content, they found TX tiles also displayed two transitions and concluded that the overall stability of TX and DX tiles is comparable (Figure 1.6A).[32] Beyond that, they also examined the thermal stability of conventional Holliday junctions, which have T_ms higher than antijunctions and mesojunctions (involving one or two nick points in the backbone), indicating that more flexible stacking domains in the latter junctions destabilize the base pairing interactions that flank the junction point (Figure 1.6B).[34] Another study from their group investigated PX tiles and demonstrated the thermally preferred formation of PX tiles over juxtaposed parallel (JX_1) tiles (Figure 1.6C).[33] Compared to simple duplexes, both PX and JX_1 tiles have comparable enthalpic gains, but higher entropic penalties due to the formation of more compact crossovers, resulting in kcal/mol-bp penalties in free energy.

To develop more complex and larger structures, researchers covalently linked four Holliday junctions together and created four-arm tiles (4x4) that were subsequently used to assemble 2D arrays (Figure 1.6D).[9] An accurate thermal study of 4x4 tiles and their arrays was performed by the Niemeyer group[19] using fluorescence spectroscopy. Compared to previous studies using UV absorbance measurements, they observed two distinguishable transitions for the periodic lattice formation; the lower temperature transition reflected the cooperative formation of 2D arrays from the individual tiles through sticky ends associations (Figure 1.6E). This study demonstrated the accuracy of applying FRET pairs to provide full thermodynamic characterization of tile assembly and array growth.

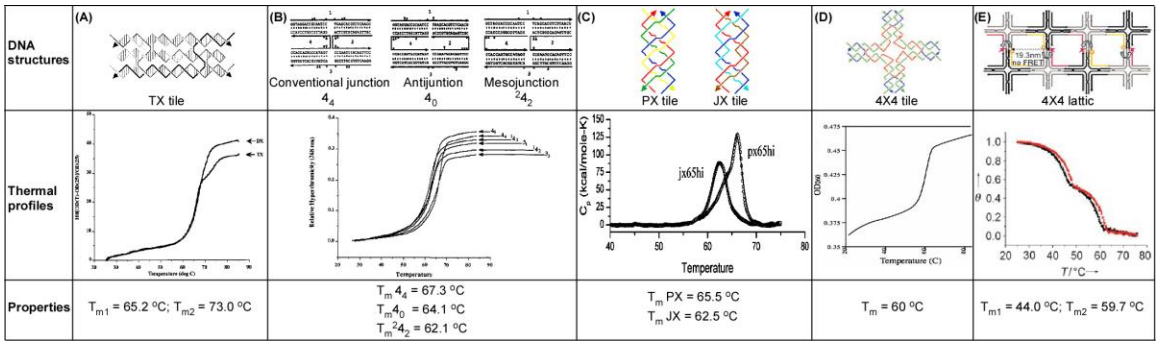

Figure 1.6 Examples of thermodynamic analyses of complex DNA tiles and tile array formation. (A) TX tile[32]. (Adapted with permission from ref 32. Copyright 2000 American Chemical Society.) (B) Holliday junction, antijunction and mesojunction tiles[34]. (Adapted with permission from ref 34. Copyright 1992 American Chemical Society.) (C) PX and JX tiles[33]. (Adapted from Biophysical Journal, 97, Spink, C. H.; Ding, L.; Yang, Q.; Sheardy, R. D.; Seeman, N. C.: Thermodynamics of forming a parallel DNA crossover, 528-38, 2009, with permission from Elsevier.) (D) 4x4 tile[9]. (From ref 9. Adapted with permission from AAAS.) (E) 4x4 lattice[19]. The reported T_m values are listed.

Recently, researchers have begun to uncover the thermodynamic properties of more complex DNA nanostructures such as DNA origami, although a more thorough study of these structures has yet to be achieved, and new approaches to de-convolute the energetics are needed. Dietz and co-workers[17] reported higher melting temperatures than folding temperatures for a series of 3D origami structures (Figure 1.7C), which is in agreement with a study from the Liu group[21] that compared the thermal profiles of 2D (Figure 1.7A) and 3D origami (Figure 1.7B). We observed that 2D origami structures exhibit good overlap between the folding/melting curves, indicating a highly cooperative and energetically favorable scaffold topology, in contrast to 3D structures that displayed a 7-10 ℃ hysteresis. FRET probes were used to study the local environment and thermal behavior of several partially formed origami structures, and the nearly homogenous assembly of 2D origami was verified. The diverse formation/dissociation behavior of the 3D origami depended on the scaffold path and staple arrangement, which presumably

causes a much slower formation rate in the cooling phase (Figure 1.7D). The long scaffold strand, under the direction of hundreds of staple strands, must overcome a relatively higher energy barrier to realize the complicated folding pathway. The disassembly likely occurs in steps, as the parallel double helices may dissociate from both ends toward the middle, until the final structure is completely dissolved at higher temperatures. However, the folding occurs slowly and strands located at different positions appear to incorporate into the final structure within a narrow temperature range, albeit at a much lower temperature than the melting temperature.

The Liu group also performed systematic thermodynamic studies of tile-tile interactions.[13,14] We evaluated multivalent sticky-end association between two complementary multi-helical DNA tiles and found that increasing the number of inter-tile interactions enhanced dimer stability, and changing the relative positions of the sticky ends resulted in unique superstructure T_ms and free energy changes. The formation of dimer structures from more flexible tiles was shown to proceed with favorable enthalpic gains due to reduced energetic strain, but involved much higher entropic penalties because of the order induced on the tiles, resulting in an overall lower thermal stability (Figure 1.7E).

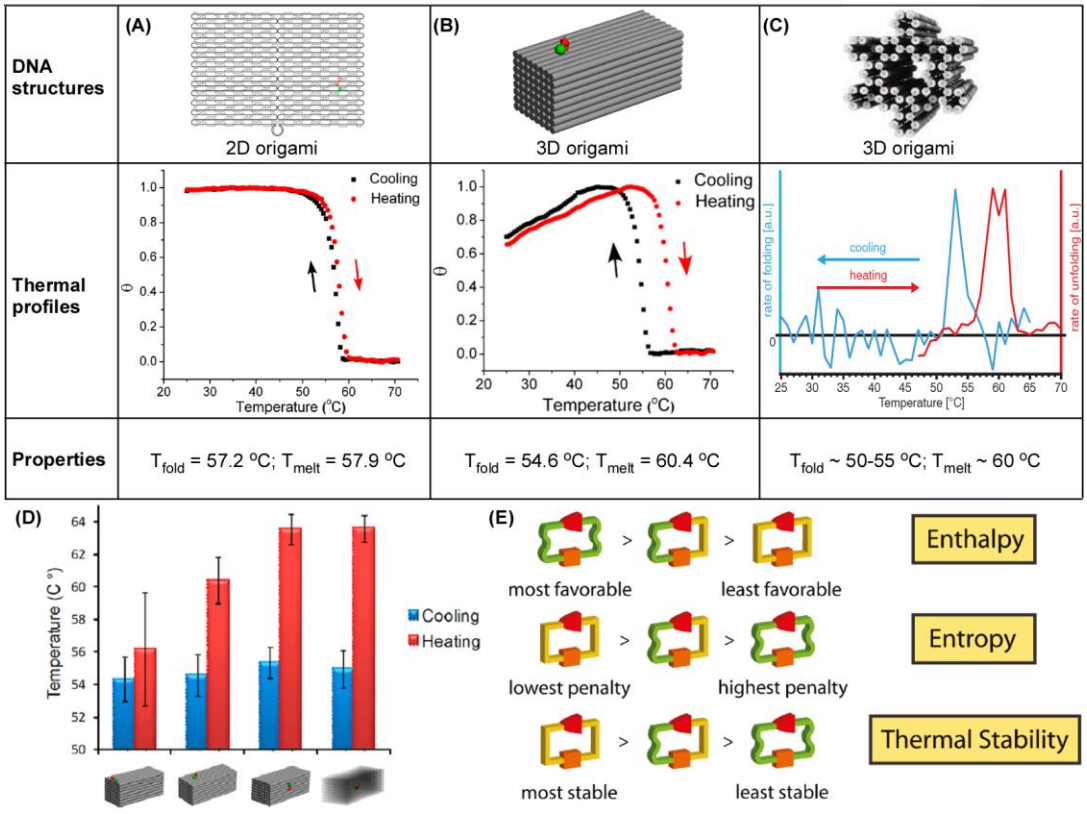

Figure 1.7 Examples of thermodynamic analyses of DNA origami and tile-tile interactions. (A) 2D[21] and (B[21]-C[17]) various 3D origami and the corresponding thermal profiles reported. (D) Evaluating cooperativity during the assembly/disassembly of different parts of a 3D cuboid origami structure.[21] (From ref 17. Reprinted with permission from AAAS.) (E) Illustration depicting the thermodynamic stabilities of dimers formed from DX tiles with varying flexibility.[14]

All of the previously described studies have provided useful quantitative, thermodynamic information describing discrete DNA motifs and periodic arrays. By carefully comparing thermal profiles, the less favorable conformational arrangements such as parallel crossovers and complex scaffold topologies were revealed. The existence of extended, undisrupted, double helical domains, higher GC content, greater numbers of longer sticky ends with favorable positions, and higher Mg^{2+} concentration can significantly improve the stability and formation of DNA nanostructures.

1.3.2 Rapid and isothermal assembly of DNA nanostructures

Based on knowledge of the thermodynamic and kinetic characteristics of DNA assembly, researchers have begun to develop isothermal techniques that facilitate faster and milder assembly of DNA nanostructures. Fan and co-workers used rationally designed "edge" strands to nucleate DNA origami based nanoribbons and nanotubes in a single-pot, where the size of the tubes was controllable and the assembly occurred within 10-20 minutes (Figure 1.8A).[36] This assembly strategy is significantly faster than the standard protocol that involves heating the DNA mixture and slowly cooling it over 12 hours. The Dietz group demonstrated that DNA origami can be folded within a few minutes with high yield at a fixed temperature, typically at the low temperature boundary of the folding curve of the thermodynamic profile (Figure 1.8B).[17] Yin and co-workers examined assembly over a wide range of constant temperatures, from 15 ℃ to 70 ℃, and successfully assembled scaffoldless single-stranded tile (SST) structures over 12 hours under various buffer conditions (Figure 1.8C).[37] Winfree and co-workers attempted to optimize strand displacement reactions using deprotector or catalyst strands and successfully demonstrated the isothermal assembly (at room temperature) of >10 μm long nanotubes from DX tiles.[10] It seems that rapid hybridization at a constant temperature just below the melting point ensures successful and efficient assembly. Rapid and isothermal assembly conditions have significantly shortened sample preparation times and can potentially facilitate the application of functional modifications with unique buffer and temperature restrictions.

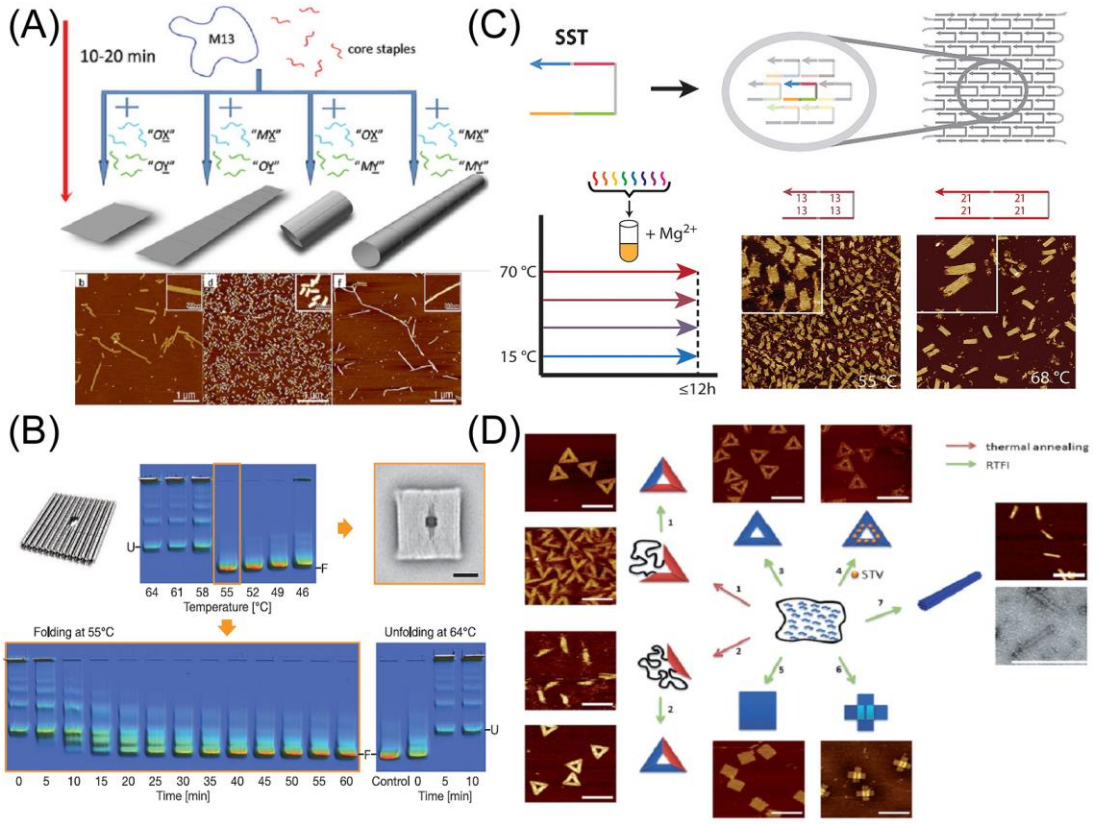

Figure 1.8. Examples of rapid and isothermal assembly of DNA nanostructures. (A) One pot annealing of combinatorial origami structures and the corresponding AFM images of the products.[36] (Adapted with permission from ref 36. Copyright 2013 American Chemical Society.) (B) Time dependent folding and unfolding of 3D origami at constant temperature analyzed by native gel electrophoresis, and the corresponding TEM image of the product.[17] (From ref 17. Reprinted with permission from AAAS.) (C) Illustration of SST structures, the isothermal assembly protocol used, and the corresponding AFM images of the products.[37] (Adapted with permission from ref 37. 2013 American Chemical Society.) (D) Schematics and AFM images of different origami assembly strategies, all achieved at room temperature with reducing concentration of formamide.[39] (Adapted with permission from ref 39).

Chemicals and detergents have also been employed to enhance the assembly of DNA structures at even lower temperatures. In 2008, Simmel and co-workers demonstrated that slowly reducing the concentration of formamide facilitates the isothermal assembly of DNA origami.[38] Recently, the Gothelf group reported the construction of DNA origami and SSTs at room temperature in 30-40% formamide[39] with relatively high yield (Figure 1.8D). The ability to assemble complex DNA nanostructures

at room temperature is ideal for applications in which the DNA structures serve as scaffolds for other thermally sensitive functional molecules, such as proteins, because high temperature assembly is often detrimental to such molecules.

1.4 Biological applications of functional DNA nanostructures

1.4.1 Broad applications of DNA nanostructures

The growth and development of DNA nanotechnology has culminated in a variety of interesting structures and reports. Researchers in this field have a series of tools in hand to speculate internal relationships, manipulate the DNA nanostructures, and explore their applications in the areas of nanoscale organization of nanoparticles, smart drug delivery systems, DNA computing, and the creation of complex, bio-mimetic functional materials, which makes DNA nanotechnology one of the most booming transdisciplinary research fields.[41-43]

As a programmable and addressable platform, DNA nanostructures afford fine positional control of molecules, making it possible to engineer interactive networks of physical, chemical, and biological species with nanometer precision.[41, 43] By displaying molecules from rationally designed DNA platforms with such precision, researchers have studied various distance- and spatially-dependent interactions related to electrical conductivity like metal particles[44], Quantum Dots[45], fluorescence energy transfer[46], and simple and cascading enzyme catalysis.[3, 43] (Figure 1.9A, B)

With predictable and reliable inter- and intra- molecular interactions: i.e. adenine-thymine (A-T) and cytosine-guanine (C-G) base pairing, DNA tiles have also served as basic elements in molecular computation, encoding numerical values for accurate and multi-parallel calculations.[51, 52] Similar to electronic circuits, deliberately designed DNA

motifs with eligible input, output and signaling strands have been programmed to implement gated logic functions. The action of most DNA logic gates involves optimization of strand displacement reactions, where the kinetic and thermodynamic properties of DNA toehold and hairpin structures play a key role in accurate, efficient, and fast calculation.[10, 35] (Figure 1.9C)

Different from other biomimicry strategies that identify, adapt, and modify existing biological components, DNA nanostructures can be designed from the bottom-up, leveraging the ability to control individual components, predict their location and the strength and duration of interacting component, and synthesis of higher-order and complex functional systems in order to create functional macromolecules and complex architectures (e.g., enzymes cascade pathways[3], artificial photosynthetic reaction centers[50], bio-chemical devices like molecular motor spiders[6], etc.). (Figure 1.9D, E)

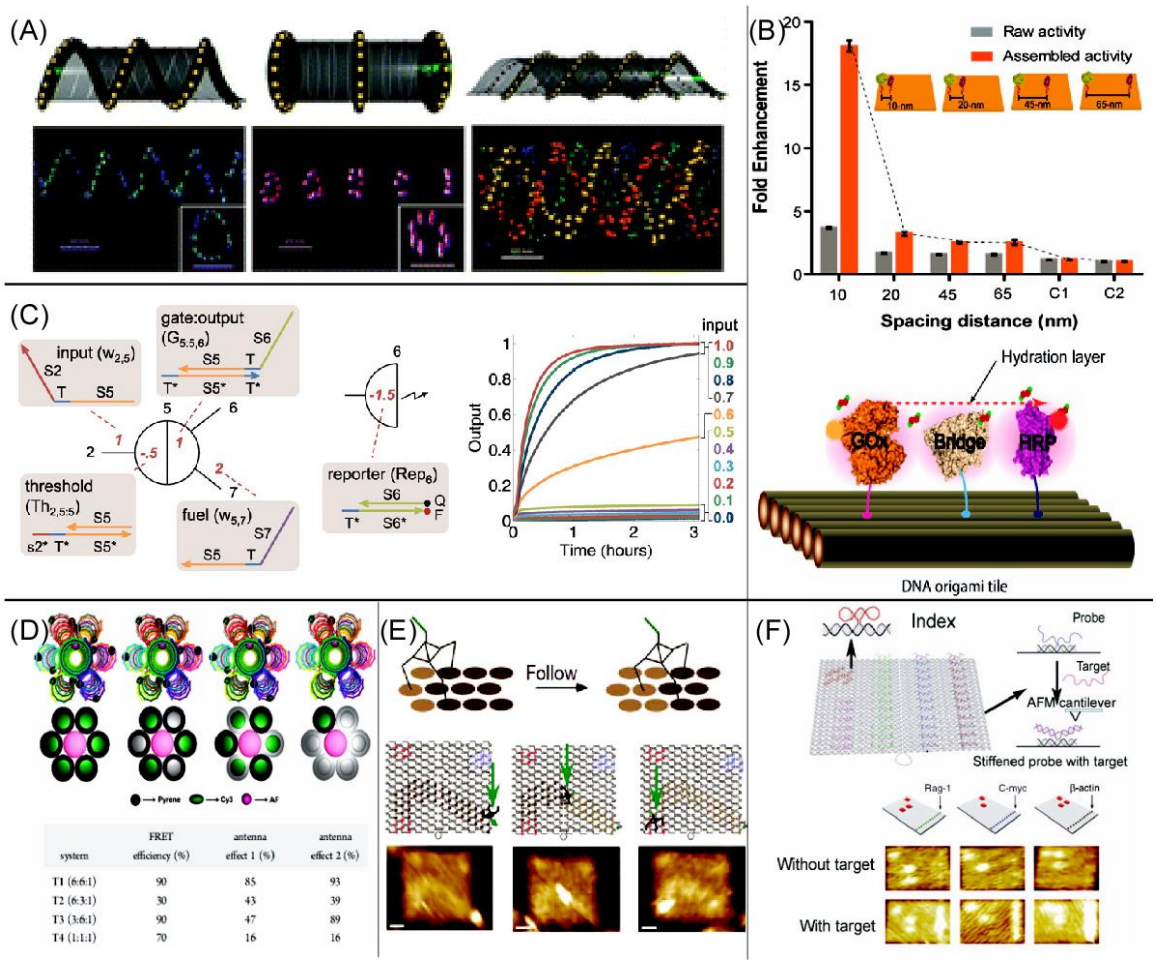

Figure 1.9 Representative examples of the broad applications of DNA nanotechnology. (A) Organized AuNPs on self-assembled DNA tubules.[44] (B) Distance controlled GOx/HRP cascade on DNA origami.[3] (C) Example of DNA computing by strand displacement.[51] (D) Artificial light harvesting antenna on a DNA device.[46] (E) Walking of a DNA robot along prescriptive landscapes.[6] (F) Biomolecular detection by functional DNA origami.[53] (Adapted with permission from refs 44, 3, 51, 46, 6, 53)

Finally, DNA nanostructures have been used as modules for the diagnosis and treatment of diseases owing to their stability, biocompatiblilty, and propensity for modification. They can also be used as transportation systems for loading, delivering and releasing drugs or other cargo to target specific organelles and cells for diagnostic and therapeutic applications.[47] Further, DNA nanostructures and nanoarrays that are modified with compounds capable of binding and signaling through synthesis, hybridization, or

conjugation, provide promising platforms for multiplex detection of nucleic acids, proteins, and other biologically relevant molecules at the single molecule or single cell level. For example, rationally designed DNA/RNA probes with complementary sequences displayed from the surface of DNA structures can be applied to detect target DNA/RNA molecules *in vitro*/*in vivo*;[53] (Figure 1.9F) Aptamers, which are *in vitro* selected DNAs/RNAs that have high binding affinity to a broad range of biomolecules, can be easily modified within DNA motifs for multifunctional diagnosis, cell surface recognition, intracellular pathway interruption or inducing cell-cell interactions.[48] The potential for cellular integration and triggered structural transformation[4] make DNA nano devices very promising candidates for drug delivery and therapy. Detecting DNA nanostructures *in vivo*/in cells can be achieved by association with Quantum Dots[49] or fluorophores[5], by co-localization analysis.

1.4.2 Diversity of T cell receptors

In the human body there are two classes of immune response systems to fight against exogenous infectious pathogens: innate immune systems that react rapidly but in a non-specific manner without generating memory to fight against future infection; and adaptive immune systems that react relatively slowly but generate a memory response that reacts to repeated exposure.[47] The immune cells that are involved in the latter system are classified as lymphocytes, including B and T lymphocytes, as well as immunoglobulin. Usually, adaptive immune responses are initiated by recognition between T cell receptors (TCRs) on the surface of T cells and antigenic peptide- major histocompatibility complexes (MHCs) on the surface of antigen presenting cells

(APCs).[54] (Figure 1.10) The TCR co-receptor CD4 bound to class II MHCs simulate T cells to transform into mature helper T cells that release T cell cytokines to activate other immune cells like B cells; while TCR co-receptor CD8 bound to class I MHCs promots T cell transformation into mature cytotoxic T cells that kill APCs.

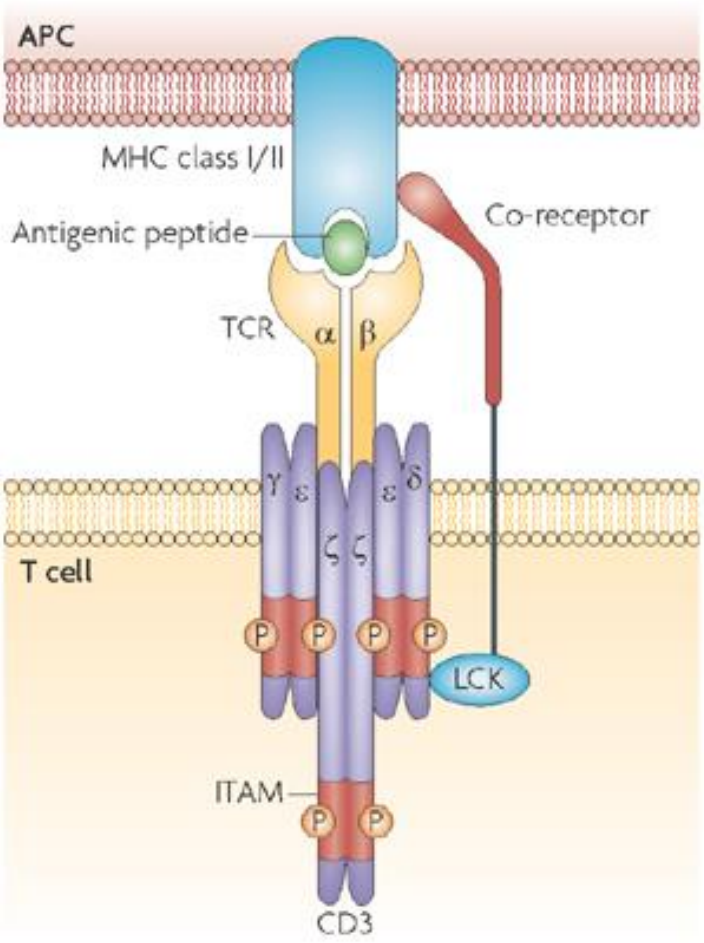

Figure 1.10 Illustration of TCR bound to the antigenic peptide‑MHC complex.[54] (Adapted with permission from ref 54)

TCR is heterodimer protein, typically composed of two peptide chains, α and β in the majority of T cells, or γ and δ in around 5% T cells. (Figure 1.10) Each α and β peptide contains a variable domain and a constant domain, where the huge variation in

the V region ensures specificity and affinity to recognize different antigenic peptide-MHC complexes.[57] In Figure 1.11A, there are three complementarity determining regions (CDR), that play key roles in the interactions with antigenic peptides or MHC molecules, among which CDR3 is mainly responsible for recognition of antigenic peptides. Understanding exactly how CDR3 of TCRαβ affects these interactions can open the door to understanding the comprehensive T cell immune response.[57-59]

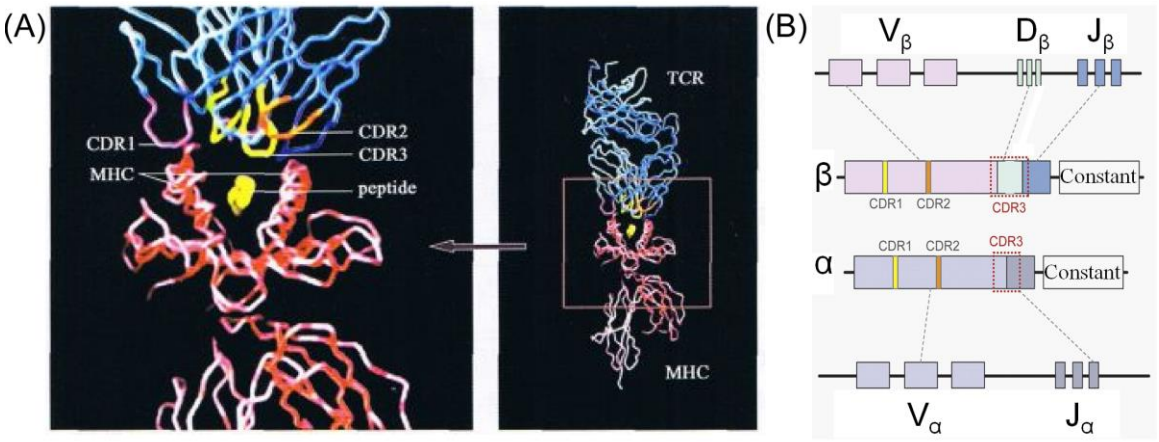

Figure 1.11 Illustration of TCRαβ peptides and gene segments. (A) TCR and antigenic peptide-MHC complex structure, with highlighted CDR region.[55] (B) The diversity of TCRs is generated from rearrangement of gene segments.[56] (Adapted with permission from ref 55, 56)

The immune system must be able to recognize and respond to virtually any invading microorganism. The specificity of the adaptive immune response is derived from the fact that a lymphocyte can only recognize and bind to one antigen. Thus, one of the most important characteristics of T cells is their immense diversity. First, in order to generate such diversity, developing T cells rearrange a defined set of variable (V), diversity (D), and joining (J) gene coding segments of TCRβ and V, and D segments of TCRα, with N-

nucleotide addition and subtraction at the joints of these gene segments, resulting in a semi-random CDR3 repertoire of immune receptors.[56, 57] (Figure 1.11B) Second, random mutation both in the thymus and peripheral circulatory systems can increase random variation. CDR3 diversity generated by recombination of gene segments has been directly estimated for each chain separately as approximately 10^7 unique sequences in humans[62], and only slightly lower in mice[63]. Further diversity is generated by pairing of rearranged α and β chains to form the heterodimer TCR.[57, 58] Pairing between different α and β chains results in a potentially greater than several million-fold increase in TCR diversity: completely non-random pairing of TCRα and TCRβ chains would result in a total diversity of ~10^7 unique TCRs, while completely random pairing of any heavy and light or α and β chains would result in a maximum total combinatorial diversity of ~10^{18} unique TCRs. Therefore, although the repertoire evolves as the adaptive immune system responds to pathogens or other challenges, at any given time the diversity of a typical human TCRα/β repertoire is at least 10^7 unique T cell clones.[59, 60]

This diversity due to pairing of individual chains has not been systematically examined for T cells. The brute force method of sequencing both TCR chains at the single cell level is financially unfeasible for large naïve cell populations; each sequencing reaction costs around $2, so for a single naïve mouse with 10^7 total cells this would be a $20,000,000 experiment.[64] Molecular strategies for linking TCRV_α and V_β mRNA have not been adequately developed to generate suitable input material for standard multiplex deep sequencing of naïve cell CDR3 regions that would provide information on both chains from a single cell. The major limitation to such approaches is that hybrid structures, generated by transfection with oligonucleotides complementary to the constant

regions of the cell receptor mRNA, result in activation of nucleases that destroy the template and therefore, preclude sequence analysis.[65, 66]

Current technologies allow for analysis of CDR3 diversity within either α or β TCRs, but no current methods exist for obtaining both CDR3s from individual cells from large polyclonal populations: single cell sequencing remains too expensive while molecular strategies for obtaining linked CDR3 information from single cells have not been adequately developed.

1.5 Projects

1.5.1 Thermodynamics of 2D and 3D DNA origami

Understanding the thermodynamic properties of complex DNA nanostructures, including rationally designed two- and three-dimensional (2D and 3D, respectively) DNA origami, facilitates more accurate spatiotemporal control and effective functionalization of the structures by other elements. In this work fluorescein and tetramethylrhodamine (TAMRA), a Förster resonance energy transfer (FRET) dye pair, were incorporated into selected staples within various 2D and 3D DNA origami structures. We monitored the temperature-dependent changes in FRET efficiency that occurred as the dye-labeled structures were annealed and melted and subsequently extracted information about the associative and dissociative behavior of the origami. In particular, we examined the effects of local and long-range structural defects (omitted staple strands) on the thermal stability of common DNA origami structures. The results revealed a significant decrease in thermal stability of the structures in the vicinity of the defects, in contrast to the negligible long range effects that were observed. Furthermore, we probed the global assembly and disassembly processes by comparing the thermal behavior of the FRET pair

at several different positions. We demonstrated that the staple strands located in different areas of the structure all exhibit highly cooperative hybridization but have distinguishable melting temperatures depending on their positions. This work underscores the importance of understanding fundamental aspects of the self-assembly of DNA nanostructures and can be used to guide the design of more complicated DNA nanostructures, to optimize annealing protocols and manipulate functionalized DNA nanostructures.

1.5.2 Integration, stabilization and separation of DNA nanostructures from cells/cell lysate

We assembled several tiles and DNA origami nanostructures of differing shape, size and probes, and investigated their interaction with cells and lysate obtained from various normal and cancerous cell lines. We first investigated the size-dependent integration of DNA structures in cells by confocal microscope. Then we separated and analyzed the origami−lysate mixtures using agarose gel electrophoresis and recovered the DNA structures for functional assay and subsequent microscopic examination. Our results demonstrate that DNA origami nanostructures are stable in cell lysate and can be easily separated from lysate mixtures, in contrast to natural, single- and double-stranded DNA. Atomic force microscope (AFM) and transmission electron microscope (TEM) images show that the DNA origami structures are fully intact after separation from cell lysate and hybridize to their targets, verifying the superior structural integrity and functionality of self-assembled DNA origami nanostructures relative to conventional oligonucleotides. The stability and functionality of DNA origami structures in cell lysate validate their use for biological applications, for example, as programmable molecular rafts or disease detection platforms.

1.5.3 Using DNA origami to quantify functional TCRαβ repertoires without single cell sorting

The immune system must be able to recognize virtually any pathogen (diversity) while maintaining enough cells specific for each pathogen in order to mount an effective response (protection). T cells generate diversity by imprecise joining of gene segments to generate α/β heterodimeric receptors. Linking sequence information for TCRα and TCRβ pairs from individual cells has been problematic due to the cost of single cell sorting and inadequate molecular approaches for linking the α and β mRNAs encoding these proteins from individual cells. We developed novel DNA origami nanostructures to capture and protect both TCRα and TCRβ mRNA from individual cells, which can then be physically linked via a unique dual-primed reverse-transcription and ligation reaction, followed by multiplex PCR to generate individual amplicons containing both TCR from individual cells for use in next generation sequencing. We demonstrated high efficiency transfection and recovery of DNA origami, optimized methods for purification with bound TCR mRNA, and validated this approach with transgenic T cells expressing a known TCR sequence. This approach is directly amenable to single cell analysis of other immune receptors (or other species) by relatively simple modifications of the origami sequences, and could be applied to virtually any heterogeneous cell population for which sequence information on any two genes is required.

1.6 Reference:

(1) Ke, Y.; Bellot, G.; Voigt, N. V.; Fradkov, E.; Shih, W. M. *Chem. Sci.* **2012**, *3*, 2587.

(2) Ke, Y.; Ong, L. L.; Shih, W. M.; Yin, P. *Science* **2012**, *338*, 1177-83.

(3) Fu, J.; Liu, M.; Liu, Y.; Woodbury, N. W.; Yan, H. *J. Am. Chem. Soc.* **2012**, *134*, 5516-9.

(4) Douglas, S. M.; Bachelet, I.; Church, G. M. *Science* **2012**, *335*, 831-4.

(5) Lin, C.; Jungmann, R.; Leifer, A. M.; Li, C.; Levner, D.; Church, G. M.; Shih, W. M.; Yin, P. *Nat. Chem.* **2012**, *4*, 832-9.

(6) Lund, K.; Manzo, A. J.; Dabby, N.; Michelotti, N.; Johnson-Buck, A.; Nangreave, J.; Taylor, S.; Pei, R.; Stojanovic, M. N.; Walter, N. G.; Winfree, E.; Yan, H. *Nature* **2010**, *465*, 206-10.

(7) Seeman, N. C.; Kallenbach, N. R. *Annu. Rev. Biophys. Biomol. Struct.* **1994**, *23*, 53-86.

(8) Ke, Y.; Liu, Y.; Zhang, J.; Yan, H. *J. Am. Chem. Soc.* **2006**, *128*, 4414-4421.

(9) Yan, H.; Park, S. H.; Finkelstein, G.; Reif, J. H.; LaBean, T. H. *Science* **2003**, *301*, 1882-4.

(10) Zhang, D. Y.; Hariadi, R. F.; Choi, H. M.; Winfree, E. *Nat. Commun.* **2013**, *4*, 1965.

(11) Han, D.; Pal, S.; Liu, Y.; Yan, H. *Nat. Nanotech.* **2010**, *5*, 712-717.

(12) Rothemund, P. W.; Papadakis, N.; Winfree, E. *PLoS Biol.* **2004**, *2*, e424.

(13) Nangreave, J.; Yan, H.; Liu, Y. *Biophys. J.* **2009**, *97*, 563-71.

(14) Nangreave, J.; Yan, H.; Liu, Y. *J. Am. Chem. Soc.* **2011**, *133*, 4490-7.

(15) Song, J.; Arbona, J. M.; Zhang, Z.; Liu, L.; Xie, E.; Elezgaray, J.; Aime, J. P.; Gothelf, K. V.; Besenbacher, F.; Dong, M. *J. Am. Chem. Soc.* **2012**, *134*, 9844-7.

(16) SantaLucia, J., Jr.; Turner, D. H. *Biopolymers* **1997**, *44*, 309-19.

(17) Sobczak, J. P.; Martin, T. G.; Gerling, T.; Dietz, H. *Science* **2012**, *338*, 1458-61.

(18) Reed, G. H.; Kent, J. O.; Wittwer, C. T. *Pharmacogenomics* **2007**, *8*, 597-608.

(19) Sacca, B.; Meyer, R.; Feldkamp, U.; Schroeder, H.; Niemeyer, C. M. *Angew. Chem. Int. Ed. Engl.* **2008**, *47*, 2135-7.

(20) Morrison, L. E.; Stols, L. M. *Biochemistry* **1993**, *32*, 3095-104.

(21) Wei, X.; Nangreave, J.; Jiang, S.; Yan, H.; Liu, Y. *J. Am. Chem. Soc.* **2013**, *135*, 6165-76.

(22) Pinheiro, A. V.; Nangreave, J.; Jiang, S.; Yan, H.; Liu, Y. *ACS Nano.* **2012**, *6*, 5521-30.

(23) Marky, L. A.; Kallenbach, N. R.; McDonough, K. A.; Seeman, N. C.; Breslauer, K. J. *Biopolymers* **1987**, *26*, 1621-1634.

(24) SantaLucia, J., Jr.; Hicks, D. *Annu. Rev. Biophys. Biomol. Struct.* **2004**, *33*, 415-40.

(25) SantaLucia, J., Jr. *Proc. Natl. Acad. Sci. USA* **1998**, *95*, 1460-5.

(26) Howard, K. P. *J. Chem. Educ.* **2000**, *77*, 1469.

(27) Hou, M. H.; Lin, S. B.; Yuann, J. M.; Lin, W. C.; Wang, A. H.; Kan Ls, L. *Nucleic acids Res.* **2001**, *29*, 5121-8.

(28) Rauzan, B.; McMichael, E.; Cave, R.; Sevcik, L. R.; Ostrosky, K.; Whitman, E.; Stegemann, R.; Sinclair, A. L.; Serra, M. J.; Deckert, A. A. *Biochemistry* **2013**, *52*, 765-72.

(29) Fu, T. J.; Seeman, N. C. *Biochemistry* **1993**, *32*, 3211-20.

(30) Chen, H. L.; Schulman, R.; Goel, A.; Winfree, E. *Nano Lett.* **2007**, *7*, 2913-9.

(31) Rinker, S.; Liu, Y.; Yan, H. *Chem. Commun.* **2006**, 2675-7.

(32) LaBean, T. H.; Yan, H.; Kopatsch, J.; Liu, F.; Winfree, E.; Reif, J. H.; Seeman, N. C. *J. Am. Chem. Soc.* **2000**, *122*, 1848-1860.

(33) Spink, C. H.; Ding, L.; Yang, Q.; Sheardy, R. D.; Seeman, N. C. *Biophys. J.* **2009**, *97*, 528-38.

(34) Du, S. M.; Zhang, S.; Seeman, N. C. *Biochemistry* **1992**, *31*, 10955-63.

(35) Zhang, D. Y.; Winfree, E. *J. Am. Chem. Soc.* **2009**, *131*, 17303-17314.

(36) Fu, Y.; Zeng, D.; Chao, J.; Jin, Y.; Zhang, Z.; Liu, H.; Li, D.; Ma, H.; Huang, Q.; Gothelf, K. V.; Fan, C. *J. Am. Chem. Soc.* **2013**, *135*, 696-702.

(37) Myhrvold, C.; Dai, M.; Silver, P. A.; Yin, P. *Nano Lett.* **2013**, *13*, 4242-8.

(38) Jungmann, R.; Liedl, T.; Sobey, T. L.; Shih, W.; Simmel, F. C. *J. Am. Chem. Soc.***2008**, *130*, 10062-10063.

(39) Zhang, Z.; Song, J.; Besenbacher, F.; Dong, M.; Gothelf, K. V. *Angew. Chem. Int. Ed. Engl.* **2013**, *52*, 9219-23.

(40) Rothemund, P. W. *Nature.* **2006**, *440*, 297-302.

(41) Lin, C., Liu, Yan., Yan, H. *Biochemistry*, **2009**, *8*, 1663‑74.

(42) Pinheiro, A. V., Han, D., Shih, W. M. , Yan, H. *Nature Nanotech.* **2011**, 6, 763‑72.

(43) Fu, J., Liu, M., Liu, Y., Yan, H. *Acc. Chem. Res.* 2012, **45**, 1215‑26.

(44) Sharma, J., Chhabra, R., Cheng, A., Brownell, J., Liu, Y., Yan, H. *Science*, **2009**, 323, 112-6.

(45) Deng, Z., Samanta, A., Nangreave, J., Yan, H., Liu, Y. *J. Am. Chem. Soc.*, **2012**, 134, 17424‑27.

(46) Dutta, P. K.; Varghese, R.; Nangreave, J.; Lin, S.; Yan, H.; Liu, Y. *J. Am. Chem. Soc.* **2011**, 133, 11985‑ 93.

(47) Liu, X., Liu, Y., Yan, H. *Israel Journal of Chemistry, Special Issue on Supramolecular Chemistry for Materials and Medicine*, **2013**, 53, 555-66.

(48) Liu, X., Yan, H., Liu, Y., Chang, Y. *Small*, **2011**, 7, 1673‑82.

(49) Zhong, H., Zhang, Q. L., Zhang, S. S. *Chem-Eur J* 2011, 17, 8388-94.

(50) Dutta, P. K., Lin, S., Loskutov, A., Levenberg, S., Saer, R., Beatty, J. T., Liu, Y., Yan, H., Woodbury, N. *J. Am. Chem. Soc.* **2014**, 136, 4599‑ 604.

(51) Qian., L., Winfree, E. *Science*, **2011**, 332, 1196-201.

(52) Qian., L., Winfree, E., Bruck, J. *Nature*, **2011**. 475, 368-72.

(53) Ke, Y.; Lindsay, S.; Chang, Y.; Liu, Y.; Yan, H. *Science*, **2008**, 319, 180‑3.

(54) Gascoigne, N. R. *Nat. Rev. Immunol.* **2008**, 11, 895-900.

(55) http://shiyan.ebioe.com//13444.htm

(56) Kazena, A. R., Adamsa, E. J. *Proc. Natl. Acad. Sci. USA* **2011**, 108, 11743-4.

(57) Davis, M. M., Bjorkman, P. J. *Nature*, **1988**. 6181, 395-402.

(58) Newell, E. W., Davis, M. M. *Nat. Biotechnol*. **2014**, 32, 149-57.

(59) Donermeyer, D. L., Weber, K. S., Kranz, D. M., Allen, P. M. *J. Immunol.* **2006**, 177, 6911-9.

(60) Arstila, T.P., Casrouge, A., Baron, V., Even, J., Kanellopoulos, J., Kourilsky, P. *Science*, **1999**. 5441, 958-61.

(61) Casrouge, A., Beaudoing, E., Dalle, S., Pannetier, C., Kanellopoulos, J., Kourilsky, P. *J. Immunol*, **2000**, 11, 5782-7.

(62) Arnaout, R., Lee, W., Cahill, P., Honan, T., Sparrow, T., Weiand, M., Nusbaum, C., Rajewsky, K., Koralov, S. B. *PLoS ONE* **2011**, 8, e22365.

(63) Travers, P., M., Walport, M. Janeway, C. *Janeway's immunobiology*. Garland Science, **2008**.

(64) Dash, P., McClaren, J. L., Oguin, T. H., Rothwell, W., Todd, B., Morris, M. Y., Becksfort, J., Reynolds, C., Brown, S. A., Doherty, P. C., Thomas, P. G. *J Clin Invest*, **2011**. 1, 288-95.

(65) Asirvatham, A.J. Gregoriea, C. J., Hub, Z., Magnera, W. J., B. Tomasi, T. B. *Mol Immunol*, **2008**. 45, 1995-2006.

(66) Zhang, N., Bevan, M. J. *Proc Natl Acad Sci USA*, **2010**. 50, 21629-34.

Chapter 2

THERMODYNAMICS OF 2D AND 3D DNA ORIGAMI

Adapted with permission from Wei, X.; Nangreave, J.; Jiang, S.; Yan, H.; Liu, Y. Mapping the Thermal Behavior of DNA Origami Nanostructures. *J. Am. Chem. Soc*. **2013**, 16, 6165-6176.

2.1 Abstract

Understanding the thermodynamic properties of complex DNA nanostructures, including rationally designed two- and three-dimensional (2D and 3D, respectively) DNA origami, facilitates more accurate spatiotemporal control and effective functionalization of the structures by other elements. In this work fluorescein and tetramethylrhodamine (TAMRA), a Förster resonance energy transfer (FRET) dye pair, were incorporated into selected staples within various 2D and 3D DNA origami structures. We monitored the temperature-dependent changes in FRET efficiency that occurred as the dye-labeled structures were annealed and melted and subsequently extracted information about the associative and dissociative behavior of the origami. In particular, we examined the effects of local and long-range structural defects (omitted staple strands) on the thermal stability of common DNA origami structures. The results revealed a significant decrease in thermal stability of the structures in the vicinity of the defects, in contrast to the negligible longrange effects that were observed. Furthermore, we probed the global assembly and disassembly processes by comparing the thermal behavior of the FRET pair at several different positions. We demonstrated that the staple strands located in different areas of the structure all exhibit highly cooperative hybridization but have distinguishable melting temperatures depending on their positions. This work underscores the importance of understanding fundamental aspects of the self-assembly of DNA nanostructures and can be used to guide the design of more complicated DNA nanostructures, to optimize annealing protocol and manipulate functionalized DNA nanostructures.

2.2 Introduction

DNA nanotechnology is a rapidly evolving field that exploits the unique properties of DNA for nanoscale engineering. In particular, DNA origami technology has attracted considerable attention for a variety of applications.[1-3] DNA origami is a technique in which a long single stranded viral genome (referred to as a scaffold, generally derived from the M13mp18 bacteriophage) is folded into predefined 2D or 3D structures through interactions with a large number of short DNA oligonucleotides (staples).[4-6] The unique features of DNA origami, e.g. addressability at each staple position, high pixel density and nanometer scale resolution, make the precise organization of selected biomolecules and nanoparticles possible. The potential applications of DNA nano-architectures continued to expand with the construction of increasingly complex DNA origami structures.[7,8]

Achieving more advanced DNA origami designs and effective functionalization by other bio-molecules and nanoparticles is likely to require a deeper understanding of the thermodynamic properties and behavior of the DNA origami platform.[9] Several previous studies examined the assembly and disassembly of DNA nanostructures, based on either the change in ultraviolet (UV) absorbance that occurs upon formation of double helical secondary structure or by means of a nucleic acid stain (SYBR Green) that can detect the presence of single and double stranded DNA.[10-12] However, these methods suffer from limited accuracy and detailed information about the local structure of the DNA origami cannot be determined from global average measurements. Song et al. used an atomic force microscope (AFM) to visualize the transformation of a DNA origami structure which exhibited a rough transition based on relatively coarse temperature

control (1 ℃/min). The experiments were conducted at a solid-liquid interface and it is possible that the behavior of the origami in their study does not reflect that in solution. In addition, scanning the sample with an AFM probe is likely to disturb the structural integrity of the DNA nanostructures.[13] Recently, Sobczak et al. used real-time fluorometric monitoring and cryogenic reaction quenching to probe the thermal folding and unfolding of 3D DNA origami nanostructures. Their study revealed intriguing differences between the assembly and melting transitions, though at a global level.[14]

Förster resonance energy transfer (FRET) is a convenient way to monitor molecular association and dissociation events.[15,16] With FRET, the efficiency of energy transfer depends on several factors including the distance between the donor and acceptor fluorophores. DNA origami is particularly compatible with FRET based reporting as adjacent staples can be easily functionalized with FRET dyes.[17,18] When the temperature is low the origami structures are fully assembled and the FRET dyes are close together, resulting in efficient energy transfer. As the temperature increases the structures destabilize and the dye labeled strands begin to dissociate from the scaffold resulting in negligible energy transfer. FRET based monitoring of DNA nanostructure assembly and disassembly can be used to overcome the technical barriers faced by UV absorption and DNA staining methods because the corresponding fluorescence energy transfer events have no correlation with the presence of extra unlabeled DNA strands; thus, the background interference is minor which permits more accurate measurement. The behavior of each individual staple, including the dye labeled strands, is highly cooperative and it is reasonable to propose that FRET between two representative individual strands will reliably reflect the overall thermal behavior of the structure. On

the other hand, FRET is sensitive enough to detect the nanometer scale changes in distance that are connected to underlying structural changes elicited by a variety of factors, including the presence or absence of structural elements in close proximity to the reporter molecules. This makes is possible to probe the behavior of very specific areas of the origami structure.[19,20]

We previously used a FRET based strategy to study the thermodynamic behavior of small, interacting DNA tiles. The number and relative position of the sticky end connections between the tiles, and the flexibility and rigidity of the core elements of the tiles themselves were systematically varied and the effects on the thermal stability of the assembled structures were determined.[21,22] In the current study we used the same FRET method to reveal the global and local stability of more complex DNA origami structures.

Initially, we established the thermodynamic characteristics of fully-assembled 2D and 3D origami as signified by the transition temperature of representative staple-scaffold interactions. Next, we held the position of the FRET dyes constant as we induced defects in the origami structures (i.e. selective omission of staples) at various distances from the reporter molecules. The results allowed us to determine the effects of distant and local defects on the stability of the origami in the vicinity of the reporter molecules. We further probed the effects of local defects on nanostructure stability by systematically removing individual staples or small groups of staples directly adjacent to the FRET dyes. Finally, we attempted to determine if the origami exhibit uniform stability across their entire structure or if different areas of the structure are more susceptible to destabilization. Here, the stability was examined when the reporter dyes were moved to different positions in the structure.

The FRET studies here reveal subtle details about the formation and dissociation of 2D and 3D DNA origami nanostructures that reflect both local and long range factors. This work has allowed us to gain a deeper understanding of the thermodynamic behavior of DNA origami structures and the hybridization of individual staple strands to the scaffold at the molecular level.

2.3 Design of FRET labeled 2D and 3D DNA origami

For each experimental design we selected two neighboring staple strands in the DNA origami structures and modified them with FRET donor (fluorescein) and acceptor (TAMRA) dyes, respectively, as shown in Figure 2.1A. The distance between the dyes in the fully-assembled DNA origami are comparable to (or smaller than) the Forster distance (~ 5 nm), permitting observation of the changes in FRET efficiency that occur during the assembly/disassembly processes.[16,23] In addition, the donor and acceptor dye labeled staples were designed to bind to different segments of the scaffold (i.e. different helices in the final product) to report on global structural changes. Assembly and disassembly of the DNA origami structures was induced by the ramping the temperature up and down. At very high temperatures the FRET efficiency is low because the dye labeled staples are dissociated from the scaffold and are relatively far apart. As the temperature is decreased the dye labeled strands begin to associate with the scaffold and are close together in the final product, thus, the FRET efficiency is relatively high.

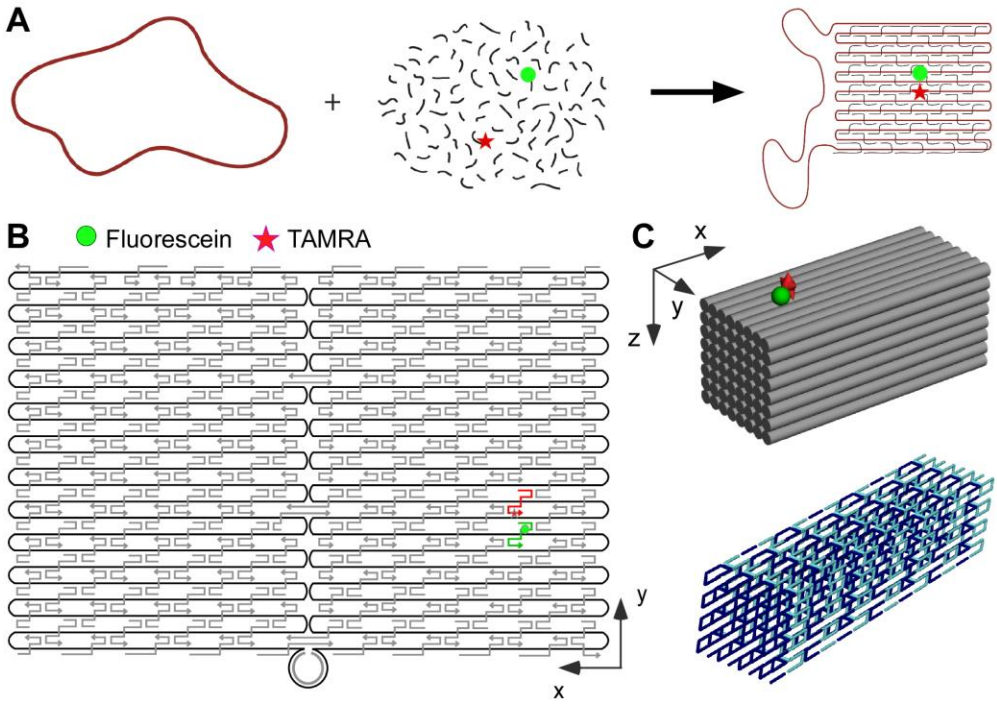

Figure 2.1 FRET based monitoring of DNA nanostructure assembly and disassembly. (A) Schematic representation of the self-assembly of a DNA origami structure from a circular scaffold and collection of complimentary staple strands. Two selected staples are modified with FRET donor (fluorescein, green circle) and acceptor (TAMRA, red star) dyes, respectively. (B) Rectangular DNA origami structure used to investigate assembly/disassembly in 2D. Note the position of the FRET dyes on different helical rows in the lower right hand quadrant. (C) Cuboid DNA origami structure used to investigate assembly/disassembly in 3D. The upper diagram depicts a FRET pair on the top surface of the structure. The lower diagram shows the layer by layer staple organization (alternative layers are shown in dark and light blue).

We selected a common rectangular design (24 parallel helices) to investigate the thermodynamic behavior of 2D DNA origami (Figure 2.1B).[4] Here, most staples are 32 nucleotides (nts) long and can be divided into three consecutive domains (8 nt, 16 nt, and 8 nt) that bind to unique regions of the scaffold, respectively, bridging three adjacent helices. As shown in Figure 1, the donor and acceptor dye-modified staples are designed to bind to the scaffold such that they bring the FRET pair into close proximity upon

formation of the origami structure. Figure 1B depicts one of three FRET dye positions that were analyzed.

We also explored the thermodynamic behavior of a 3D DNA origami cuboid structure composed of 8 x 8 helices bound in a square lattice.[24] In this design, the staples are grouped into 14 layers along the helical axis (x direction). Four different FRET dye positions were investigated, including the one depicted in Figure 2.1C. For all 2D and 3D designs (Figures 5 & 6), the distance between the donor and acceptor dye is estimated to be approximately 3-4 nm in the fully-assembled structure.

2.4 Materials and Methods

2.4.1 Preparation of DNA nanostructures

M13mp18 was purchased from New England Biolabs (Ipswich, MA, USA) and used without purification. All oligonucleotides used to assemble the DNA structures, including the fluorescein (excitation: 495 nm, emission: 520 nm) and TAMRA (excitation: 559 nm, emission: 583 nm) internally labeled strands, was purchased from Integrated DNA Technologies, Inc. (www.idtdnacom). Dye labeled strands were HPLC purified and all other staple strands were used without purification.

In general, each 2D DNA origami structure was assembled by mixing M13 viral DNA (final concentration of 50 nM and final volume of 20 μL) with 100 nM dye labeled staples and 250 nM unmodified staples. All 2D samples were assembled in 1× TAE Mg2+ buffer, which contains 40 mM Tris base, 20 mM acetate acid, 2 mM EDTA, and 12.5 mM Mg2+ at pH 8.0. Most 3D DNA origami structures were assembled at the same M13 concentration as the 2D structures, with a molar ratio 1:2:10 of M13: dye-modified

staples: unmodified staples. The same reaction buffer (1× TAE buffer) was used for assembly of the 3D structures, but with a higher Mg2+ concentration (16 mM).

2.4.2 Real-time monitoring of the assembly/disassembly processes

The fluorescence thermal curves were measured in eight-well optical tube strips using a MX3005P real-time thermocycler (Stratagene). After mixing the M13 scaffold with the staples, 20 μL of each sample was pipetted into Stratagene optical tube strips and closed with Stratagene optical caps. The samples were heated at 95 ℃ for 5 min and the fluorescence emission of fluorescein (522 nm) was monitored with an excitation of 492 nm. For rectangular origami, the temperature was reduced from 80 ℃ to 25 ℃ at a rate of 0.1 ℃/min. For cuboid origami, the temperature was reduced at 0.1 ℃/min from 80 ℃ to 75 ℃, 0.1 ℃/2 min from 75 ℃ to 65 ℃, 0.1 ℃/3 min from 65 ℃ to 40 ℃ and 0.1 ℃/2 min from 40 ℃ to 25 ℃. Heating cycles were performed in the same manner: after one cooling cycle the samples were held at 25 ℃ for 10 min and upon excitation at 492 nm, the fluorescence emission was monitored while the temperature was increased from 25 ℃ to 80 ℃ at a rate of 0.1 ℃/min for rectangular origami and the slower reverse rate for cuboid origami as described above. All experiments were repeated at least in duplicate to ensure reproducibility. For all the nanostructures investigated, two samples were prepared with identical experimental conditions: One sample contained the donor and acceptor modified staples (fully assembly FRET structure), whereas the second sample contained only the donor fluorophore and corresponding unlabeled oligomer as the reference. This scheme allowed for the measurement of the decrease in donor emission resulting from energy transfer to the TAMRA acceptor to calculate the FRET efficiency. This method also

allowed for the variations in the donor's fluorescence as a result of changes in temperature to be taken into account.

2.5 Results and discussion

2.5.1 Data Analysis

The fluorescence thermal curves were measured using a PCR thermocycler (MX3005P, Stratagene) capable of monitoring the real-time change in fluorescence of the reporter dyes as a function of temperature. For all the nanostructures investigated, two samples were prepared with identical experimental conditions: one sample contained both the donor (fluorescein) and acceptor (TAMRA) dyes, whereas the second sample contained only the donor fluorophore and corresponding unlabeled acceptor oligomer as the reference (Figure 2.2A). This scheme allowed for the measurement of the decrease in fluorescein emission resulting from energy transfer to TAMRA to calculate the FRET efficiency (Figure 2.2B).

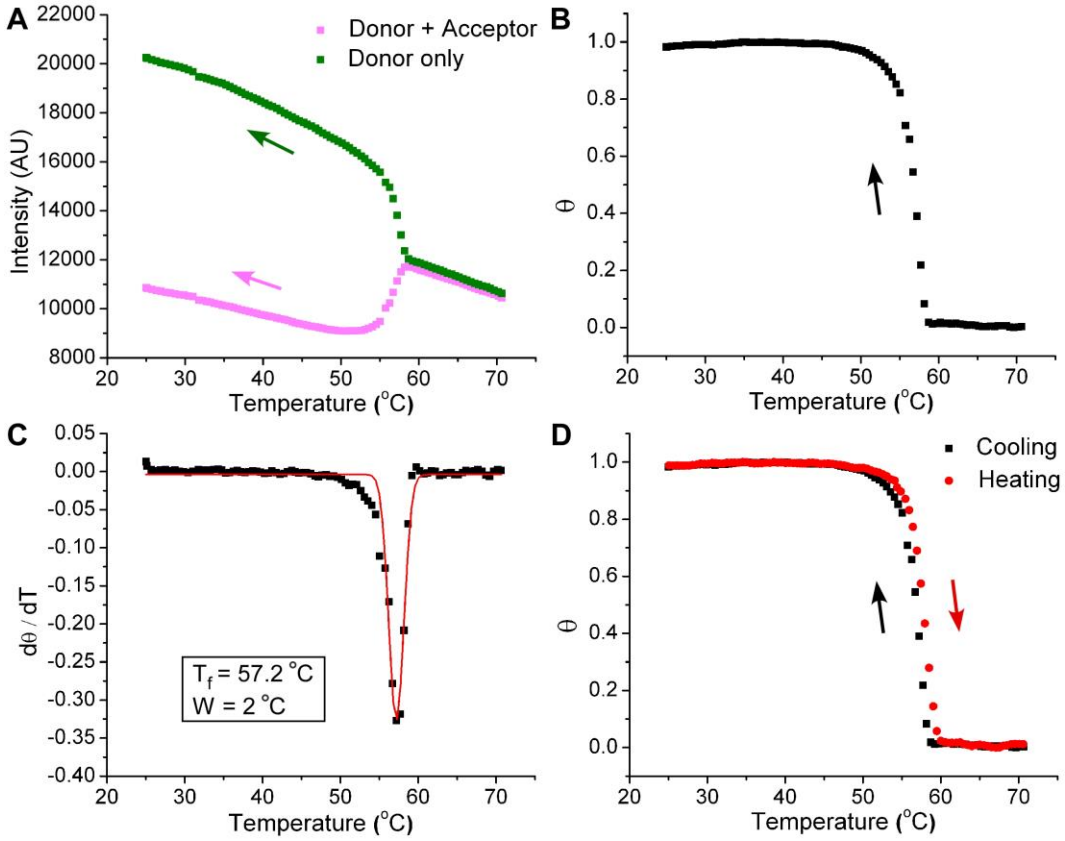

Figure 2.2 Procedure to determine the transition temperatures of DNA origami structures. All data presented in this figure corresponds to the unmodified, rectangular DNA origami reference structure. Each sample was heated at 95 ℃ for 5 min and the fluorescence emission of fluorescein at 522 nm was monitored with 492 nm excitation. For rectangular origami, the temperature was reduced from 80 ℃ to 25 ℃ at 0.1 ℃/min for the cooling cycle and vice-versa for the heating cycle. For cuboid origami, the temperature was reduced at 0.1 ℃/min from 80 ℃ to 75 ℃, 0.1 ℃/2 min from 75 ℃ to 65 ℃, 0.1 ℃/3 min from 65 ℃ to 40 ℃ and 0.1 ℃/2 min from 40 ℃ to 25 ℃ for the cooling cycle and vice-versa for the heating cycle. (A) A plot of the fluorescent emission of fluorescein (donor) versus temperature. The data was collected during the assembly phase (cooling), with the green and pink traces corresponding to the donor only and fully-assembled donor-acceptor structures, respectively. The arrows indicate the direction of the cooling temperature sweep. (B) The normalized FRET efficiency (θ) of the same sample as a function of temperature. The arrow indicates the cooling temperature sweep. (C) A plot of the first derivative of the data shown in B as a function of temperature. The curve is fitted by a Gaussian function to identify the transition temperature (T_f) and the width of the transition (W). (D) An overlay of the normalized FRET efficiency plots corresponding to cooling (black) and heating cycles (red) that reveals the reversible assembly and disassembly of the structure. The arrows indicate the direction of temperature sweep (black for cooling and red for heating).

The fluorescence of the donor (in the absence of the acceptor) gradually increased as the sample was cooled from 80 ℃, until a rapid increase in fluorescence was observed at 57-58 ℃ (dotted green trace in Figure 2.2A). This sharp change in the fluorescence intensity of the donor was also observed during the heating cycle (e.g. Figure S2.4). The sharp transition observed in the donor only sample is coincident with that observed in the fully-assembled donor-acceptor sample (pink dotted trace in Figure 2.2A), reflecting the temperature at which the dye-modified staples hybridize to the scaffold strand.

The nearly linear, temperature dependent change in the fluorescence quantum yield of fluorescein that we observed has been reported previously.[25-27] However, the sharp increase in fluorescence intensity (~ 40%) that occurred upon hybridization of the dye-modified staple cannot be explained by the temperature dependence of the dye. Pinheiro et al. recently reported a ~ 30-40% increase in the fluorescence intensity of fluorescein upon formation of double helical DNA adjacent to the site of the dye modification (5' dye labeled staple).[28] The increase in fluorescence was accompanied by a decrease in anisotropy, indicating a reduced interaction between the dye and the neighboring DNA bases upon formation of double helical DNA. Here, all dye modifications are at internal positions of staples and similarly, we anticipate that the interaction of the dye with adjacent nucleotides limits the exposure of the dye to the solvent, restricts its rotational dynamics, and contributes to quenching of its fluorescence. Hybridization of staples to the scaffold at positions adjacent to the dye modification are expected to release the dye from its interactions so that it gains exposure to a more polar environment and displays a significant increase in the quantum yield.

On the other hand, the fluorescence intensity of the donor is expected to undergo a dramatic decrease upon formation of the DNA origami structure, as the distance between the FRET pair in the fully-assembled structure is small enough for efficient energy transfer to occur. Apparently, the FRET interaction dominates when the acceptor is present as demonstrated by the data shown in Figure 2.2A (pink dots).

The FRET efficiency (E), which is related to the change in distance between the FRET donor and acceptor, is defined by the following equation:

$$E = (I_D - I_{DA})/I_D \qquad (1)$$

Where I_D and I_{DA} are the fluorescent intensity of the donor in the absence or presence of the acceptor, respectively. Assuming that the system is given adequate time to reach equilibrium at each temperature, the variation in FRET efficiency is expected to reflect any temperature dependent structural changes. Consequently, normalized FRET efficiencies are proportional to the fraction of assembled structures (θ):

$$\theta = (E - E_{min})/(E_{max} - E_{min}) \qquad (2)$$

Where E_{min} represents the minimum FRET efficiency that is present when the structure is completely dissociated (high temperatures) and E_{max} represents the maximum FRET efficiency that is observed when the structures are fully assembled (low temperatures). Thus, FRET efficiency is normalized between 0 and 1 where "θ=0" represents the fully dissociated state while "θ=1" indicates complete formation of the DNA origami.

From a plot of θ versus temperature T, we can identify the transitions that correspond to assembly or disassembly of the origami during the cooling and heating cycles, respectively (an example cooling profile is shown in Figure 2.2B). The transition observed during the cooling cycle is referred to as the temperature of formation (T_f),

while the one observed during the heating cycle is referred to as the melting temperature (T_m). A plot of the first derivative of θ ($d\theta/dT$) versus temperature (T) is fit by a Gaussian function to yield the midpoints (T_f or T_m) and width (w) of the transition (Figure 2.2C). Overlaying the cooling and heating thermal curves for the same sample indicates the reversibility of the transition (Figure 2.2D).

The results of such an analysis can be used to understand more about the thermal behavior of 2D and 3D DNA origami structures. For example, the transition temperatures indicate the stability of the FRET modified region, while the shape of the transition provides information about the cooperativity of staple hybridization. In general, higher transition temperatures reflect more stable interactions. Smooth, sharp transitions indicate rapid, cooperative assembly in which the system reaches equilibrium in a narrow temperature range. In addition, it is possible to follow the thermal characteristics of donor and acceptor modified staples separately to gain insight in the mechanism of annealing and melting at the molecular level.

2.5.2 2D and 3D reference structures

First, the experimental and data analysis methods described above were used to determine the transition temperatures of a basic and a 3D DNA origami structure (Figures S2.1 and S2.2 and Tables S2.1-S2.4). The transition temperatures (T_f and T_m) of the 2D rectangular origami structure are 57.2 ± 1.0 ℃ and 57.9 ± 1.3 ℃, respectively (Figure 2.2D). The minimal discrepancy in temperature between the cooling and heating cycle transitions, and the sharp features of the transitions reveal that the structure is reversibly assembled/disassembled at approximately 57 ℃ to 58 ℃. The data also indicates that the 2.2D origami structure forms and dissociates relatively rapidly such that the system can

indeed be considered to be at equilibrium at each measurement temperature. We also demonstrated that the rates of temperature change in the cooling and heating cycles, for both 2D and 3D samples, are slow enough to ensure equilibrium at each temperature (Table S2.5).

However, clear hysteresis between the cooling and heating curves was observed for the 8 x 8 layer 3D cuboid origami structure (Figure 2.6A), with a T_f of 54.6 ± 1.3 ℃ and a T_m of 60.4 ± 1.4 ℃ (corresponding to the dye positions depicted in Figure 2.1C). We propose that the ~ 6 ℃ difference between T_f and T_m is due to the complex folding interactions that occur between various layers in the structures, making the assembly process much slower than the melting process. A more detailed discussion of these results can be found in section G below.

2.5.3 Scaffold to staple ratio

Next, we wanted to confirm whether or not the ratio between the M13 scaffold and the staple strands has an effect on the thermal characteristics of the assembly/disassembly process. Typically, the molar ratio of the M13 scaffold to the staples is 1:5 for 2D origami, and 1:10 for 3D origami. Here, we held the M13 to dye-modified staple ratio at 1:2, and evaluated 1:1 and 1:5 ratios of M13 to unmodified staples. We also performed other experiments in which we held the ratio of M13 to unmodified staples at 1:5, while we examined 1:1, 1:2, and 1:5 M13 to dye-modified staple ratios. The results of these experiments are listed in Table 2.1A.

A. Transition temperatures measured from 2D DNA origami

M13:FRET	M13:staples	Cooling T_f (℃)	Heating T_m (℃)
1:2	1:1	55.6 ±0.9	57.6 ±1.3
1:2	1:5	57.2 ±1.0	57.9 ±1.3
1:1	1:5	57.2 ±0.9	57.7 ±1.4
1:5	1:5	57.5 ±0.9	58.3 ±1.0

B. Transition temperatures measured from 3D DNA origami

M13:FRET	M13:staples	Cooling T_f (℃)	Heating T_m (℃)
1:2	1:1	48.3 ±3.3	57.9 ±2.4
1:2	1:5	53.5 ±1.2	60.0 ±1.4
1:2	1:10	54.6 ±1.3	60.4 ±1.4
1:5	1:10	54.6 ±1.1	60.9 ±1.3
1:5	1:15	54.2 ±1.5	60.4 ±1.6

Table 2.1 The effect of the scaffold (M13) to staple ratios. (A) No significant differences were observed for the 2D structure, except for a 1:1 ratio of M13 to staples which induced a T_f 1-2 ℃ lower than the other cases. (B) No significant differences were observed in the 3D structure, except for a 1:1 ratio of M13 to staples where the cooling and heating values are significant lower. In all cases, a 6-7 ℃ difference between T_f and T_m was observed, except for a 1:1 ratio where a 9 ℃ difference was observed.

The melting temperatures are very close in all cases; however, the temperature of formation is slightly reduced for experiments with a 1:1 ratio of M13 to staples. This result is expected because without excess staples to accelerate the hybridization and M13 scaffold folding processes, it takes longer to reach equilibrium at each temperature. In addition, any truncated staples in solution (the staples were not purified before use) can bind to the scaffold and lower the thermal stability, further reducing the T_f. When the ratio of the scaffold to the unmodified staples was kept constant (1:5) and the ratio of the scaffold to the dye-modified staples was varied, the T_f and T_m showed no significant difference. This result confirmed that the dye-modified staples and FRET based method described here are reliable reporters of the thermal behavior in such a system. We used a

1:2 of M13 to dye-modified staples and a 1:5 of M13 to unmodified staples for all subsequent studies of the 2D DNA origami structure.

Note that the general practice when assembling the 2D rectangular structure used in these experiments is to omit the outermost layers of staples (adjacent to the ends of the helices on both sides) in order to reduce the non-specific end to end base stacking between structures. We measured the thermal transitions of the rectangular structure with and without the outermost staples and determined that the transition temperatures were nearly the same (0.1 to 0.3 ℃ difference for T_f and T_m, respectively) for both situations (Figure S2.4 and S2.5). For the sake of consistency and overall structural integrity, we included the outermost layers in the experiments described herein.

The folding path of the M13 scaffold is more complex in 3D origami structures, with more compact structural characteristics than observed in 2D. Thus, a higher ratio of the unmodified staples to the scaffold (typically 10:1) was used to improve the yield. For the experiments described here we held the ratio between the scaffold and the dye labeled staples at 1:2 while changing the ratio of M13 to unmodified staples from 1:1, 1:5 to 1:10. We observed a very small difference in the T_f (~ 1 ℃), while the T_m was similar for both 1:5 and 1:10 ratios; however, T_f is significantly reduced (5-6 degrees) and the width of the transition is larger (3.3 ℃ vs. 1.2 ℃), indicating a much slower formation when there are no excess staples (Table 2.1B). The melting temperature, T_m, is also significantly lower (2-3 degrees). The 3D origami with a 1:1 ratio of scaffold to staple strands may have some strand mismatches or base-pairs missing at random positions due to a less than 100% yield of the full length staple strands in the synthesis, which is consistent with the result we obtained for the 2D origami. Next we analyzed samples in

which the ratio of M13 to dye-modified staples was held at 1:5, while 1:10 and 1:15 ratios of M13 to unmodified staples were tested. Again, similar T_f and T_m values were obtained for both cases (Table 2.1B). Our results suggest that it is not necessary to use a relatively high molar ratio of M13 to staples for 3D DNA origami structures. However, most reports of 3D DNA origami describe a 1:10 ratio of M13 to staples and in an effort to remain relevant, we used a 1:2:10 ratio of M13 to dye-modified staples to unmodified staples for experiments with the cuboid structure.

We also evaluated the effect of concentration on origami folding and melting. For 2D origami the transition temperature of folding, T_f, is higher when the concentration is higher and lower when the concentration decreases (Table S2.6A). This is likely because the staples have a lower probably of encountering and interacting with the scaffold at lower concentrations. However, the transition temperature of melting (dissociation) T_m is similar because the unfolding rate is not affected as much by the concentration. For the 3D origami, the folding trend is the same as 2D origami but the absolute temperature values are even larger (Table S2.6B). The dissociation temperature was reduced a few degrees when the concentration decreased. The complicated folding of cuboid origami that more relies on dynamic dissociation and incorporation (on and off) may cause this phenomenon. In our study, we chose 50 nM as the standard concentration to reduce the impact of hysteresis.

2.5.4 Global stability of 2D structures

DNA origami is widely utilized as an addressable scaffold with selected staple strands often modified as target probes or by chemical linkers. Understanding the thermodynamic behavior of DNA origami structures is important to guarantee the

stability, integrity, and functionality of the modifications. In this study, we induced various “defects” (staple deletions) to the structures, both close to and far from the FRET reporter dyes, and examined the local and long-range impact of the deletions on the stability of the structures. The inclusion of structural defects and integrity of the resulting structures was confirmed by Atomic force microscopy (AFM) (Figure S2.3).

First we examined the relationship between the two halves of the origami structure that are naturally divided by the folding path of the scaffold. Here, all the staples on the “left” side of the origami were intentionally omitted from the sample mixture such that only the “right” side of the structure (where the FRET dyes are positioned) could form (Figure 2.3A, left). Compared to the fully-assembled reference structure, the transition temperatures of the half origami structure were only ~ 0.1 ℃ lower, which is within experimental error. This result suggests that the assembly and disassembly of the two halves of the 2D DNA origami rectangle are completely independent of each other, most likely due to the discontinuous arrangement of the scaffold strand across the width of the structure. It is reasonable to conclude that each side of the 2D structure can be manipulated without having an adverse effect on the stability of the other half.

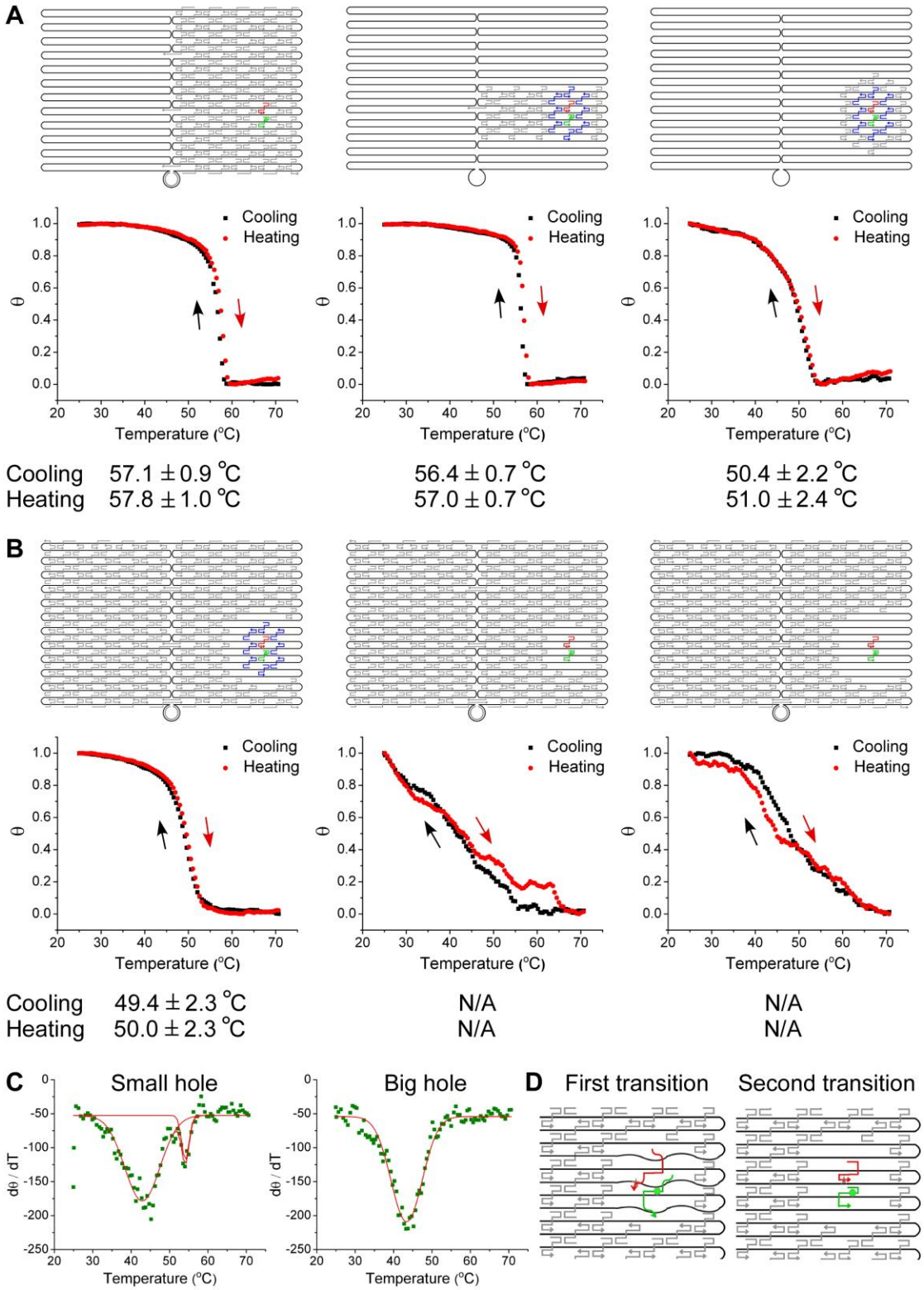

Figure 2.3 The effect of various structural defects on transition temperatures. For A and B, the upper panels depict the design while the lower panels present the corresponding

thermal melting curves from which the transition temperatures were determined. Note that the position of the reporter dyes is the same for all designs. (A) From left to right: half origami, 7-helix core, and 2-layer cluster structures. (B) From left to right: ring-hole, small-hole, and big-hole structures. The 8 staple strands in the first layer encircling the dyes are highlighted (shown in dark and light blue). The transitions corresponding to the small-hole and big-hole structures could not be reliably fit from the FRET data, so the transition temperatures are not reported here. (C) Plots of the derivative of fluorescence signal of the donor only sample for the small-hole and big-hole structures, respectively (cooling cycle, complete data sets are shown in Figures S10 and S11). Gaussian fits of the plots (red lines) yielded transition temperatures of formation (T_f) of 42.9 ±4.6 ℃ and 54.1 ±1.0 ℃ for the small-hole structure, and 43.4 ± 4.1 ℃ for the big-hole structure. (D) Proposed model to depict the transitions observed during the cooling cycle.

Next, we further omitted groups of staples designed to bind to the scaffold above and below the position of the FRET reporter dyes, leaving a seven-helix core surrounding the fluorophores (Figure 2.3A, middle). Both transition temperatures (T_f and T_m) decreased by ~ 0.7-0.9 ℃ compared to the fully-assembled reference structure, though the shape of the transitions remained the same. The sharp transitions confirm the highly cooperative activity of the staples surrounding the reporter dyes, while the minimal difference in transition temperatures (compared to the reference) suggests that the number of helices in the core is sufficient to maintain the structural integrity of the abbreviated structure.

We went on to delete all but two layers of staples surrounding the FRET dyes (Figure 2.3A, right). A dramatic 6-7 ℃ drop (compared to the reference) in both transition temperatures was observed, with a slight broadening of the transition curves. This suggests that the reporter dyes are not sufficiently stabilized by the surrounding double helical structure and that the self-assembly of the staples is less cooperative. Direct comparison of the scenarios depicted in the middle and right panel of Figure 2.3A implies that the staples which are designed to bind to the same stretch of scaffold (along

the same helical row) as the reporter dyes are more important in stabilizing the area than those along other helices.

We subsequently focused on the presence/absence of staples only in the two staple layers immediately encircling the reporter dyes. We sought to identify how significantly, if at all, do these staples affect the local stability of the structure, and what staples specifically have the largest impact. We examined samples in which the first (8 staples, "small-hole"), second (14 staples, "ring-hole), or both (big-hole) layers of staples surrounding the reporter dyes were omitted (Figure 2.3B). Of the three groups, only the ring-hole sample (first layer of staples surrounding the reporter dyes is present) exhibited sharp, relatively high transition temperatures ~ 50 ℃ (comparable to the design shown in Figure 2.3A, right). In the experiments described here, it is apparent that omitting the second layer of staples interferes with the association of the dye-modified strands with the scaffold, possible due to increased local flexibility.

The other two groups (small-hole and the big-hole structures) exhibited extremely broad transitions ranging from 35-50 ℃ (see complete data set in Figures S2.10, S2.11). Here, the transition temperatures could not be accurately determined due to the smaller amplitude of the fluorescence intensity change compared to the background, an indication that binding equilibrium was not achieved at each temperature. One possible explanation for the low signal to noise ratio is related to the flexibility of unpaired regions of the scaffold strand. It is likely that the increased flexibility of the scaffold at positions directly adjacent to the reporter site interferes with the formation of crossovers between adjacent helices and close helical packing, resulting in a larger distance between the FRET dyes. Fortunately, the donor only samples corresponding to these groups exhibited

more obvious transitions than the fully-assembled donor-acceptor samples (Figure 2.3C, S2.10-S2.11). It should be noted that the position of the donor dye modification is in the middle of the 16 nt long domain of the corresponding staple, not one of the 8 nt terminal domains as is the case for the acceptor dye. Thus, we might expect that the donor modified staple is subject to more efficient hybridization to the scaffold than the acceptor modified staple.

A comparison of the donor only and fully-assembled donor-acceptor pair data corresponding to these two samples (small-hole and big-hole) also supports this explanation (Figures 2.3C and S2.10-2.11). For the small-hole design, the donor only sample exhibited two clear transitions at 42.9±4.6 ℃ and 54.1±1.0 ℃ (cooling cycle). In Figure 2.3D, the narrower transition observed at ~54℃ can be attributed to the hybridization of the 16 nt long domain of the staples, while the broader transition at ~43℃ reflects hybridization of the two 8 nt domains. In the small-hole design only the first layer of staple strands encircling the reporter site are absent so that the 8 nt staple domains have the opportunity to bind to complementary regions of the scaffold on adjacent helical rows and form crossovers. However, in the big-hole structure there are two layers of absent staples and a single broad transition is observed 43.4±4.1℃. In this case it is likely that only the 16 nt domain binds to the scaffold, and not the 8 nt domains.

The much lower transition temperatures and broader transition curves for the small-hole and large-hole structures (compared to the ring-hole structure) indicate that the layer of staples immediately encircling the dye labeled strands plays a more critical role in stabilizing the local structure than other layers.

2.5.5 Local stability of 2D structures

Based on the previous results we further investigated the influence of individual staples surrounding the FRET dyes. A close inspection of Figure 4A reveals the pattern of staples directly adjacent to the reporter site. We distinguished each staple by specifying its cardinal direction (N, NE, E, SE, S, SW, W, and NW) relative to the position of the FRET dyes. We systematically removed each "cardinal" staple one at a time, or groups of three adjacent staples and examined the resulting stability of the structures (Figures 2.4A, S2.12-S2.23).

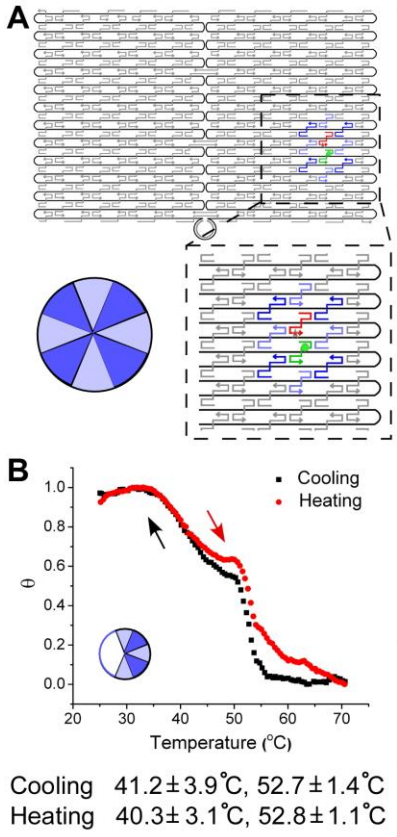

	Direction	Cooling T_f (°C)	Heating T_m (°C)
	North	53.7 ± 2.0, 58.5 ± 0.6	53.9 ± 1.9, 59.0 ± 0.6
	East	46.5 ± 6.6, 55.1 ± 2.3	44.0 ± 9.0, 55.4 ± 2.6
	South	51.1 ± 2.5, 58.3 ± 0.9	51.3 ± 2.8, 58.6 ± 1.0
	West	41.2 ± 3.9, 52.7 ± 1.4	40.3 ± 3.1, 52.8 ± 1.1
	N	57.6 ± 1.0	58.2 ± 1.2
	NE	56.7 ± 1.1	57.2 ± 1.5
	E	50.7 ± 2.2, 58.2 ± 0.8	50.8 ± 2.2, 58.4 ± 1.0
	SE	51.5 ± 2.1, 58.2 ± 0.8	51.6 ± 2.1, 58.5 ± 1.3
	S	57.7 ± 1.1	58.2 ± 1.2
	SW	56.8 ± 1.4	57.2 ± 1.5
	W	44.8 ± 4.7, 56.1 ± 1.3	42.0 ± 2.7, 56.1 ± 1.2
	NW	56.9 ± 1.2	57.2 ± 1.3

Figure 2.4 Systematic evaluation of local structural defects. (A) Spotlight on the FRET reporter dye position and the surrounding staples. Note that there are 8 staples in the first layer that encircle the dyes (shown in dark and light blue). The staples were selectively omitted one at a time or in clusters of three. In the table on the right, the pie chart depicts the omitted staple(s) position (white slices denote omitted staples). The cardinal direction of the omitted staples is also specified in the table. The remaining two columns in the table correspond to the assembly and melting transition temperatures, respectively. Multiple transitions are listed when applicable. (B) Sample data corresponding to omission of staple cluster W (three staples to the left of the FRET reporter dyes). Two clearly distinguishable transitions are observed in both the cooling and heating cycles.

Omitting staples N or S resulted in no change in the transition temperatures or shape of the transitions (Figures S2.16, S2.20 and data listed in the right table in Figure 2.4A), as compared to the reference structure. This result was expected as these staples are the most removed from the reporter site, bound to entirely different scaffold rows than the FRET dyes. Removing NE, NW or SW staples resulted in a ~ 1 ℃ drop in the transition temperatures (right table in Figure 2.4A and Figures S2.17, S2.23, S2.21). This

particular group of staples is designed to bind to the helical scaffold rows directly surrounding the FRET dyes. Defects in these locations may produce a small perturbation to the local thermal stability of the structure.

The result is more complicated when E, SE, and W staples were omitted (right table in Figure 2.4A and Figures S2.18, S2.19, S2.22). When E or SE staples were absent two transitions were observed: a small and narrow transition at the same temperature as the reference origami structure (58 ℃), and a more dominant, broader transition 6-7 degrees lower (~51-52 ℃). When staple W was omitted, the first transition was 2 degrees lower than the reference (~56 ℃), and the second transition occurred at a drastically lower temperature (~ 40 ℃). It is important to point out that these three staples bind directly to the same helical row as the FRET dyes. It is evident that a single staple omission at any of these positions directly impacts hybridization of the FRET modified strands to the scaffold, and that centrally located staples (relative to the overall structure) are very important in stabilizing the reporter site (as opposed to those close to the end of the helices).

Generally speaking, we anticipate that omitting a larger number of staples will lead to a more significant decrease in stability. For example, we expect that omitting three staples will be more destabilizing than a single defect. However, it is also important to understand the subtle effects of various defect patterns. For all four cases in which groups of three staples were omitted, two clear transitions were observed (results shown in the right table in Figure 2.4A, complete data set shown in Figures S2.12-S2.15). For example, omitting three staples on the N or S sides of the reporter dyes had a similar effect - a small and sharp transition at 58 ℃ and a large and slightly broader transition at

51 or 53 ℃, respectively, were observed. As shown in Figure 2.4B, omitting clusters of staples from the E and W sides of the reporter dyes resulted in much broader transitions that were skewed toward lower temperatures (50 ℃ and ~40 ℃ for the first and second transition, respectively). Overall, the results here reflect the same trends as were observed for single staple omission experiments.

2.5.6 Mechanism of assembly in 2D

By comparing the thermal curves corresponding to the donor only and fully-assembled donor-acceptor samples we were able to develop several hypothesis about the DNA origami assembly process. We theorize that the mechanism proposed in Figure 3D can be used to explain all the observations thus far. For example, consider the situation in which there are staple defects in the area immediately surrounding the reporter site. If one of the omitted staples is designed to bind to the same helical row as the dye-modified staples then the scaffold strand in the vicinity of the defect is expected to be quite flexible. We propose that during the assembly (cooling) process the dye-modified staples approach the scaffold and hybridize to the complementary domains in a stepwise manner. First, the 16 nt central domain of the staples will bind to the scaffold leaving the two 8 nt terminal domains freely dangling. Here, the FRET donor (fluorescein) is located in the longer central domain and the initial binding event will be reflected by the increase in fluorescence intensity of the donor only sample. Simultaneously, binding of the 16 nt domain of the FRET acceptor (TAMRA) modified staple will be echoed by a slight increase in FRET efficiency as the dyes are brought closer together than when they are freely diffusing in solution. As the temperature of the sample is gradually reduced, the flexibility and dynamics of the unbound portions of the scaffold are also reduced,

facilitating binding of the remaining 8 nt domains of the dye-modified staples. Finally, the formation of crossovers between neighboring helices fixes the structure, bringing the FRET dyes together for efficient energy transfer. Because the FRET acceptor is located in an 8 nt domain of the corresponding staple, this binding event will be reflected by maximum energy transfer between dyes. In summary, we propose that the first observed transitions reflect binding of longer staple domains while the second transitions at lower temperatures reflect binding of shorter staple domains. Melting of the assembled structures occurs in a similar manner, with the 8 nt domains of the staples dissociating from the scaffold first, followed by the 16 nt domain at higher temperatures. The presence of multiple transitions for various structures is also explained by a similar mechanism.

Based on this simplified representation of DNA origami assembly and disassembly processes we expect to observe a single transition in the donor-only samples, as the dye modification is within the longer staple domain that should bind to the scaffold in a single step. However, there were several cases in which multiple transitions were observed. In a few cases (i.e. Figure S2.19-S2.20) two distinct transitions that coincided with those seen in the fully-assembled donor-acceptor sample were observed. In all of these situations selected staples directly adjacent to the donor modified staple were omitted (i.e. cluster S, W, E, or SE).

The appearance of multiple transitions in the donor only data can be partially explained by the quenching effect of ssDNA on the fluorescence of fluorescein. During the assembly phase, the 16 nt domain of the donor modified staple binds to the scaffold forming a double helix. This event releases the dye of its interaction with neighboring

single stranded DNA bases which reduces the quenching of the donor's fluorescence and therefore increases the emission of the donor. However, when there is other single stranded DNA present (either from unpaired sections of the scaffold or dangling domains of other partially bound staples), it also has an opportunity to interact with the donor and partially quench its fluorescence. The emission of the donor may undergo a second increase when the dangling domains finally associate with the scaffold and release the dye from any remaining interactions. We also observed three transitions in the donor only data corresponding to omission of staple cluster S, which is likely the result of similar events.

Interestingly, if the helical rows that the donor modified staple is bound to are completely surrounded by staples (no omissions) then the second transition was not observed. In those cases binding of the 16 nt domain was not distinguishable from the shorter 8 nt domains. For example, the sample in which cluster N was omitted displayed a single transition at ~58 ℃ in the donor-only sample (Figure S2.13). Meanwhile, a second transition at ~53 ℃ was observed for the fully-assembled donor-acceptor sample. The second transition is likely due to step-wise binding of the acceptor dye-modified staple rather than the donor modified staple.

2.5.7 Heterogeneity of assembly

In all the previously described experiments the dye-modified staples reflected the status of a small area (position 1) in the lower right quadrant of the rectangular structure. To determine if the assembly of the 2D DNA origami rectangle occurs homogeneously across the structure, we also examined several other reporter dye positions (Figure 2.5). We positioned the dyes along the seam between the two domains of the rectangle

(position 2) and also in the center of the left side (position 3). We examined fully-assembled structures as references, and also simulated several defect states, including the half structure, ring-hole, small-hole, and big-hole defects.

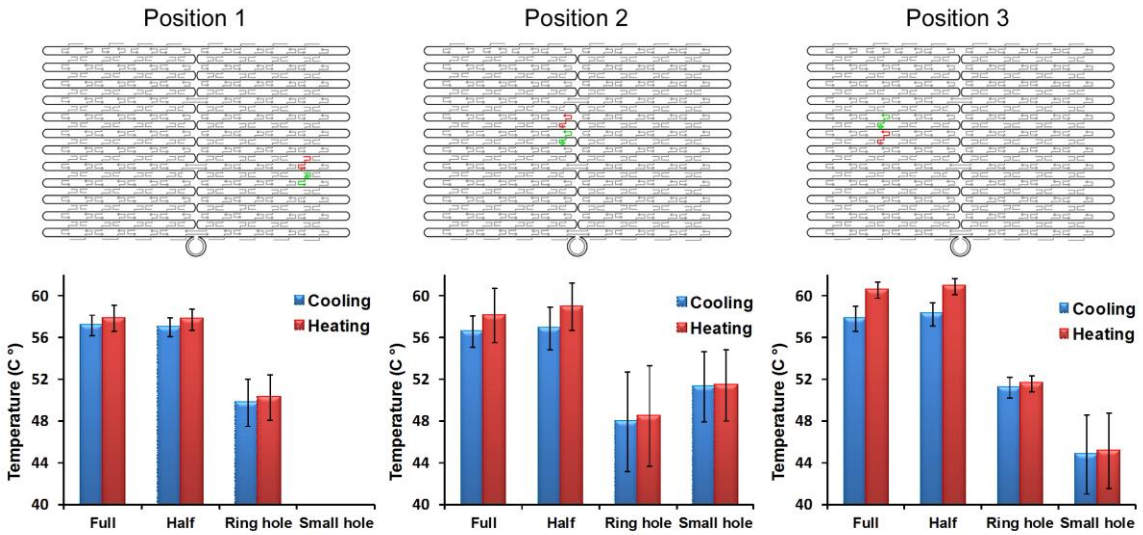

Figure 2.5 Evaluating the homogeneity of assembly across a 2D rectangular structure. The upper panels show the three different areas that were examined, as indicated by the presence of FRET reporter dyes (shown in green and red). Position 1 is close to the edge in the lower right quadrant (same design as previous study); position 2 is located along the seam created by the scaffold folding path; and position 3 is in the approximate center of the left side of the structure. The lower panels present the transition temperatures corresponding to all the designs investigated (including the reference structure, half origami, ring-hole and small-hole structures) at each position. All results corresponding to the big and small hole structures at position 1 are not presented since they cannot be reliably fit. For those designs that displayed multiple transitions, only the higher temperature one is shown. The error bars represents the transition widths and the standard deviation of the measurements is much smaller than the transition width. The data is also listed in Table S2.7.

The thermal curves corresponding to the fully-assembled structures show that position 3 (Figure S2.30) exhibits the highest T_m (~61 ℃), approximately 2.7 ℃ higher than position 1 (Figure S2.4) and 2.4 ℃ higher than position 2 (Figure S2.25). These results indicate that staples are more easily dissociated from terminal helical positions,

rather than interior ones (the seam connects two independent halves, each with helical termini). Thus, melting is likely to be initiated from the far left and right helical ends and on both sides of the seam. The T_m transition is narrowest at position 3 and broadest at position 2. From this we can speculate that dissociation of staples from the outside layers of the scaffold will cause the M13 in these areas to become progressively more flexible and promote dissociation of the interior staples.

Interestingly, the T_f of the three reference structures differs by less than ~1 ℃ (position 3 > position 1 > position 2). Similar to the melting data, the T_f transition is also slightly broader at the seam. Taken together, these results suggest that there exists some form of structural stress along the seam that causes binding to occur more slowly and at a slightly lower temperature than at the other positions. A comparison of the raw cooling data for the three positions shows that the difference between the donor-only and the fully-assembled donor-acceptor samples is the smallest at the most shielded position (position 3) while the largest at the seam (position 2). The results indicate that either the assembly yield or the stability of the dye labeled staples is lowest at the seam.

The transition temperatures of the position 2 and 3 labeled half origami structures reflect a similar trend as position 1, with less than 1 ℃ difference between the fully and half assembled structures (Figure S2.26, S2.31). This further supports the notion that each side of the rectangular DNA origami structure is independent of the other.

The thermal transitions corresponding to the ring-hole and small-hole defects at position 3 occur at lower temperatures than at positions 2 and 1 (Figure S2.32-S2.34, S2.27-S2.29), when the transitions were reliably fit. This suggests that insulated reporter positions are more sensitive to local structural changes than more accessible ones. Here,

the slightly enhanced stability of the region depends on the presence of all the surrounding staples to fix the DNA helices in place. Apparently inducing defects along the edges is less likely to cause damage to the structural integrity of the area than in more centrally located positions.

2.5.8 Assembly in 3D

Our study already demonstrated the extremely reversible and highly cooperative nature of the assembly/disassembly process for 2D DNA origami structures. However, assembling a 3D origami structure, a cuboid for example, not only involves a much more complicated scaffold folding path, but also a far more elaborate staple pattern. Many of the staples in 3D structures weave back and forth and bridge more distant helices than in 2D structures. The efficient formation of 3D structures requires more rigorous cooperation among the staples, which is experimentally achieved by annealing for longer times with slower temperature ramps and higher salt concentrations.

We were most interested in monitoring the assembly and disassembly phases at the molecular level. To achieve this we examined four different reporter dye positions within a cuboid structure, reflecting various levels of insulation by other structural elements (Figure 2.6A). The staples along the length of the cuboid structure are separated into 14 layers (x direction) that are numbered from 1 to 14 (left to right) as shown in Figure 1C. There are 8 helices in the y and z directions, numbered from 1 to 8 from back to front and from top to bottom. The coordinates of the FRET dyes at each position are: (2,6,1)-(2,4,1); (3,4,1)-(4,3,1); (6,8,3)-(6,8,5); and (7,4,4)-(6,4,5); respectively, as shown in Figure 6A. The reporter dyes at the first position are fully exposed to solution at the boundary between the top and side faces of the structure. The dyes at the second and third

positions are slightly less accessible on the top and front face, respectively. The dyes at the last position are buried inside the structure when it is fully assembled (Figure 2.6A).

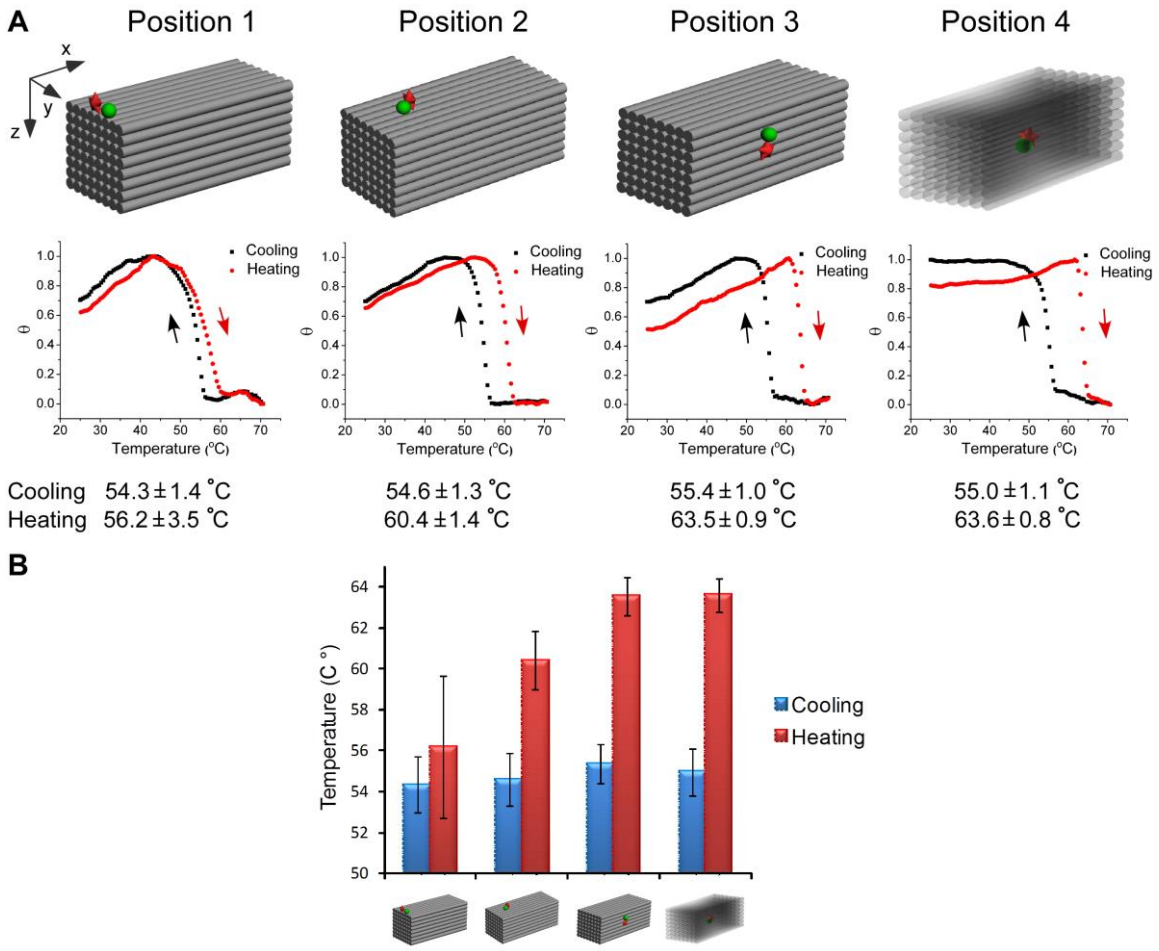

Figure 2.6 Evaluating the assembly of a 3D cuboid structure. (A) The upper panels show the four different areas of the cuboid that were examined, as indicated by the presence of FRET reporter dyes (shown in green and red). The lower panels present the corresponding thermal transitions during the cooling (black) and heating phases (red). (B) A plot summarizing the transition temperatures of the four positions. The error bars represent the widths of the transitions. No significant difference in T_f was observed among the positions. The T_m was dramatically higher for those positions farthest from the end of the helices.

The T_f (cooling) corresponding to the four positions vary by only one degree, ranging from 54.3 to 55.4 ℃ with the more interior positions exhibiting noticeably

sharper transitions than the exterior ones. The results suggest that the assembly of 3D origami occurs uniformly across the structure. We surmise that the structure is relatively loose and unstable at temperatures above T_f, and forms rapidly at and below the transition temperature in a highly cooperative process of staple hybridization.

However, the T_m (heating) corresponding to the four positions vary widely (Figure 2.6B). The lowest T_m (56.2 ℃) was observed at position 1, indicating that dissociation of the most accessible staples occurs first. The T_m corresponding to position 2, a less exposed position, is four degrees higher (60.4 ℃). Positions 3 and 4, farthest from the ends of the helices, exhibited melting temperatures approximately seven degrees higher (63.5 ℃ and 63.6 ℃, respectively), than position 1. Thus, it is apparent that dissociation proceeds gradually from the staples closest to the termini of the helices to the innermost positions. The transition curves corresponding to the inner positions are sharper than those of the outer ones, indicating that the outer staples are not as stable and dissociate more slowly. Note that there is no significant difference in T_m when the reporter dyes are located on staples with the same x-coordinate, regardless of whether or not they are on the surface of the structure or buried in the interior (position 3 vs position 4). Careful examination of the staple binding patterns reveals that the staples with different x-coordinates do not interact with one another, while those with the same coordinate participate in crossovers with four to five neighboring helices. This arrangement of staples makes it less likely that melting will proceed in the direction perpendicular to the helical axis.

2.6 Conclusion

In this study we used a FRET based method to probe the structural integrity and association/dissociation of DNA origami at the molecular level, unlike other strategies that evaluate average global behavior. The sensitivity and precision of our method allowed us to investigate the influence of scaffold to staple ratios, and the presence or absence of staples close to and far from selected reporter sites, on the stability of 2D and 3D structures. We also examined the homogeneity of staple hybridization across entire structures. We observed that the folding and unfolding of 2D structures is very consistent in different areas of the same structure, with evidence of rapid and cooperative staple hybridization. Weak positional effects were observed; more interior positions were more stable, and also more sensitive to local structural defects, than those along the edges and seam. Assembly and disassembly of structures in 3D was not as consistent, with staples at the most accessible positions melting gradually first, followed by rapid dissociation of inner layer staples.

The results draw attention to the importance of scaffold folding paths and staple binding patterns in the thermal stability of origami structures, with a sharp difference in stability observed for unique structural arrangements. This information can be used to guide and optimize the rational design of scaffold folding paths and staple arrangements in more complex DNA nanostructures for high yield and stability.

In addition, the detailed melting behavior that is accessible by our method can be used to tailor annealing protocols for shorter, more efficient assembly conditions. Current annealing protocols often involve heating DNA mixtures to very high temperatures and cooling to room temperature over long periods of time. The results here

suggest that it may not be necessary to heat the mixtures to such a high temperature initially, which could be important to DNA systems that involve other more fragile molecules such as folded proteins. Sobczak et al. have already demonstrated the ability to optimize annealing protocols for origami structures by considering temperature.[14] Further studies of the local and global thermal behavior of DNA origami and other DNA nanostructures will facilitate optimization of assembly temperatures and times. Overall, the information gathered from this study can lead to more stable DNA structures with significantly enhanced integrity.

Improving the stability and integrity of DNA origami will allow researchers to effectively modify and functionalize the underlying nanostructures. Understand how to efficiently and accurately fold and disassemble DNA nanostructures will, ultimately improve our ability to manipulate and control such systems.[29-33] This may lead to broader application of the technology.

2.7 References

(1) Pinheiro, A. V.; Han, D.; Shih, W. M.; Yan, H. *Nat. Nanotechnol.* **2011**, *6*, 763.

(2) Nangreave, J.; Han, D.; Liu, Y.; Yan, H. *Curr. Opin. Chem. Biol.* **2010**, *14*, 608.

(3) Seeman, N. C. *Mol. Biotechnol.* **2007**, *37*, 246.

(4) Rothemund, P. W. *Nature* **2006**, *440*, 297.

(5) Dietz, H.; Douglas, S. M.; Shih, W. M. *Science* **2009**, 325, 725.

(6) Douglas, S. M.; Dietz, H.; Liedl, T.; Hogberg, B.; Graf, F.; Shih, W. M. *Nature* **2009**, 459, 414.

(7) Gu, H.; Chao, J.; Xiao, S. J.; Seeman, N. C. *Nat. Nanotechnol.* **2009**, *4*, 245.

(8) Seeman, N. C. *Annu. Rev. Biochem.* **2010**, *79*, 65.

(9) Castro, C. E.; Kilchherr, F.; Kim, D. N.; Shiao, E. L.; Wauer, T.; Wortmann, P.; Bathe, M.; Dietz, H. *Nat. Methods* **2011**, *8*, 221.

(10) Sobey, T. L.; Renner, S.; Simmel, F. C. *J. Phys. Condens. Matter* **2009**, *21*, 034112.

(11) Rajendran, A.; Endo, M.; Katsuda, Y.; Hidaka, K.; Sugiyama, H. *J. Am. Chem. Soc.* **2011**, *133*, 14488.

(12) Mergny, J. L.; Lacroix, L. *Oligonucleotides* **2003**, *13*, 515.

(13) Song, J.; Arbona, J. M.; Zhang, Z.; Liu, L.; Xie, E.; Elezgaray, J.; Aime, J. P.; Gothelf, K. V.; Besenbacher, F.; Dong, M. *J. Am. Chem. Soc.* **2012**, *134*, 9844.

(14) Sobczak, J. P. J.; Martin, T. G.; Gerling, T.; Dietz, H. *Science* **2012**, *338*, 1458.

(15) Forster, T. *Discuss. Faraday Soc.* **1959**, 7.

(16) Lilley, D. M. J.; Wilson, T. J. *Curr. Opin. Chem. Biol.* **2000**, *4*, 507.

(17) Liedl, T.; Simmel, F. C. *Anal. Chem.* **2007**, *79*, 5212.

(18) Stein, I. H.; Schuller, V.; Bohm, P.; Tinnefeld, P.; Liedl, T. *Chem. Phys. Chem.* **2011**, 12, 689.

(19) Sacca, B.; Meyer, R.; Feldkamp, U.; Schroeder, H.; Niemeyer, C. M. *Angew. Chem. Int. Ed.* **2008**, *47*, 2135.

(20) Sacca, B.; Meyer, R.; Niemeyer, C. M. *Nat. Protoc.* **2009**, *4*, 271.

(21) Nangreave, J.; Yan, H.; Liu, Y. *Biophys. J.* **2009**, *97*, 563.

(22) Nangreave, J.; Yan, H.; Liu, Y. *J. Am. Chem. Soc.* **2011**, *133*, 4490.

(23) Dacres, H.; Wang, J.; Dumancic, M. M.; Trowell, S. C. *Anal. Chem.* **2010**, *82*, 432.

(24) Ke, Y.; Douglas, S. M.; Liu, M.; Sharma, J.; Cheng, A.; Leung, A.; Liu, Y.; Shih, W. M.; Yan, H. *J. Am. Chem. Soc.* **2009**, *131*, 15903.

(25) Bowen, E. J.; Sahu, J. *J. Phys. Chem.* **1959**, *63*, 4.

(26) You, Y.; Tataurov, A. V.; Owczarzy, R. *Biopolymers* **2011**, *95*, 472.

(27) Sjoback, R.; Nygren, J.; Kubista, M. *Biopolymers* **1998**, *46*, 445.

(28) Pinheiro, A. V.; Nangreave, J.; Jiang, S.; Yan, H.; Liu, Y. *ACS Nano.* **2012**, *6*, 5521.

(29) Deng, Z.; Samanta, A.; Nangreave, J.; Yan, H.; Liu, Y. *J. Am. Chem. Soc.* **2012**, 134, 17424.

(30) Ding, B.; Wu, H.; Xu, W.; Zhao, Z.; Liu, Y.; Yu, H.; Yan, H. *Nano letters* **2010**.

(31) Pal, S.; Deng, Z.; Ding, B.; Yan, H.; Liu, Y. *Angew. Chem. Int. Ed.* **2010**, 49, 2700.

(32) Bell, N. A.; Engst, C. R.; Ablay, M.; Divitini, G.; Ducati, C.; Liedl, T.; Keyser, U. F. *Nano letters* **2012**, 12, 512.

(33) Douglas, S. M.; Bachelet, I.; Church, G. M. *Science* **2012**, 335, 831.

Chapter 3

INTEGRATION, STABILIZATION AND SEPARATION OF DNA NANOSTRUCTURES FROM CELLS/CELL LYSATE

Adapted with permission from Mei, Q.; Wei, X.; Su, F.; Liu, Y.; Youngbull, C.; Johnson, R.; Lindsay, S.; Yan, H.; Meldrum, D. Stability of DNA Origami Nanoarrays in Cell Lysate. *Nano Lett.* **2011**, 4, 1477-1482.

3.1 Abstract

We assembled several tiles and DNA origami nanostructures of differing shape, size and probes, and investigated their interaction with cells and lysate obtained from various normal and cancerous cell lines. We first investigated the size-dependent integration of DNA structures in cells by confocal microscope. Then we separated and analyzed the origami−lysate mixtures using agarose gel electrophoresis and recovered the DNA structures for functional assay and subsequent microscopic examination. Our results demonstrate that DNA origami nanostructures are stable in cell lysate and can be easily separated from lysate mixtures, in contrast to natural, single- and double-stranded DNA. Atomic force microscope (AFM) and transmission electron microscope (TEM) images show that the DNA origami structures are fully intact after separation from cell lysate and hybridize to their targets, verifying the superior structural integrity and functionality of self-assembled DNA origami nanostructures relative to conventional oligonucleotides. The stability and functionality of DNA origami structures in cell lysate validate their use for biological applications, for example, as programmable molecular rafts or disease detection platforms.

3.2 Introduction

Scaffolded DNA origami is a relatively new technique that uses hundreds of short "staple" DNA oligonucleotides to direct the folding of a single-stranded DNA scaffold, typically the 7249 nucleotide (nt) long M13 viral DNA genome, into a predefined structure.[1-3] This is an attractive method to construct nanoscale objects because of the ease and convenience of design, low production cost, high assembly yield, and unparalled addressability of the resulting origami structures. Many 2D[1] and 3D nanoarchitectures[4-8] assembled by this technique have been used to pattern various materials, serve as nanoscale rulers for single molecule imaging,[9] act as platforms for molecular robotics,[10] and observe single molecule chemical reactions.[11] In addition to these purposes, the distinctive properties of DNA origami structures make them particularly interesting for potential biological applications. The size of DNA origami nanostructures, the existence of well developed chemistries and enzymatic methods to modify their nucleotides and functionalities, and their biocompatibility permit their use in cellular studies. DNA origami has already been used as an addressable support to place proteins at precise positions and intermolecular distances,[12-14] and for label-free detection of RNA hybridization, which suggests a potential to assay for gene expression at the single molecule level.[15] Most recently, Seeman and co-workers[16] developed an elegant strategy to use DNA origami as a molecular chip to detect single nucleotide polymorphism (SNP), further demonstrating the potential of DNA nanostructures for biological applications. With the developments in high-speed atomic force microscopy (AFM)[17,18] and super-

resolution fluorescence imaging,[19] DNA origami nanostructures are more readily characterized, further encouraging their utilization in single cell studies.

Though significant progress has been made over the past several decades in single cell proteomic analysis, most new methods are performed as end point analyses and provide only a snapshot of cell status. These problems are exacerbated by the low abundance of rare proteins and disease markers, whose presence is often difficult, if not impossible, to detect. With DNA origami, it may be possible to develop a platform that can be used for single, live cell analysis, with sufficient sensitivity to provide an accurate picture of intracellular dynamics. Microfluidic technologies for mixing[20-23] in situ cell lysis[24-29] and subsequent electrophoretic separation[30-33] of cellular components have recently been developed by several research groups. It is our goal to apply the latest technologies to construct a microfluidic device consisting of a mixing chamber, lysis chamber, and electrophoretic channel to analyze cell-integrated, DNA origami platforms for cellular analysis. However, before DNA origami can be used to probe real-time cellular behavior, or as a disease detection or diagnosis tool, several issues must be addressed. For example, it is well-known that oligonucleotides may be unstable and easily degraded in cellular environments.[34, 35] Therefore, it is critical to establish the stability of DNA origami structures in intra- and extracellular environments and determine whether or not they can be separated intact from cell lysate.

Here we investigated the stability of a series of DNA origami structures in cell lysates from a number of normal and cancerous cell lines and their ability to be separated from the cell lysate mixtures (Figure 3.1). The concentration of cells used to prepare the lysate (and therefore the amount of enzymes and other cellular material) was varied,

along with DNA structure/lysate incubation time and temperature to determine if the DNA origami structures were stable under a wide variety of conditions. Several well-studied, 2D and 3D DNA origami nanostructures were assembled and purified following published methods.[1, 7] Cell lysate was prepared by mixing cells with mammalian cell lysis buffer (50 mM Tris-HCl, 150 mM NaCl, 0.1% SDS, 0.5% deoxycholic acid and protease inhibitor), followed by centrifugation to remove nuclear DNA and cell membrane debris. After the purified DNA origami structures were incubated with cell lysate, separation was performed by nondenaturing agarose gel electrophoresis. The morphological integrity of the structures was verified by direct visualization with AFM and transmission electron microscopy (TEM).

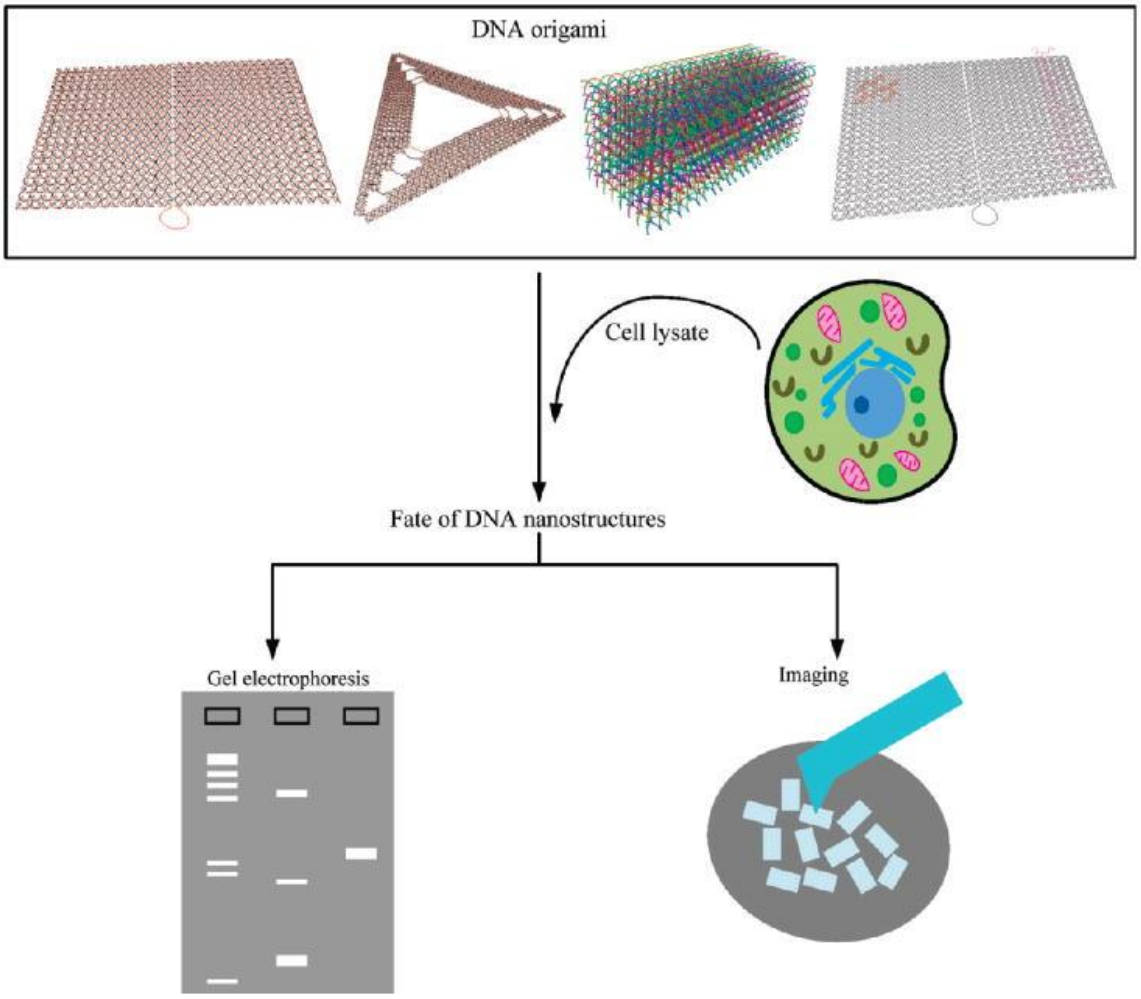

Figure 3.1 Investigating the fate of DNA nanostructures in cell lysate. (Adapted with permission from Stability of DNA Origami Nanoarrays in Cell Lysate. *Nano Lett.* **2011**, 4, 1477-1482. Copyright 2011 American Chemical Society.)

3.3 Materials and Methods

3.3.1 Reagents and Materials

The mammalian cell lysis kit, phosphate buffered saline (PBS), hydrocortisone, insulin, cholera toxin and calcium chloride were obtained from Sigma-Aldrich (Saint Louis, MI). M13mp18 single-stranded DNA and Lambda DNA were purchased from New England Biolabs Inc (Ipswich, MA). All of the DNA helper strands were

synthesized by Integrated DNA Technologies (Coralville, IA) and normalized to 100 μM in 96 well plates without further purification. Synthetic β-actin RNA was also purchased from IDT and purified by RNase-free HPLC in factory. Total RNA isolation kit, RNase-free DNase, and RNA fragmentation reagent were obtained from Ambion (Austin, TX). Dulbecco's Modified Eagle's Medium (DMEM), DMEM: F12 medium, keratinocyte serum-free medium, horse serum, human recombinant Epidermal Growth Factor (hrEGF), fetal bovine serum (FBS), penicillin/streptomysin solution, Bovine Pituitary Extract (BPE), trypsin, agarose and SYBR Green I were purchased from Invitrogen (Carlsbad, CA).

3.3.2 Assembly of DNA Origami

M13 viral ssDNA (10 nM or 20 nM) was mixed with the corresponding set of helper strands at a molar ratio of 1:5 or 1:10 in 1 x TAE/Mg buffer containing 100 mM Tris, 50 mM acetic acid, 5 mM EDTA and 12.5 mM magnesium acetate (pH 8.0) to form the 2D rectangular, 2D triangular, or 3D cuboid origami, respectively. The origami samples were annealed and assembled in an Eppendorf thermocycler (Hauppauge, NY) from 94 ℃ to room temperature over 12 h or 24 h for the 2D or 3D origami. Excess helper strands were removed using Microcon centrifuge filters YM-100 (Millipore, Bedford, MA).

3.3.3 Cell Lines

CP-A cells (metaplastic human esophageal epithelial cell line) were kindly provided by Dr. Brian J. Reid at the Fred Hutchison Cancer Research Center. MCF-10A (non-tumorigenic mammary epithelial cell line) and MDA-MB-231 cells (metastatic breast

cancer cell line) were provided by Dr. Thea Tlsty, University of California, San Francisco. HeLa (human cervical cancer cell line) and End1/E6E7 (normal endocervical epithelial cell line) were purchased from American Type Culture Collection (ATCC, Manassas, VA).

3.3.4 Cell Cultures

CP-A cells were cultured in keratinocyte serum-free medium supplemented with BPE and hrEGF. End1/E6E7 cells were grown in the same medium for CP-A cells plus calcium chloride (0.013 g/L). HeLa and MDA-MB-231 cells were cultured in DMEM medium supplemented with 10% FBS and 100 unit/mL penicillin: 100 μg/mL streptomycin solutions. MCF-10A cells were cultured in DMEM: F12 medium supplemented with 5% horse serum, 0.5 μg/mL hydrocortisone, 20 ng/mL hrEGF, 10 μg/mL insulin, 100ng/mL cholera toxin and 100 unit/mL penicillin: 100 μg/mL streptomycin solutions. All the cells were cultured in 25 or 75 cm2 flasks to ~ 80% confluency and incubated at 37 ℃ under 5% CO2 atmosphere.

3.3.5 Cell Lysis

The lysis solution contains 50 mM Tris-HCl, 150 mM NaCl, 0.1% SDS, 0.5% deoxycholic acid and protease inhibitor at the ratio of 1:100. Cells were washed with PBS and detached from the flask with 0.05% trypsin for CP-A, MDA-MB-231 and MCF-10A cells and with 0.25% trypsin for HeLa and End1/E6E7 cells. After trypsin treatment, cells were centrifuged at 900 rpm for 3 minutes and resuspended in 1mL of 1X PBS. Cells

(106) were lysed in 500 uL of the lysis solution and incubated on ice for 20 min on a shaker. The lysates were then centrifuged at 17000 x g at 4 ℃ for 30 min. Finally, the supernatant was removed and stored on ice or -20 ℃ for the following steps.

3.3.6 Separation of Rectangular Origami from CP-A Cell Lysates

Purified rectangular DNA origami was mixed with various concentrations of CP-A cell lysate for 1 h and 12 h on a shaker. The stability of origami was first verified by gel electrophoresis. 1% agarose slab gel containing SYBR Green I dye was prepared in 1X TAE/Mg buffer, and then immersed in the same buffer. The origami-cell lysate mixture was loaded in the gel sample wells, followed by electrophoresis for 2 h at 80 V. After electrophoresis, the gel was rinsed and imaged with a Gel Doc XR system (Bio-Rad, Hercules, CA). The band intensity was measured using Image J (National Institutes of Health, http://rsb.info.nih.gov/ij). The migration bands corresponding to assembled origami were excised from the gel for AFM imaging. Gel bands were crushed and transferred into DNA gel extraction spin column (Bio-Rad). DNA origami was recovered by centrifuging the column for 5 minutes at 13000 g.

3.3.7 Mixing Triangular and 3D Cuboid Origami with Cell Lysates

Purified triangular and 3D cuboid origami were mixed with CP-A cell lysates at room temperature for 1 h and 12 h, respectively. The sample mixtures were analyzed by agarose gel electrophoresis. The origami bands were subsequently excised from the gel and recovered. The structural integrity of the triangular and 3D cuboid origami was confirmed by AFM and TEM imaging, respectively.

3.3.8 Separation of Rectangular Origami, M13 ssDNA and λ DNA from Cell Lysates

10 nM of rectangular origami and M13 viral ssDNA and 100 nM λ DNA were added to CP-A cell lysates (5,000 or 10,000 cells) at room temperature for 1 h and 12 h respectively. Agarose gel electrophoresis was used to separate them from the cell lysate components to determine their stability (Figure 3.4 in the main text). In addition, these three DNA samples were mixed with other cell lysates, including HeLa, End1/E6E7, MDA-MB-231 and MCF-10A. The mixtures were loaded into agarose slab gels followed by electrophoresis. The gel images of three DNA structures after incubation with the various cell lysates are shown in Figure S3.2. The results show that only DNA origami can be separated from the cell lysate in all cell lines. λ DNA showed a strong interaction with all types of cell lysate, nonspecifically shifting the bands into the gel loading wells, while the ssDNA smeared and displayed some degree of random degradation.

Preparation of Total Cellular RNA. Total RNA was extracted from HeLa cell lines and prepared by total RNA isolation kit, according to the manufacturer's instructions. Genomic DNA was removed by treating samples with RNase-free DNase. The purified RNA was kept at -80 ℃ for future use or fragmentized using RNA fragmentation reagent.

3.3.9 AFM Imaging

The rectangular and triangular origami extracted from the gel (2 μL) was deposited onto a freshly cleaved mica (Ted Pella) and left to adsorb for 2 minutes. 1 X TAE/Mg buffer (30 μL) was added to the AFM liquid cell, and the samples were scanned in

tapping mode under fluid on an AFM (Digital Instruments, Veeco, Bruker, Santa Barbara, CA) with SNL-tips (Veeco).

3.3.10 TEM Imaging

The TEM sample was prepared by dropping 2 μL of 3D origami sample solution on carbon-coated grid (400 mesh, Ted Pella). Before depositing the sample, the grids were negatively glow discharged using Emitech K100X machine. After 45 seconds, the sample was wicked from the grid by filter paper. The grid was then washed with a drop of water to remove excess salt. A drop of 0.7 % uranyl formate solution was added to the grid, and excess solution was again wicked away with filter paper. The grid was treated with a second drop of uranyl formate solution for 15 seconds, and the excess solution wicked away. The grid was evaporated to dryness at room temperature. Low resolution TEM studies were carried out by using a Philips CM12 transmission electron microscope, operated at 80 kV in the bright field mode.

3.3.11 Confocal microscope imaging

The CPA cells were cultured on 96-well plate. DNA structures were mixed with cell medium at 1:3 ratio and incubated with cells without any treatment. After 4 hours or overnight, the plate was imaged by confocal microscope with live cell incubator setting. Excitation of 488 nm and emission peak of 512 nm is the channel for detecting donor dye on structure, while excitation of 488 nm and emission peak of 580 nm is the channel for detecting acceptor dye by FRET. Transparent channel was used to observe cells and

overlap of all channels were able to indicate the distribution of structures inside cells.

3.4 Results and discussion

3.4.1 Integration of DNA nanostructures and size-dependent distribution

To investigate the potential applications of DNA nanostructures as scaffold with multifunction towards live cells, a series of DNA nanostructures in different sizes and shapes are designed for cellular uptake purpose. The rational designs (Figure 3.2A, B) include a wide range of small rectangular tiles (from 2 nm × 17 nm to 21 nm × 17 nm) as well as a large rectangular origami array (60 nm × 90 nm). Selected oligonucleotides were covalently linked with a pair of fluorescence resonance energy transfer (FRET) dyes, which were used to indicate the intracellular integrity of the DNA arrays. After incubated with pre-cancerous human esophageal squamous epithelial cells (CPA), confocal microscope images are taken subsequently.

Interestingly, the cellular localization of various DNA nanostructures are size-dependent: small tiles always passed through the nuclear membrane and distributed inside the nucleus, while the large origami array only presented in the cytoplasm. (Figure 3.2C, D) Furthermore, after a long period of incubation, the change of the FRET signal intensity indicate the stability of the arrays of different size: instability of small tiles could be observed in the nucleus, while large origami remained stable for up to 4 days of incubation.

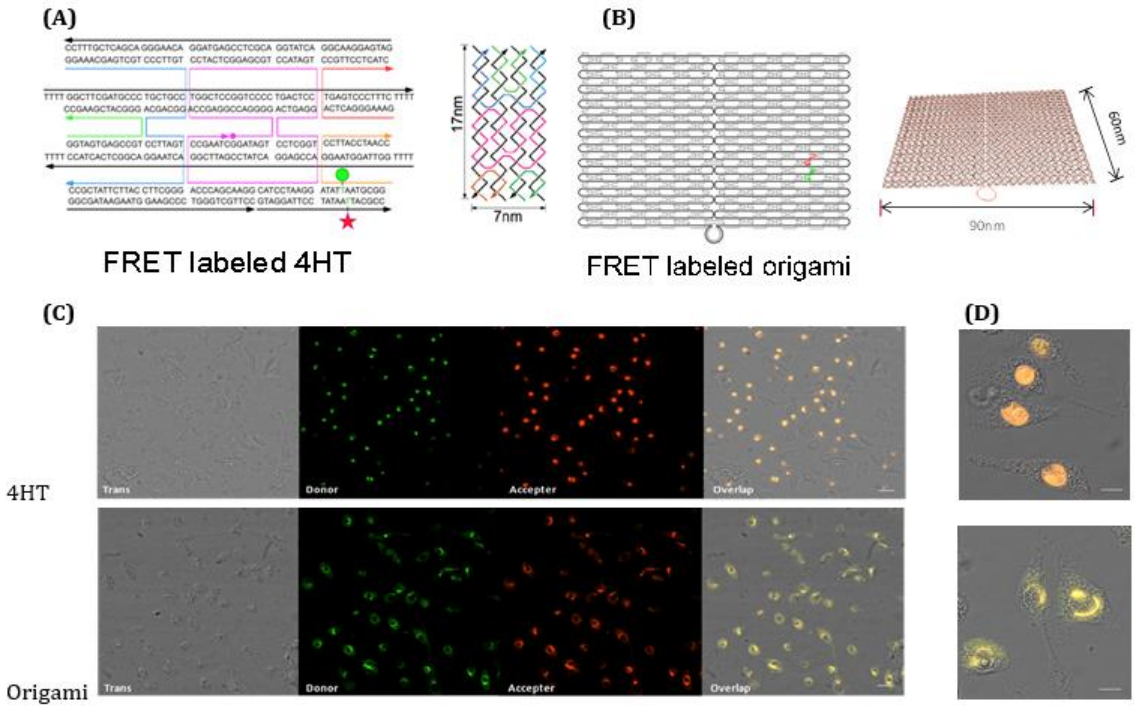

Figure 3.2 Schematic design of DNA nanostructures and size-dependent cellular uptake and distribution. (A) Design of small four helix tile structure (4HT) with FRET dye modifications. (B) Design of large origami with FRET dye modifications. (C) Confocal microscope images of cells with different DNA structures. Each individual structure was incubated with CP-A cells for 4 hours and confocal Images were subsequently collected. The green channel and red channel are selected from the emission peak of donor and acceptor dyes, according to the cell spectra. The varying color indicates different FRET efficiencies resulting from the different distances between FRET pairs. (D) For each structure, the zoom in confocal images are provided for detail information. The scale bar is 25 μm while 10 μm in zoom in images.

3.4.2 Origami stability in and separability from cell lysate

First, the stability of the same 2D, rectangular origami (90 nm × 60 nm) that was reported for label-free detection of RNA hybridization[15] was investigated. The rectangular origami was added to CP-A cell lysate (metaplastic human esophageal epithelial cell line[36]) prepared from different numbers of cells (5000 or 10000) and was

subsequently incubated for 1 or 12 h at 4 ℃ or room temperature, respectively. Native gel analysis of each reaction mixture is shown in Figure 3.3a. For each gel, lane 1 contains a 1000 bp DNA ladder, used as a marker to identify the molecular size of each band, while lanes 2 and 3 and 6 and 7 contain the DNA origami/cell lysate mixtures corresponding to the various conditions. Lane 4 contains a DNA origami sample (not mixed with cell lysate), used as a positive control to illustrate the mobility of a fully formed structure, while lane 5 contains a sample of cell lysate only, as a negative control. In lanes 2, 3, 6, and 7, the presence of a band with the same mobility as the DNA origami control in lane 4 confirms that the DNA origami structures are stable in each of the conditions and can be successfully separated from cell lysate mixtures.

The relative intensity of each band was quantified using ImageJ, and the concentration of DNA origami structures in the bands separated from the cell lysate was estimated by comparison to the intensity of the band of the positive control (Figure 3.3b). No significant differences were observed for the various conditions. It should be noted that the intensities of the origami bands from the 25 ℃ reactions were approximately 98% of those from the 4 ℃ reactions. This result suggests that the DNA origami–cell lysate mixtures are stable at room temperature, obviating the requirement for any cooling device in the future design of a microfluidic chip.

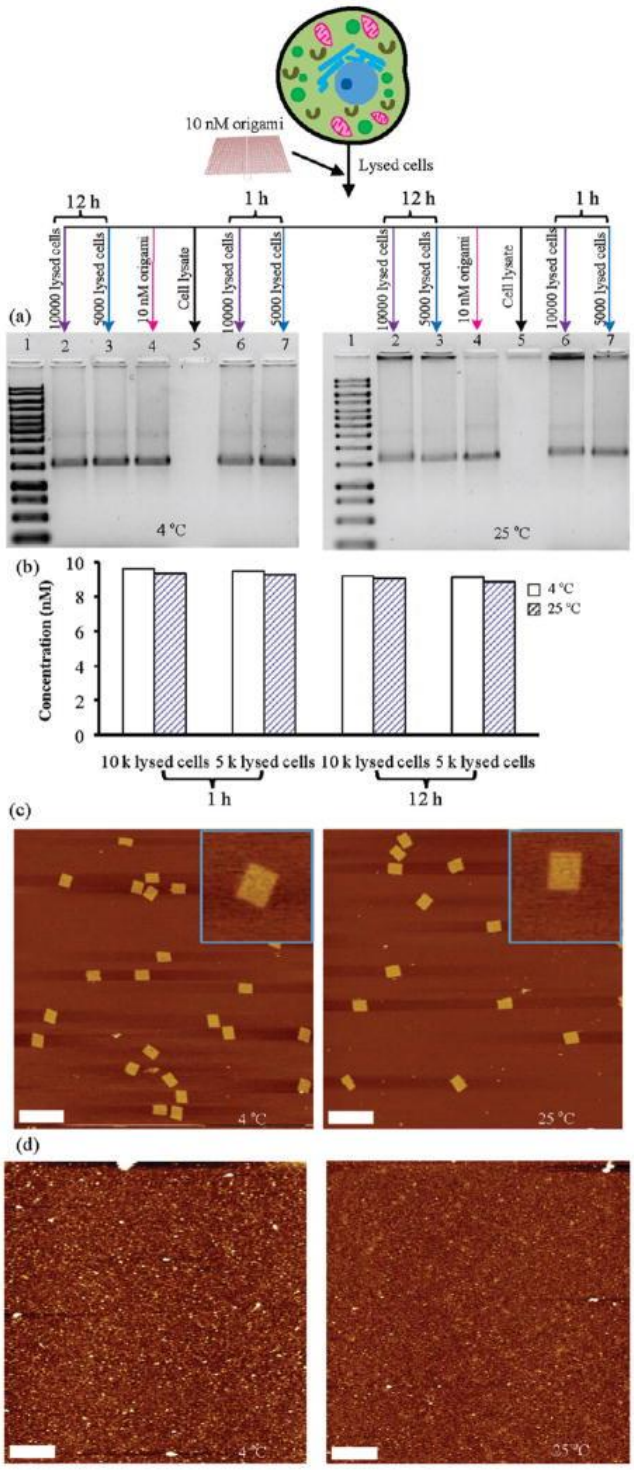

Figure 3.3 Analysis of rectangular DNA origami stability in, and separability from, CP-A cell lysate. (a) Agarose gels separate origami after incubation at 4 and 25 ℃: lane 1, 1000 bp DNA ladder; lane 2, 10000 lysed cells with origami incubated for 12 h; lane 3, 5000 lysed cells with origami incubated for 12 h; lane 4, 10 nM origami; lane 5, cell

lysate only; lane 6, 10000 lysed cells with origami incubated for 1 h; lane 7, 5000 lysed cells with origami incubated for 1 h. (b) Concentration of origami products after separation from cell lysate, estimated from the relative band intensities, compared to the control sample in lane 4. (c) Topographic images of rectangular DNA origami extracted from agarose gels. Scale bar = 300 nm (image insets in upper corners are 250 nm by 250 nm). (d) AFM images of origami/cell lysate mixtures without gel electrophoretic separation, at 4 and 25 ℃. Scale bar = 300 nm. (Adapted with permission from Stability of DNA Origami Nanoarrays in Cell Lysate. *Nano Lett.* **2011**, 4, 1477-1482. Copyright 2011 American Chemical Society.)

To further verify their structural integrity and degree of separation from the cell lysate, DNA origami structures were extracted from the gels and visualized by AFM. The AFM images in Figure 3.3c and Figure S3.1 clearly show the rectangular DNA origami structures have been separated from the cell lysate, remaining fully intact with no evidence of degradation. For comparison, a mixture of DNA origami and cell lysate (no electrophoretic separation) was directly deposited on a mica substrate for AFM readout. Figure 3.3d shows that individual DNA origami structures cannot be identified in AFM images of the mixtures with cell lysate, because broken lipid membranes, proteins, nucleic acids and cellular organelle debris obscure the nanostructures. The cell remnants adsorb to the mica surface, preventing the DNA origami structures access to the substrate. Cell lysate constituents may also adsorb to the AFM tip while scanning, reducing image quality. These results confirm that separation, electrophoretic or otherwise, is a critical step for AFM analysis of DNA origami/cell lysate mixtures.

3.4.2 Stability of different origami shapes in cell lysate

In the future, other 2D and 3D DNA origami structures may be required for tailored applications. It is therefore desirable to determine whether the shape of a structure has any influence on its stability in, or separability from, cell lysate. Two additional DNA

origami constructions, whose shape and helical density might be presumed to affect their susceptibility to enzyme digestion, were investigated: a 2D equilateral triangle (120 nm long with 30 nm wide sides) with an open, central, triangular cavity of 60 nm per side and a 3D multilayer rectangular parallelepiped structure (8 helix × 8 helix square lattice with dimensions of 16 nm × 16 nm × 30 nm). The triangular and cuboid structures were prepared, mixed with CP-A cell lysate, and separated by gel electrophoresis (Figure 3.4a). The results show that both additional DNA origami shapes can be separated from CP-A cell lysate, with no significant damage to the structures. A small amount of the triangular DNA origami structure remained in the wells, reflecting the known tendency of these structures to self-associate by base-stacking at the corner to form larger aggregates. The structures were subsequently extracted from the gels and imaged using AFM and TEM, as shown in panels b and c of Figure 3.4, respectively. The results indicate that regardless of size or shape, DNA origami structures are stable in, and separable from, a variety of cell lysate mixtures under the investigated conditions. The ability of these synthetic DNA structures to resist association with any cellular components and degradation by the DNA enzymes in the cell lysate might not have been predicted, considering how readily native DNA (both single stranded and double stranded) can interact with various DNA binding proteins and be digested in the intracellular environment. It is possible that the cellular machinery and enzymes do not recognize DNA in an origami structure as they normally would, or perhaps cannot access it given the relatively compact arrangement of DNA helixes due to limited steric accessibility. In addition, origami structures have a very high negative charge density, which may

contribute to the inaccessibility of cellular components and enzymes to DNA origami surfaces.

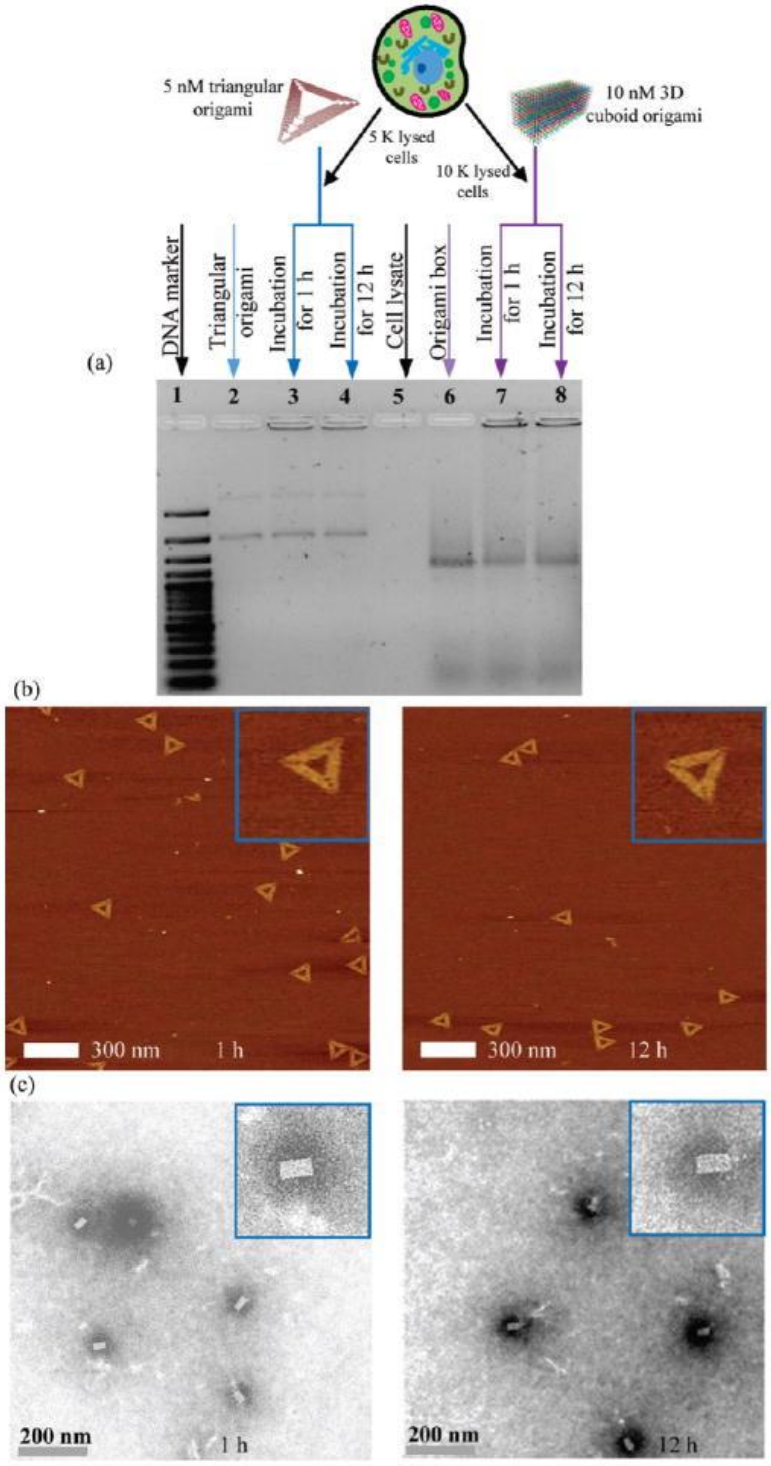

Figure 3.3 Stability of different origami shapes in CP-A cell lysate. (a) Agarose gel electrophoresis of 2D triangular origami and 3D cuboid origami after incubation with CP-A cell lysate: lane 1, 1 kbp DNA ladder; lane 2, 5 nM triangular origami; lanes 3 and 4, triangular origami incubated with cell lysate for 1 and 12 h; lane 5, cell lysate; lane 6, 10 nM origami cube; lanes 7 and 8, 10 nM origami cube incubated with cell lysate for 1 and 12 h. (b) AFM images of triangular DNA origami after separation from CP-A lysate. Images insets are 250 nm by 250 nm. (c) TEM images of 3D cuboid origami after separation from CP-A lysate. Images insets are 125 nm by 125 nm. (Adapted with permission from Stability of DNA Origami Nanoarrays in Cell Lysate. *Nano Lett.* **2011**, 4, 1477-1482. Copyright 2011 American Chemical Society.)

3.4.3 Relative stabilities of origami, ssDNA and dsDNA in cell lysate

To determine the interaction of cell lysate with traditional DNA and compare the results to those of DNA origami structures, representative single- and double-stranded DNA were also tested. It was expected that the natural, noncompact structure of single- and double-stranded DNA should be less resistant to interaction with, and degradation by, the components in cell lysate. M13mp18 viral DNA, which acts as the scaffold strand in the assembly of DNA origami, was selected as the representative single-stranded DNA; λ DNA, ~47 kbp from *E. coli*, was used as the double-stranded DNA. Mixtures of single-and double-stranded DNA with cell lysate were prepared in the same way as the rectangular DNA origami–lysate mixture. After 1 or 12 h of 25 ℃ incubation in CP-A lysate, only the DNA origami remained unchanged as shown in the gel images in Figure 3.5. Notably, after only 1 h of incubation with cell lysate, comparing the gels from the untreated and treated samples, the single-stranded M13 mp18 viral DNA and double-stranded λ DNA were completely altered, as evidenced by the disappearance of their representative bands. After treatment with cell lysate, the single-stranded DNA did not run as a single band but was smeared throughout the lane: the appearance of products with smeared faster mobility indicates that some of the single-stranded DNA was

digested by cellular enzymes; the products with smeared slower mobility indicate severe protein binding and maybe some degradation. In the case of λDNA, nearly the entire sample of double-stranded DNA remained in the gel well. It is likely that the double-stranded DNA was interacting with some component in the cell lysate, possibly becoming entangled with cellular proteins. DNA origami is better able to maintain its integrity in cell lysate compared to single- and double-stranded DNA, likely because the rigidity, compact organization, and charge density of the origami structure decrease its susceptibility to degradation and propensity to interact with lysate components.

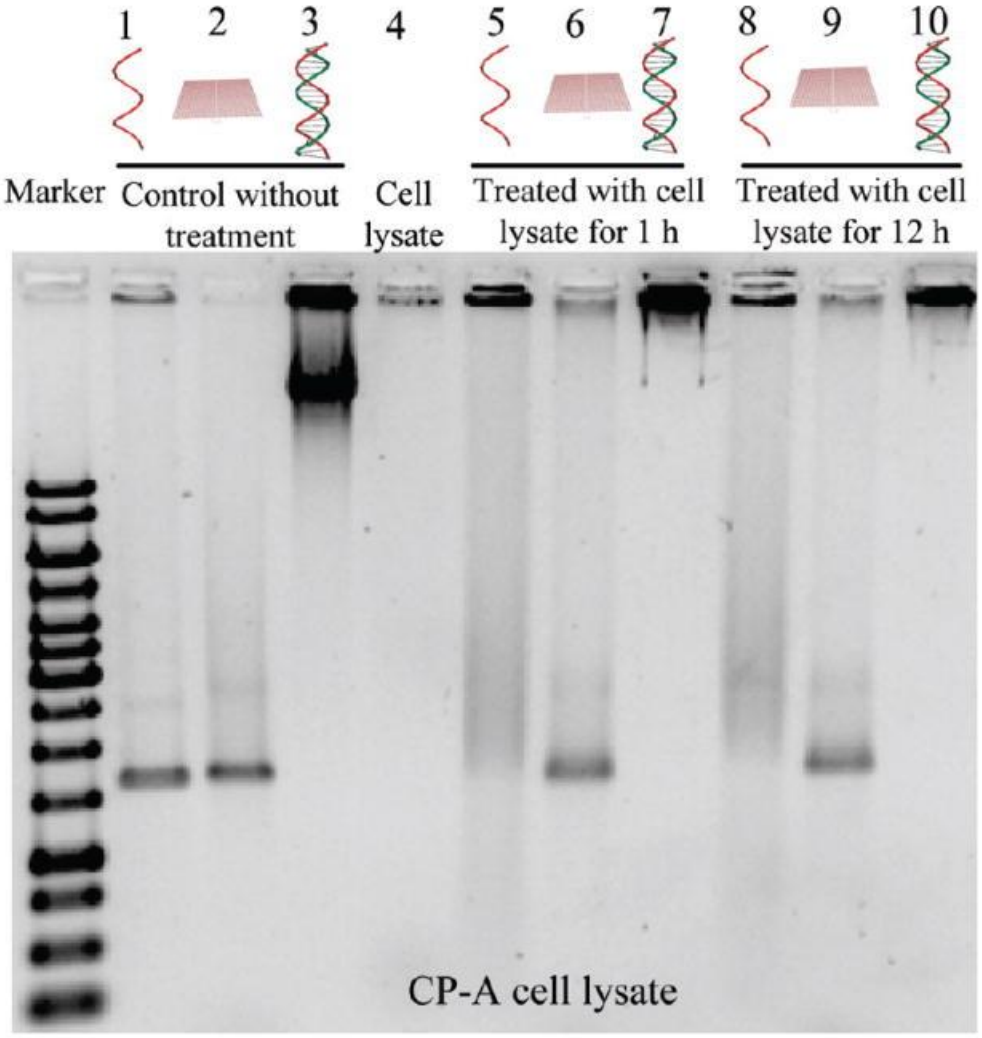

Figure 3.5 Relative stabilities of rectangular origami, single-stranded M13 viral DNA and double-stranded λ DNA in CP-A cell lysate. Agarose gel electrophoresis confirms that only origami is separable from cellular debris: lane 1, 10 nM M13; lane 2, 10 nM origami; lane 3, 25 ng/μLλ DNA; lane 4, cell lysate; lanes 5–7, M13, origami and λ DNA incubated with cell lysate for 1 h at 25 ℃, respectively; lanes 8–10, M13, origami, and λ DNA incubated with cell lysate for 12 h at 25 ℃, respectively. (Adapted with permission from Stability of DNA Origami Nanoarrays in Cell Lysate. *Nano Lett.* **2011**, 4, 1477-1482. Copyright 2011 American Chemical Society.)

Cell-line-dependent effects of lysate on the stability and separation of DNA origami structures were also investigated. Normal End1/E6E7, MCF-10A and cancerous HeLa & MDA-MB-231 cells (see detailed description in SI) were lysed and separately mixed and incubated with DNA origami, double-stranded λ DNA, and single-stranded M13mp18 viral DNA. Figure S3.2 shows the results of agarose gel separation of the mixtures, with each cell line exhibiting similar patterns to those of the CP-A cell lysate experiments. No notable cell line dependent effects were observed, and the results confirm that only the folded structure of DNA origami is stable in the various cell lysates. Most of the double-stranded λ DNA remained in the wells when mixed with the cell lysates, possibly because of entanglement with proteins in the lysate mixture.

3.4.4 Functional assay of origami with interaction of cell lysate

Finally, to confirm the functionality of DNA origami with interaction of cell lysate, a region of humanβ-actin gene (40 bases long) was linked as a capture probe onto the rectangular-shaped origami and then mixed with HeLa cell lysate. Twelve copies of probe were aligned into each strand on the right edge of the origami, while a sequence not found in the human genome was selected as a control and located at the same position as the probe (Figure S3.6). Six of the dumbbell-shaped structures were placed on the upper left corner as index feature to orient the image, as described previously.[15] Detailed

sequences of the probe, control, and index can be found in the Table S3.4. After 1 and 12 h room temperature incubation with lysate prepared from various numbers of cells, origami with a capture probe was successfully separated from cell lysate as shown in Figure 3.6a. The gel images show that DNA origami/probe is still separable from the lysate, even after 12 h of incubation. The origami bands were cut from the gel for further functional assay. First synthetic RNA with complementary sequence to the probes (40 bases) was reacted with probe origami. AFM images of hybridized origami, such as in Figure 3.6c, revealed that the target hybridization can be visualized as bright features along the line of the probes, while no such binding was evident on the control (Figure 3.6b). Two more targets, fragmentized total cellular RNA and total cellular RNA, were prepared and reacted with probe-bearing origami after recovering from cell lysate. Those total cellular RNA should contain the mRNA for β-actin gene that is complementary to the probes. The AFM images of panels d and e of Figure 3.6 confirmed the obvious hybridization between probe origami and total cellular RNA, but no target binding on the control probe line as shown in panels b and c of Figure S3.7. Excess total cellular RNA was observed as aggregated dots on the mica surface (Figure 3.6e and Figure S3.7c). These results indicate that the single-stranded probes are not digested by cellular enzymes and remain functional for RNA hybridization after exposure to the cell lysate even for 12 h.

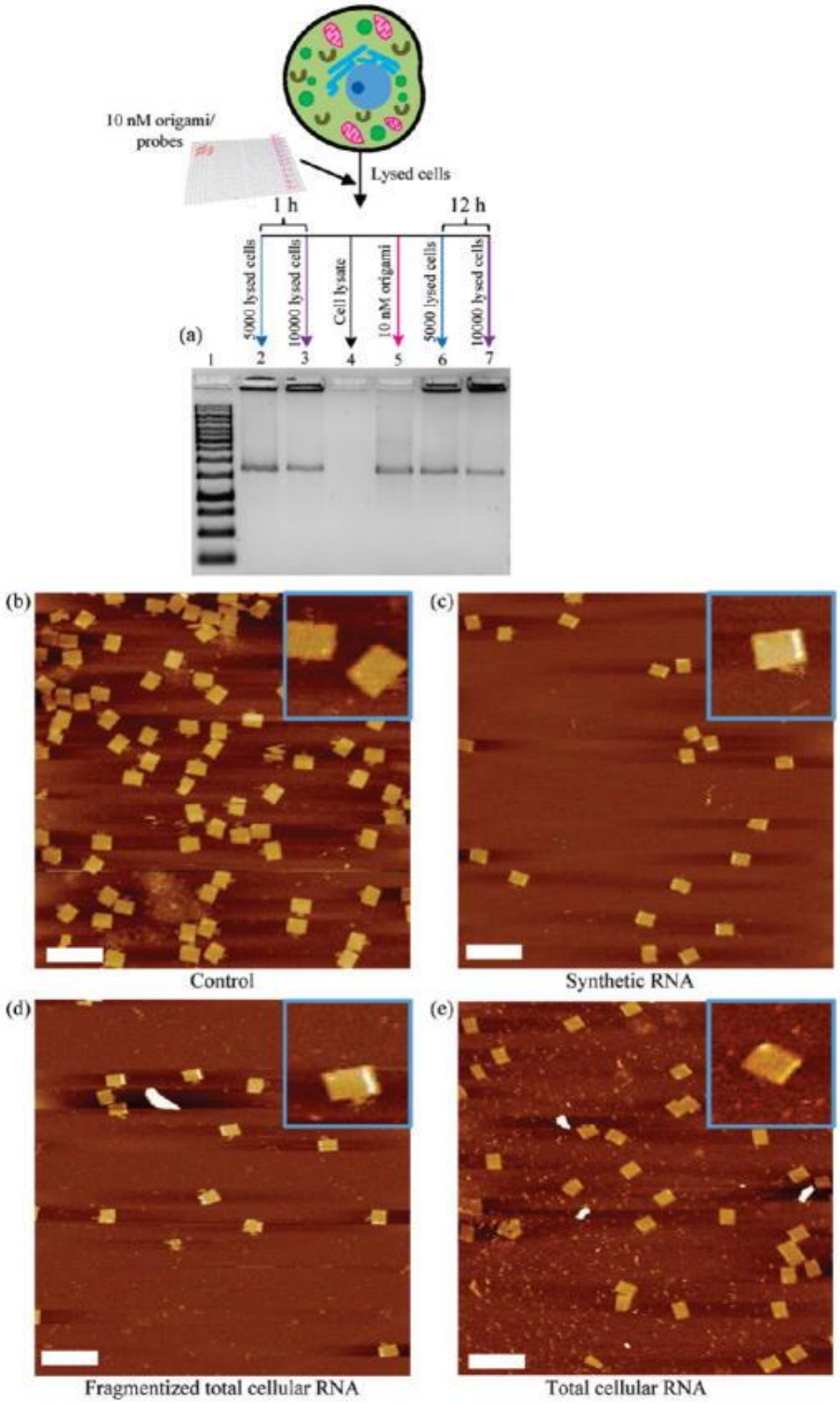
10 nM origami/
probes
Lysed cells
1 h
12 h
5000 lysed cells
10000 lysed cells
Cell lysate
10 nM origami
5000 lysed cells
10000 lysed cells
(a)
1
2
3
4
5
6
7
(b)
(c)
Control
Synthetic RNA
(d)
(e)
Fragmentized total cellular RNA
Total cellular RNA

Figure 3.6 Functional assay of single-stranded probe-bearing DNA origami nanostructure after mixing with HeLa cell lysate. (a) Each DNA origami carries a line of probes positioned near the right edge and is recovered after incubation with HeLa cell lysate using agarose gel: lane 1, 1 kbp DNA ladder; lane 2, 5000 lysed cells with probe bearing DNA origami incubated for 1 h; lane 3, 10000 lysed cells with probe bearing DNA origami incubated for 1 h; lane 4, cell lysate only; lane 5, 10 nM probe bearing DNA origami; lane 6, 5000 lysed cells with probe bearing DNA origami incubated for 12 h; lane 7, 10000 lysed cells with probe bearing DNA origami incubated for 12 h. (b–e) Topographic AFM images of the DNA origami with three different targets after separation from HeLa cel lysate. (b) Control probes mixed with synthetic RNA target. (c) Binding to synthetic RNA. (d) Binding to fragmentized total cellular RNA. (d) Binding to total cellular RNA. Scale bar = 300 nm (image insets are 250 nm by 250 nm). (Adapted with permission from Stability of DNA Origami Nanoarrays in Cell Lysate. *Nano Lett.* **2011**, 4, 1477-1482. Copyright 2011 American Chemical Society.)

3.5 Conclusion

In summary, we have demonstrated the successful electrophoretic separation of a variety of DNA origami nanostructures from the lysates of several cell lines. The structural integrity of the resulting DNA origami was verified by AFM and TEM imaging, confirming that the structures can be separated from cell lysate without degradation or damage. We also established that DNA origami structures are stable in lysate mixtures for at least 12 h at room temperature, in contrast to natural, single- and double-stranded DNA configurations. Finally, we confirmed that DNA probe origami is not only stable but also functional after extended exposure to cell lysate. These results imply that DNA origami should remain stable in intracellular conditions and has the potential to serve as an in vitro diagnostic platform. Collectively, the experimental results encourage the development of an integrated, microfluidic chip for origami separation after cell lysis. This type of integrated device could be used for single cell proteomic analysis and provide sufficient sensitivity to ascertain an accurate picture of intracellular dynamics.

3.6 References

(1) Rothemund, P. W. K. *Nature* **2006**, 440, 297.

(2) Kuzuya, A.; Komiyama, M. *Nanoscale* **2010**, 2, 310.

(3) Nangreave, J.; Han, D.; Liu, Y.; Yan, H. *Curr. Opin. Chem. Biol.* **2010**, 14, 608.

(4) Douglas, S. M.; Dietz, H.; Liedl, T.; Hogberg, B.; Graf, F.; Shih, W. M. *Nature* **2009**, 459, 414.

(5) Andersen, E. S.; Dong, M.; Nielsen, M. M.; Jahn, K.; Subramani, R.; Mamdouh, W.; Golas, M. M.; Sander, B.; Stark, H.; Oliveira, C. L. P.; Pedersen, J. S.; Birkedal, V.; Besenbacher, F.; Gothelf, K. V.; Kjems, J. *Nature* **2009**, 459, 73.

(6) Ke, Y. G.; Douglas, S. M.; Liu, M. H.; Sharma, J.; Cheng, A. C.; Leung, A.; Liu, Y.; Shih, W. M.; Yan, H. *J. Am. Chem. Soc.* **2009**, 131, 15903.

(7) Dietz, H.; Douglas, S. M.; Shih, W. M. *Science* **2009**, 325, 725.

(8) Kuzuya, A.; Komiyama, M. *Chem Commun* **2009**, 4182.

(9) Endo, M.; Katsuda, Y.; Hidaka, K.; Sugiyama, H. *J. Am. Chem. Soc.* **2010**, 132, 1592.

(10) Lund, K.; Manzo, A. J.; Dabby, N.; Michelotti, N.; Johnson-Buck, A.; Nangreave, J.; Taylor, S.; Pei, R. J.; Stojanovic, M. N.; Walter, N. G.; Winfree, E.; Yan, H. *Nature* **2010**, 465, 206.

(11) Voigt, N. V.; Torring, T.; Rotaru, A.; Jacobsen, M. F.; Ravnsbaek, J. B.; Subramani, R.;Mamdouh,W.; Kjems, J.;Mokhir, A.; Besenbacher, F.; Gothelf, K. V. *Nat. Nanotechnol*. **2010**, 5, 200.

(12) Rinker, S.; Ke, Y. G.; Liu, Y.; Chhabra, R.; Yan, H. *Nat. Nanotechnol*. **2008**, 3, 418.

(13) Kuzuya, A.; Kimura, M.; Numajiri, K.; Koshi, N.; Ohnishi, T.; Okada, F.; Komiyama, M. *Chem Bio Chem* **2009**, 10, 1811.

(14) Kuzyk, A.; Laitinen, K. T.; Torma, P. *Nanotechnology* **2009**, 20.

(15) Ke, Y. G.; Lindsay, S.; Chang, Y.; Liu, Y.; Yan, H. *Science* **2008**, 319, 180.

(16) Subramanian, H. K. K.; Chakraborty, B.; Sha, R.; Seeman, N. C. *Nano Lett*. **2011**, 11, 910.

(17) Kodera, N.; Yamamoto, D.; Ishikawa, R.; Ando, T. *Nature* **2010**, 468, 72.

(18) Sannohe, Y.; Endo, M.; Katsuda, Y.; Hidaka, K.; Sugiyama, H. *J. Am. Chem. Soc.* **2010**, 132, 16311.

(19) Steinhauer, C.; Jungmann, R.; Sobey, T. L.; Simmel, F. C.; Tinnefeld, P. *Angew. Chem., Int. Ed.* **2009**, 48, 8870.

(20) Glasgow, I.; Batton, J.; Aubry, N. *Lab Chip* **2004**, 4, 558.

(21) Howell, P. B.; Mott, D. R.; Fertig, S.; Kaplan, C. R.; Golden, J. P.; Oran, E. S.; Ligler, F. S. *Lab Chip* **2005**, 5, 524.

(22) Mei, Q.; Xia, Z.; Xu, F.; Soper, S. A.; Fan, Z. H. *Anal. Chem*. **2008**, 80, 6045.

(23) Stroock, A. D.; Dertinger, S. K. W.; Ajdari, A.; Mezic, I.; Stone, H. A.; Whitesides, G. M. *Science* **2002**, 295, 647.

(24) Bienvenue, J. M.; Duncalf, N.; Marchiarullo, D.; Ferrance, J. P.; Landers, J. P. J. *Forensic Sci*. **2006**, 51, 266.

(25) Chen, X.; Cui, D. F.; Liu, C. C.; Li, H.; Chen, *J. Anal. Chim. Acta* **2007**, 584, 237.

(26) Kim, J.; Jang, S. H.; Jia, G. Y.; Zoval, J. V.; Da Silva, N. A.; Madou, M. J. *Lab Chip* **2004**, 4, 516.

(27) McClain, M. A.; Culbertson, C. T.; Jacobson, S. C.; Allbritton, N. L.; Sims, C. E.; Ramsey, *J. M. Anal. Chem*. **2003**, 75, 5646.

(28) Mun, B. P.; Jung, S. M.; Yoon, S. Y.; Kim, S. H.; Lee, J. H.; Yang, S. *Microfluid. Nanofluid.* **2010**, 8, 695.

(29) Schilling, E. A.; Kamholz, A. E.; Yager, P. *Anal. Chem*. **2002**, 74, 1798.

(30) Das, C.; Zhang, J.; Denslow, N. D.; Fan, Z. H. *Lab Chip* **2007**, 7, 1806.

(31) Fan, R.; Vermesh, O.; Srivastava, A.; Yen, B. K. H.; Qin, L. D.; Ahmad, H.; Kwong, G. A.; Liu, C. C.; Gould, J.; Hood, L.; Heath, J. R. *Nat. Biotechnol*. **2008**, 26, 1373.

(32) Hatch, A. V.; Herr, A. E.; Throckmorton, D. J.; Brennan, J. S.; Singh, A. K. *Anal. Chem*. **2006**, 78, 4976.

(33) Hellmich, W.; Pelargus, C.; Leffhalm, K.; Ros, A.; Anselmetti, D. *Electrophoresis* **2005**, 26, 3689.

(34) Barton, G. M.; Medzhitov, R. *Proc. Natl. Acad. Sci. U.S.A.* **2002**, 99, 14943.

(35) Mitchell, P. *Nat. Biotechnol*. **2001**, 19, 1013.

(36) Palanca-Wessels, M. C.; Barrett, M. T.; Galipeau, P. C.; Rohrer, K. L.; Reid, B. J.; Rabinovitch, P. S. *Gastroenterology* **1998**, 114, 295.

Chapter 4

USING DNA ORIGAMI TO QUANTIFY FUNCTIONAL TCRαβ REPERTOIRES WITHOUT SINGLE CELL SORTING

4.1 Abstract

The immune system must be able to recognize virtually any pathogen (diversity) while maintaining enough cells specific for each pathogen in order to mount an effective response (protection). T cells generate diversity by imprecise joining of gene segments to generate α/β heterodimeric receptors. Linking sequence information for TCRα and TCRβ pairs from individual cells has been problematic due to the cost of single cell sorting and inadequate molecular approaches for linking the α and β mRNAs encoding these proteins from individual cells. We developed novel DNA origami nanostructures to capture and protect both TCRα and TCRβ mRNA from individual cells, which can then be physically linked via a unique dual-primed reverse-transcription and ligation reaction, followed by multiplex PCR to generate individual amplicons containing both TCR from individual cells for use in next generation sequencing. We demonstrated high efficiency transfection and recovery of DNA origami, optimized methods for purification with bound TCR mRNA, and validated this approach with transgenic T cells expressing a known TCR sequence. This approach is directly amenable to single cell analysis of other immune receptors (or other species) by relatively simple modifications of the origami sequences, and could be applied to virtually any heterogeneous cell population for which sequence information on any two genes is required.

4.2 Introduction

In order for the immune system to recognize and combat a diverse array of pathogens, T cells express a large repertoire of clonotypic αβ dimeric T cell receptors (TCR), resulting in an enormous number of specificities at the population level.[1] TCR diversity is due to two processes. First, somatic recombination of V and J gene segments for the TCRα chain and V, D, and J segments for the TCRβ chain, together with junctional diversity, results in ~10^6 unique sequences of diverse TCRα and TCRβ.[2-4] Second, pairing between different TCRα and TCRβ chains results in a potential one million-fold increase in TCR diversity: completely non-random pairing of each TCRβ with a single TCRα would result in a total diversity of ~10^6 unique TCRs, while completely random pairing of any TCRβ with any TCRα would yield a maximum combinatorial diversity of ~10^{12} unique TCRs. A central problem in immunology is that the immune system must balance diversity in immune populations with maintenance of sufficient precursor cells that are specific for any given pathogen to mount an effective response. Quantitatively defining this balance between diversity and protection has been problematic, in large part due to the lack of methods for quantitating total TCR diversity. Despite quantitation of sequence diversity independently for TCRα and TCRβ chains in the naïve T cell repertoire in both humans and mice, pairing of different TCR α and β chains have precluded accurate measurement of TCR combinatorial diversity.[3, 4] Current technologies allow for analysis of complementarity determining region 3 (CDR3) diversity, within either the α or β TCR, but no current methods exist for obtaining both CDR3s from individual cells from large polyclonal populations. Single cell sequencing

remains too expensive[5], while molecular strategies for obtaining linked CDR3 information from single cells have not been adequately developed[6, 7]. In addition to lacking information about diversity attributable to α/β chain pairing, we also lack a quantitative understanding of overall T cell receptor diversity in general. Thus far, TCR diversity has been described in terms of simple summary statistics such as the number of distinct TCRs (based solely on analysis of TCRβ chain sequences), which is analogous to species richness or the Simpsons diversity index in ecology that provides a single number to describe the relative abundance of different species.[8]

With predictable Watson-Crick base-pairing, biocompatibility, and ease of chemical and biological functional modification, DNA nanostructures are an excellent platform for intracellular capture and detection.[9-11] In particular, scaffolded DNA origami[12] is fully addressable and large enough for multi-functional modification and steric inhibition of enzymatic access and degradation, and has already been shown to capture targeted mRNAs.[13, 14] We exploited these features and developed a novel strategy to determine the contribution of pairing of different TCRα and TCRβ chains to total T cell receptor repertoire diversity using DNA origami nanostructures to specifically bind the constant region of TCRα and TCRβ mRNAs from individual cells and protect these hybrid structures from destruction. Together with Illumina paired end deep sequencing technology in which individual DNA amplicons containing CDR3 information from both TCRα and TCRβ from individual cells, we can obtain linked sequences for both rearranged TCRα and TCRβ chains from individual cells, and thereby estimate the contribution of TCRαβ pairing to total TCR diversity.

4.3 Experimental design

We engineered DNA origami nanostructures to specifically capture and protect TCRα and TCRβ mRNAs. In order to maximize the possibility of binding to diverse mRNAs, we targeted the constant (C) region of either the TCRα or TCRβ mRNA coding sequences for binding. To optimize and verify our strategy, CD8+ T cells from P14 TCR-transgenic mice were applied as model cells for *in vivo* analysis, while TCR α and β RNA with same sequence were prepared by *in vitro* transcription for *in vitro* testing. The secondary structures of known P14 TCR α and β mRNA were analyzed and single stranded loop regions were bound by a pair of complimentary, 16 nt single stranded probes extended from the surface of rectangular origami. (Figure S4.1) To increase the success of binding and minimize errors, 6 repeating pairs of binding probes for capturing either TCRα or TCRβ mRNA were displayed in two lines from each origami, thus, a single origami structure is designed to capture multiple copies of both TCR α and β mRNA. (Figure 4.1) Site-directed attachment of fluorescent dyes (Fluorescein and TAMRA) and biotin labeled staples were used to facilitate detection of transfected cells and subsequent isolation and purification, respectively, of transfected DNA origami nanostructures from cell lysate with bound TCR mRNAs. (Figure 4.1)

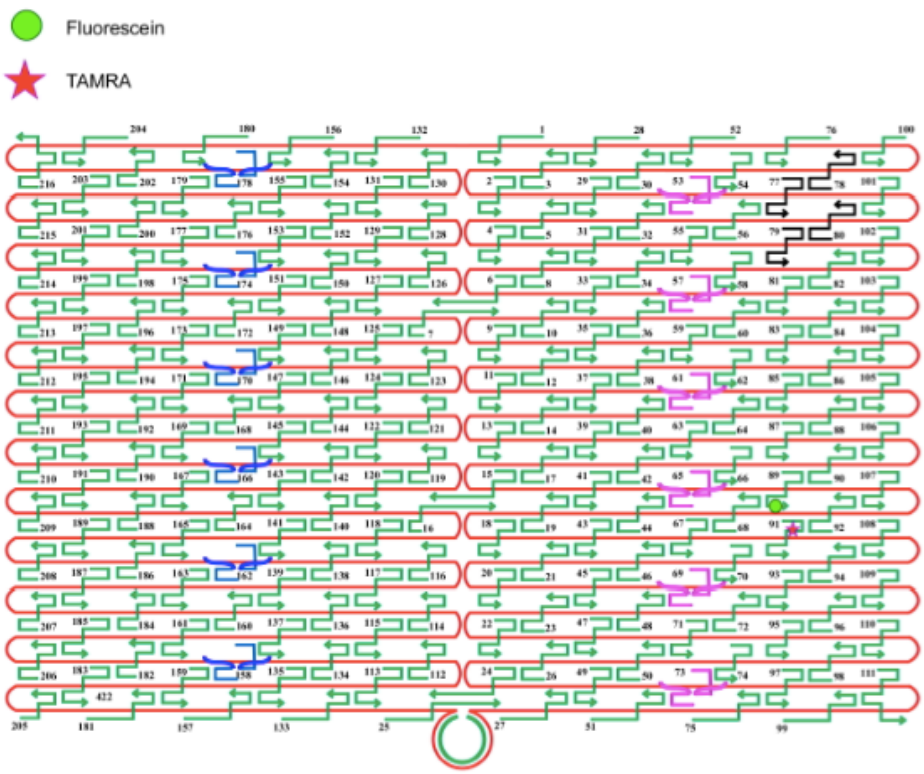

Figure 4.1 Multi-functional DNA origami nanostructure. Basic DNA origami design showing M13 circular ssDNA (red line) folded into a rectangular shape and stabilized by staple primers (green lines).[12] Two selected lines of staples with extended pairs of complementary sequences to the conserved regions of TCRα or TCRβ (pink and blue lines respectively) were used for binding targeted TCR mRNA. Other staples are biotinylated (black lines) for purification, or have fluorescent probes (green dot, red star) attached for monitoring.

The intracellular capture of target mRNAs was realized by transfection of multi-functional DNA origami nanostructures into T cells to bind and protect both TCR mRNAs. The cells were subsequently lysed and origamis with bound mRNAs were isolated. The novel flexible DNA linker was used to assist in dual-primer reverse transcription (RT), ligation and polymerase chain reaction (PCR) amplification, followed by paired-end deep sequencing, so that the CDR3 information of both α and β chains

from individual cells are integrated into one PCR product. Therefore, the linked sequence information for both TCR chains was obtained from individual cells, without the need for single cell sorting. (Figure 4.2) This approach was first demonstrated *in vitro* with a P14 TCR mRNA system and then *in vivo* with T cells from P14 transgenic mice. Finally, we are planning to estimate total TCR diversity in the pre-immune T cell repertoire of mice, including a quantitative description of the frequency and distribution of T cell receptors.

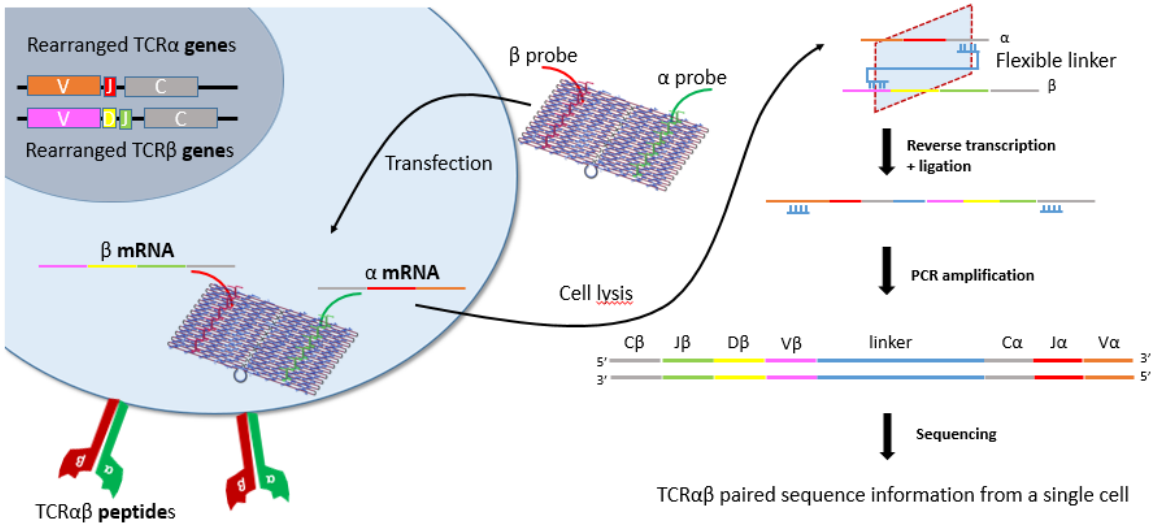

Figure 4.2 Strategy of using multifunctional DNA origami to obtain linked sequence information of both TCR α and β from single cells without single cell sorting. Antigen-reactive T cells are obtained by flow cytometry using labeled antigens, and transfected by DNA origami nanostructures containing extended sequences complimentary to both α and β constant region mRNAs. DNA origami molecules bind and protect intracellular α and β mRNAs within single cells that are then lysed and origami with bound mRNAs, re-isolated and purified. Using a dual-primer multiplex reverse transcription reaction, with an exonuclease deficient RT enzyme that does not displace downstream primers, intervening α and β CDR3 sequences are "filled in" and intermediate products ligated by T4 ligase. The cDNA is then amplified by standard V-C multiplex PCR to obtain a pool of amplification products suitable for Illumina paired end sequencing. Each amplicon will thus provide sequence-paired information of both α and β from an individual cells without the need for single cell sorting.

4.4 Materials and Methods

4.4.1 DNA origami assembly and purification

To prepare DNA origami, we used M13mp18 purchased from New England Biolabs (Ipswich, MA, USA) directly without purification. All oligonucleotides were purchased from Integrated DNA Technologies, Inc. (www.idtdnacom). Dye labeled strands were HPLC purified; probe extended strands and biotin labeled strands were purified by denaturing polyacrylamide gel electrophoresis (PAGE); all other staple strands were directly used without purification.

When assembling origami, M13 (final concentration of 50 nM), 3X dye labeled staples, probe strands and biotin labeled strands, and 5X unmodified staples were mixed in 1 × TAE Mg2+ buffer (40 mM Tris base, 20 mM acetate acid, 2 mM EDTA, and 12.5 mM Mg2+ at pH 8.0). A PCR thermal cycler was used to heat samples to 95 ℃ and slowly cooled to 4 ℃ over 12 hours. The assembled origami was separated from excess strands using 100 kDa Microcon centrifugal filter devices (Millipore, USA).

4.4.2 Linker preparation

Two 100 nt oligonucleotides, T1 and T2, with phosphate labeled 5’ ends were purchased from Integrated DNA Technologies and purified by denaturing PAGE. A 20 nt short oligonucleotide that was complementary to last 10 nt at the 3’ end of T1 and the first 10 nt at the 5’ end of T2 was also purchased from Integrated DNA Technologies and used without purification. Equal amounts of purified T1 and T2 were mixed with 10X the short complementary strand and annealed from 45 ℃ to 4 ℃ over 1.5 hr. New England Biolabs T4 DNA Ligase Kit was subsequently applied overnight at room temperature.

The ligated 200 nt linker was purified from the final product by denaturing PAGE. The concentration of linker was estimated by measuring absorbance at 260 nm.

4.4.3 Harvesting T cells from mice and sorting CD8+ T cells

The spleen from each mouse was extracted and deposited them into 1.5 mL tubes with 1mL RPMI-complete media. To digest the spleen and lyse the RBCs, first, we poured the spleen/media into a 70 μM cell strainer over one half of a petri dish and added 1 mL RPMI-complete media to the strainer using an eye dropper. Next, we used the base of a plunger from a 3 mL syringe to smash the spleen through the strainer and rinsed the plunger and strainer several times with RPMI-complete media. We then added the collection to a 15 mL tube and centrifuged at 1200 rpm, 5 min. After pouring off the supernatant we flicked the tube to re-suspend the cells. Then we added 1 mL ACK lysis buffer and incubated the solution for 2 minutes at room temperature to quench the lysis buffer with RPMI-complete buffer. After centrifuging again we poured off the supernatant and re-suspended the cells in 750 μL MACS buffer (mixture of 20 mL autoMACS rinsing solution and 1mL MACS BSA stock solution).

Sorting CD8+ T cells by MACS fit: we mixed collected cells with 50 μL MACS CD8a (Ly-2) Microbeads and incubated for 30 minutes at 4 ℃. We then added 5 mL MACS buffer and centrifuged to rinse the cells (2X) and re-suspended the cells in 1 mL MACS buffer. We used a MACS MS column with magnet to capture the CD8+ T cells. After washing off the unbounded cells, we removed the column from the magnet and used the plunger to slowly elute the CD8+ T cells with 1 mL MACS buffer. Finally, we placed the cells on ice until use.

4.4.4 TCR RNA *in vitro* transcription

Total RNA was extracted from purified CD8+ T cells from a P14 mouse using a Qiagen RNeasy Kit. We reverse transcribed TCR mRNA using a Qiagen Omniscript RT kit and PCR amplified using a *Taq* Polymerase Kit. We performed TOPO TA Cloning with 3 μL of the above product, 1 μL salt solution, 1 μL TOPO vector and 2 μL H_2O and incubated at room temperature for 5 minutes. We placed the product on ice until use.

Chemically transformed E. coli cells were prepared with a One Shot TOP10 cell line. LB plates containing 50 μg/mL ampicillin were prepared and placed in a 37 ℃ incubator for at least 30 minutes prior to use. We added 2 μL of the TOPO cloning reaction from above to one vial of pre-thawed OneShot chemically competent E. coli cells and incubated for 30 minutes on ice. We heat shocked the cells for 30 seconds by holding in a 42 ℃ water bath and immediately transfered the cells to ice. We added 250 μL of room temperature S.O.C. media and shook the tube on a horizontal shaker (200 rpm) for 1 hour at 37 ℃. Then we spread 10-50 μL on pre-warmed selective LB plates and incubated the plates overnight at 37 ℃.

The next day we picked 2-6 individual colonies and used them to inoculate individual tubes containing LB media supplemented with 50 μG/mL ampicillin (pre-warmed to 37 ℃). Incubated tubes were put on a horizontal shaker (200 rpm) for 6-12 hours at 37 ℃.

Plasmid DNA was isolated using a PureLink Quick Plasmid Miniprep Kit. For sequencing, we used either M13Forward or M13Reverse primers. Agarose gel electrophoresis was used to analyze the transformants at about 950 bp. If a low

concentration of DNA was found, M13F/M13R primers were used to amplify the plasmid DNA for use in *in vitro* transcription.

I*n vitro* transcription was performed using a MEGAscript T7 *in vitro* Transcription Kit for 4 hours at 37 ℃. The final concentration of the RNA product was estimated by absorbance at 260 nm. We then placed the RNA at -20 ℃ until use.

4.4.5 Capture *in vitro* transcript TCR RNAs with origami

Target TCR RNA α/β/α & β and prepared origami with corresponding probes were mixed at a ratio of 2:1, 10:1, 20:1 RNA:probes (6X the origami amount) in 1× TAE Mg2+ buffer and incubated at 37 ℃ for 1 hour. Origamis without probes were used as the control group. 1% agarose gel electrophoresis and AFM were used to analyze origami binding capability.

4.4.6 Transfection of CD8+ T cells with DNA origami

An ECM 830 BTX electroporator was applied to transfect origami into cells. 100 μL of ~1x10^6 purified CD8+ T cells were mixed with 25 μL, 50 nM purified origami and placed into a new BTX electroporation cuvette (Blue Cap, 2mm Gap). Electroporation was performed at 300 V for 5 minutes. Then the sample was removed from the cuvette and pipetted into a 96 well plate. After removing as much sample as possible from the cuvette, it was rinsed with 100 μL Lonza Mouse T cell Nucleofector Media and pipetted into the same well. The lid was placed on a 96 well plate and incubated overnight in a 37 ℃ /5% CO2 incubator. The same amount of origami without probes or same volume of 1×TAE Mg2+ buffer was applied as control groups with same amount of cells.

4.4.7 Lysing cells and isolating DNA origami with bound cellular mRNA

The plate was centrifuged at 1300 rpm for 3 minutes and flicked the media from the plate. The cells were re-suspended in 100 µL of 1% NP-40 cell lysis buffer and incubated on the plate for 1 hour on ice. One Sigma Prep Spin Column was prepared for each sample. 50 µL of Streptavidin Agarose Resin was pre-loaded into the spin column with 500 µL 1X TAE-Mg2+ and centrifuged at 2000 rpm for 10 seconds. The effluent was discarded and the bottom of the column was capped. Lysate from the 96 well plates were pipetted into the columns and the samples were incubated for 30 minutes at room temperature, shaking every 10 minutes by hand. The cap was removed from the column and centrifuged at 2000 rpm for 10 seconds. We washed 5X with 500 µL 1X TAE-Mg2+ buffer, leaving only the biotin labeled origami with captured RNA on the resin. The bottom of the column was capped again and placed into a new tube for the next step.

4.4.8 Reverse transcription (RT)

Reverse transcription was performed directly in the column. The RT master mix was prepared using a Qiagen Omniscript RT Kit (15 µL H2O, 2 µL Buffer, 2 µL dNTPs, 1 µL Ribolock RNase Inhibitor, 1 µL Cβ RT primer (100 µM), 3 µL linker primer (10-15 µM), 1 µL Reverse Transcriptase). The mixture was directly pipetted into the capped sample column and incubated for 1 hour at 37 ℃.

4.4.9 Ligation

Ligation was also peformed directly in the column. The ligation master mix was prepared using a New England Biolabs T4 DNA Ligase Kit (7 µL Buffer, 2 µL T4 DNA Ligase). The mix was directly pipetted into the sample column and incubated for 1 hour at room temperature.

4.4.10 Elution of cDNA and PCR amplification

The cap was removed from the sample and the column was incubated for 5 minutes on a 95 ℃ heat block. The column was centrifuged at 2000 rpm for 30 seconds to elute the cDNA into the tube. The column was discarded and the cDNA was kept on ice until use.

PCR reactions was performed in standard PCR tubes using a Phire Green Hot Start II DNA Polymerase Kit (9.5 μL H2O, 4 μL Buffer, 2 μL dNTPs, 0.5 μL DMSO, 0.75 μL Cβ PCR primer (100 μM), 0.75 μL Vα PCR primer (100 μM), 0.70 μL DNA Polymerase and 2 μL cDNA Sample above). PCR was performed on a thermocycler at 98 ℃ for 30 seconds, with 30 to 40 cycles of 98 ℃ 5 second denaturation, 45 ℃ 7 second annealing, 72 ℃ 7 second extension, then 72 ℃ 60 second further extension and final sample hold at 4 ℃.

4.4.11 Analyzing and purifying products by gel electrophoresis for sequencing

The PCR products were applied to a 2% agarose gel in 1x TAE buffer for 1 hour, 110 V. According to the 100 bp dsDNA ladder, the band of expected length was excised and recovered using a Promega Wizard SV gel & PCR clean up system. The purified PCR product was sent for sequencing by DNASU Sanger Sequencing Services.

4.5 Results and discussion

4.5.1 Ability to capture targeted RNA on origami

Gel electrophoresis and atomic force microscopy (AFM) were applied to verify the formation of multifunctional DNA origami and their ability to bind to TCRα and TCRβ mRNA sequences using *in vitro* transcribed P14 TCR α and β RNA. Multi-probe origami

was first exposed to TCRβ RNA only to verify the specificity of binding. The gel result shows that after binding, the origami-RNA complex has retarded migration, and as the RNA to probe ratio increases the band shifts even farther upward, indicating the capture of multiple RNAs on single origami structures. (Figure 4.3A) AFM was used to directly visualize TCR mRNA binding; the images show a single line of bound mRNAs when only one species of TCR RNA present , demonstrating that origami with both TCR target probes displayed can selectively bind to the correct RNA, without any random, non-specific interactions. (Figure 4.3B) We observed similar results when both TCR RNAs were evaluated. The pattern of gel migration demonstrates the ability of both types of TCR mRNA probes displayed from the origami to selectively capture multiple copies of the targets. (Figure 4.3C) We further confirmed our strategy by AFM; the images show that both lines of probes are bound by RNA when both species are present in the sample. (Figure 4.3D) Because the probes displayed from the origami are designed to target region C of the TCR RNAs and the *in vitro* binding conditions include simple incubation at 37 ℃ for one hour without any preprocessing of the RNA or additional chemical accelerate treatment, we expect that the intracellular binding efficient of origami after transfection into cells should be the same.

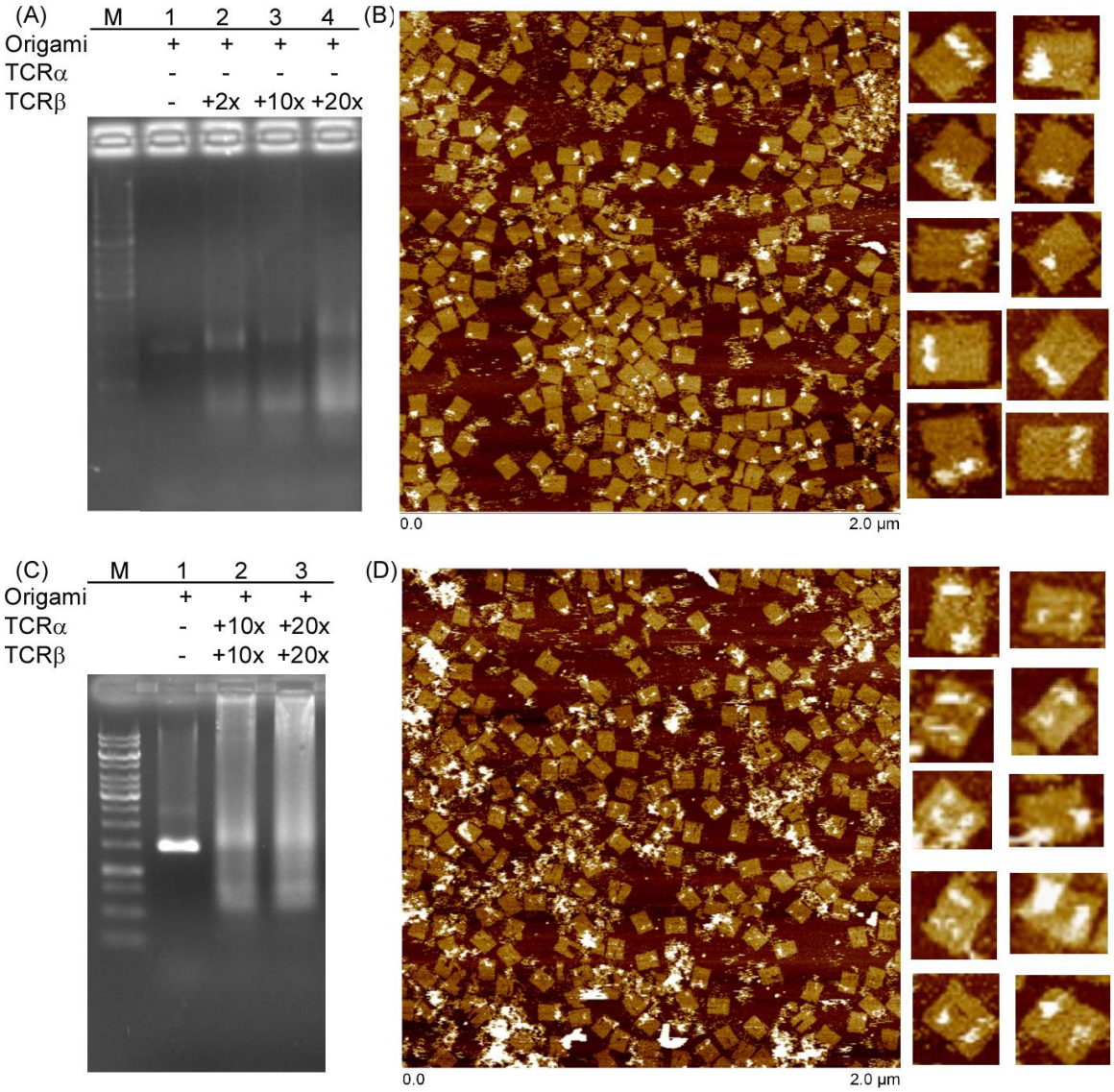

Figure 4.3 Binding of multi-probe DNA origami to *in vitro* transcribed P14 TCR mRNA. (A) Agarose gel to verify a single TCR RNA binds specifically to multi-probe origami. Lane M: 1kb ladder, Lanes 1: control origami without RNA, Lane 2: Origami incubated with TCRβ RNA at a 2:1 ratio of probe:RNA, Lane 3: Origami with TCRβ RNA at a 10:1 ratio of probe:RNA, Lane 4: Origami incubated with TCRβ RNA at a 20:1 ratio of probe:RNA, The number of RNAs binding to each origami may not be the same, so, the origami complex band migrates slowly and is smeared. (B) Selected AFM images of TCRβ RNA only binding origami. Left panel image is 2 µm and right panel images are representative zoom in areas to show binding. (C) Agarose gel to verify both TCR RNAs binding to multi-probe origami. Lane M: 1kb ladder, Lanes 1: control origami without RNA, Lane 2: Origami incubated with TCRαβ RNA at a 10:1 ratio of probe:RNA, Lane 3: Origami with TCRαβ RNA at a 20:1 ratio of probe:RNA. Slower band migration and smearing can be observed. (D) Selected AFM images of both

TCRαβ RNAs binding origami. Left panel image is 2 μm and right panel images are representative zoom in areas to show binding.

4.5.2 Transfection of DNA origami into B cells

The origami nanostructures bearing the designed probes were delivered into T cells for intracellular binding by transfection. To ensure the structural integrity and the efficiency of transfection, electroporation was selected to temporarily open the pore size of the cell membrane and increase the accessibility of nano scale DNA origami into cells. Fluorescently labeled DNA origami inside transfected T cells were visualized by fluorescence-activated cell sorting (FACS). The transfection efficiency dramatically increased when the incubation time increased and reached greater than 80% for overnight or two day incubation. (Figure 4.4) We selected overnight incubation for practical reasons and to guarantee that sufficient origami was transfected into cells and to minimize the chance of origami or bound TCR mRNA degradation.

To verify that the DNA origami nanostructures had actually entered transfected cells, rather than binding non-specifically to the cell surface, we pre-treated the transfected cells with DNase, followed by FACS analysis. Furthermore, we verified that DNase treatment resulted in destruction of origami. (Figure S4.2)

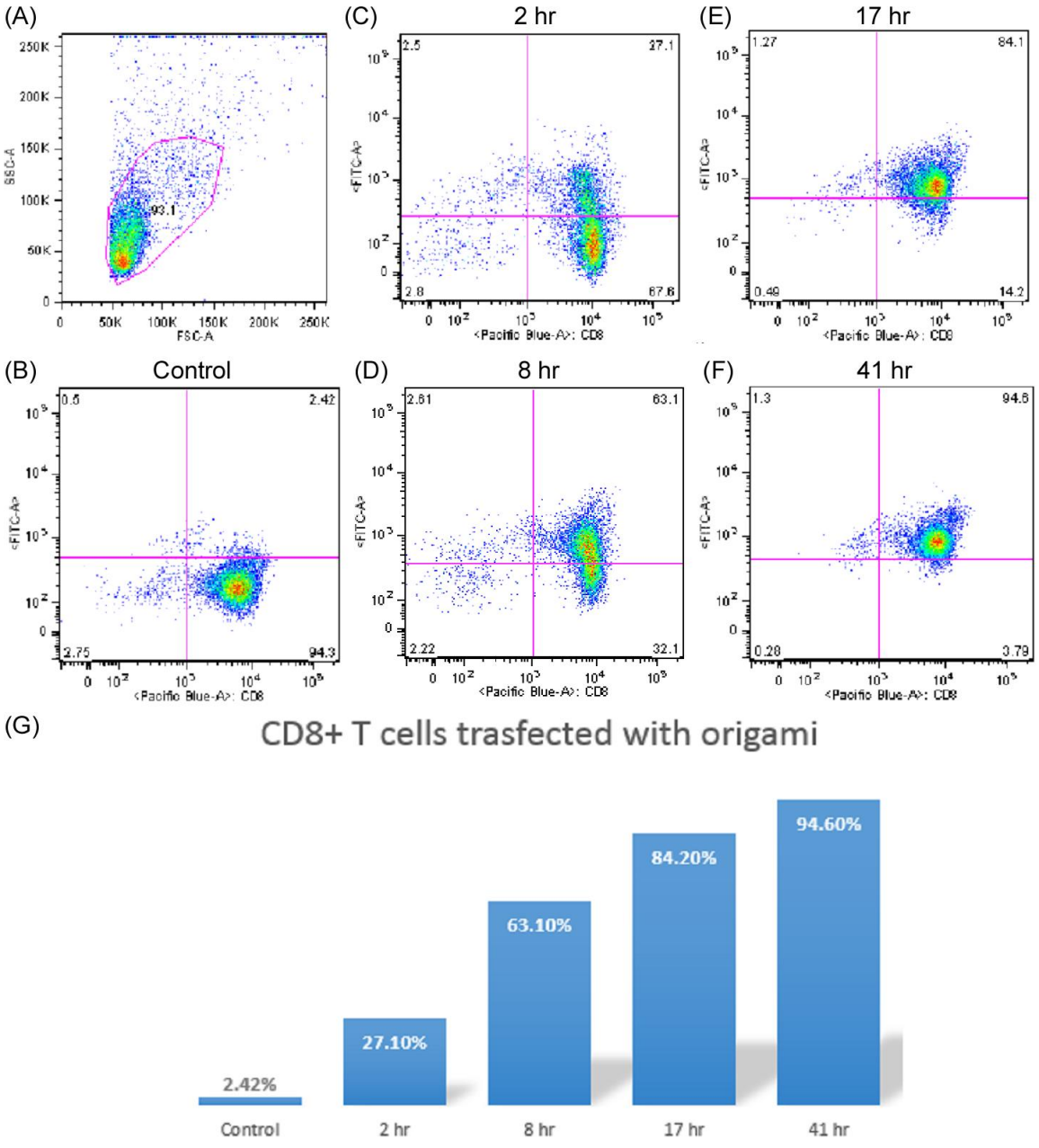

Figure 4.4 Transfection efficiency of P14 CD8+ T cells with DNA origami as determined by FACS. (A) Dot plot of cell population after transfection for 2 hours. (B) Lymphocytes from P14 mice were mock transfected as a negative control. The X axis is antibody staining of CD8+ cells and the Y axis is FITC fluorescent intensity from cells transfected with fluorescein dye labeled origami. The upper right panel is the target distribution. (C)-(F) Lymphocytes transfected with origami and sorted after 2 hours, 8 hours, 17 hours and 41 hours as described. (G) Bar graph to summarize the transfection efficiency of CD8+ T cells with functional origami.

4.5.3 Extracting origami from cells and amplifying target RNA

Gentle cell lysis was applied to break the cells and release, re-isolate and purify the multi-functional origami nanostructures with bound TCR mRNAs from cell lysate. By using a gentle, non-ionic detergent, the origami with protruding probes remains stable and maintains its structural integrity during incubation, even with bound RNA. (Figure 4.5A) Thus, origami is an effective platform to capture intracellular TCR_{α} and TCR_{β} mRNAs.

The following isolation and purification steps used to separate origami with bound RNAs from excess, unbound free RNAs and other cellular debris in the cell lysate, utilize selected, biotin modified staple strands that strongly bind to immobilized streptavidin beads. This approach maximizes the stability of bound cellular mRNAs on origami while efficiently removing unbound RNAs.

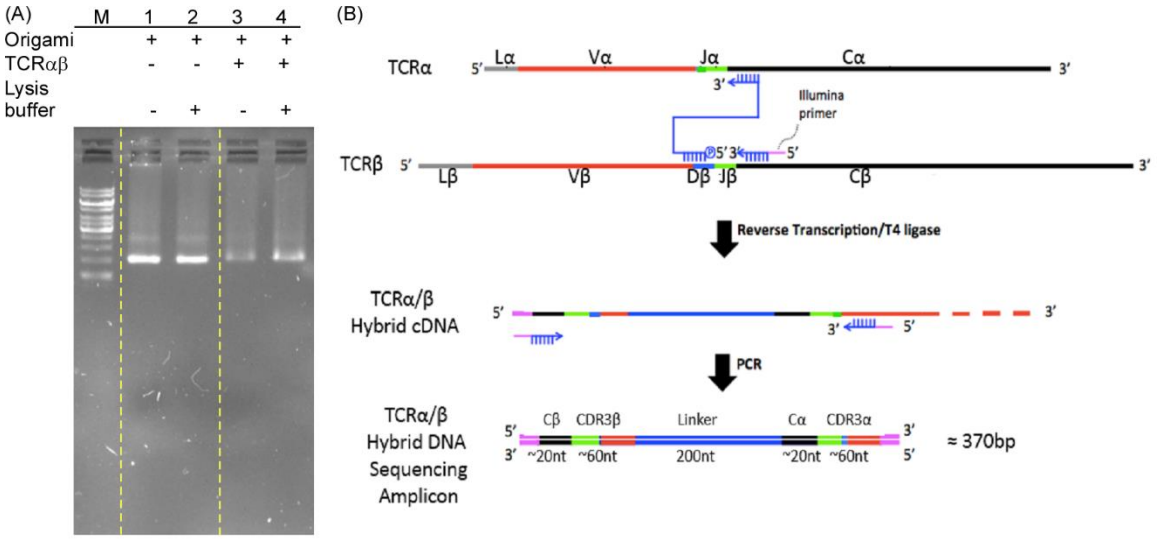

Figure 4.5 Isolating origami with bound mRNAs and the amplification strategy used to link TCR pair information. (A) Stability of origami with/without bound RNAs in cell lysis buffer. The pure origami in lysis buffer bands (lane 2) have the same mobility as the control band (lane 1) on a 1% agarose gel. Origami with bound RNA are also stable (lane 4) compared to the control band (Lane 3). (B) Reverse transcription, ligation, PCR amplification and TCR CDR3 sequencing. A dual-primer reverse transcription reaction using an upstream Cβ primer and a pool of downstream Vβ-linker-Cα primers are annealed and the first strand synthesized using an MMuLV exonuclease deficient RT enzyme to minimize downstream primer displacement. Intermediate products are ligated with T4 ligase, resulting in linked CDR3 information from both mRNAs into a single cDNA molecule. PCR amplification was performed by a single Cβ primer and a pool of Vα primers. Finally, the mixture of amplicons containing both TCRα and TCRβ CDR3 information from single cells are evaluated by standard Illumina paired end sequencing.

A novel, multiplex, dual-primer T-ligation-PCR system was developed to amplify rearranged TCRαβ cDNA "hybrids". A flexible single stranded linker is added to the system after origamis with bound RNA pairs are isolated. The 5' end of the linker binds to the Vβ region and the 3' end of the linker is complementary to the Cα region and also serves as a RT primer of TCRα. The length of the linker is the approximate distance between the two lines of probes on the same origami, such that the linker is within the range accessible to both TCRαβ RNA bound to a single origami, but not long enough to link RNAs from different origami. With the help of the linker, the upstream and

downstream reverse transcribed intermediate structures are ligated using a T4 RNA/DNA dependent ligase, resulting in "hybrid" cDNA that contains CDR3 information from the two mRNA species. Multiplex PCR is then utilized to generate a pool of amplicons containing paired CDR3 information from the same origami, and thus, from the same cell. Finally, an entire population of amplification products can be sequenced simultaneously and the sequences aligned by specific genes, including CDR3 sequences identifying the T cell composition of the original sample. The whole process is illustrated in Figure 4.5B.

4.5.4 Identifying TCRα and TCRβ mRNA sequences

After isolation and purification, we first confirmed whether the captured RNA was still immobilized and protected by the origami, and capable of being reverse transcribed and amplified using our system. The bands corresponding to the correct amplicons from either the TCR α or β mRNAs migrate the same distance as the positive control. Origami without probes to capture RNAs did not get amplified since the free RNAs were completely removed after purification. (Figure 4.6A) The results demonstrate that the origami stabilizes the RNAs during the purification treatment and that the bound RNAs are accessible to the following amplification. The amplicons resulting from the complete RT-ligation-PCR approach matched the predicted length. (Figure 4.6B)

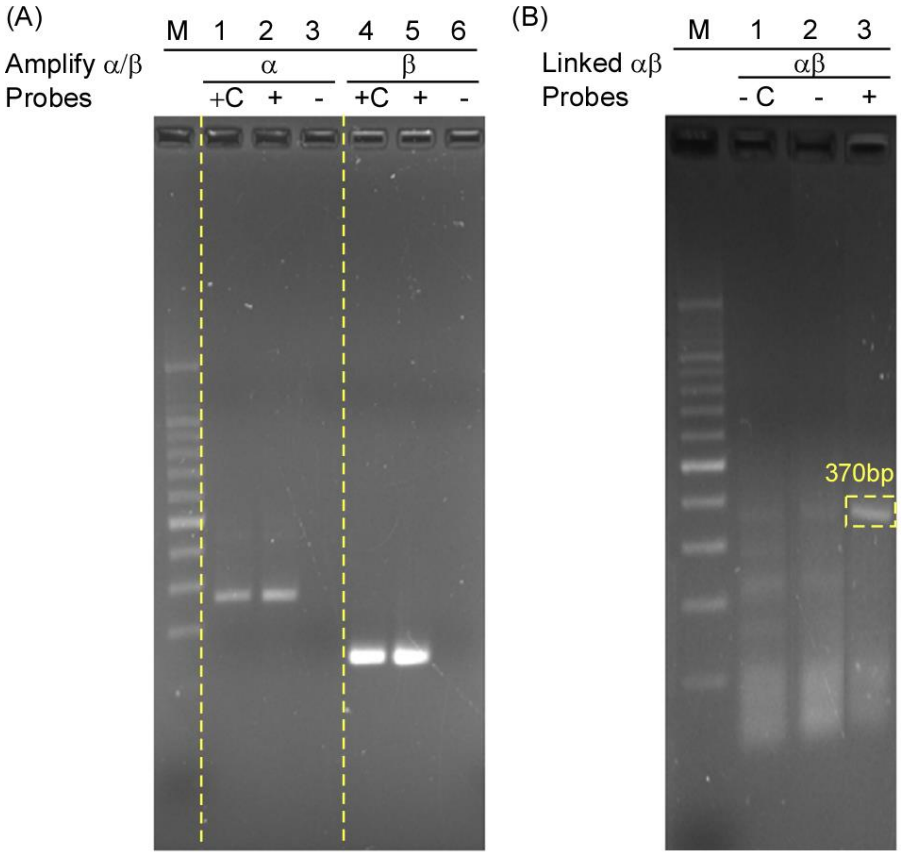

Figure 4.6 Gel verification of RT-PCR amplification of TCR α or β mRNAs and RT-ligation-PCR linked amplicons from both RNAs. (A) Amplification of only TCR α or β mRNA. Lane 1 is the positive control of TCRα only without origami and isolation. Lane 2 is the amplification of bound TCRα RNA on multi-probe origami after purification. Lane 3 is negative control of origami without probes. Lanes 4-6 are similar TCRβ text samples. (B) The final amplicons of RT-ligation-PCR exhibit the correct 370 bp length on 2% agarose gel (Lane 3). Lane 1 is a negative control of free RNA that cannot be linked due to a large distance. Lane 2 is another negative control of origami without probes.

The amplicons obtained from P14 T cells were purified from gel and subjected to conventional sequencing. The obtained sequences are identical to the theoretical sequences, including partial V, full J, partial C of published P14 TCRα, followed by the linker sequence, and partial V, full D and J, partial C of P14 TCRβ. (Figure 4.7)

Therefore, we can easily obtain CDR3 information for both TCRα and TCRβ, as we expected.

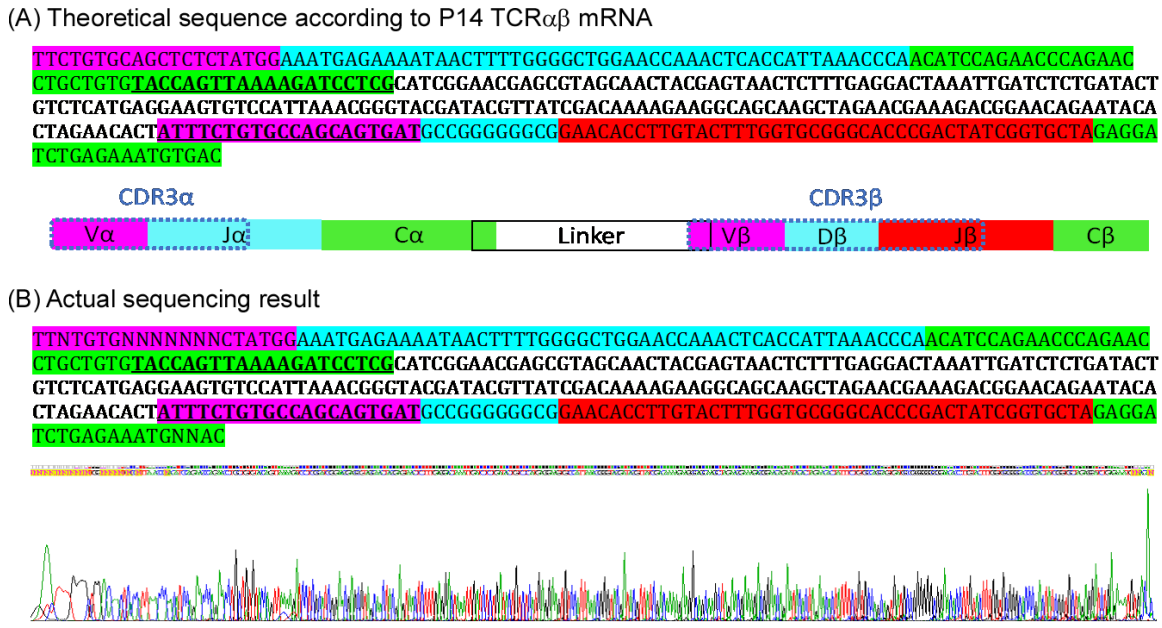

Figure 4.7 Dual-primer RT-ligation-PCR sequencing result. (A) Theoretical sequence according to published P14 CDR3 for both TCRα and TCRβ as well as the linker sequence. The sequences of specific regions are indicated with corresponding colors. (B) The actual obtained sequencing result is identical to part A.

4.6 Conclusions

We developed a novel strategy to evaluate paired TCRαβ RNA information in individual cells from a large cell population. Multifunctional origami was efficiently transfected into cells, captured the target mRNA within the cells, stabilized and protected RNA from degradation, and together with the mRNAs, ultimately isolated from cell lysate and amplified into amplicons that were analyzed. Most importantly, the addressability of origami affords a universal linking method to integrate information from

pair of individual RNAs into one cDNA strand, avoiding the need for single cell sorting when analyzing gene sequences from single cells within heterogeneous cell populations. This technique can easily be adapted to different systems for different targets such as analysis of cells from other species, cells expressing other immunoreceptors, or specific mutations in cancer cells or cancer stem cells, by relatively simple modifications to the DNA origami nanostructure.

Although we only performed this approach in transgenic P14 T cells to demonstrate proof of principle, it is possible to apply this approach to the analysis of heterodimeric T cell receptors and establish rapid identification of heterogeneous T cells in the pre-immune repertoire. The knowledge of linked TCRα and TCRβ sequences from human cells is critical for thoroughly understanding immune competence in aging individuals (decreasing diversity) or individuals undergoing bone marrow transplants after radiation and chemotherapy (increasing diversity).

Conventional approaches for antibody development involve single cell sorting of antibody-producing plasma T cells, fusion of sorted clones with immortalized cell lines to generate hybridomas, propagation of hybridomas *in vitro*, and screening of hybridomas for antigen binding. Such approaches are time-consuming, costly, and have inherent biases in the selection and survival of T cells. The DNA origami nanostructure approach provides a much more rapid process for antibody development, requiring only transfection of antigen-binding T cell populations, linking TCR_{α} and TCR_{β} mRNA into a single cDNA via the unique molecular biology strategy facilitated by the nanostructure geometry, sequence analysis of linked TCR, and construction of single-chain antibody

phage-display libraries for screening. This approach requires only days-weeks, rather than the weeks-months associated with traditional approaches for antibody identification.

4.7 References

(1) Nikolich-Zugich, J., Slifka, M. K., Messaoudi, I. *Nat Rev Immunol*, **2004**. 2, 123-32.

(2) Davis, M. M., Bjorkman, P. J. *Nature*, **1988**. 6181, 395-402.

(3) Arstila, T.P., Casrouge, A., Baron, V., Even, J., Kanellopoulos, J., Kourilsky, P. *Science*, **1999**. 5441, 958-61.

(4) Casrouge, A., Beaudoing, E., Dalle, S., Pannetier, C., Kanellopoulos, J., Kourilsky, P. *J. Immunol*, **2000**, 11, 5782-7.

(5) Dash, P., McClaren, J. L., Oguin, T. H., Rothwell, W., Todd, B., Morris, M. Y., Becksfort, J., Reynolds, C., Brown, S. A., Doherty, P. C., Thomas, P. G. *J Clin Invest*, **2011**. 1, 288-95.

(6) Asirvatham, A.J. Gregoriea, C. J., Hub, Z., Magnera, W. J., B. Tomasi, T. B. *Mol Immunol*, **2008**. 45, 1995-2006.

(7) Zhang, N., Bevan, M. J. *Proc Natl Acad Sci USA*, **2010**. 50, 21629-34.

(8) Quigley, M.F., Greenaway, H. Y., Venturi, V., Lindsay, R., Quinn, K. M.,Seder, R. A., Douek, D. C., Davenport, M. P., Price, D. A. *Proc Natl Acad Sci U S A*, **2010**. 45, 19414-9.

(9) Lin, C., Liu, Yan., Yan, H. *Biochemistry*, **2009**, *8*, 1663‑74.

(10) Pinheiro, A. V., Han, D., Shih, W. M. , Yan, H. *Nature Nanotech.* **2011**, 6, 763‑72.

(11) Fu, J., Liu, M., Liu, Y., Yan, H. *Acc. Chem. Res.* 2012, **45**, 1215‑26.

(12) Rothemund, P. W. *Nature.* **2006**, *440*, 297-302.

(13) Ke, Y.; Lindsay, S.; Chang, Y.; Liu, Y.; Yan, H. *Science*, **2008**, 319, 180‑3.

(14) Mei, Q., Wei, X., Su, F., Liu, Y., Youngbull, C., Johnson, R., Lindsay, S., Yan, H. and Meldrum, D., *Nano Lett*, **2011**. 11:1477-82.

Chapter 5

PERSPECTIVES ON THERMODYNAMIC STUDIES AND BIOLOGICAL APPLICATIONS OF DNA NANOSTRUCTURES

5.1 Future directions of thermodynamic studies

Researchers in DNA nanotechnology have put significant effort into designing more complicated and functional assemblies, and are exploring an ever wider range of applications, but have long been lacking vital information about the thermodynamics and kinetics of the structures to guide them. Uncovering the intricate details of the assembly process will allow us to thoroughly understand, expertly control, and efficiently optimize structural design and applications.

Although the current tools and techniques available have already revealed much about the thermodynamic and kinetic properties of DNA nanostructures, there are many remaining challenges to unravel the complexities of their behavior. For example, the rate of crossover formation during the assembly of DNA tile motifs has rarely been studied, and is an important factor that influences the outcomes of assembly. In addition, the folding/disassociation behavior of DNA origami structures is still largely unknown due to the great number of interactions between many strands, and it is important for researchers to continue developing appropriate analytical tools, approaches, and models to better understand the kinetic behavior of complex DNA nanostructures.

Today, dynamic and transformable structures are mostly achieved by strand displacement reactions, where the transformation of a pre-formed structure is triggered by external fuel strands.[1, 2] In the future, it may be possible to realize structural transformations by subtly controlling temperature fluctuations (and thus energy

input/release). Recently, advanced techniques like cryo-electron microscopy (cryo-EM)[3] and all-atom molecular dynamics (MD)[4] have been applied to reveal additional characteristics of dynamic DNA nanostructures. These methods may provide precise and perceptual macro- and microscopic analyses of these complex structures.

With a substantial understanding of the thermodynamic and kinetic properties of DNA nanostructures, including the stabilities and energy requirements to achieve certain designs, one can identify the ideal temperatures for assembly and predict the rates of nanostructure formation, which will lead to improved design outcomes (higher yield, faster rate), efficient suppression of the formation of unwanted side-products and avoid the labor-intensive, trial-and-error approach. Moreover, software that takes these parameters into account can potentially predict the outcomes of any sequence design, optimize the strand sequences, lengths of sticky ends and positions of crossovers, etc. A database may be established for screening the most frequent and efficient motifs for practical, customized conditions. Both experimental and theoretical researchers can benefit from this, and eventually much of the design process can be automated.

5.2 Perspectives of biological applications

Based on more accurate control and stabilization, biocompatible DNA nanostructures can be utilized for many attractive applications. By optimizing the capture sequences, interactions, and orientations of components more carefully, DNA structures can serve as ideal platforms to arrange and organize other materials. Employing milder assembly conditions will ensure more stable immobilization and minimize the damage to individual components.

The suitable size of DNA nanostructures, as well as their biocompatibility and signaling capacity makes them ideal platforms for in cell or *in vivo* detection. In the previous chapter, I proposed a strategy to capture biomolecules in cells for subsequent analysis. Moreover, co-localized detection can be realized as well if fluorescent signaling is turned on when a target has been detected.[5] This can be applied to *in vivo* diagnostics, for minimal cost, risk and time.

Controllable, predicable and dynamically transformable DNA structures[6] are very good candidates to mimic or control biological processes which require accurate control over stoichiometry and timing. They can participate in *in vivo* regulation, and even dual-direction regulation in the future, by carefully designing switchable DNA nanostructures to promote forward reactions under one set of conditions and inhibit or trigger backward reactions in other conditions. It is also possible to achieve *in vivo* therapies[7], e.g. controlled dynamic drug release with specific interaction, activation and actuatation at specific locations and certain time points.

One outstanding feature of DNA nanostructures compared to other nano scale particles is the integration of multiple functions on individual structures, which can be realized by simple chemical reactions. This can significantly reduce the number of nano particles, each of which serves a different purpose, required for one procedure. For example, vaccine based DNA nanostructures can be developed to trigger multiple correlative immune responses when recognized by certain cellular receptors, minimizing other risks.[8]

In summary, a thorough understanding of the DNA assembly process will guide structural designs, reduce accumulated errors during self-assembly, and optimize the

conditions for preparation, manipulation, and functionalization of DNA nanostructures, ultimately benefiting both upstream design and downstream applications. Meanwhile, the excellent characteristics of DNA nanostructures and the countless potential multi-functionalization strategies will continue to contribute to biological and biomedical fields and will likely lead to breakthroughs of broad application.

5.3 References

(1) Han, D.; Pal, S.; Liu, Y.; Yan, H. *Nat. Nanotech.* **2010**, *5*, 712-717.

(2) Zhang, F.; Nangreave, J.; Liu, Y.; Yan, H. *Nano Lett.* **2012**, *12*, 3290-5.

(3) Bai, X. c.; Martin, T. G.; Scheres, S. H. W.; Dietz, H. *Proc. Natl. Acad. Sci. USA* **2012**, *109*, 20012-20017.

(4) Yoo, J.; Aksimentiev, A. *Proc. Natl. Acad. Sci. USA* **2013**, *110*, 20099-104.

(5) Lin, C.; Jungmann, R.; Leifer, A. M.; Li, C.; Levner, D.; Church, G. M.; Shih, W. M.; Yin, P. *Nat. Chem.* **2012**, *4*, 832-9.

(6) Liu, M., Fu, J., Hejesen, C., Yang, Y., Woodbury, N. M., Gothelf, K., Liu, Y., Yan, H. *Nature Comm*. **2013**, 4, 2127.

(7) Lee, H. , Lytton-Jean, A. K. R., Chen, Y., Love, K. T., Park, A. I., Karagiannis, E. D., Sehgal, A., Querbes, W., Zurenko, C. S., Jayaraman, M., Peng, C. G., Charisse, K., Borodovsky, A., Manoharan, M., Donahoe, J. S., Truelove, J., Nahrendorf, M., Langer, R., Anderson, D. G. *Nat. Nanotechnol.* **2012** , 7 , 389 .

(8) Liu, X., Xu, Y., Yu, T., Craig, C., Liu, Y., Yan, H., Chang, Y. *Nano Letters*, **2012**, 12, 4254‑9.

Bibliography

Chapter 1 References

(1) Ke, Y.; Bellot, G.; Voigt, N. V.; Fradkov, E.; Shih, W. M. *Chem. Sci.* **2012**, *3*, 2587.

(2) Ke, Y.; Ong, L. L.; Shih, W. M.; Yin, P. *Science* **2012**, *338*, 1177-83.

(3) Fu, J.; Liu, M.; Liu, Y.; Woodbury, N. W.; Yan, H. *J. Am. Chem. Soc.* **2012**, *134*, 5516-9.

(4) Douglas, S. M.; Bachelet, I.; Church, G. M. *Science* **2012**, *335*, 831-4.

(5) Lin, C.; Jungmann, R.; Leifer, A. M.; Li, C.; Levner, D.; Church, G. M.; Shih, W. M.; Yin, P. *Nat. Chem.* **2012**, *4*, 832-9.

(6) Lund, K.; Manzo, A. J.; Dabby, N.; Michelotti, N.; Johnson-Buck, A.; Nangreave, J.; Taylor, S.; Pei, R.; Stojanovic, M. N.; Walter, N. G.; Winfree, E.; Yan, H. *Nature* **2010**, *465*, 206-10.

(7) Seeman, N. C.; Kallenbach, N. R. *Annu. Rev. Biophys. Biomol. Struct.* **1994**, *23*, 53-86.

(8) Ke, Y.; Liu, Y.; Zhang, J.; Yan, H. *J. Am. Chem. Soc.* **2006**, *128*, 4414-4421.

(9) Yan, H.; Park, S. H.; Finkelstein, G.; Reif, J. H.; LaBean, T. H. *Science* **2003**, *301*, 1882-4.

(10) Zhang, D. Y.; Hariadi, R. F.; Choi, H. M.; Winfree, E. *Nat. Commun.* **2013**, *4*, 1965.

(11) Han, D.; Pal, S.; Liu, Y.; Yan, H. *Nat. Nanotech.* **2010**, *5*, 712-717.

(12) Rothemund, P. W.; Papadakis, N.; Winfree, E. *PLoS Biol.* **2004**, *2*, e424.

(13) Nangreave, J.; Yan, H.; Liu, Y. *Biophys. J.* **2009**, *97*, 563-71.

(14) Nangreave, J.; Yan, H.; Liu, Y. *J. Am. Chem. Soc.* **2011**, *133*, 4490-7.

(15) Song, J.; Arbona, J. M.; Zhang, Z.; Liu, L.; Xie, E.; Elezgaray, J.; Aime, J. P.; Gothelf, K. V.; Besenbacher, F.; Dong, M. *J. Am. Chem. Soc.* **2012**, *134*, 9844-7.

(16) SantaLucia, J., Jr.; Turner, D. H. *Biopolymers* **1997**, *44*, 309-19.

(17) Sobczak, J. P.; Martin, T. G.; Gerling, T.; Dietz, H. *Science* **2012**, *338*, 1458-61.

(18) Reed, G. H.; Kent, J. O.; Wittwer, C. T. *Pharmacogenomics* **2007**, *8*, 597-608.

(19) Sacca, B.; Meyer, R.; Feldkamp, U.; Schroeder, H.; Niemeyer, C. M. *Angew. Chem. Int. Ed. Engl.* **2008**, *47*, 2135-7.

(20) Morrison, L. E.; Stols, L. M. *Biochemistry* **1993**, *32*, 3095-104.

(21) Wei, X.; Nangreave, J.; Jiang, S.; Yan, H.; Liu, Y. *J. Am. Chem. Soc.* **2013**, *135*, 6165-76.

(22) Pinheiro, A. V.; Nangreave, J.; Jiang, S.; Yan, H.; Liu, Y. *ACS Nano.* **2012**, *6*, 5521-30.

(23) Marky, L. A.; Kallenbach, N. R.; McDonough, K. A.; Seeman, N. C.; Breslauer, K. J. *Biopolymers* **1987**, *26*, 1621-1634.

(24) SantaLucia, J., Jr.; Hicks, D. *Annu. Rev. Biophys. Biomol. Struct.* **2004**, *33*, 415-40.

(25) SantaLucia, J., Jr. *Proc. Natl. Acad. Sci. USA* **1998**, *95*, 1460-5.

(26) Howard, K. P. *J. Chem. Educ.* **2000**, *77*, 1469.

(27) Hou, M. H.; Lin, S. B.; Yuann, J. M.; Lin, W. C.; Wang, A. H.; Kan Ls, L. *Nucleic acids Res.* **2001**, *29*, 5121-8.

(28) Rauzan, B.; McMichael, E.; Cave, R.; Sevcik, L. R.; Ostrosky, K.; Whitman, E.; Stegemann, R.; Sinclair, A. L.; Serra, M. J.; Deckert, A. A. *Biochemistry* **2013**, *52*, 765-72.

(29) Fu, T. J.; Seeman, N. C. *Biochemistry* **1993**, *32*, 3211-20.

(30) Chen, H. L.; Schulman, R.; Goel, A.; Winfree, E. *Nano Lett.* **2007**, *7*, 2913-9.

(31) Rinker, S.; Liu, Y.; Yan, H. *Chem. Commun.* **2006**, 2675-7.

(32) LaBean, T. H.; Yan, H.; Kopatsch, J.; Liu, F.; Winfree, E.; Reif, J. H.; Seeman, N. C. *J. Am. Chem. Soc.* **2000**, *122*, 1848-1860.

(33) Spink, C. H.; Ding, L.; Yang, Q.; Sheardy, R. D.; Seeman, N. C. *Biophys. J.* **2009**, *97*, 528-38.

(34) Du, S. M.; Zhang, S.; Seeman, N. C. *Biochemistry* **1992**, *31*, 10955-63.

(35) Zhang, D. Y.; Winfree, E. *J. Am. Chem. Soc.* **2009**, *131*, 17303-17314.

(36) Fu, Y.; Zeng, D.; Chao, J.; Jin, Y.; Zhang, Z.; Liu, H.; Li, D.; Ma, H.; Huang, Q.; Gothelf, K. V.; Fan, C. *J. Am. Chem. Soc.* **2013**, *135*, 696-702.

(37) Myhrvold, C.; Dai, M.; Silver, P. A.; Yin, P. *Nano Lett.* **2013**, *13*, 4242-8.

(38) Jungmann, R.; Liedl, T.; Sobey, T. L.; Shih, W.; Simmel, F. C. *J. Am. Chem. Soc.***2008**, *130*, 10062-10063.

(39) Zhang, Z.; Song, J.; Besenbacher, F.; Dong, M.; Gothelf, K. V. *Angew. Chem. Int. Ed. Engl.* **2013**, *52*, 9219-23.

(40) Rothemund, P. W. *Nature.* **2006**, *440*, 297-302.

(41) Lin, C., Liu, Yan., Yan, H. *Biochemistry*, **2009**, *8*, 1663‑74.

(42) Pinheiro, A. V., Han, D., Shih, W. M. , Yan, H. *Nature Nanotech.* **2011**, 6, 763‑72.

(43) Fu, J., Liu, M., Liu, Y., Yan, H. *Acc. Chem. Res.* 2012, **45**, 1215‑26.

(44) Sharma, J., Chhabra, R., Cheng, A., Brownell, J., Liu, Y., Yan, H. *Science*, **2009**, 323, 112-6.

(45) Deng, Z., Samanta, A., Nangreave, J., Yan, H., Liu, Y. *J. Am. Chem. Soc.*, **2012**, 134, 17424‑27.

(46) Dutta, P. K.; Varghese, R.; Nangreave, J.; Lin, S.; Yan, H.; Liu, Y. *J. Am. Chem. Soc.* **2011**, 133, 11985‑ 93.

(47) Liu, X., Liu, Y., Yan, H. *Israel Journal of Chemistry, Special Issue on Supramolecular Chemistry for Materials and Medicine*, **2013**, 53, 555-66.

(48) Liu, X., Yan, H., Liu, Y., Chang, Y. *Small*, **2011**, 7, 1673‑82.

(49) Zhong, H., Zhang, Q. L., Zhang, S. S. *Chem-Eur J* 2011, 17, 8388-94.

(50) Dutta, P. K., Lin, S., Loskutov, A., Levenberg, S., Saer, R., Beatty, J. T., Liu, Y., Yan, H., Woodbury, N. *J. Am. Chem. Soc.* **2014**, 136, 4599‑ 604.

(51) Qian., L., Winfree, E. *Science*, **2011**, 332, 1196-201.

(52) Qian., L., Winfree, E., Bruck, J. *Nature*, **2011**. 475, 368-72.

(53) Ke, Y.; Lindsay, S.; Chang, Y.; Liu, Y.; Yan, H. *Science*, **2008**, 319, 180‑3.

(54) Gascoigne, N. R. *Nat. Rev. Immunol.* **2008**, 11, 895-900.

(55) http://shiyan.ebioe.com//13444.htm

(56) Kazena, A. R., Adamsa, E. J. *Proc. Natl. Acad. Sci. USA* **2011**, 108, 11743-4.

(57) Davis, M. M., Bjorkman, P. J. *Nature*, **1988**. 6181, 395-402.

(58) Newell, E. W., Davis, M. M. *Nat. Biotechnol*. **2014**, 32, 149-57.

(59) Donermeyer, D. L., Weber, K. S., Kranz, D. M., Allen, P. M. *J. Immunol.* **2006**, 177, 6911-9.

(60) Arstila, T.P., Casrouge, A., Baron, V., Even, J., Kanellopoulos, J., Kourilsky, P. *Science*, **1999**. 5441, 958-61.

(61) Casrouge, A., Beaudoing, E., Dalle, S., Pannetier, C., Kanellopoulos, J., Kourilsky, P. *J. Immunol*, **2000**, 11, 5782-7.

(62) Arnaout, R., Lee, W., Cahill, P., Honan, T., Sparrow, T., Weiand, M., Nusbaum, C., Rajewsky, K., Koralov, S. B. *PLoS ONE* **2011**, 8, e22365.

(63) Travers, P., M., Walport, M. Janeway, C. *Janeway's immunobiology*. Garland Science, **2008**.

(64) Dash, P., McClaren, J. L., Oguin, T. H., Rothwell, W., Todd, B., Morris, M. Y., Becksfort, J., Reynolds, C., Brown, S. A., Doherty, P. C., Thomas, P. G. *J Clin Invest*, **2011**. 1, 288-95.

(65) Asirvatham, A.J. Gregoriea, C. J., Hub, Z., Magnera, W. J., B. Tomasi, T. B. *Mol Immunol*, **2008**. 45, 1995-2006.

(66) Zhang, N., Bevan, M. J. *Proc Natl Acad Sci USA*, **2010**. 50, 21629-34.

Chapter 2 References

(1) Pinheiro, A. V.; Han, D.; Shih, W. M.; Yan, H. *Nat. Nanotechnol.* **2011**, *6*, 763.

(2) Nangreave, J.; Han, D.; Liu, Y.; Yan, H. *Curr. Opin. Chem. Biol.* **2010**, *14*, 608.

(3) Seeman, N. C. *Mol. Biotechnol.* **2007**, *37*, 246.

(4) Rothemund, P. W. *Nature* **2006**, *440*, 297.

(5) Dietz, H.; Douglas, S. M.; Shih, W. M. *Science* **2009**, 325, 725.

(6) Douglas, S. M.; Dietz, H.; Liedl, T.; Hogberg, B.; Graf, F.; Shih, W. M. *Nature* **2009**, 459, 414.

(7) Gu, H.; Chao, J.; Xiao, S. J.; Seeman, N. C. *Nat. Nanotechnol.* **2009**, *4*, 245.

(8) Seeman, N. C. *Annu. Rev. Biochem.* **2010**, *79*, 65.

(9) Castro, C. E.; Kilchherr, F.; Kim, D. N.; Shiao, E. L.; Wauer, T.; Wortmann, P.; Bathe, M.; Dietz, H. *Nat. Methods* **2011**, *8*, 221.

(10) Sobey, T. L.; Renner, S.; Simmel, F. C. *J. Phys. Condens. Matter* **2009**, *21*, 034112.

(11) Rajendran, A.; Endo, M.; Katsuda, Y.; Hidaka, K.; Sugiyama, H. *J. Am. Chem. Soc.* **2011**, *133*, 14488.

(12) Mergny, J. L.; Lacroix, L. *Oligonucleotides* **2003**, *13*, 515.

(13) Song, J.; Arbona, J. M.; Zhang, Z.; Liu, L.; Xie, E.; Elezgaray, J.; Aime, J. P.; Gothelf, K. V.; Besenbacher, F.; Dong, M. *J. Am. Chem. Soc.* **2012**, *134*, 9844.

(14) Sobczak, J. P. J.; Martin, T. G.; Gerling, T.; Dietz, H. *Science* **2012**, *338*, 1458.

(15) Forster, T. *Discuss. Faraday Soc.* **1959**, 7.

(16) Lilley, D. M. J.; Wilson, T. J. *Curr. Opin. Chem. Biol.* **2000**, *4*, 507.

(17) Liedl, T.; Simmel, F. C. *Anal. Chem.* **2007**, *79*, 5212.

(18) Stein, I. H.; Schuller, V.; Bohm, P.; Tinnefeld, P.; Liedl, T. *Chem. Phys. Chem.* **2011**, 12, 689.

(19) Sacca, B.; Meyer, R.; Feldkamp, U.; Schroeder, H.; Niemeyer, C. M. *Angew. Chem. Int. Ed.* **2008**, *47*, 2135.

(20) Sacca, B.; Meyer, R.; Niemeyer, C. M. *Nat. Protoc.* **2009**, *4*, 271.

(21) Nangreave, J.; Yan, H.; Liu, Y. *Biophys. J.* **2009**, *97*, 563.

(22) Nangreave, J.; Yan, H.; Liu, Y. *J. Am. Chem. Soc.* **2011**, *133*, 4490.

(23) Dacres, H.; Wang, J.; Dumancic, M. M.; Trowell, S. C. *Anal. Chem.* **2010**, *82*, 432.

(24) Ke, Y.; Douglas, S. M.; Liu, M.; Sharma, J.; Cheng, A.; Leung, A.; Liu, Y.; Shih, W. M.; Yan, H. *J. Am. Chem. Soc.* **2009**, *131*, 15903.

(25) Bowen, E. J.; Sahu, J. *J. Phys. Chem.* **1959**, *63*, 4.

(26) You, Y.; Tataurov, A. V.; Owczarzy, R. *Biopolymers* **2011**, *95*, 472.

(27) Sjoback, R.; Nygren, J.; Kubista, M. *Biopolymers* **1998**, *46*, 445.

(28) Pinheiro, A. V.; Nangreave, J.; Jiang, S.; Yan, H.; Liu, Y. *ACS Nano.* **2012**, *6*, 5521.

(29) Deng, Z.; Samanta, A.; Nangreave, J.; Yan, H.; Liu, Y. *J. Am. Chem. Soc.* **2012**, 134, 17424.

(30) Ding, B.; Wu, H.; Xu, W.; Zhao, Z.; Liu, Y.; Yu, H.; Yan, H. *Nano letters* **2010**.

(31) Pal, S.; Deng, Z.; Ding, B.; Yan, H.; Liu, Y. *Angew. Chem. Int. Ed.* **2010**, 49, 2700.

(32) Bell, N. A.; Engst, C. R.; Ablay, M.; Divitini, G.; Ducati, C.; Liedl, T.; Keyser, U. F. *Nano letters* **2012**, 12, 512.

(33) Douglas, S. M.; Bachelet, I.; Church, G. M. *Science* **2012**, 335, 831.

Chapter 3 References

(1) Rothemund, P. W. K. *Nature* **2006**, 440, 297.

(2) Kuzuya, A.; Komiyama, M. *Nanoscale* **2010**, 2, 310.

(3) Nangreave, J.; Han, D.; Liu, Y.; Yan, H. *Curr. Opin. Chem. Biol.* **2010**, 14, 608.

(4) Douglas, S. M.; Dietz, H.; Liedl, T.; Hogberg, B.; Graf, F.; Shih, W. M. *Nature* **2009**, 459, 414.

(5) Andersen, E. S.; Dong, M.; Nielsen, M. M.; Jahn, K.; Subramani, R.; Mamdouh, W.; Golas, M. M.; Sander, B.; Stark, H.; Oliveira, C. L. P.; Pedersen, J. S.; Birkedal, V.; Besenbacher, F.; Gothelf, K. V.; Kjems, J. *Nature* **2009**, 459, 73.

(6) Ke, Y. G.; Douglas, S. M.; Liu, M. H.; Sharma, J.; Cheng, A. C.; Leung, A.; Liu, Y.; Shih, W. M.; Yan, H. *J. Am. Chem. Soc.* **2009**, 131, 15903.

(7) Dietz, H.; Douglas, S. M.; Shih, W. M. *Science* **2009**, 325, 725.

(8) Kuzuya, A.; Komiyama, M. *Chem Commun* **2009**, 4182.

(9) Endo, M.; Katsuda, Y.; Hidaka, K.; Sugiyama, H. *J. Am. Chem. Soc.* **2010**, 132, 1592.

(10) Lund, K.; Manzo, A. J.; Dabby, N.; Michelotti, N.; Johnson-Buck, A.; Nangreave, J.; Taylor, S.; Pei, R. J.; Stojanovic, M. N.; Walter, N. G.; Winfree, E.; Yan, H. *Nature* **2010**, 465, 206.

(11) Voigt, N. V.; Torring, T.; Rotaru, A.; Jacobsen, M. F.; Ravnsbaek, J. B.; Subramani, R.;Mamdouh,W.; Kjems, J.;Mokhir, A.; Besenbacher, F.; Gothelf, K. V. *Nat. Nanotechnol*. **2010**, 5, 200.

(12) Rinker, S.; Ke, Y. G.; Liu, Y.; Chhabra, R.; Yan, H. *Nat. Nanotechnol*. **2008**, 3, 418.

(13) Kuzuya, A.; Kimura, M.; Numajiri, K.; Koshi, N.; Ohnishi, T.; Okada, F.; Komiyama, M. *Chem Bio Chem* **2009**, 10, 1811.

(14) Kuzyk, A.; Laitinen, K. T.; Torma, P. *Nanotechnology* **2009**, 20.

(15) Ke, Y. G.; Lindsay, S.; Chang, Y.; Liu, Y.; Yan, H. *Science* **2008**, 319, 180.

(16) Subramanian, H. K. K.; Chakraborty, B.; Sha, R.; Seeman, N. C. *Nano Lett*. **2011**, 11, 910.

(17) Kodera, N.; Yamamoto, D.; Ishikawa, R.; Ando, T. *Nature* **2010**, 468, 72.

(18) Sannohe, Y.; Endo, M.; Katsuda, Y.; Hidaka, K.; Sugiyama, H. *J. Am. Chem. Soc.* **2010**, 132, 16311.

(19) Steinhauer, C.; Jungmann, R.; Sobey, T. L.; Simmel, F. C.; Tinnefeld, P. *Angew. Chem., Int. Ed.* **2009**, 48, 8870.

(20) Glasgow, I.; Batton, J.; Aubry, N. *Lab Chip* **2004**, 4, 558.

(21) Howell, P. B.; Mott, D. R.; Fertig, S.; Kaplan, C. R.; Golden, J. P.; Oran, E. S.; Ligler, F. S. *Lab Chip* **2005**, 5, 524.

(22) Mei, Q.; Xia, Z.; Xu, F.; Soper, S. A.; Fan, Z. H. *Anal. Chem*. **2008**, 80, 6045.

(23) Stroock, A. D.; Dertinger, S. K. W.; Ajdari, A.; Mezic, I.; Stone, H. A.; Whitesides, G. M. *Science* **2002**, 295, 647.

(24) Bienvenue, J. M.; Duncalf, N.; Marchiarullo, D.; Ferrance, J. P.; Landers, J. P. J. *Forensic Sci*. **2006**, 51, 266.

(25) Chen, X.; Cui, D. F.; Liu, C. C.; Li, H.; Chen, *J. Anal. Chim. Acta* **2007**, 584, 237.

(26) Kim, J.; Jang, S. H.; Jia, G. Y.; Zoval, J. V.; Da Silva, N. A.; Madou, M. J. *Lab Chip* **2004**, 4, 516.

(27) McClain, M. A.; Culbertson, C. T.; Jacobson, S. C.; Allbritton, N. L.; Sims, C. E.; Ramsey, *J. M. Anal. Chem*. **2003**, 75, 5646.

(28) Mun, B. P.; Jung, S. M.; Yoon, S. Y.; Kim, S. H.; Lee, J. H.; Yang, S. *Microfluid. Nanofluid.* **2010**, 8, 695.

(29) Schilling, E. A.; Kamholz, A. E.; Yager, P. *Anal. Chem*. **2002**, 74, 1798.

(30) Das, C.; Zhang, J.; Denslow, N. D.; Fan, Z. H. *Lab Chip* **2007**, 7, 1806.

(31) Fan, R.; Vermesh, O.; Srivastava, A.; Yen, B. K. H.; Qin, L. D.; Ahmad, H.; Kwong, G. A.; Liu, C. C.; Gould, J.; Hood, L.; Heath, J. R. *Nat. Biotechnol*. **2008**, 26, 1373.

(32) Hatch, A. V.; Herr, A. E.; Throckmorton, D. J.; Brennan, J. S.; Singh, A. K. *Anal. Chem*. **2006**, 78, 4976.

(33) Hellmich, W.; Pelargus, C.; Leffhalm, K.; Ros, A.; Anselmetti, D. *Electrophoresis* **2005**, 26, 3689.

(34) Barton, G. M.; Medzhitov, R. *Proc. Natl. Acad. Sci. U.S.A.* **2002**, 99, 14943.

(35) Mitchell, P. *Nat. Biotechnol*. **2001**, 19, 1013.

(36) Palanca-Wessels, M. C.; Barrett, M. T.; Galipeau, P. C.; Rohrer, K. L.; Reid, B. J.; Rabinovitch, P. S. *Gastroenterology* **1998**, 114, 295.

Chapter 4 References

(1) Nikolich-Zugich, J., Slifka, M. K., Messaoudi, I. *Nat Rev Immunol*, **2004**. 2, 123-32.

(2) Davis, M. M., Bjorkman, P. J. *Nature*, **1988**. 6181, 395-402.

(3) Arstila, T.P., Casrouge, A., Baron, V., Even, J., Kanellopoulos, J., Kourilsky, P. *Science*, **1999**. 5441, 958-61.

(4) Casrouge, A., Beaudoing, E., Dalle, S., Pannetier, C., Kanellopoulos, J., Kourilsky, P. *J. Immunol*, **2000**, 11, 5782-7.

(5) Dash, P., McClaren, J. L., Oguin, T. H., Rothwell, W., Todd, B., Morris, M. Y., Becksfort, J., Reynolds, C., Brown, S. A., Doherty, P. C., Thomas, P. G. *J Clin Invest*, **2011**. 1, 288-95.

(6) Asirvatham, A.J. Gregoriea, C. J., Hub, Z., Magnera, W. J., B. Tomasi, T. B. *Mol Immunol*, **2008**. 45, 1995-2006.

(7) Zhang, N., Bevan, M. J. *Proc Natl Acad Sci USA*, **2010**. 50, 21629-34.

(8) Quigley, M.F., Greenaway, H. Y., Venturi, V., Lindsay, R., Quinn, K. M.,Seder, R. A., Douek, D. C., Davenport, M. P., Price, D. A. *Proc Natl Acad Sci U S A*, **2010**. 45, 19414-9.

(9) Lin, C., Liu, Yan., Yan, H. *Biochemistry*, **2009**, *8*, 1663‑74.

(10) Pinheiro, A. V., Han, D., Shih, W. M. , Yan, H. *Nature Nanotech.* **2011**, 6, 763‑72.

(11) Fu, J., Liu, M., Liu, Y., Yan, H. *Acc. Chem. Res.* 2012, **45**, 1215‑26.

(12) Rothemund, P. W. *Nature*. **2006**, *440*, 297-302.

(13) Ke, Y.; Lindsay, S.; Chang, Y.; Liu, Y.; Yan, H. *Science*, **2008**, 319, 180‑3.

(14) Mei, Q., Wei, X., Su, F., Liu, Y., Youngbull, C., Johnson, R., Lindsay, S., Yan, H. and Meldrum, D., *Nano Lett*, **2011**. 11:1477-82.

Chapter 5 References

(1) Han, D.; Pal, S.; Liu, Y.; Yan, H. *Nat. Nanotech.* **2010**, *5*, 712-717.

(2) Zhang, F.; Nangreave, J.; Liu, Y.; Yan, H. *Nano Lett.* **2012**, *12*, 3290-5.

(3) Bai, X. c.; Martin, T. G.; Scheres, S. H. W.; Dietz, H. *Proc. Natl. Acad. Sci. USA* **2012**, *109*, 20012-20017.

(4) Yoo, J.; Aksimentiev, A. *Proc. Natl. Acad. Sci. USA* **2013**, *110*, 20099-104.

(5) Lin, C.; Jungmann, R.; Leifer, A. M.; Li, C.; Levner, D.; Church, G. M.; Shih, W. M.; Yin, P. *Nat. Chem.* **2012**, *4*, 832-9.

(6) Liu, M., Fu, J., Hejesen, C., Yang, Y., Woodbury, N. M., Gothelf, K., Liu, Y., Yan, H. *Nature Comm*. **2013**, 4, 2127.

(7) Lee, H. , Lytton-Jean, A. K. R., Chen, Y., Love, K. T., Park, A. I., Karagiannis, E. D., Sehgal, A., Querbes, W., Zurenko, C. S., Jayaraman, M., Peng, C. G., Charisse, K., Borodovsky, A., Manoharan, M., Donahoe, J. S., Truelove, J., Nahrendorf, M., Langer, R., Anderson, D. G. *Nat. Nanotechnol.* **2012** , 7 , 389 .

(8) Liu, X., Xu, Y., Yu, T., Craig, C., Liu, Y., Yan, H., Chang, Y. *Nano Letters*, **2012**, 12, 4254‑9.

APPENDIX A

SUPPLEMENTAL INFORMATION FOR CHAPTER 2

(THERMODYNAMICS OF 2D AND 3D DNA ORIGAMI)

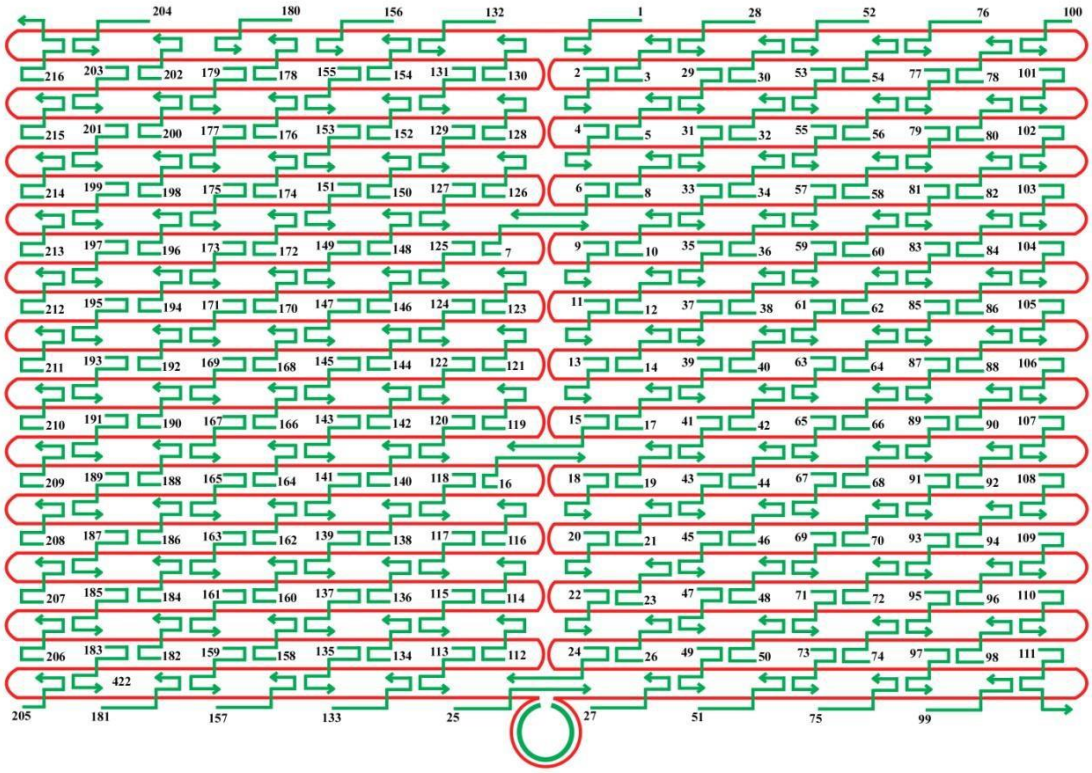

Figure S2.1. Schematic design of the reference 2D rectangular origami structure.

Table S2.1. Helper strand sequences of 2D rectangular origami.

Name	Sequence
1	CAAGCCCAATAGGAAC CCATGTACAAACAGTT
2	AATGCCCCGTAACAGT GCCCGTATCTCCCTCA
3	TGCCTTGACTGCCTAT TTCGGAACAGGGATAG
4	GAGCCGCCCCACCACC GGAACCGCGACGGAAA
5	AACCAGAGACCCTCAG AACCGCCAGGGGTCAG
6	TTATTCATAGGGAAGG TAAATATT CATTCAGT
7	CATAACCCGAGGCATA GTAAGAGC TTTTTAAG
8	ATTGAGGGTAAAGGTG AATTATCAATCACCGG
9	AAAAGTAATATCTTAC CGAAGCCCTTCCAGAG
10	GCAATAGCGCAGATAG CCGAACAATTCAACCG
11	CCTAATTTACGCTAAC GAGCGTCTAATCAATA
12	TCTTACCAGCCAGTTA CAAAATAAATGAAATA
13	ATCGGCTGCGAGCATG TAGAAACCTATCATAT
14	CTAATTTATCTTTCCT TATCATTCATCCTGAA
15	GCGTTATAGAAAAAGC CTGTTTAG AAGGCCGG
16	GCTCATTTTCGCATTA AATTTTTG AGCTTAGA
17	AATTACTACAAATTCT TACCAGTAATCCCATC
18	TTAAGACGTTGAAAAC ATAGCGATAACAGTAC
19	TAGAATCCCTGAGAAG AGTCAATAGGAATCAT
20	CTTTTACACAGATGAA TATACAGTAAACAATT
21	TTTAACGTTCGGGAGA AACAATAATTTTCCCT
22	CGACAACTAAGTATTA GACTTTACAATACCGA
23	GGATTTAGCGTATTAA ATCCTTTGTTTTCAGG
24	ACGAACCAAAACATCG CCATTAAA TGGTGGTT
25	GAACGTGGCGAGAAAG GAAGGGAA CAAACTAT

26	TAGCCCTACCAGCAGA AGATAAAAACATTTGA
27	CGGCCTTGCTGGTAAT ATCCAGAACGAACTGA
28	CTCAGAGCCACCACCC TCATTTTCCTATTATT
29	CTGAAACAGGTAATAA GTTTTAACCCCTCAGA
30	AGTGTACTTGAAAGTA TTAAGAGGCCGCCACC
31	GCCACCACTCTTTTCA TAATCAAACCGTCACC
32	GTTTGCCACCTCAGAG CCGCCACCGATACAGG
33	GACTTGAGAGACAAAA GGGCGACAAGTTACCA
34	AGCGCCAACCATTTGG GAATTAGATTATTAGC
35	GAAGGAAAATAAGAGC AAGAAACAACAGCCAT
36	GCCCAATACCGAGGAA ACGCAATAGGTTTACC
37	ATTATTTAACCCAGCT ACAATTTTCAAGAACG
38	TATTTTGCTCCCAATC CAAATAAGTGAGTTAA
39	GGTATTAAGAACAAGA AAAATAATTAAAGCCA
40	TAAGTCCTACCAAGTA CCGCACTCTTAGTTGC
41	ACGCTCAAAATAAGAA TAAACACCGTGAATTT
42	AGGCGTTACAGTAGGG CTTAATTGACAATAGA
43	ATCAAAATCGTCGCTA TTAATTAACGGATTCG
44	CTGTAAATCATAGGTC TGAGAGACGATAAATA
45	CCTGATTGAAAGAAAT TGCGTAGACCCGAACG
46	ACAGAAATCTTTGAAT ACCAAGTTCCTTGCTT
47	TTATTAATGCCGTCAA TAGATAATCAGAGGTG
48	AGATTAGATTTAAAAG TTTGAGTACACGTAAA
49	AGGCGGTCATTAGTCT TTAATGCGCAATATTA
50	GAATGGCTAGTATTAA CACCGCCTCAACTAAT
51	CCGCCAGCCATTGCAA CAGGAAAAATATTTTT
52	CCCTCAGAACCGCCAC CCTCAGAACTGAGACT

53	CCTCAAGAATACATGG CTTTTGATAGAACCAC
54	TAAGCGTCGAAGGATT AGGATTAGTACCGCCA
55	CACCAGAGTTCGGTCA TAGCCCCCGCCAGCAA
56	TCGGCATTCCGCCGCC AGCATTGACGTTCCAG
57	AATCACCAAATAGAAA ATTCATATATAACGGA
58	TCACAATCGTAGCACC ATTACCATCGTTTTCA
59	ATACCCAAGATAACCC ACAAGAATAAACGATT
60	ATCAGAGAAAGAACTG GCATGATTTTATTTTG
61	TTTTGTTTAAGCCTTA AATCAAGAATCGAGAA
62	AGGTTTTGAACGTCAA AAATGAAAGCGCTAAT
63	CAAGCAAGACGCGCCT GTTTATCAAGAATCGC
64	AATGCAGACCGTTTTT ATTTTCATCTTGCGGG
65	CATATTTAGAAATACC GACCGTGTTACCTTTT
66	AATGGTTTACAACGCC AACATGTAGTTCAGCT
67	TAACCTCCATATGTGA GTGAATAAACAAAATC
68	AAATCAATGGCTTAGG TTGGGTTACTAAATTT
69	GCGCAGAGATATCAAA ATTATTTGACATTATC
70	AACCTACCGCGAATTA TTCATTTCCAGTACAT
71	ATTTTGCGTCTTTAGG AGCACTAAGCAACAGT
72	CTAAAATAGAACAAAG AAACCACCAGGGTTAG
73	GCCACGCTATACGTGG CACAGACAACGCTCAT
74	GCGTAAGAGAGAGCCA GCAGCAAAAAGGTTAT
75	GGAAATACCTACATTT TGACGCTCACCTGAAA
76	TATCACCGTACTCAGG AGGTTTAGCGGGGTTT
77	TGCTCAGTCAGTCTCT GAATTTACCAGGAGGT
78	GGAAAGCGACCAGGCG GATAAGTGAATAGGTG
79	TGAGGCAGGCGTCAGA CTGTAGCGTAGCAAGG

80	TGCCTTTAGTCAGACG ATTGGCCTGCCAGAAT
81	CCGGAAACACACCACG GAATAAGTAAGACTCC
82	ACGCAAAGGTCACCAA TGAAACCAATCAAGTT
83	TTATTACGGTCAGAGG GTAATTGAATAGCAGC
84	TGAACAAACAGTATGT TAGCAAACTAAAAGAA
85	CTTTACAGTTAGCGAA CCTCCCGACGTAGGAA
86	GAGGCGTTAGAGAATA ACATAAAAGAACACCC
87	TCATTACCCGACAATA AACAACATATTTAGGC
88	CCAGACGAGCGCCCAA TAGCAAGCAAGAACGC
89	AGAGGCATAATTTCAT CTTCTGACTATAACTA
90	TTTTAGTTTTTCGAGC CAGTAATAAATTCTGT
91	TATGTAAACCTTTTTT AATGGAAAAATTACCT
92	TTGAATTATGCTGATG CAAATCCACAAATATA
93	GAGCAAAAACTTCTGA ATAATGGAAGAAGGAG
94	TGGATTATGAAGATGA TGAAACAAAATTTCAT
95	CGGAATTATTGAAAGG AATTGAGGTGAAAAAT
96	ATCAACAGTCATCATA TTCCTGATTGATTGTT
97	CTAAAGCAAGATAGAA CCCTTCTGAATCGTCT
98	GCCAACAGTCACCTTG CTGAACCTGTTGGCAA
99	GAAATGGATTATTTAC ATTGGCAGACATTCTG
100	TTTT TATAAGTA TAGCCCGGCCGTCGAG
101	AGGGTTGA TTTT ATAAATCC TCATTAAATGATATTC
102	ACAAACAA TTTT AATCAGTA GCGACAGATCGATAGC
103	AGCACCGT TTTT TAAAGGTG GCAACATAGTAGAAAA
104	TACATACA TTTT GACGGGAG AATTAACTACAGGGAA
105	GCGCATTA TTTT GCTTATCC GGTATTCTAAATCAGA
106	TATAGAAG TTTT CGACAAAA GGTAAAGTAGAGAATA

107	TAAAGTAC TTTT CGCGAGAA AACTTTTTATCGCAAG
108	ACAAAGAA TTTT ATTAATTA CATTTAACACATCAAG
109	AAAACAAA TTTT TTCATCAA TATAATCCTATCAGAT
110	GATGGCAA TTTT AATCAATA TCTGGTCACAAATATC
111	AAACCCTC TTTT ACCAGTAA TAAAAGGGATTCACCA GTCACACG TTTT
112	CCGAAATCCGAAAATC CTGTTTGAAGCCGGAA
113	CCAGCAGGGGCAAAATCCCTTATAAAGCCGGC
114	GCATAAAGTTCCACAC AACATACGAAGCGCCA
115	GCTCACAATGTAAAGCCTGGGGTGGGTTTGCC
116	TTCGCCATTGCCGGAA ACCAGGCATTAAATCA
117	GCTTCTGGTCAGGCTGCGCAACTGTGTTATCC
118	GTTAAAATTTTAACCAATAGGAACCCGGCACC
119	AGACAGTCATTCAAAA GGGTGAGAAGCTATAT
120	AGGTAAAGAAATCACCATCAATATAATATTTT
121	TTTCATTTGGTCAATA ACCTGTTTATATCGCG
122	TCGCAAATGGGGCGCGAGCTGAAATAATGTGT
123	TTTTAATTGCCCGAAA GACTTCAAAACACTAT
124	AAGAGGAACGAGCTTCAAAGCGAAGATACATT
125	GGAATTACTCGTTTACCAGACGACAAAAGATT
126	GAATAAGGACGTAACA AAGCTGCTCTAAAACA
127	CCAAATCACTTGCCCTGACGAGAACGCCAAAA
128	CTCATCTTGAGGCAAA AGAATACAGTGAATTT
129	AAACGAAATGACCCCCAGCGATTATTCATTAC
130	CTTAAACATCAGCTTG CTTTCGAGCGTAACAC
131	TCGGTTTAGCTTGATACCGATAGTCCAACCTA
132	TGAGTTTCGTCACCAGTACAAACTTAATTGTA
133	CCCCGATTTAGAGCTTGACGGGGAAATCAAAA

134	GAATAGCCGCAAGCGGTCCACGCTCCTAATGA
135	GAGTTGCACGAGATAGGGTTGAGTAAGGGAGC
136	GTGAGCTAGTTTCCTGTGTGAAATTTGGGAAG
137	TCATAGCTACTCACATTAATTGCGCCCTGAGA
138	GGCGATCGCACTCCAGCCAGCTTTGCCATCAA
139	GAAGATCGGTGCGGGCCTCTTCGCAATCATGG
140	AAATAATTTTAAATTGTAAACGTTGATATTCA
141	GCAAATATCGCGTCTGGCCTTCCTGGCCTCAG
142	ACCGTTCTAAATGCAATGCCTGAGAGGTGGCA
143	TATATTTTAGCTGATAAATTAATGTTGTATAA
144	TCAATTCTTTTAGTTTGACCATTACCAGACCG
145	CGAGTAGAACTAATAGTAGTAGCAAACCCTCA
146	GAAGCAAAAAAGCGGATTGCATCAGATAAAAA
147	TCAGAAGCCTCCAACAGGTCAGGATCTGCGAA
148	CCAAAATATAATGCAGATACATAAACACCAGA
149	CATTCAACGCGAGAGGCTTTTGCATATTATAG
150	ACGAGTAGTGACAAGAACCGGATATACCAAGC
151	AGTAATCTTAAATTGGGCTTGAGAGAATACCA
152	GCGAAACATGCCACTACGAAGGCATGCGCCGA
153	ATACGTAAAAGTACAACGGAGATTTCATCAAG
154	CAATGACACTCCAAAAGGAGCCTTACAACGCC
155	AAAAAAGGACAACCATCGCCCACGCGGGTAAA
156	TGTAGCATTCCACAGACAGCCCTCATCTCCAA
157	GTAAAGCACTAAATCGGAACCCTAGTTGTTCC
158	AGTTTGGAGCCCTTCACCGCCTGGTTGCGCTC
159	AGCTGATTACAAGAGTCCACTATTGAGGTGCC
160	ACTGCCCGCCGAGCTCGAATTCGTTATTACGC

161	CCCGGGTACTTTCCAGTCGGGAAACGGGCAAC
162	CAGCTGGCGGACGACGACAGTATCGTAGCCAG
163	GTTTGAGGGAAAGGGGGATGTGCTAGAGGATC
164	CTTTCATCCCCAAAAACAGGAAGACCGGAGAG
165	AGAAAAGCAACATTAAATGTGAGCATCTGCCA
166	GGTAGCTAGGATAAAAATTTTTAGTTAACATC
167	CAACGCAATTTTTGAGAGATCTACTGATAATC
168	CAATAAATACAGTTGATTCCCAATTTAGAGAG
169	TCCATATACATACAGGCAAGGCAACTTTATTT
170	TACCTTTAAGGTCTTTACCCTGACAAAGAAGT
171	CAAAAATCATTGCTCCTTTTGATAAGTTTCAT
172	TTTGCCAGATCAGTTGAGATTTAGTGGTTTAA
173	AAAGATTCAGGGGGTAATAGTAAACCATAAAT
174	TTTCAACTATAGGCTGGCTGACCTTGTATCAT
175	CCAGGCGCTTAATCATTGTGAATTACAGGTAG
176	CGCCTGATGGAAGTTTCCATTAAACATAACCG
177	TTTCATGAAAATTGTGTCGAAATCTGTACAGA
178	ATATATTCTTTTTTCACGTTGAAAATAGTTAG
179	AATAATAAGGTCGCTGAGGCTTGCAAAGACTT
180	CGTAACGATCTAAAGTTTTGTCGTGAATTGCG
181	ACCCAAATCAAGTTTTTTGGGGTCAAAGAACG
182	TGGACTCCCTTTTCACCAGTGAGACCTGTCGT
183	TGGTTTTTAACGTCAAAGGGCGAAGAACCATC
184	GCCAGCTGCCTGCAGGTCGACTCTGCAAGGCG
185	CTTGCATGCATTAATGAATCGGCCCGCCAGGG
186	ATTAAGTTCGCATCGTAACCGTGCGAGTAACA
187	TAGATGGGGGGTAACGCCAGGGTTGTGCCAAG

188	ACCCGTCGTCATATGTACCCCGGTAAAGGCTA
189	CATGTCAAGATTCTCCGTGGGAACCGTTGGTG
190	TCAGGTCACTTTTGCGGGAGAAGCAGAATTAG
191	CTGTAATATTGCCTGAGAGTCTGGAAAACTAG
192	CAAAATTAAAGTACGGTGTCTGGAAGAGGTCA
193	TGCAACTAAGCAATAAAGCCTCAGTTATGACC
194	TTTTTGCGCAGAAAACGAGAATGAATGTTTAG
195	AAACAGTTGATGGCTTAGAGCTTATTTAAATA
196	ACTGGATAACGGAACAACATTATTACCTTATG
197	ACGAACTAGCGTCCAATACTGCGGAATGCTTT
198	CGATTTTAGAGGACAGATGAACGGCGCGACCT
199	CTTTGAAAAGAACTGGCTCATTATTTAATAAA
200	GCTCCATGAGAGGCTTTGAGGACTAGGGAGTT
201	ACGGCTACTTACTTAGCCGGAACGCTGACCAA
202	AAAGGCCGAAAGGAACAACTAAAGCTTTCCAG
203	GAGAATAGCTTTTGCGGGATCGTCGGGTAGCA
204	ACGTTAGTAAATGAATTTTCTGTAAGCGGAGT
205	TTTTCGATGGCCCACTACGTAAACCGTC
206	TATCAGGGTTTTCGGTTTGCGTATTGGGAACGCGCG
207	GGGAGAGGTTTTTGTAAAACGACGGCCATTCCCAGT
208	CACGACGTTTTTGTAATGGGATAGGTCAAAACGGCG
209	GATTGACCTTTTGATGAACGGTAATCGTAGCAAACA
210	AGAGAATCTTTTGGTTGTACCAAAAACAAGCATAAA
211	GCTAAATCTTTTCTGTAGCTCAACATGTATTGCTGA
212	ATATAATGTTTTCATTGAATCCCCCTCAAATCGTCA
213	TAAATATTTTTTGGAAGAAAAATCTACGACCAGTCA
214	GGACGTTGTTTTTCATAAGGGAACCGAAAGGCGCAG

215	ACGGTCAATTTTGACAGCATCGGAACGAACCCTCAG
216	CAGCGAAAATTTTACTTTCAACAGTTTCTGGGATTTTGCTAAACTTTT
rt-rem1	AACATCACTTGCCTGAGTAGAAGAACT
rt-rem2	TGTAGCAATACTTCTTTGATTAGTAAT
rt-rem3	AGTCTGTCCATCACGCAAATTAACCGT
rt-rem4	ATAATCAGTGAGGCCACCGAGTAAAAG
rt-rem5	ACGCCAGAATCCTGAGAAGTGTTTTT
rt-rem6	TTAAAGGGATTTTAGACAGGAACGGT
rt-rem7	AGAGCGGGAGCTAAACAGGAGGCCGA
rt-rem8	TATAACGTGCTTTCCTCGTTAGAATC
rt-rem9	GTACTATGGTTGCTTTGACGAGCACG
rt-rem10	GCGCTTAATGCGCCGCTACAGGGCGC

Table S2.2. FRET labeled strands of 2D rectangular origami.

Position 1:

91- Fluorescein: TATGTAAACCTTT/iFluorT/TTAATGGAAAAATTACCT

89-TAMRA: AGAGGCATAATTTCATCTTCTGACTAT/i6-TAMN/AACTA

Position 2:

123-TAMRA: TTTTA/i6-TAMN/ATTGCCCGAAAGACTTCAAAACACTAT

121- Fluorescein: TTTCA/iFluorT/TTGGTCAATAACCTGTTTATATCGCG

Position 3:

168-TAMRA: CAATA/i6-TAMN/AATACAGTTGATTCCCAATTTAGAGAG

170- Fluorescein: TACCT/iFluorT/TAAGGTCTTTACCCTGACAAAGAAGT

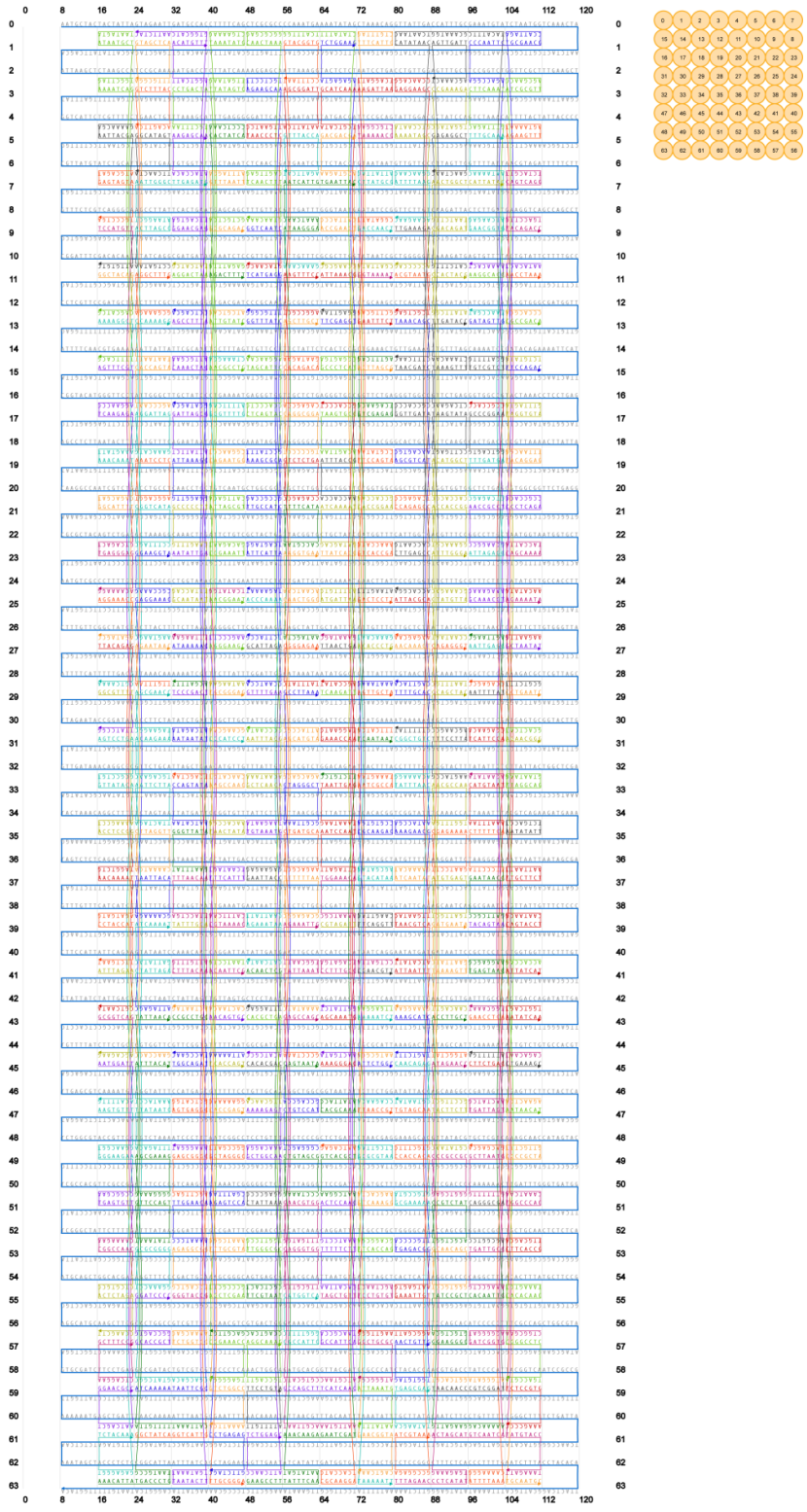

Figure S2.2. Schematic design of 3D eight-layer cuboid origami structure.

Table S2.3. Helper strand sequences of 3D eight-layer cuboid origami structure.

Name	Sequence
1-1-1	TGCTGAATGTAGCATTTAACACTG
1-2-1	ATAAATCAAGCTTAATCTCCAAAA
1-3-1	CCAAAAGGGAATGACCGTAGCAAC
1-4-1	ACCAGAACACATAACGCGACCTGC
1-1-2	TTGAAAATGAGACTCCATGTACCGAATAGATA
1-2-2	GAACGAGGATATTCACAAGAGGCTGAACGCGA
1-3-2	GAAATCCGTTTTCATCTGGCCTTGAGCAGCCT
1-4-2	CGAGAAACCAACCGATGTAGCGCGTTACCAGA
1-1-3	TATTCTAATCATATGCTTATCAACATCCTGAG
1-2-3	ATGAAAATCCTTTTTAGTTTAGTATCGTCTGA
1-3-3	GAACAAAGATCAAGAAAGAGACTAGAGGTGAG
1-4-3	GCGACATTGGTTAGAAAAACAAACATTTGAGG
1-1-4	ACGCTCAAGAAAGGAAACGCCAGATGTACCAAAAACATTA
1-2-4	ATAAAACAGATAGGGTCGTGGCGATTGAGAGAAGCTATTT
1-3-4	GATAATACTAATGAATTAGCCCGAAACCAATACATTTTTT
1-4-4	AATGGAAGGCAGGTCGAGCTGCATTCCAGCCAGATCGCAC
2-1-1	TAATAGTAATAATGCTTTTTCACG
2-2-1	TGGCTTAGAAAATCAGCAGCATCG
2-3-1	GAAAACGAAATTACGAATTGTGTC
2-4-1	ATGCAGATGAGTAGTATGCCCTGA
2-1-2	AGTTTCGTAGGAACCCTCAAGAGATTATCCGG
2-2-2	AAAAGGCTAAAGTATTAAACAAATCGTCAAAA
2-3-2	GGCTACAGCAGACGATGGCATTTTAGATAGCC
2-4-2	TCCATGTTGTCAGACTTGAGGGAGACAAAAGG
2-1-3	AGTCCTGAGCGCCTGTGTTATACAACATTTTG

2-2-3	GGCGTTTTAAAAGCCTACCTCCGGAGCAGAAG
2-3-3	TTACAGAGTAGGTCTGAACAAAATCGTCAATA
2-4-3	AGGAAACCAGATGATGCCTACCATTTCTGAAT
2-1-4	AAGTGTTTGGAACGGTGGGAAGAAGAGAGGGTTCTACAAA
2-2-4	AATGGATTCCGGCGAATGAGTGTTAATCAGCTGGAACGCC
2-3-4	GCGGTCAGCAAAAGAACGGCCAACCTCAGGAAGCTTTCCG
2-4-4	ATTTAGAAGTCGTGCCACTCTAGACCAAGCTTGCATGCCT
3-1-1	AGCCCAATCACCAGTATAATAATTGTAGCTCATTTGCGGA
3-2-1	GCGAAAGAGTCTTTACACAGTTCA
3-3-1	CCTGATAAGGCATAGTTTCAACTA
3-4-1	AAGTAAGCCGGTCATACCTTTAGCACTTAGCCATAAGGCTAATTGGGCTTGAGATG
3-1-2	TGCAGAACACAAGAAATAGAAGGCAGGATTAGGAAACATGCCAAAAGG
3-2-2	TTGTTTAAAAATCCTCAGGCAGGTAGGCTTTG
3-4-2	ATTAGAGCTAATTACAGCAAAAGAGAGGAAACCGCCAAAGGGAAGGTA
3-1-3	TTTAGACATTATAATCAAATACCTAATTCTTATTACTAGAAGCGAACC
3-2-3	GAACCACCCTTAGGTTCAAAATCAAGAATAAC
3-4-3	CGACGACAGTATCGGCGCGCGGGGGGAAACCTGTATTAGAGATTATACATCAAAAT
3-1-4	TGACCCTGTAATGCCGAGCGAAAGGGGGAAAGATTTACAT
3-2-4	CATTAAATTTTTGTTAGTTCCAGTTTATAAATTATTAACA
3-4-4	GCACCGCTGGCCAGTGGGATCCCC
4-1-1	TCCCGACTATTATTCTGATTAGCGATTGCGAACAAACTACGTGGCATCAATTCTAC
4-2-1	AGCCTTTAAGGTCATTACATGTTT
4-3-1	AGGACTAATGCTTTAACCTGACTA
4-4-1	AATATTGATTCAGTGAGGAACGAGATACCACAAAGAGCAA
4-1-2	TGGCAGATAATCATAACCAGTATAATCAGATAAATAATATGGATAGCA
4-3-2	ATAAAAACGGAGGTTGATTAAAGCCCTCAGCA

4-4-2	TATTTGCATTTACCAGGCAATAATCAAGTTTGGCCCCCTTTATCATCG
4-1-3	GGCTATCAGGTCATTGAGCTTGACGAGCGGGCGCTCATGGAGTGAGGCTCAGCTAA
4-3-3	CCGCCTGCGAATTTATGGGTTATAACGATTTT
4-4-3	GGGTACCGATTGTTTGCTTTACAATTACCTGATTTAACAATTTAAGAA
4-1-4	TGATAAATTAATACTTAAAGGGAT
4-3-4	ATCAAAAATAATTCGCAAAATCCCTTGGAACATACCGAAC
4-4-4	AAAACGACTCTGGTGCTCCAGTCGAGAGGCGGACTAATAG
5-1-1	TAAATATGCTGAAAAGAACGCCTG
5-2-1	TTATAGTCTTGATAAGATTGTATC
5-3-1	CACTATCACCCTCAAAAGACTTTT
5-4-1	GTTTAATTATTTAGGAGCGCAGAC
5-1-2	CTAAAGGAGGGTTTTGATTTTCAGCCCATCCT
5-2-2	ATCGTCACCAGAATGGCGGAACCTTGCGGGAG
5-3-2	GAGATTTGATTAGCGTCATTGACAAGGGAAGC
5-4-2	GCTGCTCACGGAAATTGACAGAATAACGGAAT
5-1-3	GCAAGCAAAAGCCAACCAACATGTCACCGAGT
5-2-3	AATAAGAATAACTATAAACACCGGTCACCAGT
5-3-3	AAGCCCTTTTTCATTTTCAATAGTAACAGTGC
5-4-3	TCATATGGCGTAAAACCATTTCAAACAATTCG
5-1-4	GGAAAAACGCTAGGGCGGCCGATTTTGCGGGAGAAGCCTT
5-2-4	ATTAAAAAAGAGTCCACGATTTAGCCTGAGAGGTTCTAGC
5-3-4	CACTAACATTTGCGTAAAATCGGCGTCTGGCCAAAATTCG
5-4-4	TAATCCTGAGCTCGAAGCCCGCTTCGGAAACCTGAGGGGA
6-1-1	GGCGCGAGCAACTAAAAGGAACAA
6-2-1	TGCTCCTTAGAAGCAATTTGCGGG
6-3-1	TTGAATCCTAACCCTCGTACAACG

6-4-1	CAGTTGAGTCAACTTTGTAACAAA
6-1-2	TAGCATTCCCACCCTCCTCAGTACGCCCAATA
6-2-2	GGTTTATCGCCTATTTAAAGCGCACCAATCCA
6-3-2	TCATGAGGGCCGCCAGTTGCCATCTCTTACCG
6-4-2	GGTCAATCTCAGTAGCATTCATTATAGAAAAT
6-1-3	AATTTACGACAATAAAGCTCAACATTGCAACA
6-2-3	GTTTTGAATAAGAATATGTAAATGACATCGCC
6-3-3	GCATTAGAGAGAAGAGGAATTACCTTTAGGAG
6-4-3	ACCCAAAAGAATTATTAGAAATAACATCAATA
6-1-4	AAAAGAGTAAACAGGAGCTGGCAAATTCAACCTCTGGAGC
6-2-4	CACACGACGGAGCCCCCTATTAAAATTTTGTTTTCCTGTA
6-3-4	CACGCTGATGGTTCCGTTGGGCGCTGCCAGTTAGGCAAAG
6-4-4	ACAACTCGCGCTCACTTTCGTAATCCAGTCACGACGTTGT
7-1-1	CAGAGCCACACAGACAGAATAGAAGTACGGTGCCTTTAAT
7-2-1	AGGCCGCTAGCGGATTAATATTCA
7-3-1	GAAACAAAGTTTACCAAGATTCAT
7-4-1	AATAGCTATTTTCATACACCGTAAATAAGGGAAAATCAACAATCATTGTGAATTAC
7-1-2	AGACGACGAGCATGTAATTACCGCCAGGCGGATGCCCCCTAGCTTGCT
7-2-2	TATTTATCGTCTCTGACCAGAGCCAAGTTTCC
7-4-2	AAAATATCTTTTTTAAGCAGAGGCGAACTGGCACAATCAAAAGGTGAA
7-1-3	CGGGAGCTCTGTCCATGCCAGCCAGTAGGGCTGCGTTAAAGCCTTAAA
7-2-3	GCCCTAAACTGATGCAAAGACGCTCGGGAGAA
7-4-3	ATCGTAACCGTGCATCCAGGGTGGTTGCGTTGTATTAAATTGGCAATTAGAAATTG
7-1-4	TATTTCAAAATATGATGTGTAGCGCCCTAAAGCAGTAATA
7-2-4	AATTGTAAACGTTAATGAACGTGGTTTGATGGGAGCCAGC
7-4-4	CGCCATTCGGGTTTTCCATGGTCA

8-1-1	TCAAGATTACAGTTAATAAGTGCCCGGAGTGAGCCCTCATCTATATTTTCATTTGG
8-2-1	TTCGAGGTAGAGAGTATCTGGAAG
8-3-1	ATTAAACGTCGTCATAGCATCAAA
8-4-1	TTATCACCCATTACCCACCGAACTAGGTAGAAGACGACGA
8-1-2	AAAGGGACTAAATAAGTAATTGAGTAGGAATCGAAACCAAGCCACCCT
8-3-2	TTAACTGAAACCACCAATTTACCGGGAGTTAA
8-4-2	CGTAGATTATTTTGTCATGATTAAGATAGCAGATCAAAATCCAAGCGC
8-1-3	AAACAAGAGAATCGATAATCGGAAGTCACGCTATATTACCCACGCAAATTCTGTCC
8-3-3	AGCAAATGCTTAGATTAATCCAATAGCCATAT
8-4-3	TAGCTGTTTCAGATGACCTTTGCCAAAATCGCTGGAAACAGAAATAGC
8-1-4	TCACCATCCGCAAGGAAATCAGAG
8-3-4	GCCAGCTTTCATCAACAAATCCTGACTCCAACAACTGATA
8-4-4	TAACGCCAGCCATTCACACATTAATTTTTCTTGGTTATCT
9-1-1	TTTCATTCCTGTTTAGAGTTAGCG
9-2-1	AAGATTAATCAGGATTGAATTTCT
9-3-1	TAAAAACCCTGCGGAAGGTAAAAT
9-4-1	CTTATGCGATTATTACGACCAACT
9-1-2	AGTTTCAGGTCGAGAGTCAGAACCTCAATAAT
9-2-2	GCTTGCAGTTCCAGTACCGTATAAAGTTGCTA
9-3-2	CGATTATACACCGGAAGCCACCAGACACCCTG
9-4-2	CGGATATTGTCACCGAAAACCATCGACTCCTT
9-1-3	TTTCATCGAATCGCCATAAAGTAATTAACCGT
9-2-3	AAATAAACCGCAAGACCCGTGTGAATTCTGGC
9-3-3	GAAACAATGTACATAAAGCGATAGAAAAATCT
9-4-3	ATAAGTTTTTCAGGTTCAAGTTACCGAACGTT
9-1-4	CCAGAACAGCGCGTAACTCGTTAGTAAAAATTTTTAGAAC

9-2-4	AATGCGCGGTCAAAGGAAGCACTAGAACGGTACAGTCAAA
9-3-4	TTGAGGAATTCACCAGGCAGGCGAATTAAATGAATATTTA
9-4-4	CCTGATTATCCTGTGTAGCTAACTGGCTGCGCATGGGCGC
10-1-1	TCAATAACCATATAACCTTTCAAC
10-2-1	CCAACAGGGAGGAAGCTCGCTGAG
10-3-1	GTCCAATAAAAATAGCACCCCCAG
10-4-1	GGAACAACATTTTAAGACAAGAAC
10-1-2	TAACGATCCGCCACCCGGTTGATAGTTTTTAT
10-2-2	TAAACAGCAACAGTGCAGCGTCATCAGTTACA
10-3-2	ACGTAATGTCAGAGCCCCAGAGCCAAGAGCAA
10-4-2	TTGAAAGACACCAATGCTTGAGCCACCACGGA
10-1-3	CGGCTGTCACAAAAGGTATTTAACGGTAATAT
10-2-3	TTTTGCACAATACCGAAAAGAACGTAGTCTTT
10-3-3	AACAAAGTGAAAACATATCAATATGAAAGGAA
10-4-3	ATTACGCATTGAATACTAACGTCAATCATATT
10-1-4	TGTAGCAAGTGCTTTCCCACCACAGCCGGAGAATCGTAAA
10-2-4	CAACAGAGGTGCCGTAGCGAAAAATATAAGCATGAGCGAG
10-3-4	AAAGCATCTTGCCCCATGAGACGGTGGTGTAGAACTGTTG
10-4-4	ATTAATTTAATGAGTGGAAATTGTAGGCGATTAAGTTGGG
11-1-1	CTCAGAACTAAAGTTTCTAAACAAAGTTGATTAGCAAACT
11-2-1	ATATTCGGCCGAAAGATGGATAGC
11-3-1	CATCTTTGGAGAGGCTGAACTAAC
11-4-1	CCAATAATACCACCGGGGAAACGTGGACAGATTAATCTTGAACTGGCTCATTATAC
11-1-2	AAGTACCGTTTCCTTAAGCAAGCCTAAGTATACCTTGAGTTTGATACC
11-2-2	TAATTTGCACATGGCTCACCACCCCCACTACG
11-4-2	CAACAGTTATGTGAGTTGATTGCTGTATGTTAGCAAAGACATTTGGGA

11-1-3	CGTATAACTACTTCTTGCCTTGCTAACGCCAATGGTTTGACCAGCTAC
11-2-3	ATGGCTATCGAGAAAAGAATCCTTCAGAGGGT
11-4-3	ATGGGATAGGTCACGTGCAACAGCGGGTGCCTTAAAAGTTGAATTATCGATGAATA
11-1-4	CCTCATATTGAGAAAGCCCGCCGCGGGTCGAGATAGAACC
11-2-4	AAAAACAGGAAGATTGCCGTCTATACGCTGGTACCTTGCT
11-4-4	GGAAGGGCGTGCTGCATATCCGCT
12-1-1	AATTTTATGGTCAGTGGCCCGGAAGGATTTTGTGTCGTCTTACATTTCGCAAATGG
12-2-1	GATAGTTGAGACCGGACCCAATTC
12-3-1	AAGGCACCGTTTAGACCTTCAAAT
12-4-1	ATTAGAGCATCAAGAGGAACGGTGAATAAAACTTTGCAAA
12-1-2	CTTCTGACAAATTTAACATGTAATCGAGAACATCATTCCACCGCCACC
12-3-2	AATTGAGCCTCAGAGCTTTGATGATAACCGAT
12-4-2	TACAGTAAAAAGAAACGCAAACGTGCAAGGCCAACCGCCTAAAACACT
12-1-3	ACTAGCATGTCAATCAGTTTTTTGGCTTAATGAACTATCGTGATTAGTAGAATATA
12-3-3	GAACCTCATTCCCTTACTTTTTCACCAGAGCC
12-4-3	CACAATTCAAGGAGCGTGAGTAACGATTCGCCGAATAACCAGTTAAGC
12-1-4	CAAAAGGGATTTTAAAGACGAGCA
12-3-4	TAACAACCCGTCGGATAGCGGTCCCAGGGCGAATTTTTGA
12-4-4	AGGGGGATGATCGGTGAAAGCCTGTGATTGCCTGGCAAAT
13-1-1	TGCGAACGCCATTAGATTCCAGAC
13-2-1	ATCGCGTTAGCGAACCCGCCGACA
13-3-1	AGAAGTTTAGTAAAATAACCTAAA
13-4-1	CAGTCAGGTCTACGTTTACAGACC
13-1-2	TCTGTATGTAGGTGTAGTTTAGTAAGAACGGG
13-2-2	CCCACGCATACAGGAGTTTAACGGCCTGAATC
13-3-2	AATACACTCCCTCAGACCGCCACCGCTAATAT

13-4-2	TGACCTTCCAGCAAAATACCATTAAGAAAATA
13-1-3	GCACTCATTTAGGCAGGTAATAAGAATAACAT
13-2-3	GCGTCTTTAATATATTTCTGACCTCTGAAAGC
13-3-3	AAGAATTGTTGCTTCTAATTAATTAATATCAA
13-4-3	AACATATACAGTACCTCAATAACGATTATCAT
13-1-4	AGAACTCACGCCGCTAGTTGCTTTTGCAATGCCTGAGTAA
13-2-4	CAGACAATTGGCCCACCAAATCAATATGTACCTAAAGATT
13-3-4	TGGTCAGTCTTCACCGTTGCAGCATCTCCGTGAAAGCCCC
13-4-4	ACCACCAGCACACAACTAAAGTGTCGGGCCTCTGACCGTA
14-1-1	TAGTTTGAAGTAGATTATGAATTT
14-2-1	AGCTTCAATTAATTCGAACCATCG
14-3-1	GGGGTAATTGCCAGAGGGCAAAAG
14-4-1	AAGAAAAAACGTTGGGAGGCTGGC
14-1-2	GTTAGTAACTCAGGAGTCACCGTACAAGTACC
14-2-2	ATGACAACTAATAAGTTGTACTGGGCTAACGA
14-3-2	ACGAAAGACCTCAGAAGCCGCCACTAACCCAC
14-4-2	AGGCGCATAGCACCATTCACCAGTAAGGTGGC
14-1-3	TATTAAACTCGAGCCAAGGCATTTTGAGTAGA
14-2-3	TTACCAACTTTCATCTTTAGTTAAACGTGGCA
14-3-3	CAGAGAGATCGCTATTGTAAATCGTCAATATC
14-4-3	CATACATAGGGAGAAATTTACATCACAAAGAA
14-1-4	CACTTGCCGTACTATGCAGGGCGCTGTGTAGGCCGGTTGA
14-2-4	GTAAGAATCCATCACCTACGTGAATAATCAGAGGAACAAA
14-3-4	ACCCTCAATGAGAGAGCCTGGCCCCGGCGGATTTCGCTAT
14-4-4	TTTGCGGACGGAAGCAATACGAGCTACGCCAGCTGGCGAA

Table S2.4. FRET labeled strands of 3D eight-layer cuboid origami structure.

Edge:

2-2-1-TAMRA: TGGCTTAGAA/i6-TAMN/AATCAGCAGCATCG

2-3-1- Fluorescein: GAAAACGAAA/iFluorT/TACGAATTGTGTC

Top surface:

3D 3-2-1- Fluorescein: GCGAAAGAGTCTT/iFluorT/ACACAGTTCA

3D 4-2-1-TAMRA: AGCCTTTAAGGTC/i6-TAMN/TTACATGTTT

Front surface middle:

6-4-2- Fluorescein: GGTCAATCTCAGTAGCATTCA/iFluorT/TATAGAAAAT

6-4-3-TAMRA: ACCCAAAAGAATTATTAGAAA/i6-TAMN/TAACATCAATA

Central inside:

6-2-3-TAMRA: GTTTTGAATAAGAATATGTA/i6-TAMN/AATGACATCGCC

7-2-2- Fluorescein: TATT/iFluorT/ATCGTCTCTGACCAGAGCCAAGTTTCC

A. Transition temperatures measured from 2D DNA origami

Cooling/Heating total time duration	Cooling T_f (℃)	Heating T_m (℃)
10 hr	57.2 ±1.0	57.9 ±1.3
24 hr	57.6 ±1.1	58.0 ±1.4

B. Transition temperatures measured from 3D DNA origami

Cooling/Heating total time duration	Cooling T_f (℃)	Heating T_m (℃)
24 hr	54.6 ±1.3	60.4 ±1.4
48 hr	53.6 ±2.3	60.7 ±1.4
87 hr	53.9 ±2.5	60.6 ±2.0

Table S2.5. Evaluating the effect of the rates of temperature change in cooling/heating on transition temperatures. The concentration and ratio of both structures are consistent with other studies. (A) For the 2D structure, the rate was constant 0.1 ℃/min from 80 ℃ to 25 ℃ over 10 hours, and compared to slower rates (0.1 ℃/2.4 min from 80 ℃ to 25 ℃ over 24 hours). No significant differences in the transition temperatures or curve shape observed. (B) For 3D structure, the cooling/heating occurred over 24 hours in most study and here compared to longer duration as 48 hours and 87 hours. No significant differences were observed when slower rates applied. Thus the rate of temperature change we chose in our study is sufficient to ensure equilibrium at each temperature.

A. Transition temperatures measured from 2D DNA origami

Concentration	Cooling T_f (℃)	Heating T_m (℃)
50 nM	57.2 ±1.0	57.9 ±1.3
10 nM	56.0 ±0.9	57.9 ±1.0
5 nM	55.0 ±1.0	57.8 ±1.0

B. Transition temperatures measured from 3D DNA origami

Concentration	Cooling T_f (℃)	Heating T_m (℃)
50 nM	54.6 ±1.3	60.4 ±1.4
10 nM	52.3 ±1.5	58.8 ±1.7
5 nM	49.7 ±2.2	57.1 ±3.1

Table S2.6. Evaluating the effect of concentration of origami on transition temperatures. The rate of temperature change and ratio of both structures are consistent with other studies. We selected 50 nM for our study which is considered to be a relatively high concentration and compared to other typical annealing concentrations, 5nM (10 times less) and 10nM (5 times less). (A) For the 2D structure, T_f is higher when the concentration increases and is lower when the concentration decreases. The difference is about 2 ℃. (B) For 3D structure, T_f is higher when the concentration increases but the absolute temperature values are even larger, different at about 5 ℃. The dissociation temperature was reduced a few degrees when the concentration decreased.

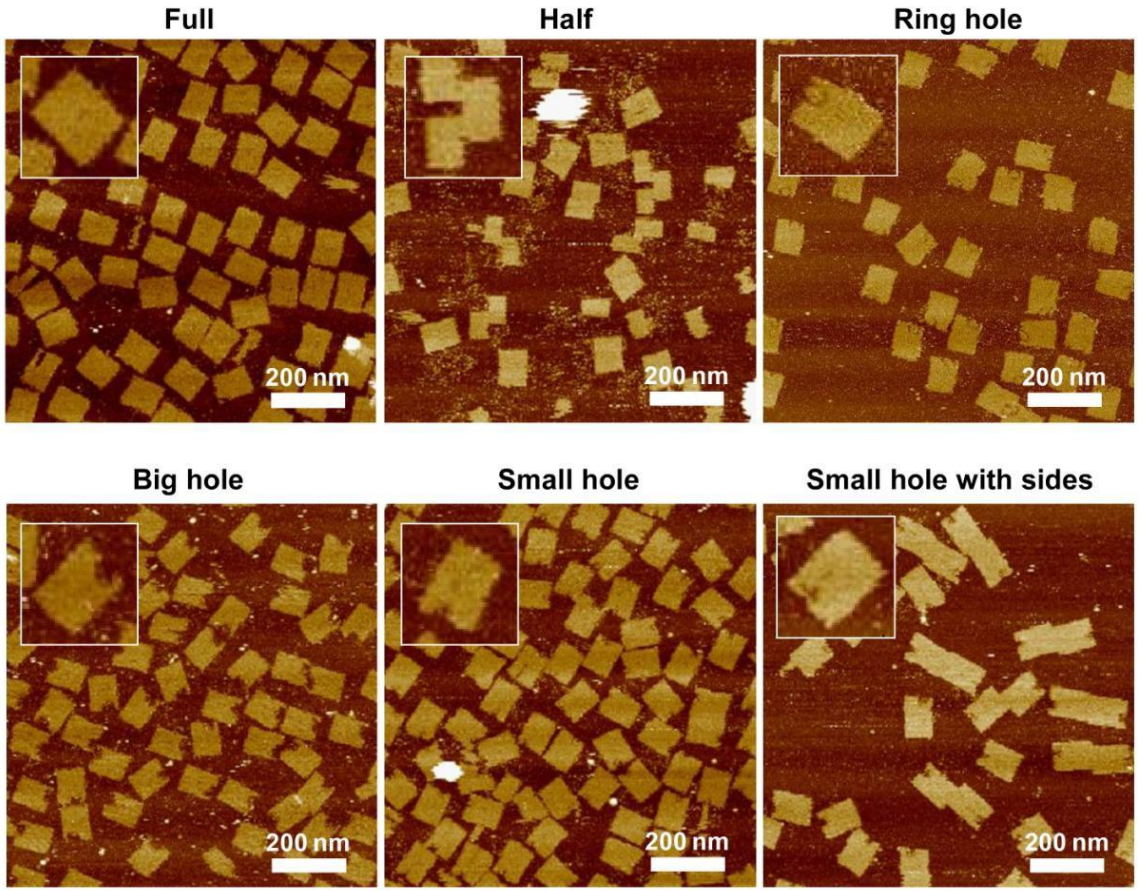

Figure S2.3. AFM characterization of the fully-assembled reference structure and the defective 2D rectangular origami structures studied in this work. All structures were annealed at the same concentrations, buffer conditions and annealing programs as were used in the thermal studies. Upper panel from left to right: full origami, half origami, ring hole at position 1. Lower panel left to right: big hole at position 1, small hole at position 1 with side edge staples excluded, small hole at position 1 with side edge staples included. Insets are zoom in images of individual structures. Defects in selected areas of the origami structures (with several staples missing) did not affect the overall integrity of the origami. With staple strands included on both sides the formation of origami is not affected but it promotes unwanted stacking interactions between individual structures.

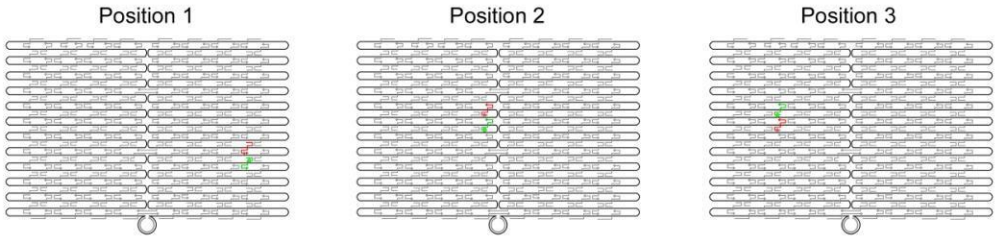

Structure	Cooling T_f (°C)	Heating T_m (°C)
Full	57.2 ± 1.0	57.9 ± 1.3
Half	57.1 ± 0.9	57.8 ± 1.0
Ring hole	49.8 ± 2.3	50.3 ± 2.2
Small hole	N/A	N/A

Cooling T_f (°C)	Heating T_m (°C)
56.6 ± 1.5	58.2 ± 2.6
56.9 ± 2.1	59.0 ± 2.2
47.9 ± 4.8	48.5 ± 4.8
30.9 ± 11.0, 51.3 ± 3.4	31.5 ± 4.9, 51.4 ± 3.4

Cooling T_f (°C)	Heating T_m (°C)
57.9 ± 1.2	60.6 ± 0.8
58.3 ± 1.1	60.9 ± 0.8
41.9 ± 2.7, 51.2 ± 1.0	42.4 ± 2.9, 51.6 ± 0.8
44.8 ± 3.8	45.2 ± 3.6

Table S2.7. Evaluating the homogeneity of origami assembly by placing the FRET pair at 3 different representative positions. The tables summarize the observed transition temperatures of various structural arrangements.

Figures S2.4-S2.38. Structural design, corresponding thermal data and analytical result of the various structures. (**A**) Schematic design: the position of the FRET reporter dyes are depicted by red (acceptor) and green (donor) staples. (**B**) Raw fluorescent intensity versus temperature result for the cooling cycle, when only the donor is present (green), or both the donor and acceptor (pink). (**C**) Raw fluorescent intensity versus temperature result for the heating cycle, when only the donor is present (blue), or both the donor and acceptor (orange). (**D**) Overlay of the normalized FRET efficiency for the cooling (black) and the heating (red) cycles. (**E**) The derivative of the cooling curve in (**D**) and corresponding Gaussian fit to yield the transition temperature of folding, T_f. (**F**) The derivative of the heating curve in (**D**) and corresponding Gaussian fit to yield the transition temperature of melting, T_m. (**G**) The derivative of the donor only cooling curve in (**B**) and the corresponding Gaussian fit to yield the transition temperature of folding, T_f'. (**H**) The derivative of the donor only heating curve in (**C**) and the corresponding Gaussian fit to yield the transition temperature of melting, T_m'.

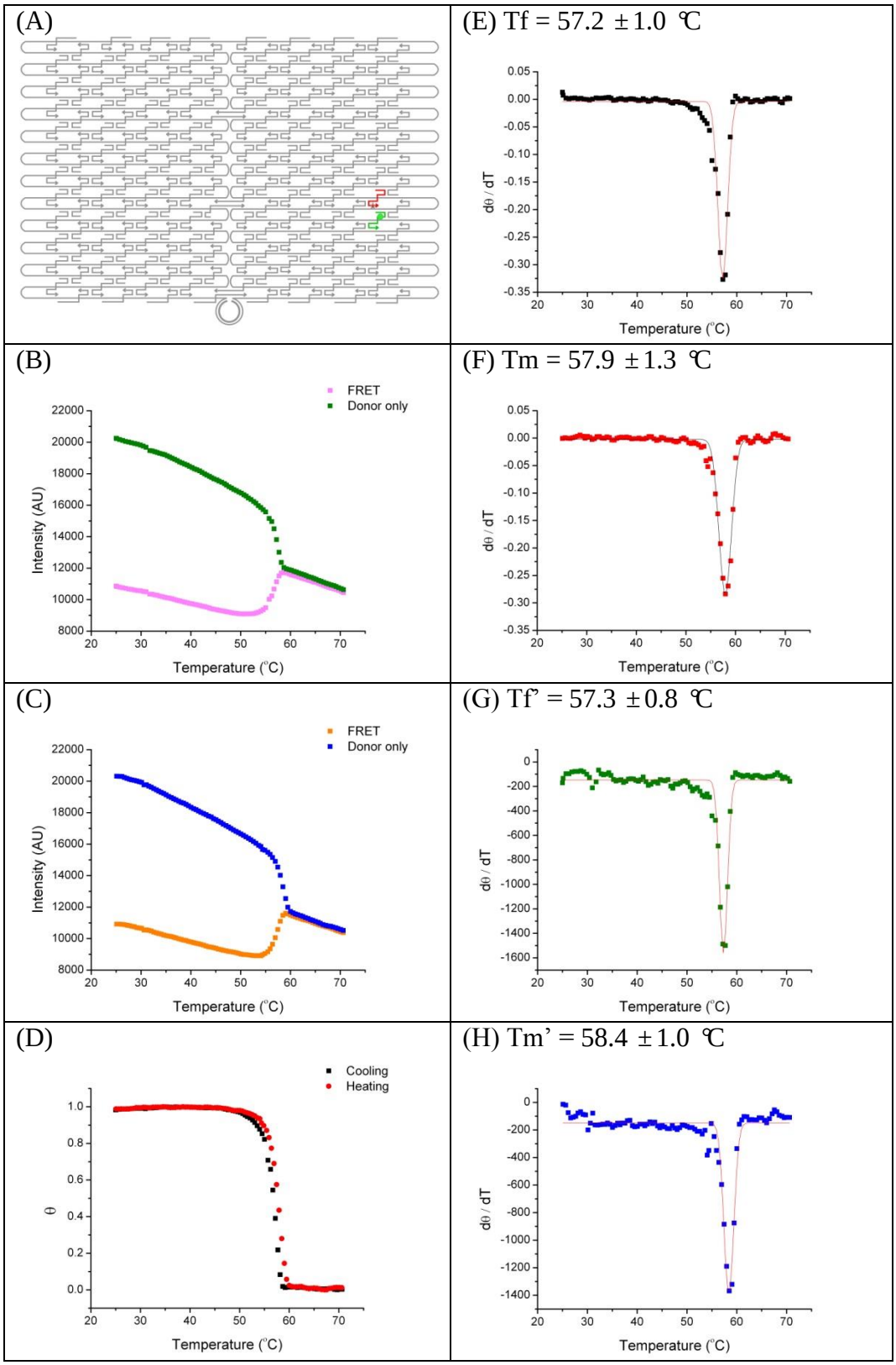

Figure S2.4. Rectangular structure with edge staples omitted

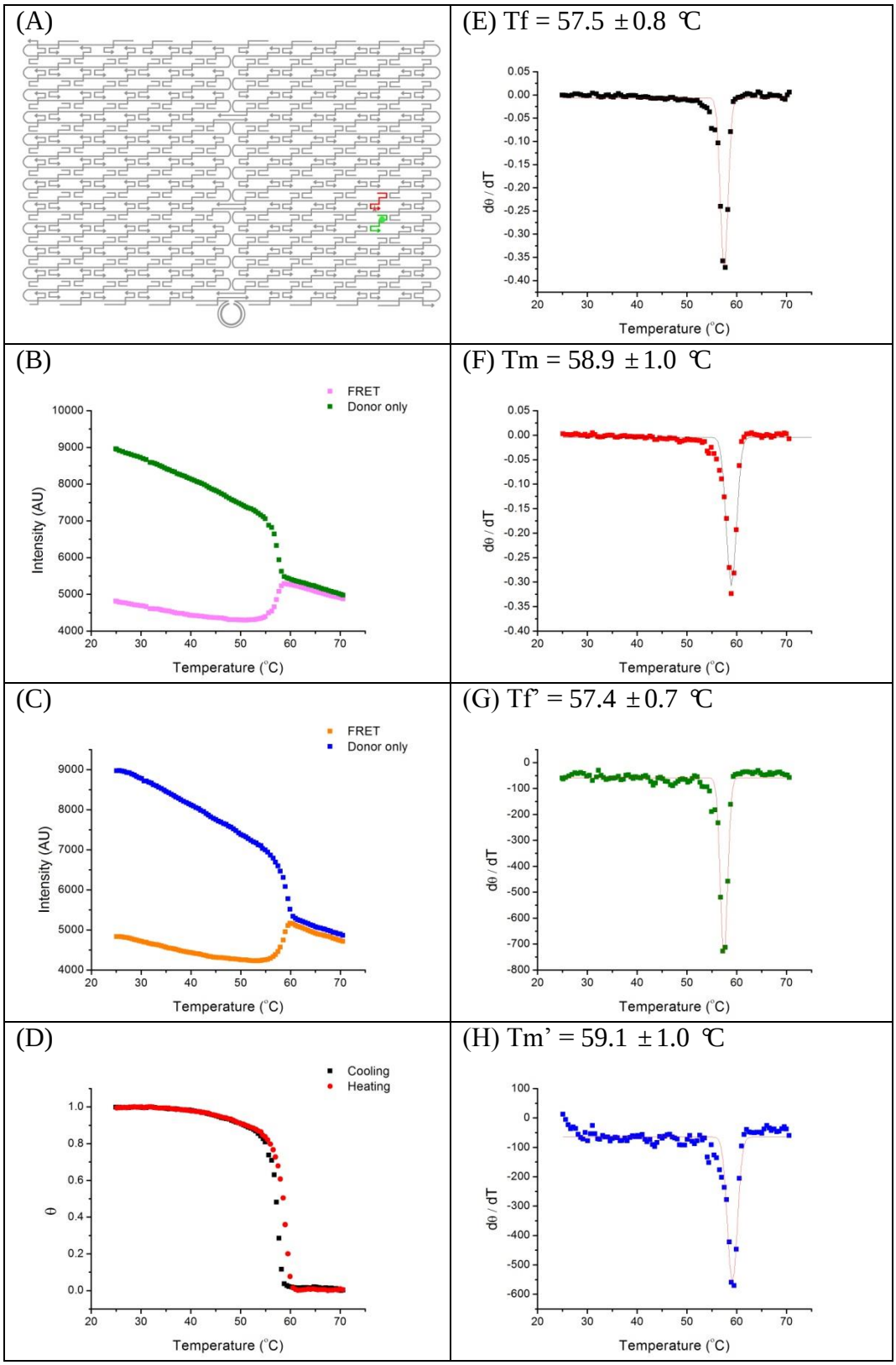

Figure S2.5. Rectangular structure (used as the reference in all 2D experiments)

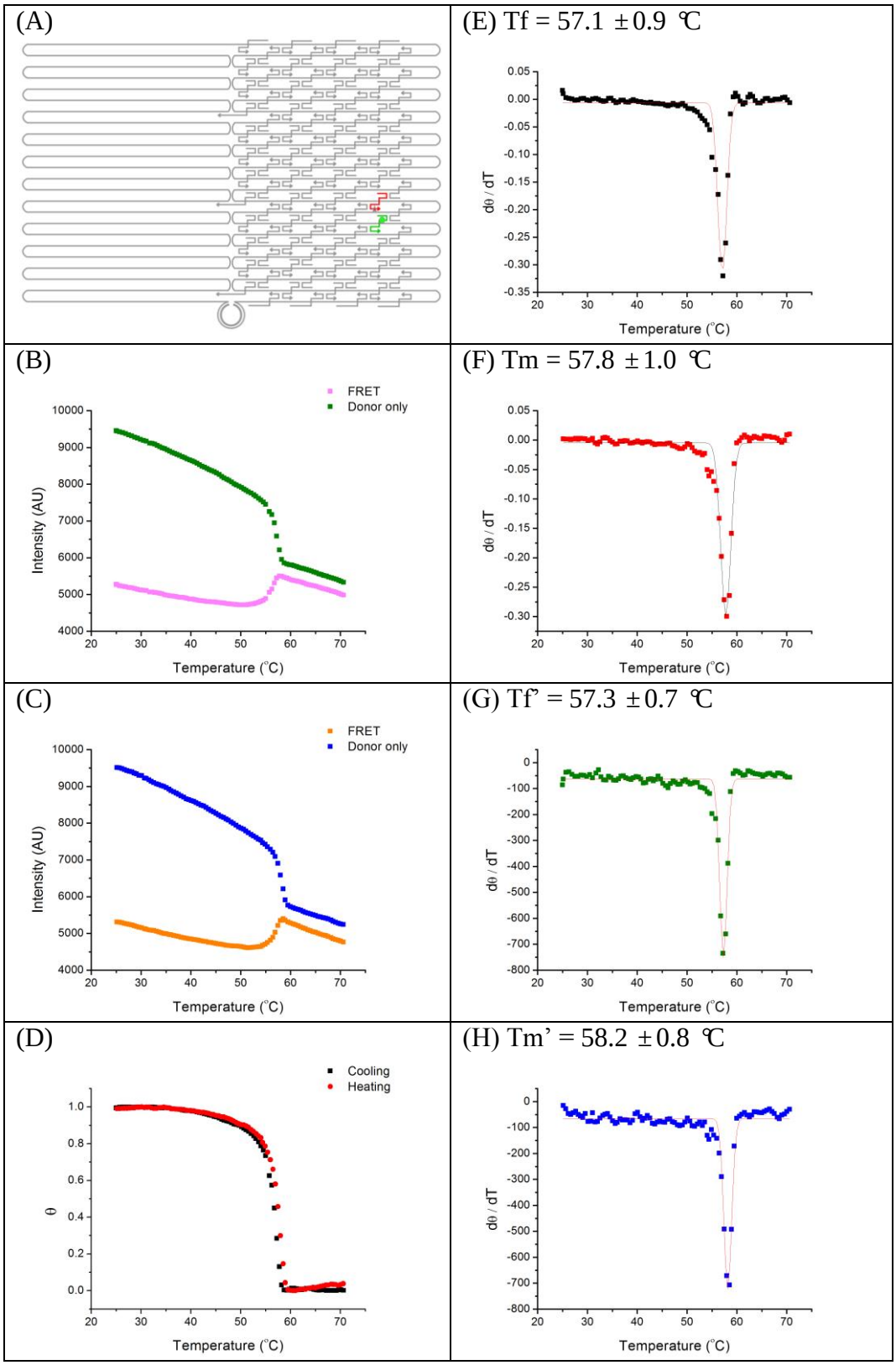

Figure S2.6. Half origami structure – position 1

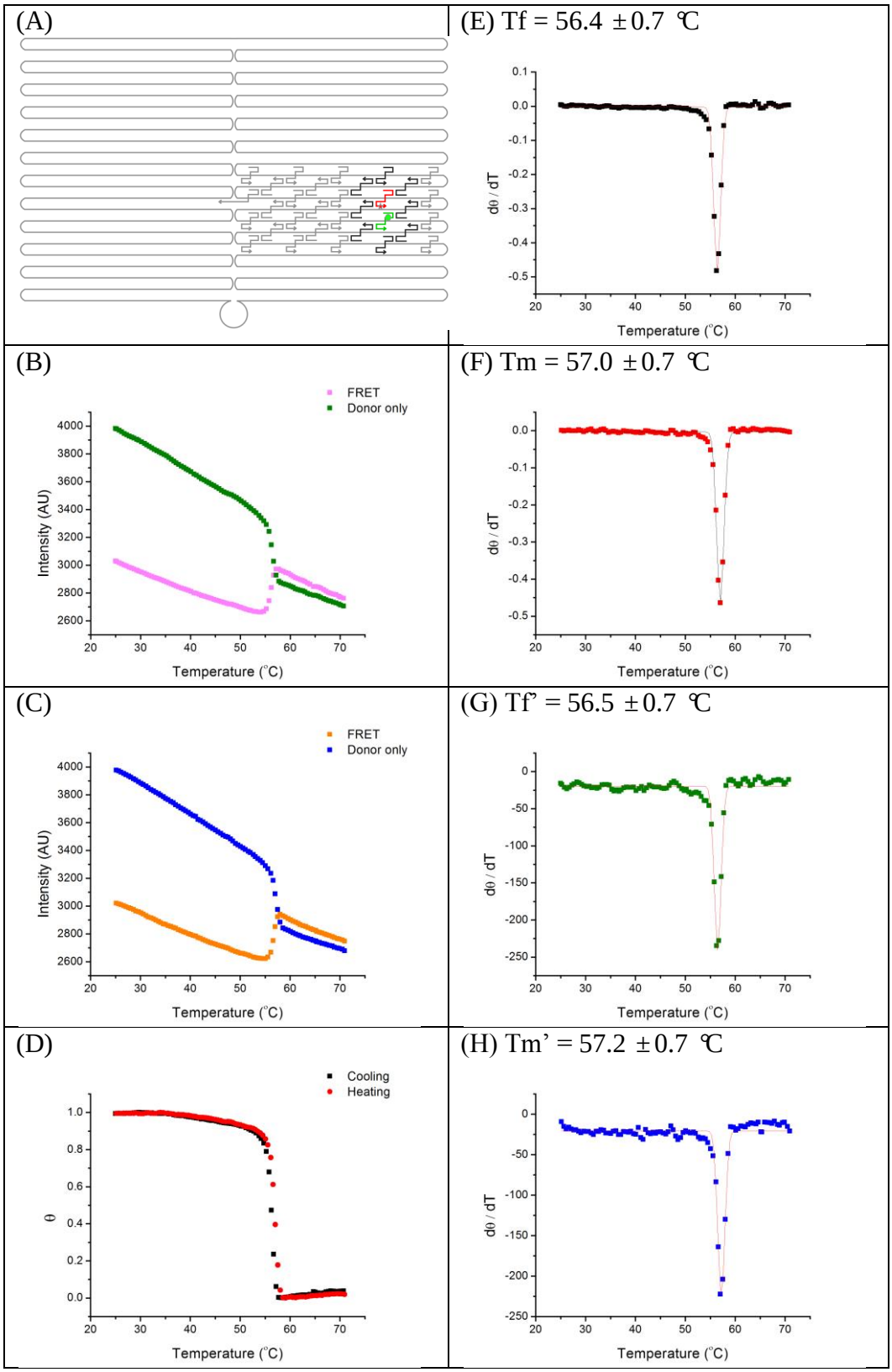

Figure S2.7. 7 helix core structure – position 1

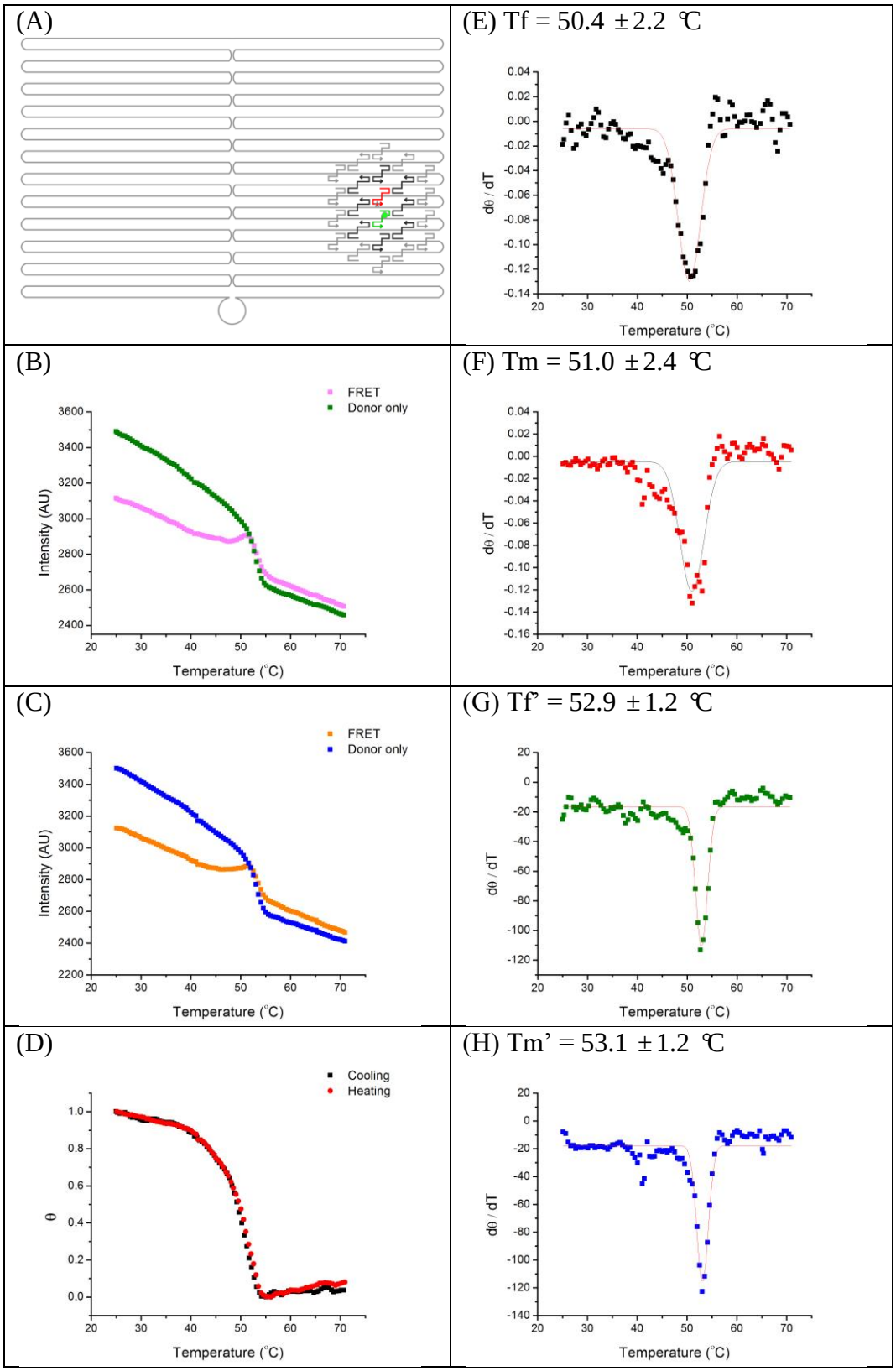

Figure S2.8. 2-layer cluster structure - position 1

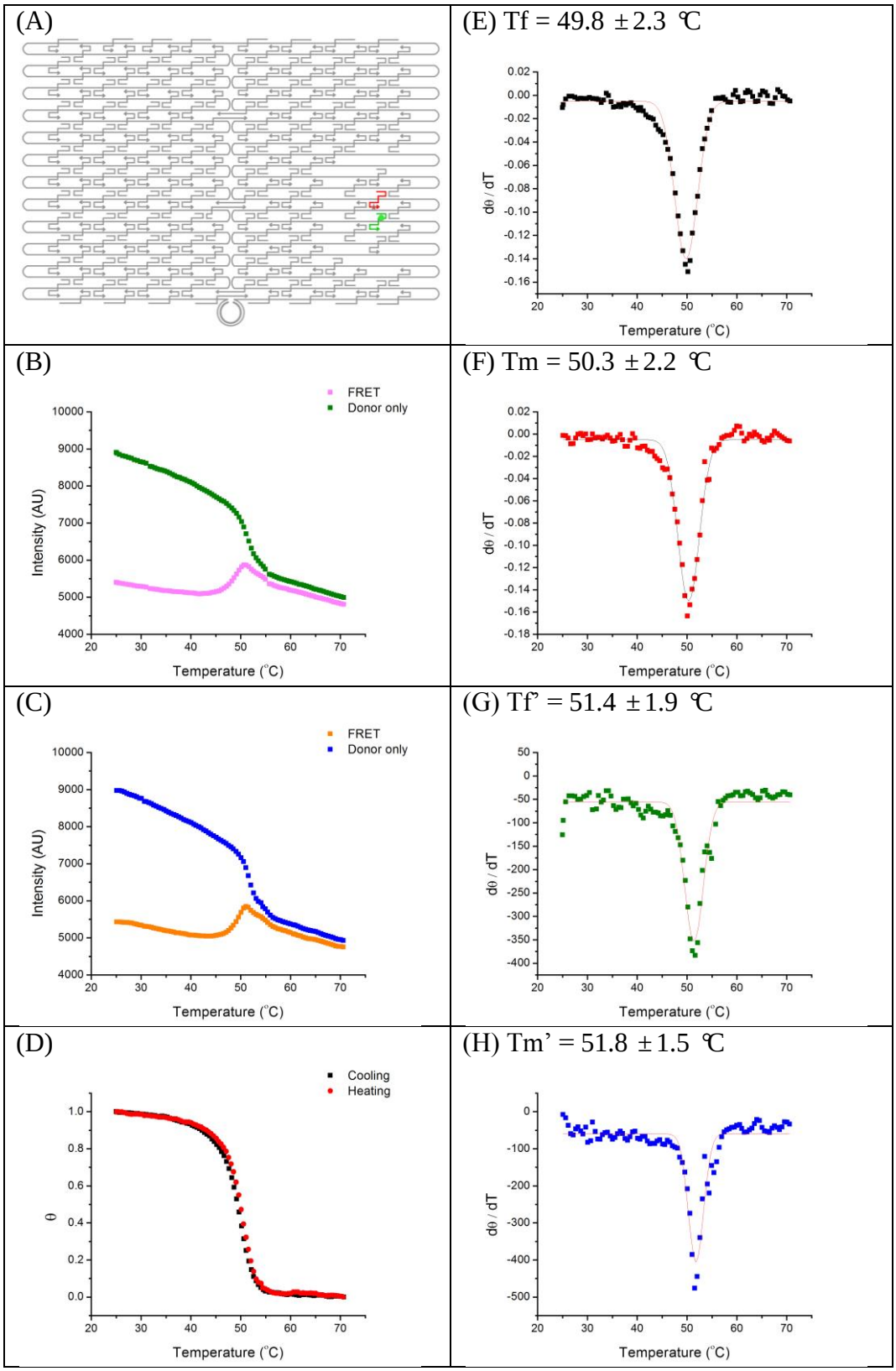

Figure S2.9. Ring-hole structure with the edge staples omitted - position 1

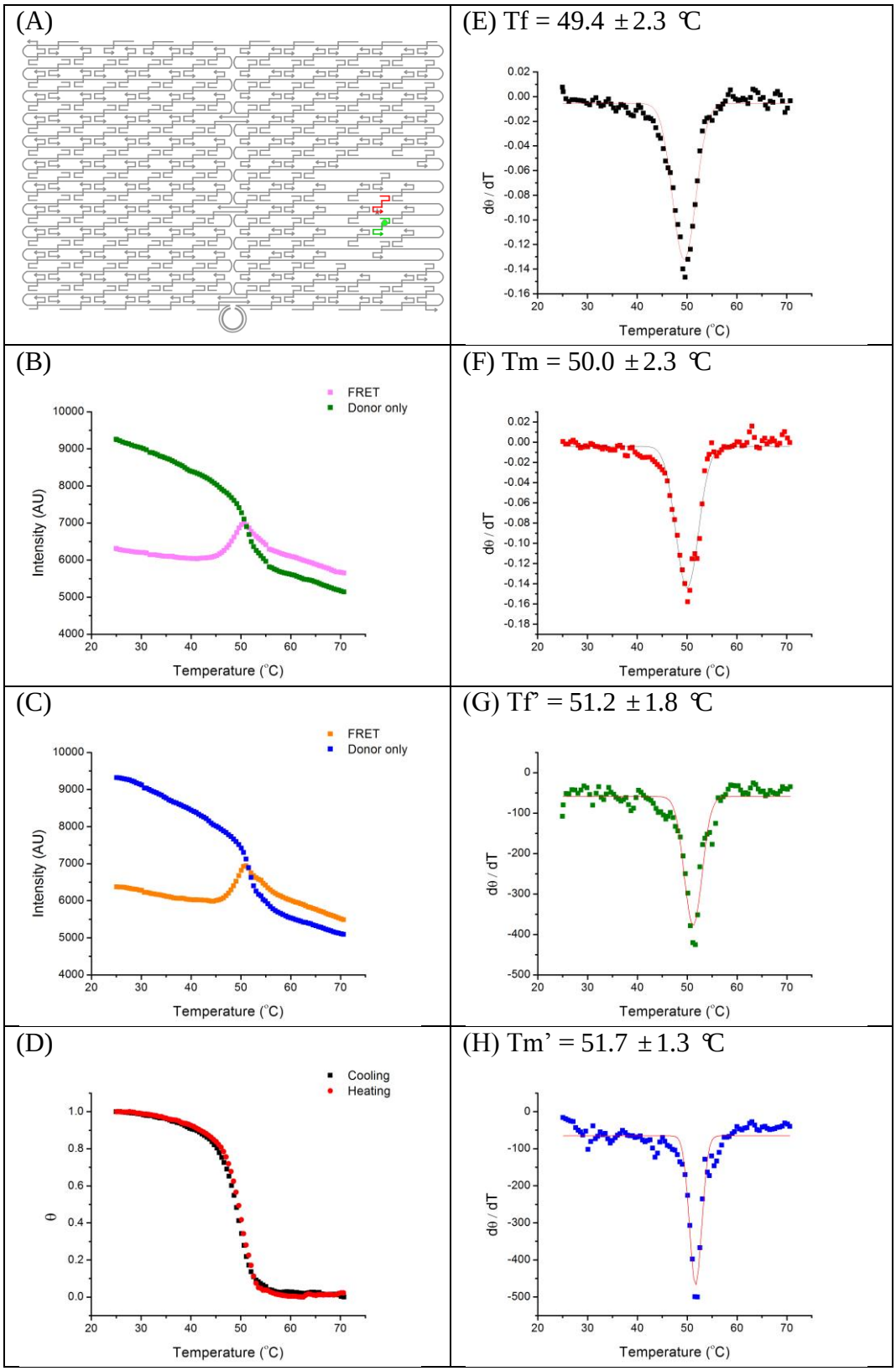

Figure S2.10. Ring-hole structure - position 1

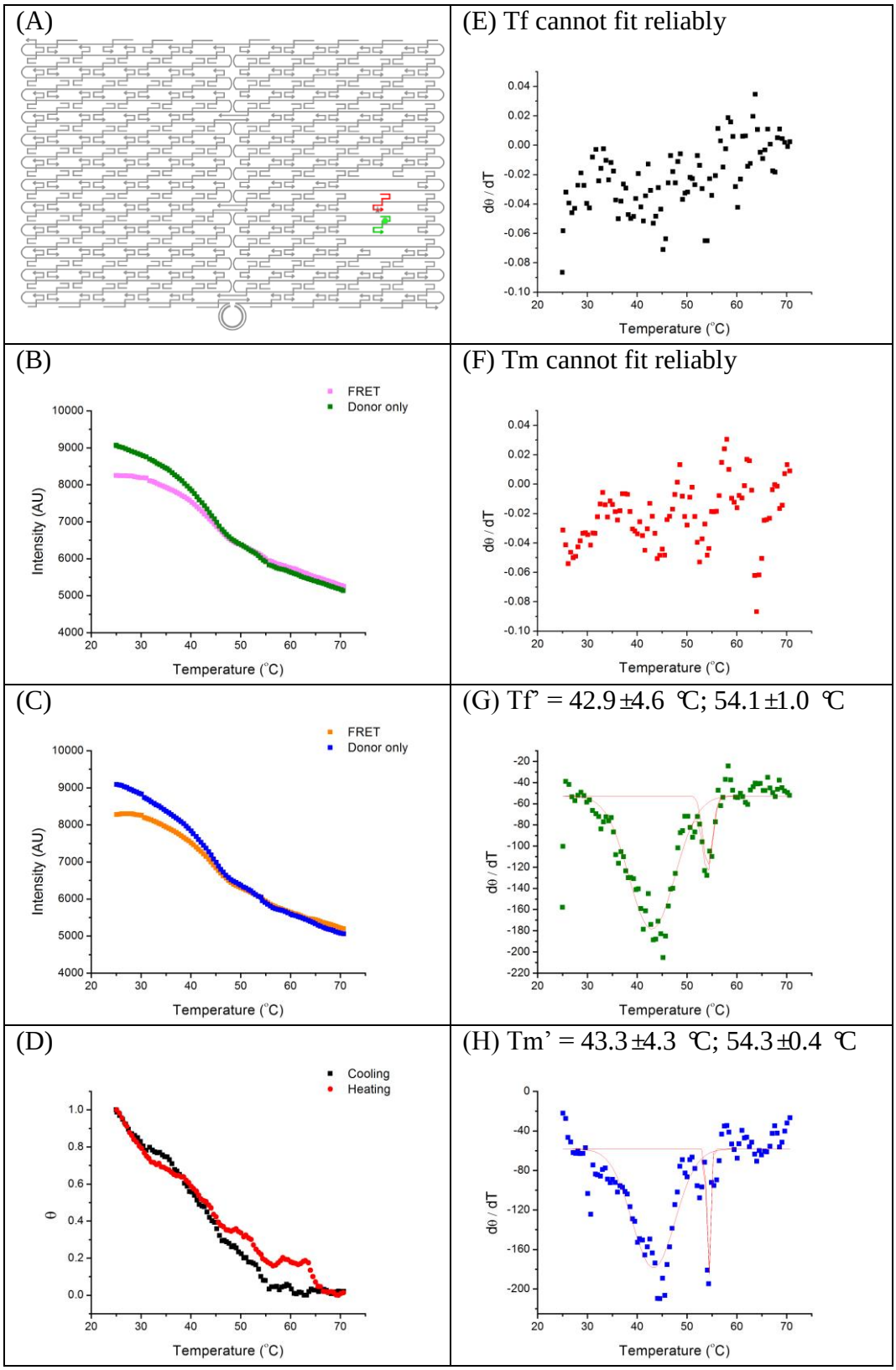

Figure S2.11. Small-hole structure - position 1

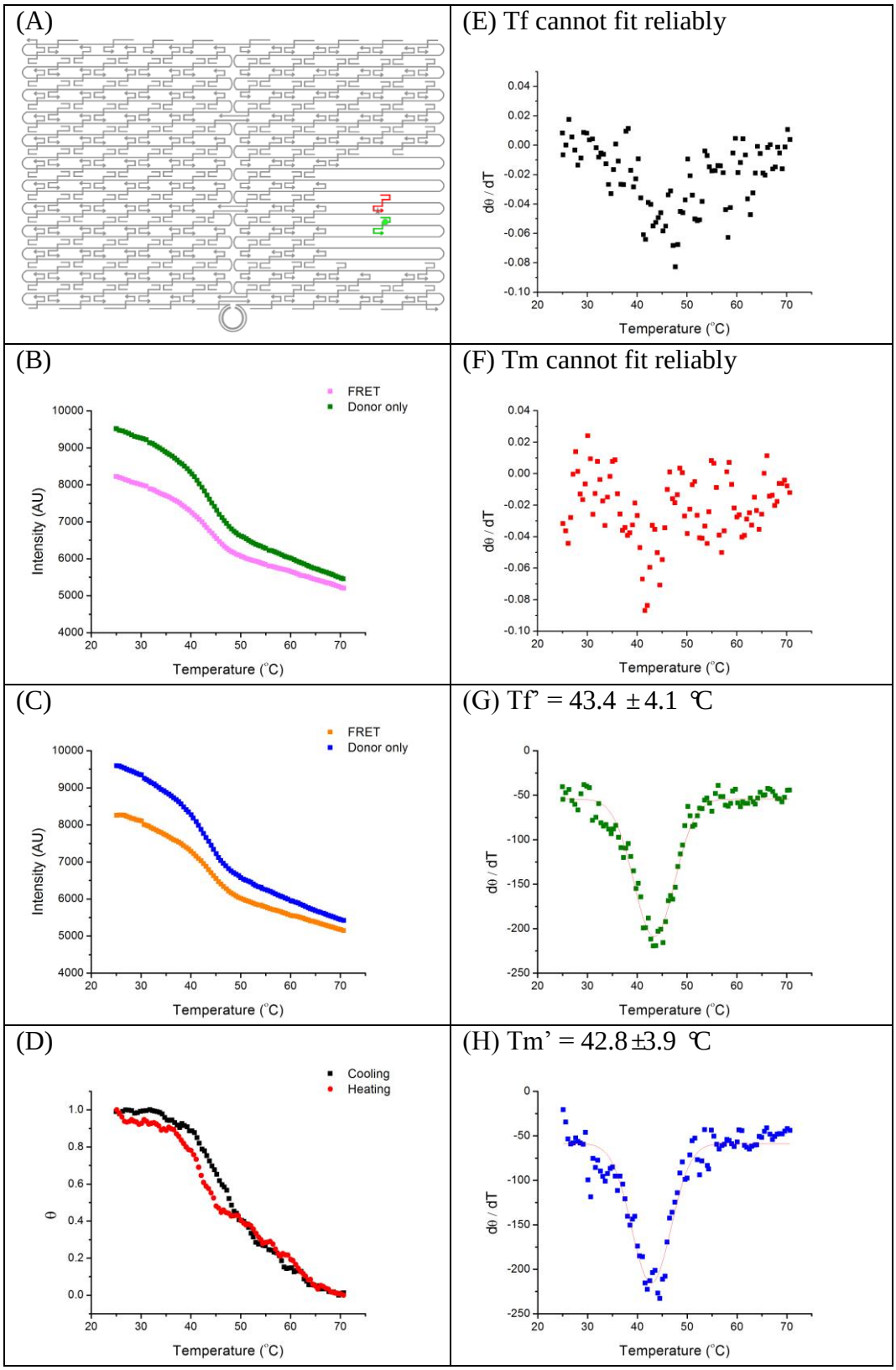

Figure S2.12. Big-hole structure - position 1

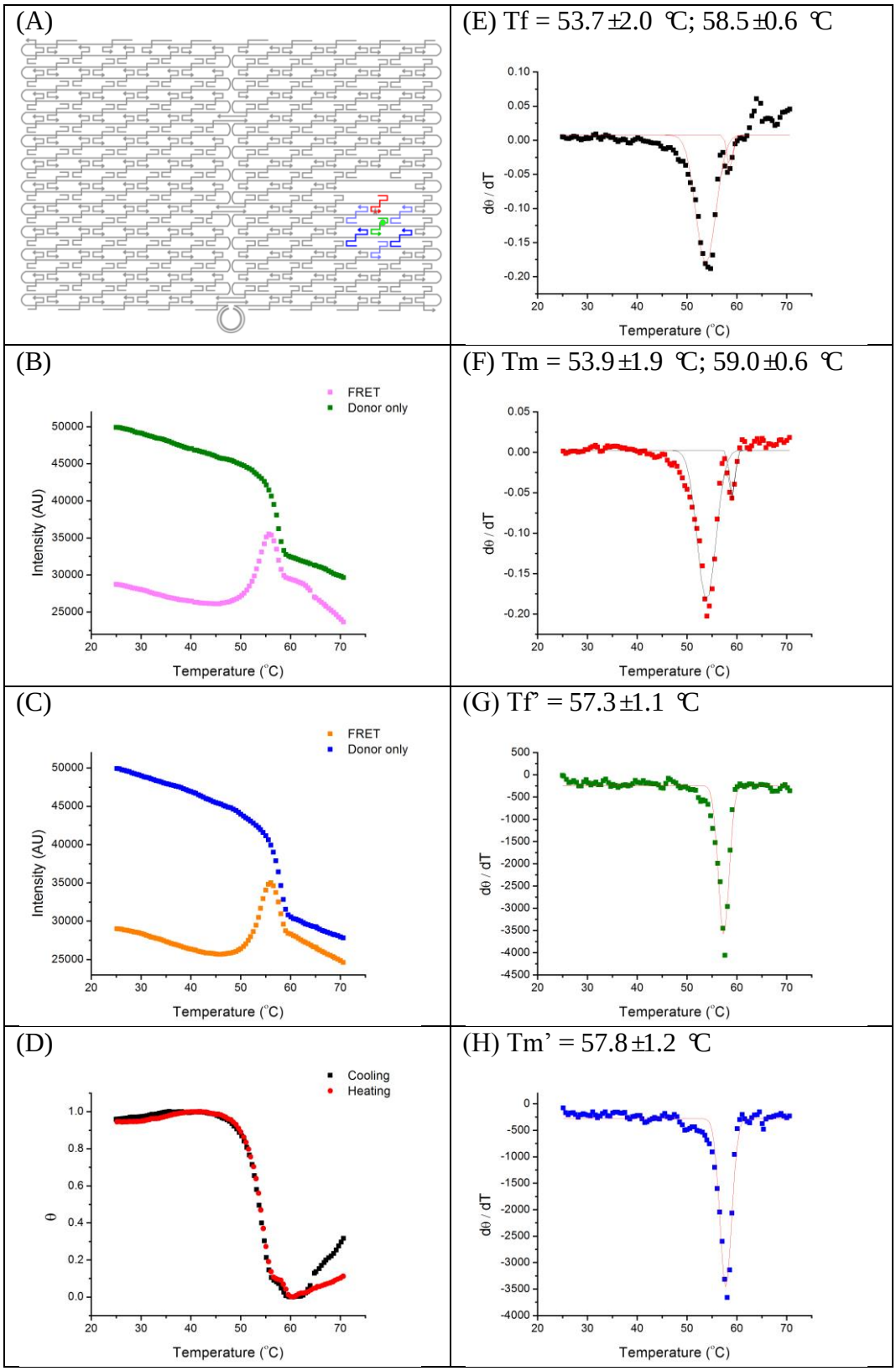

Figure S2.13. Cluster of 3 staples removed from N - position 1

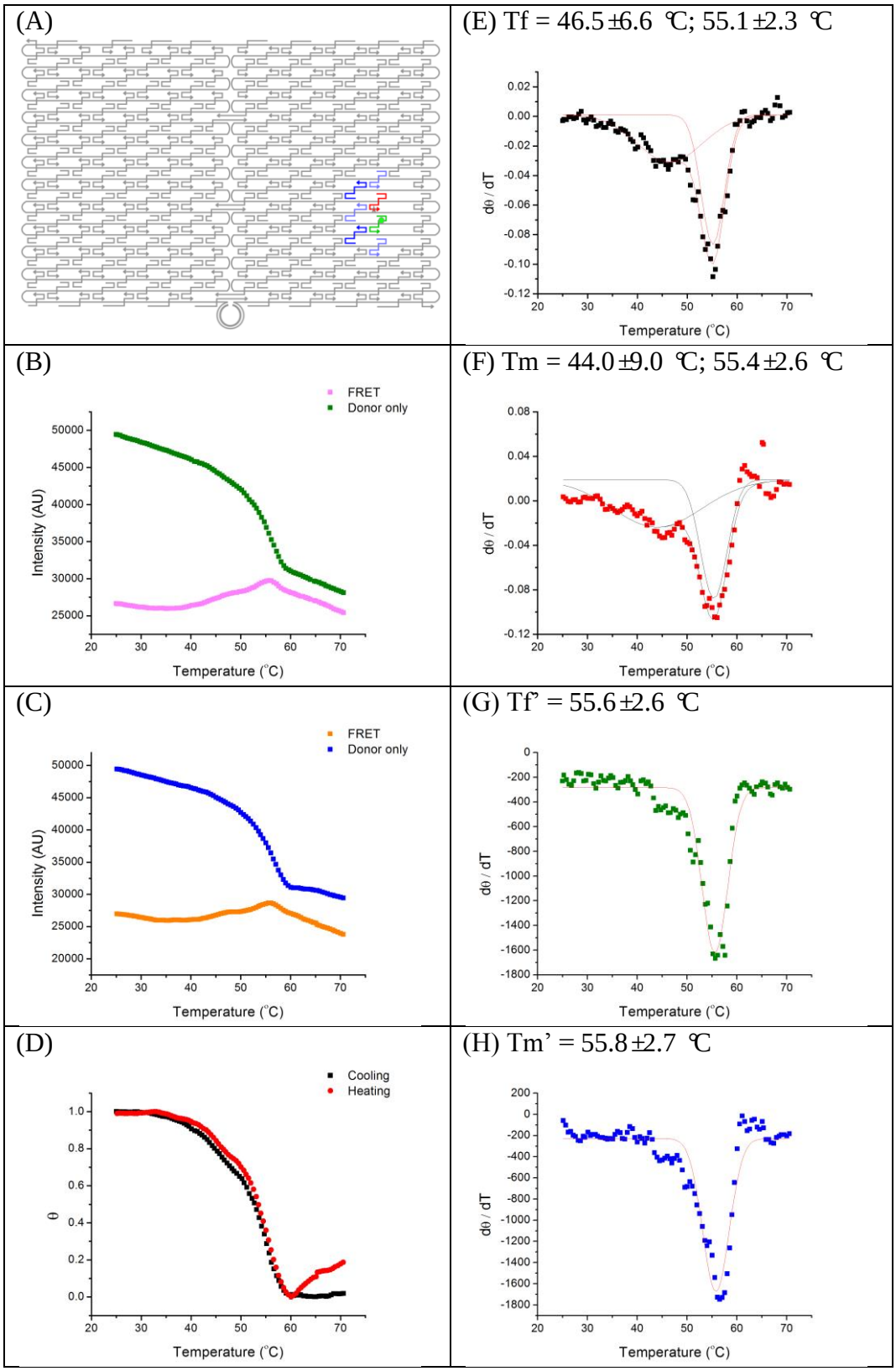

Figure S2.14. Cluster of 3 staples removed from E - position 1

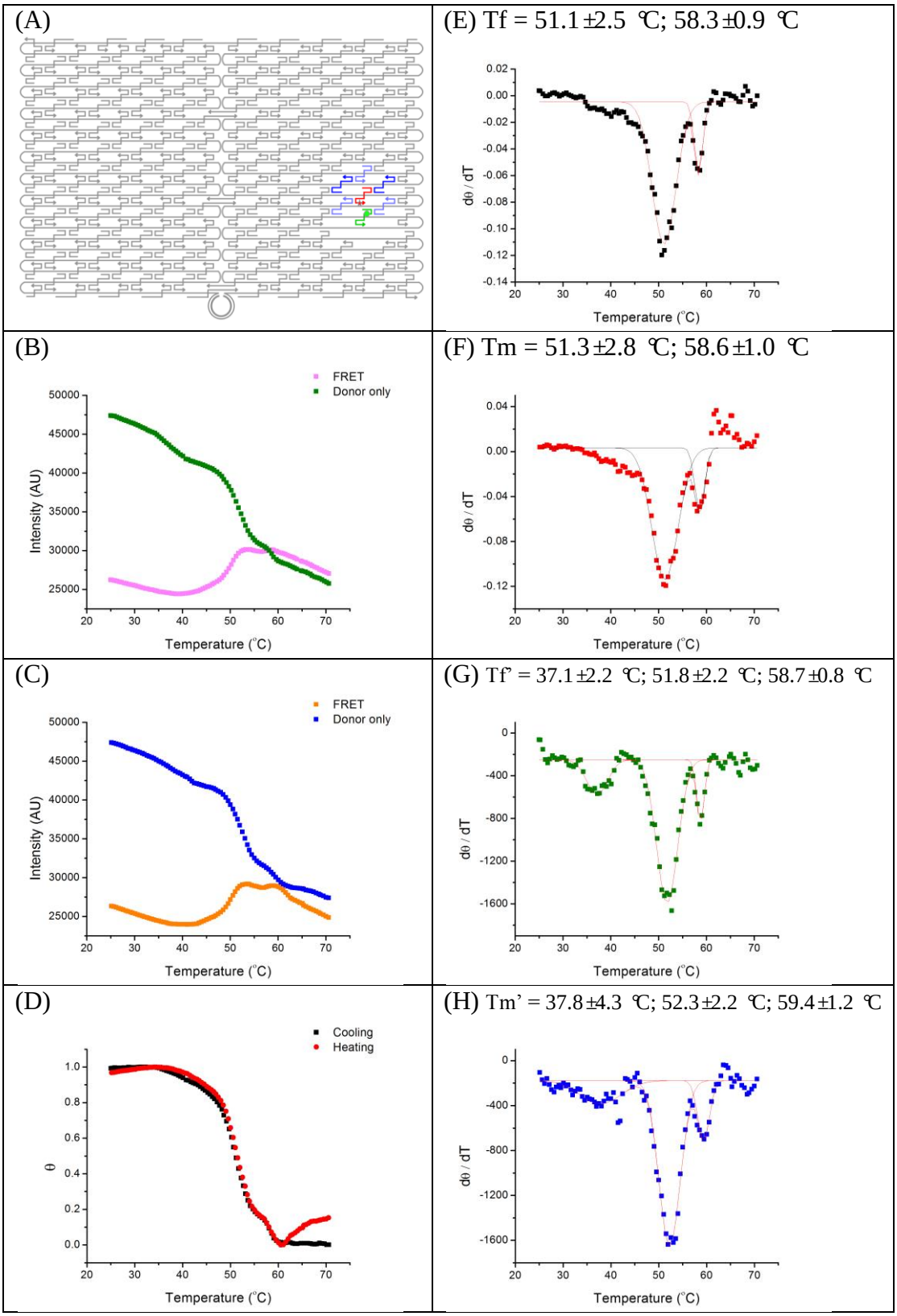

Figure S2.15. Cluster of 3 staples removed from S - position 1

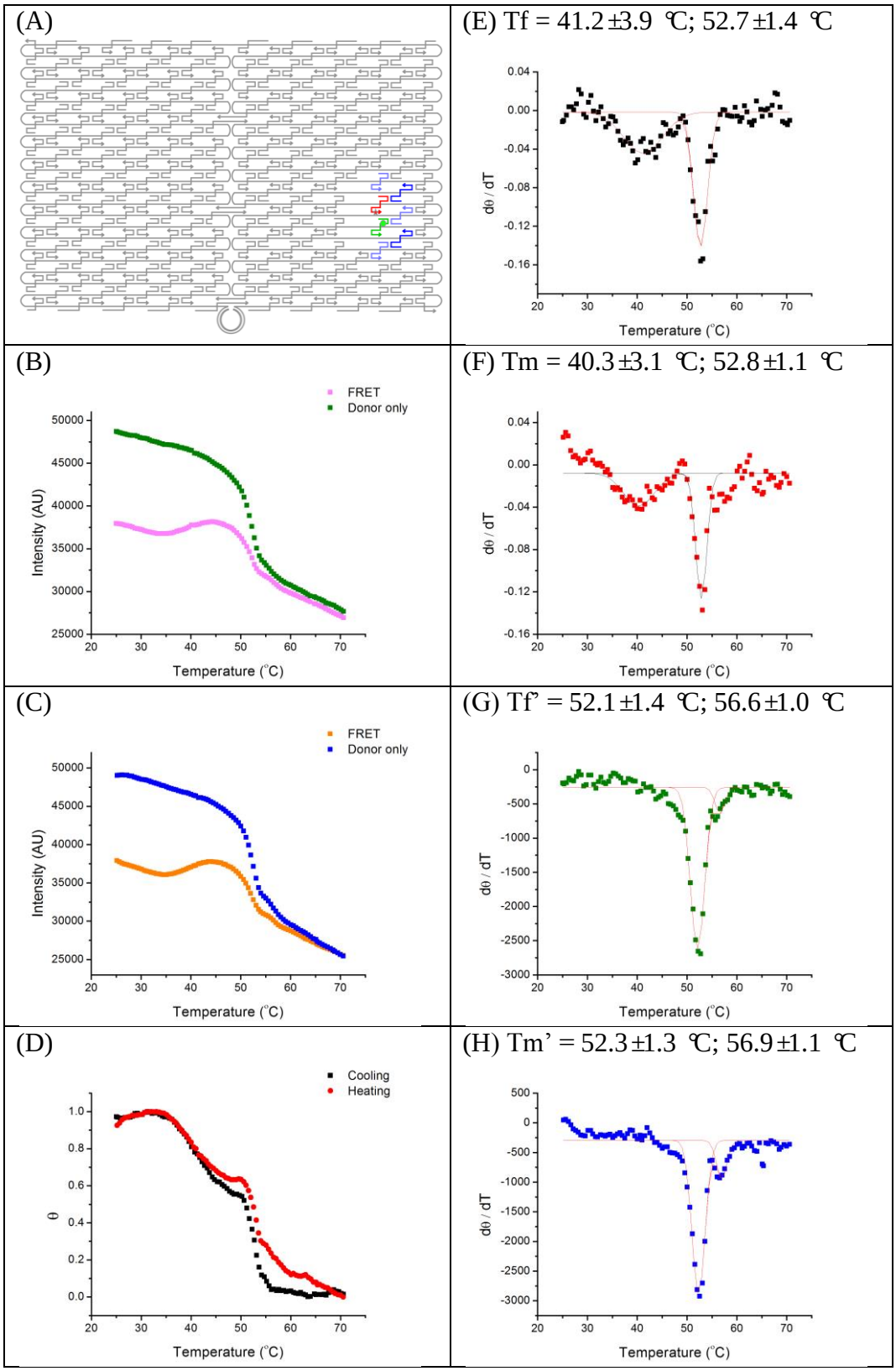

Figure S2.16. Cluster of 3 staples removed from W - position 1

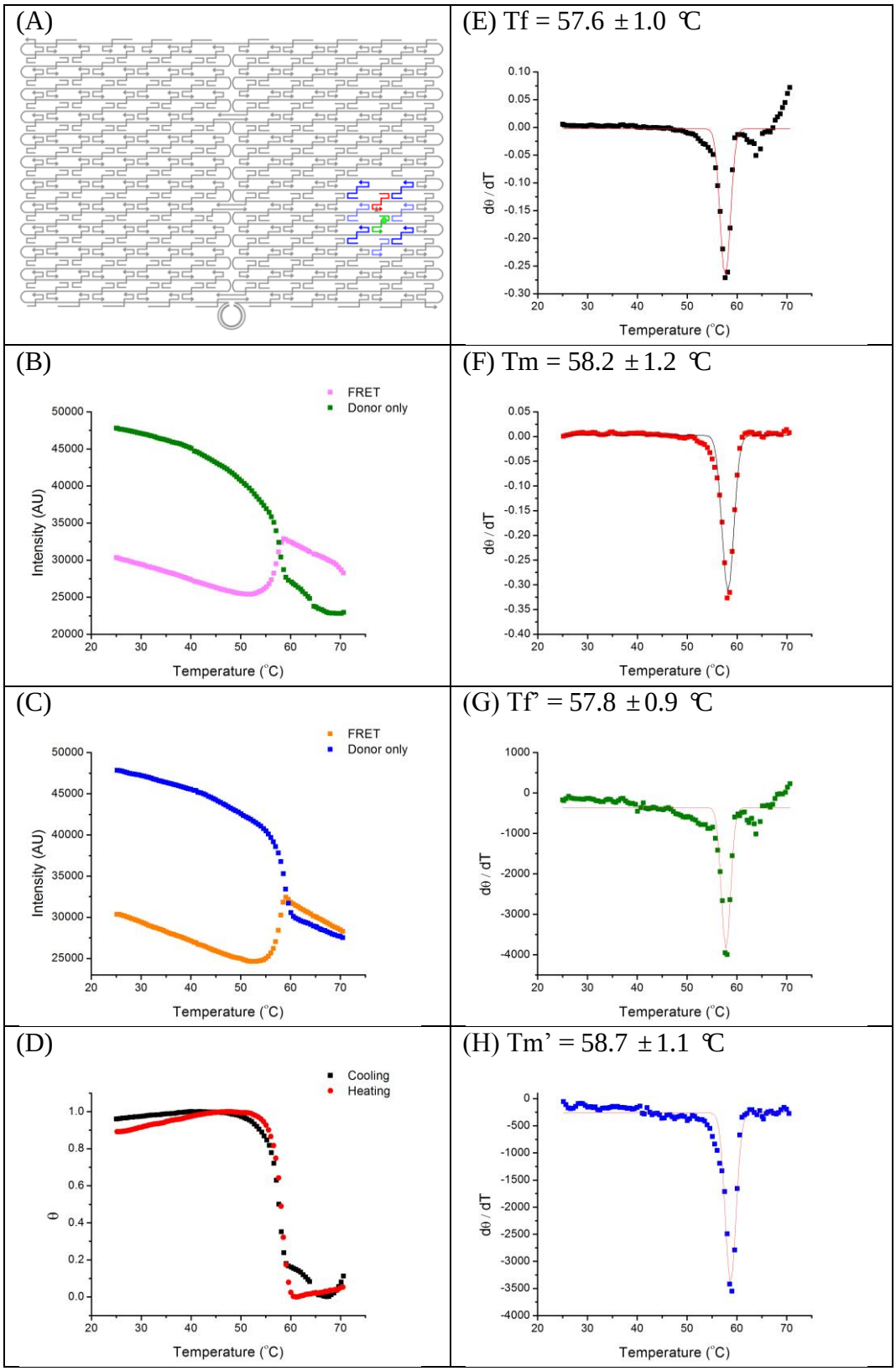

Figure S2.17. Staple N omitted - position 1

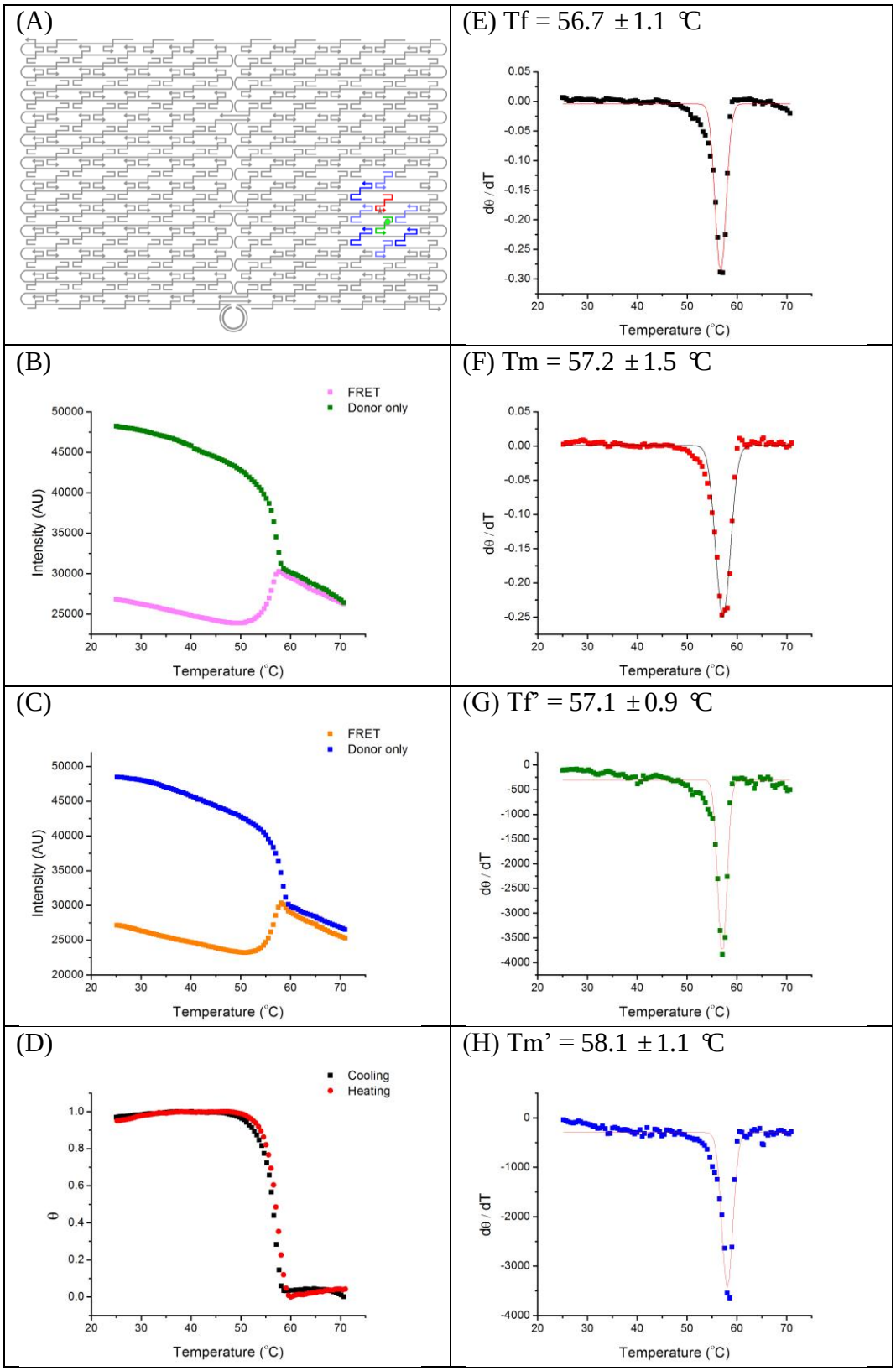

Figure S2.18. Staple NE omitted - position 1

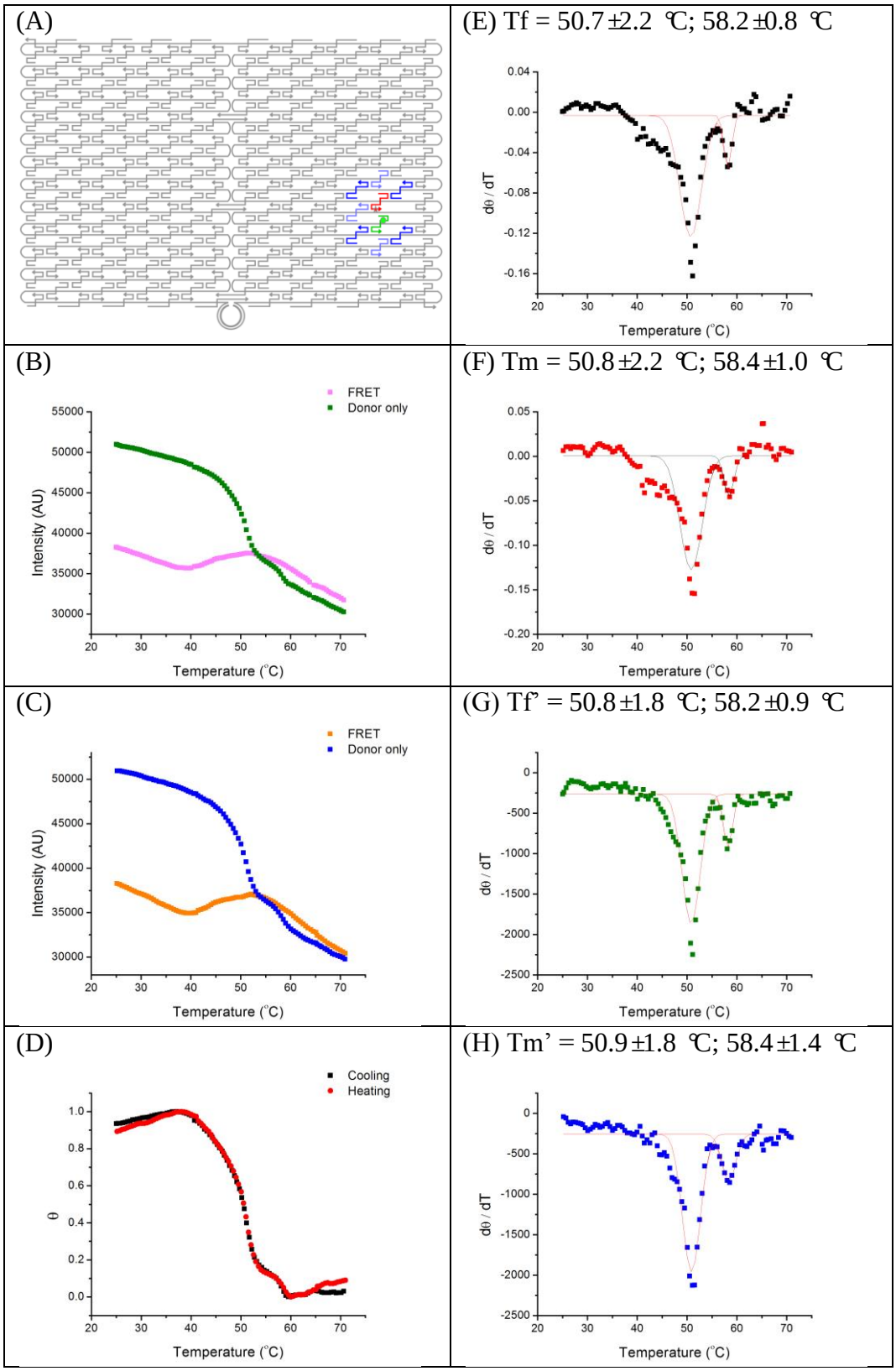

Figure S2.19. Staple E omitted - position 1

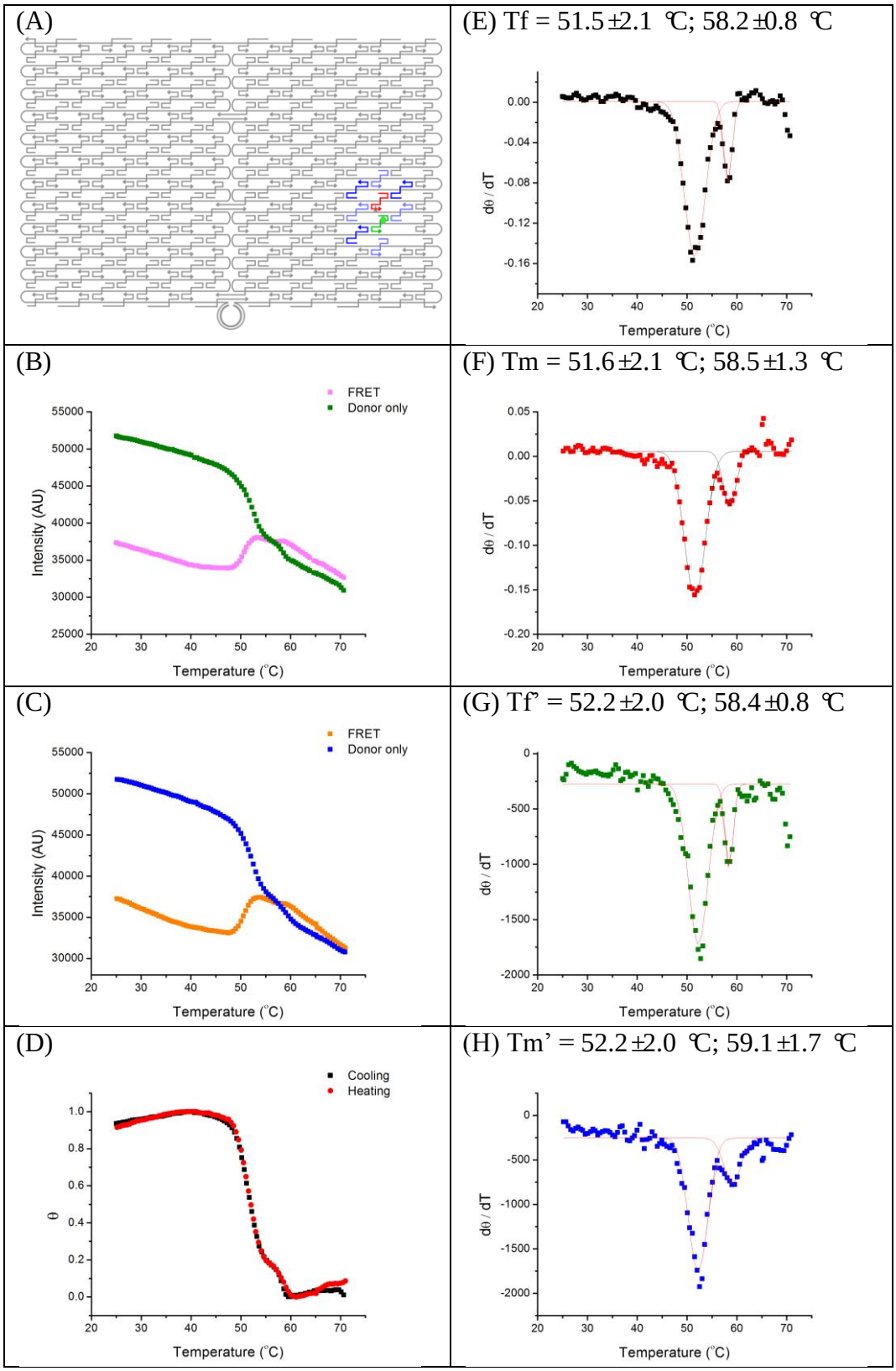

Figure S2.20. Staple SE omitted - position 1

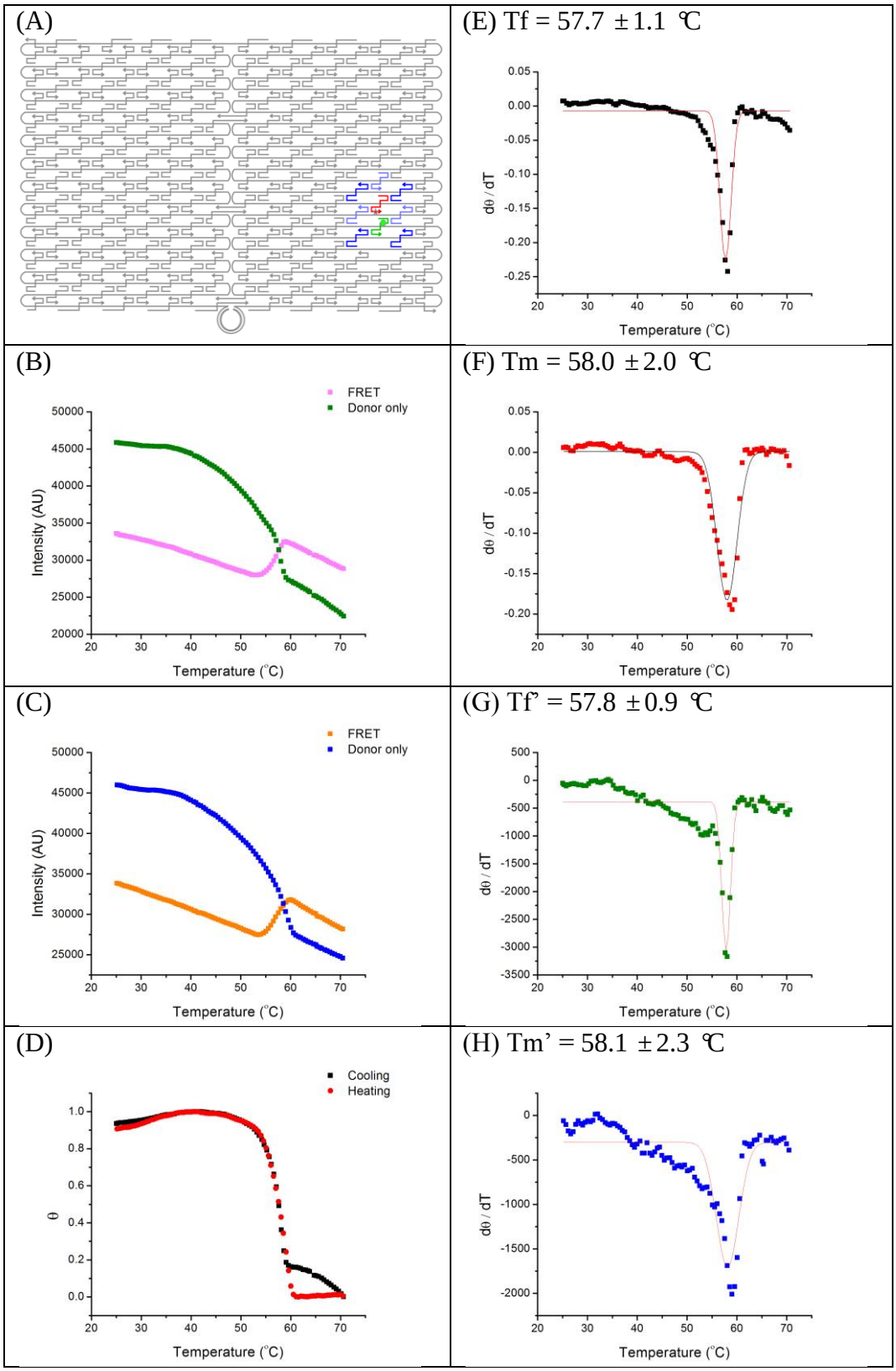

Figure S2.21. Staple S omitted - position 1

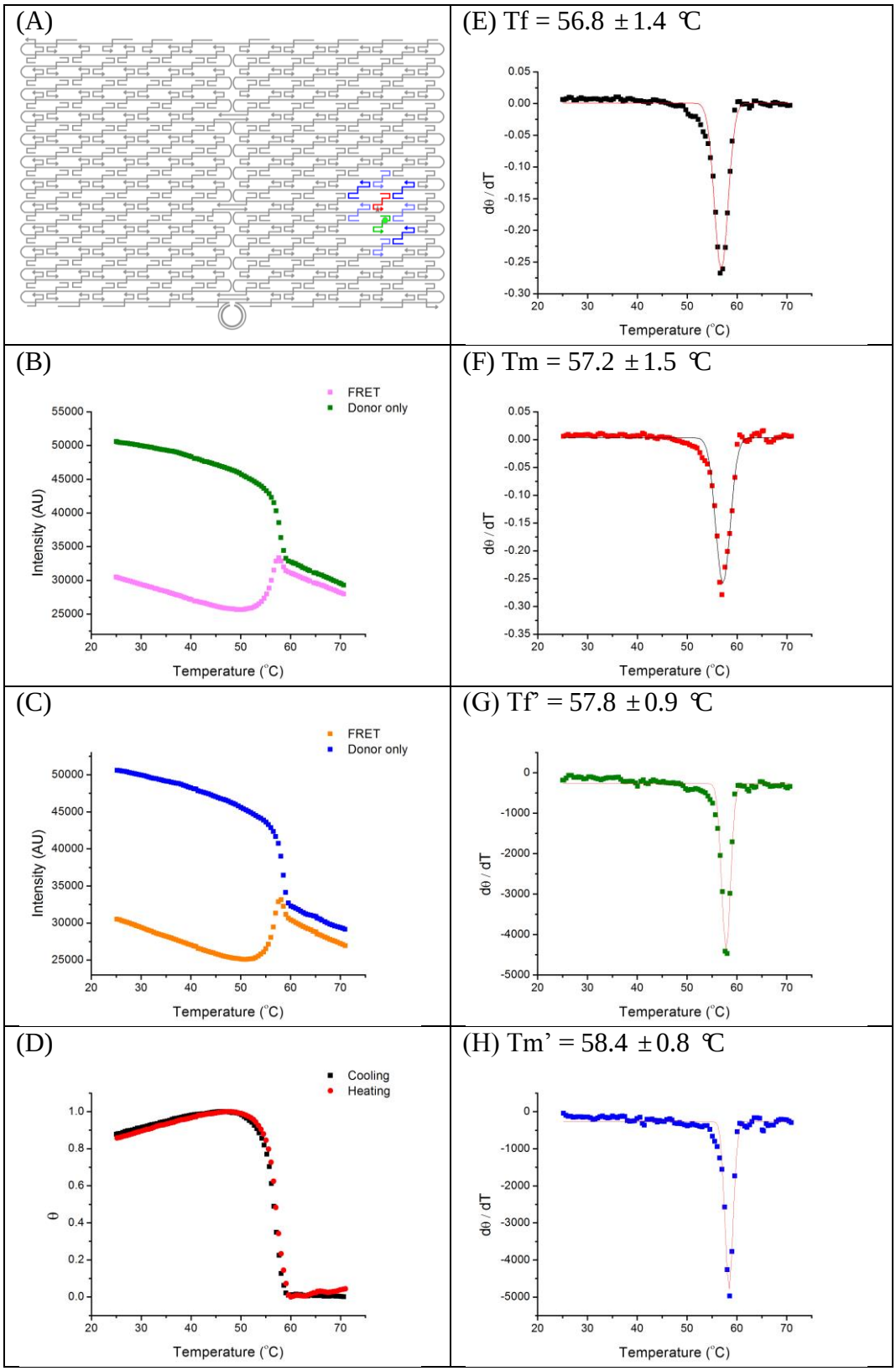

Figure S2.22. Staple SW omitted - position 1

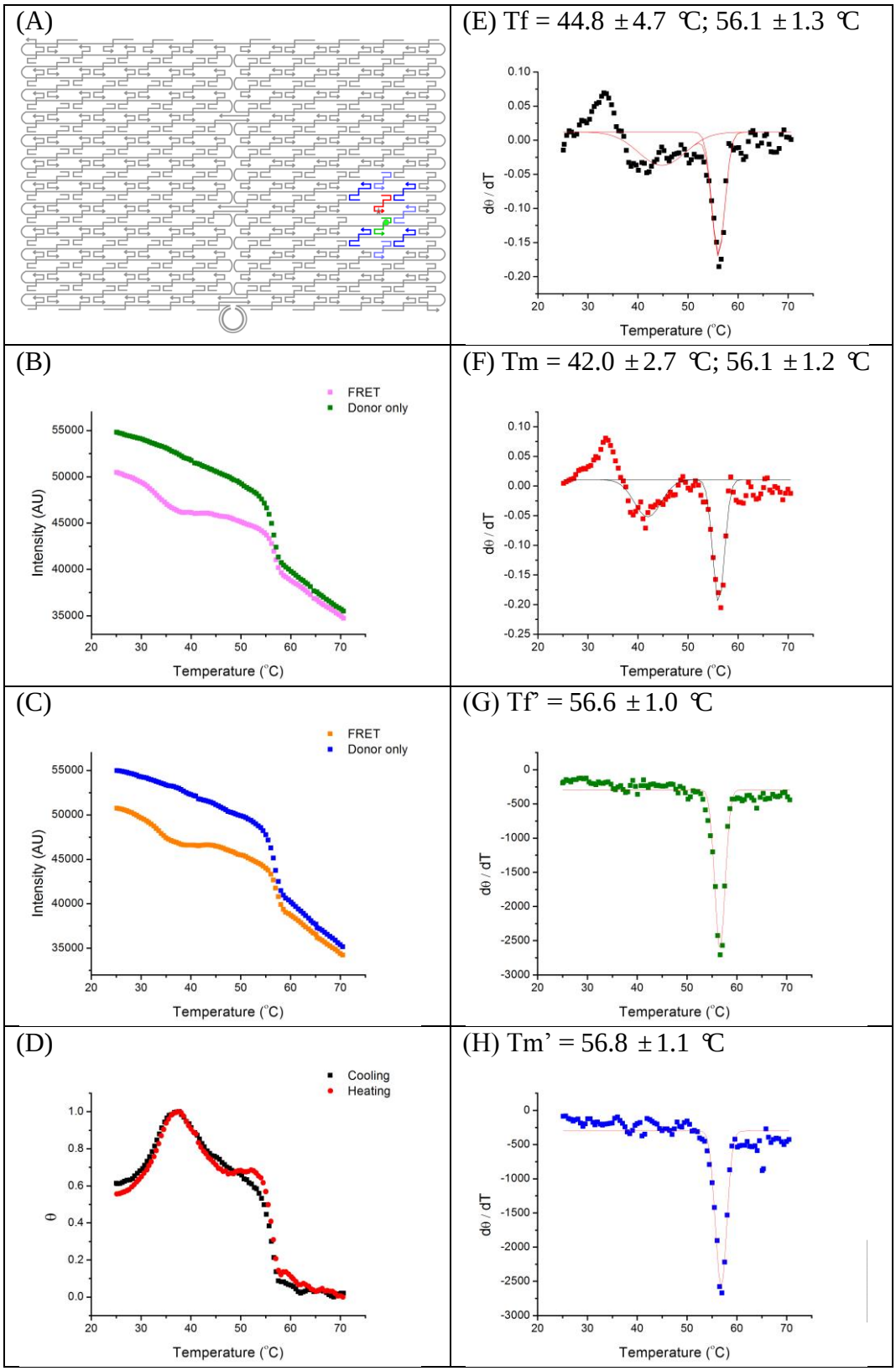

Figure S2.23. Staple W omitted - position 1

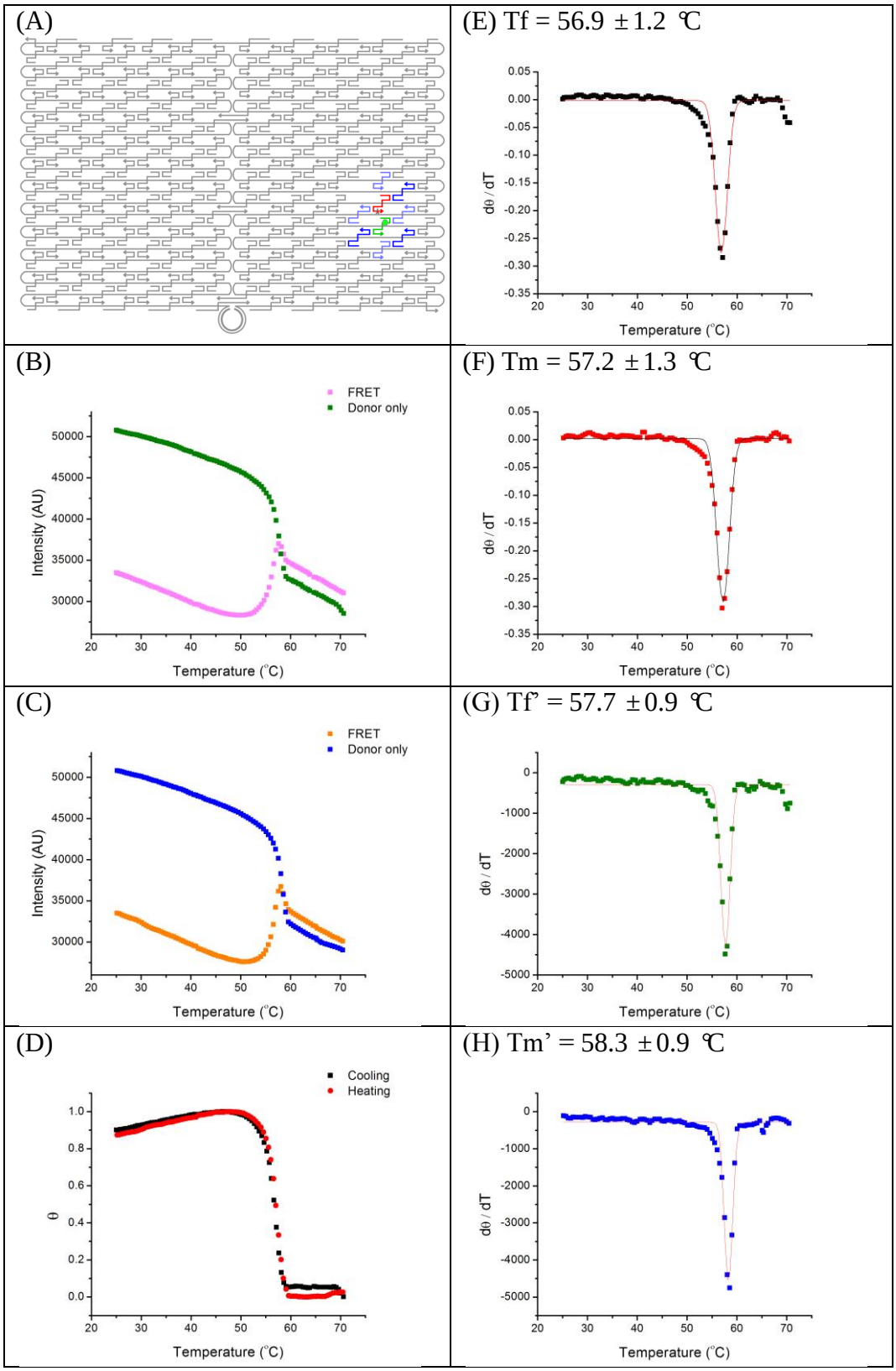

Figure S2.24. Staple NW omitted - position 1

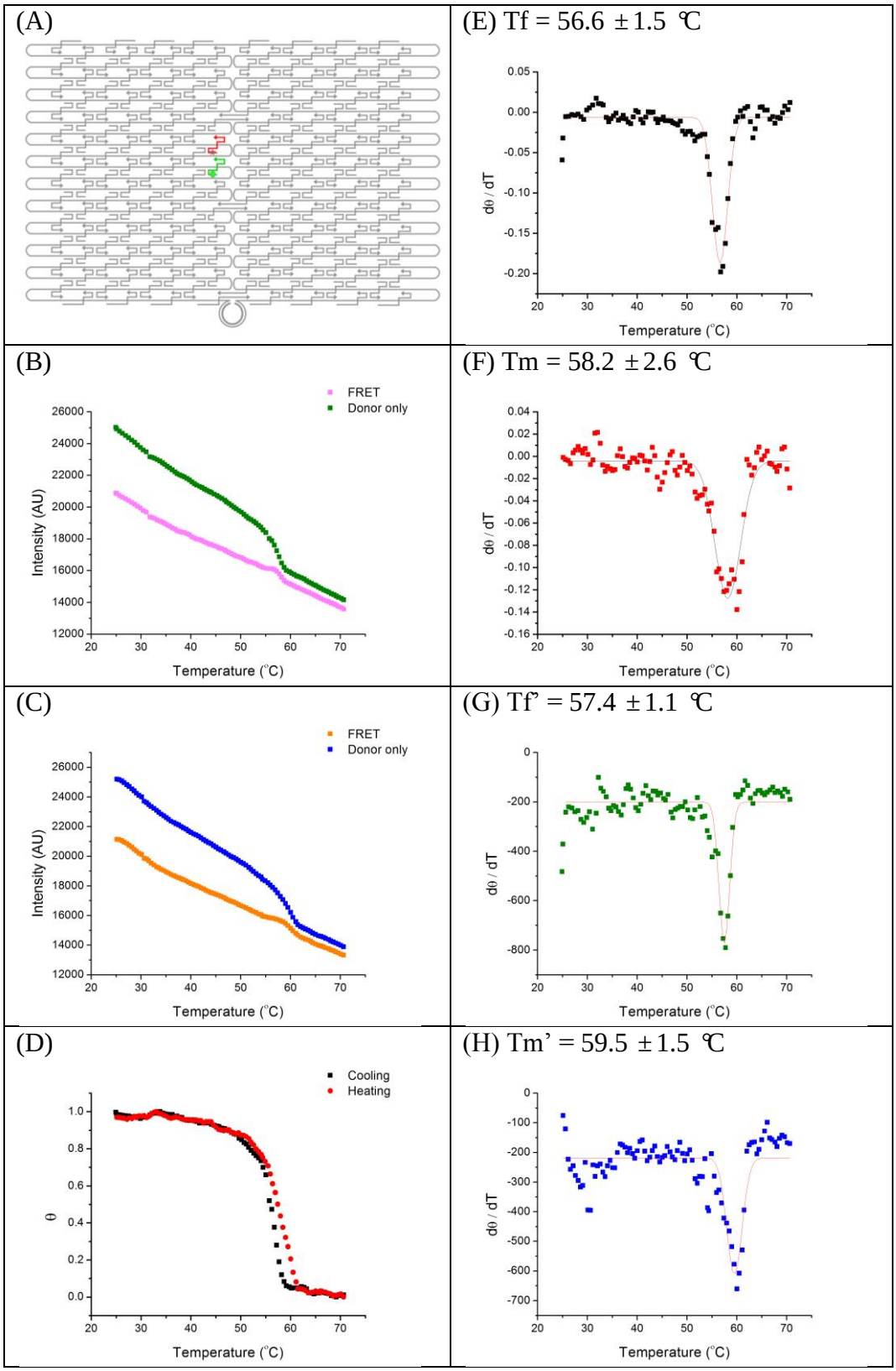

Figure S2.25. Rectangular structure - position 2 (edge staples omitted)

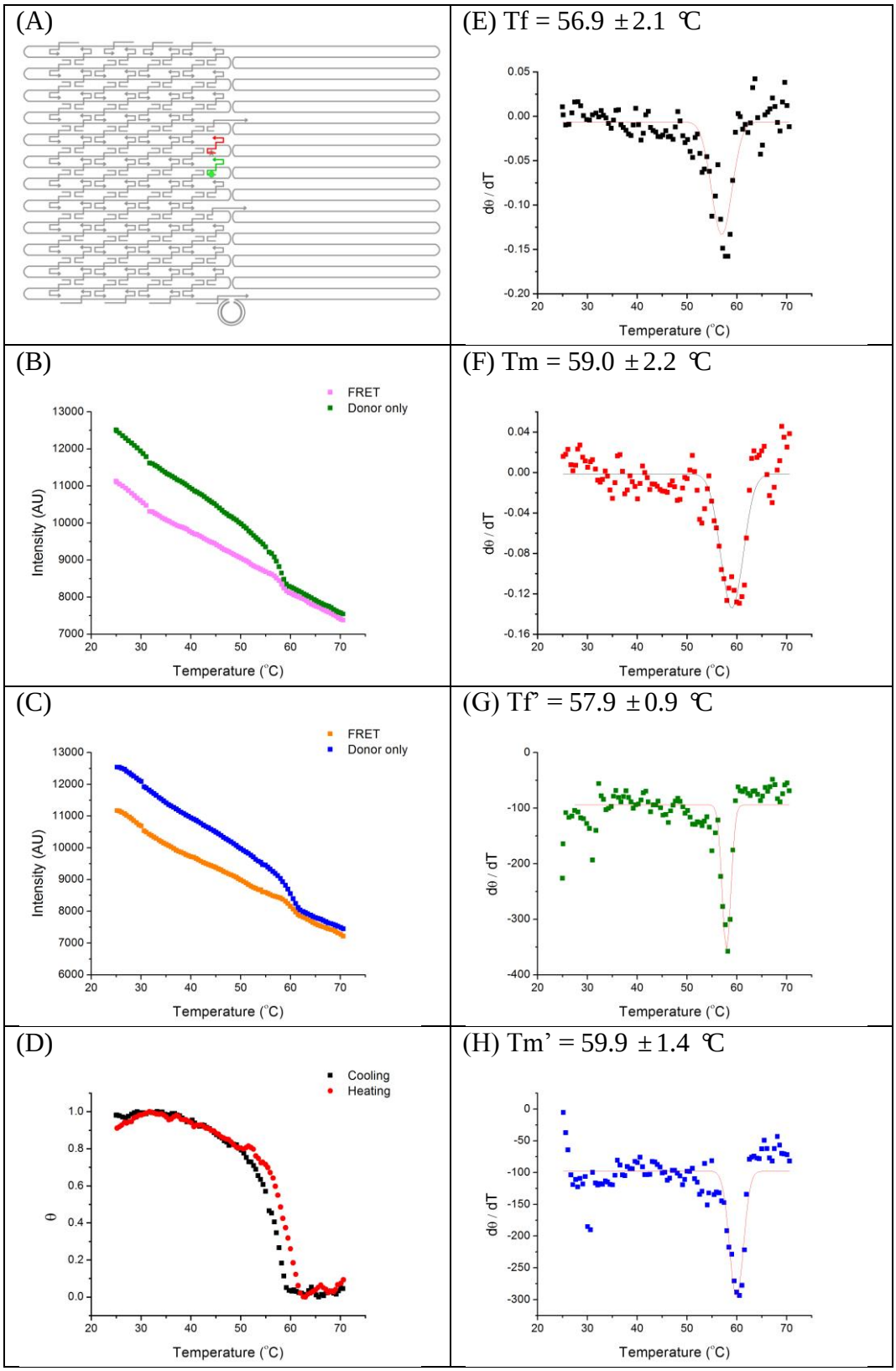

Figure S2.26. Half origami structure – position 2 (edge staples omitted)

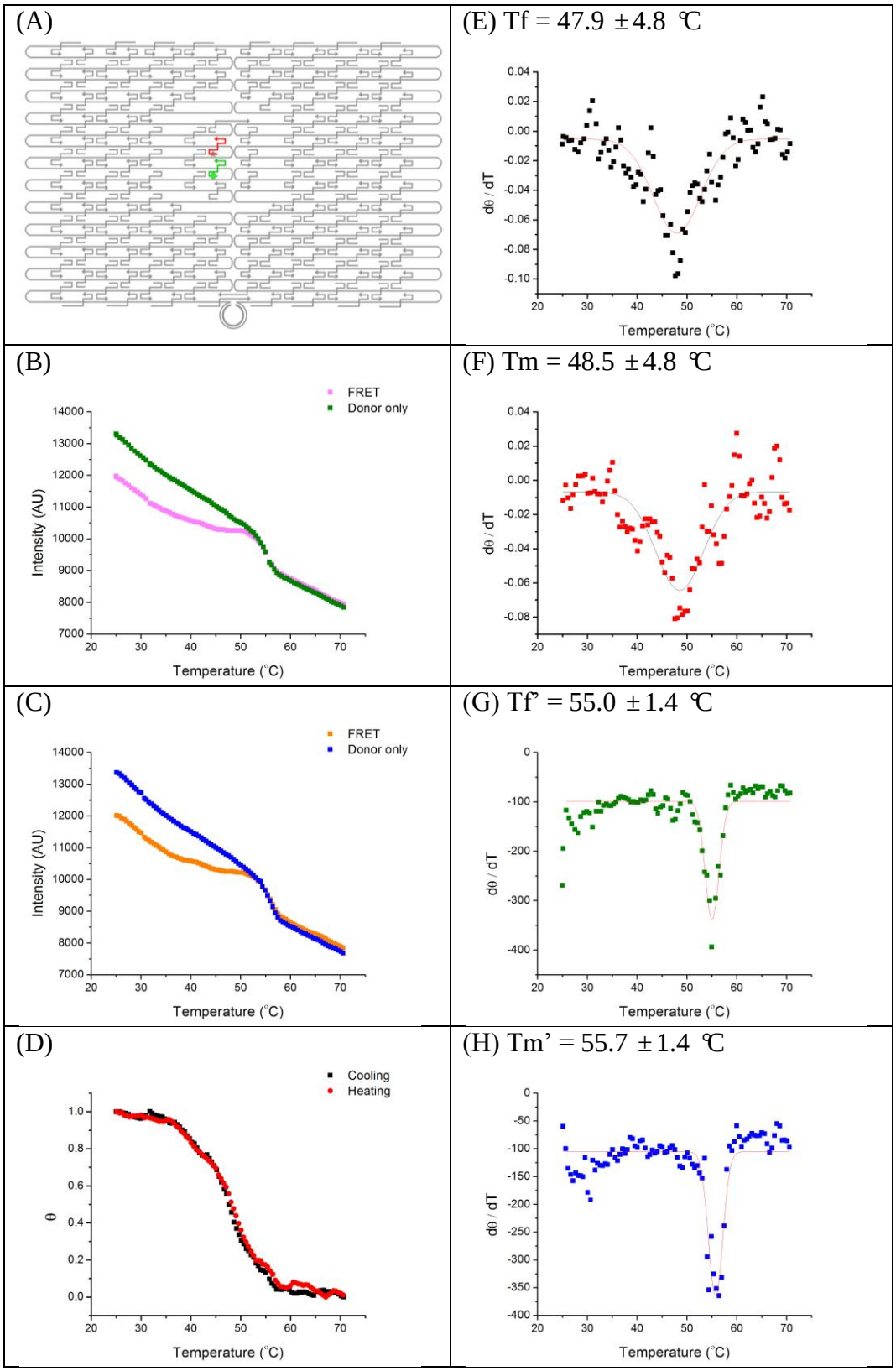

Figure S2.27. 7 helix core structure – position 2 (edge staples omitted)

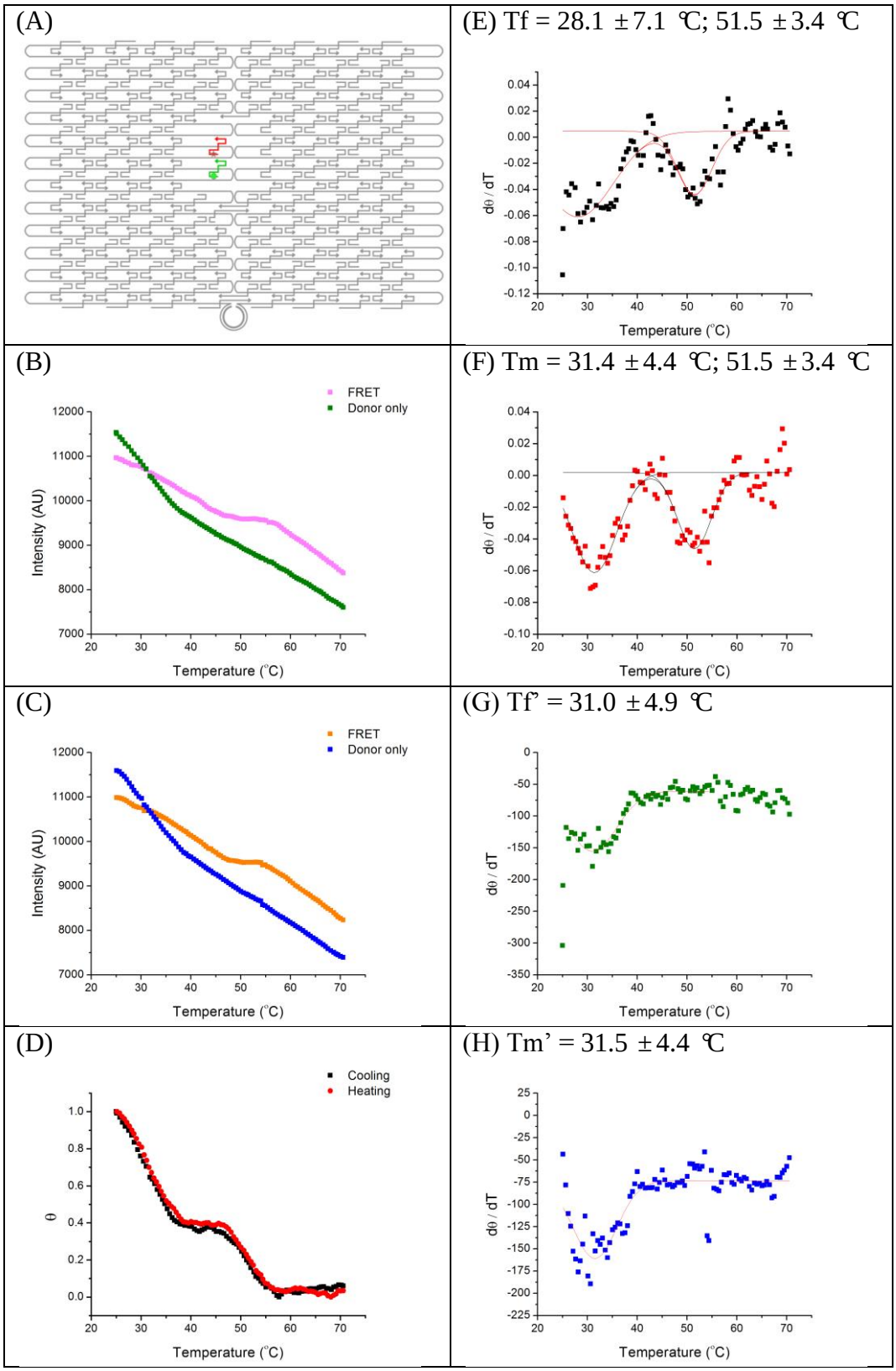

Figure S2.28. Small-hole structure – position 2 (edge staples omitted)

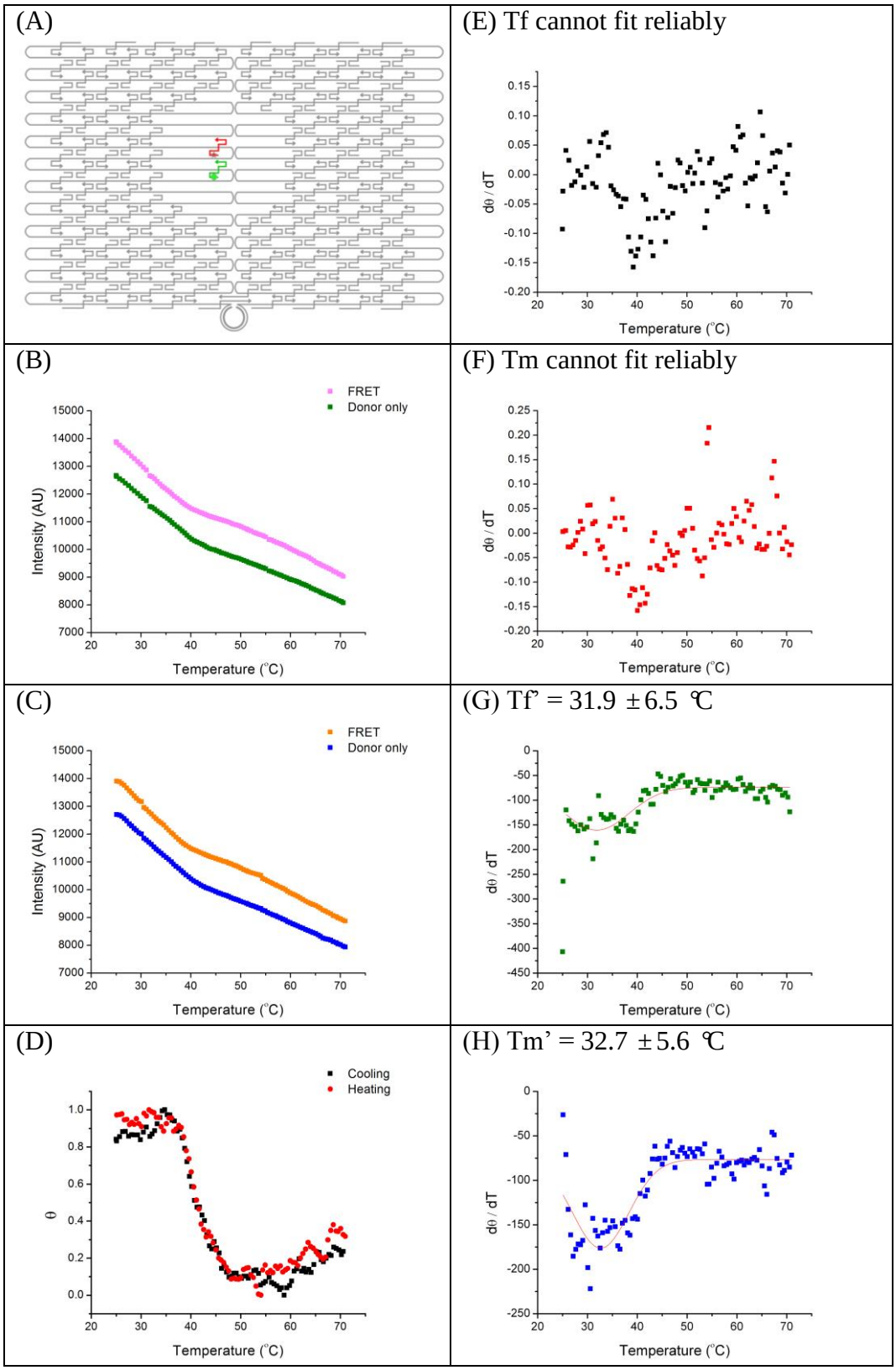

Figure S2.29. Big-hole structure – position 2 (edge staples omitted)

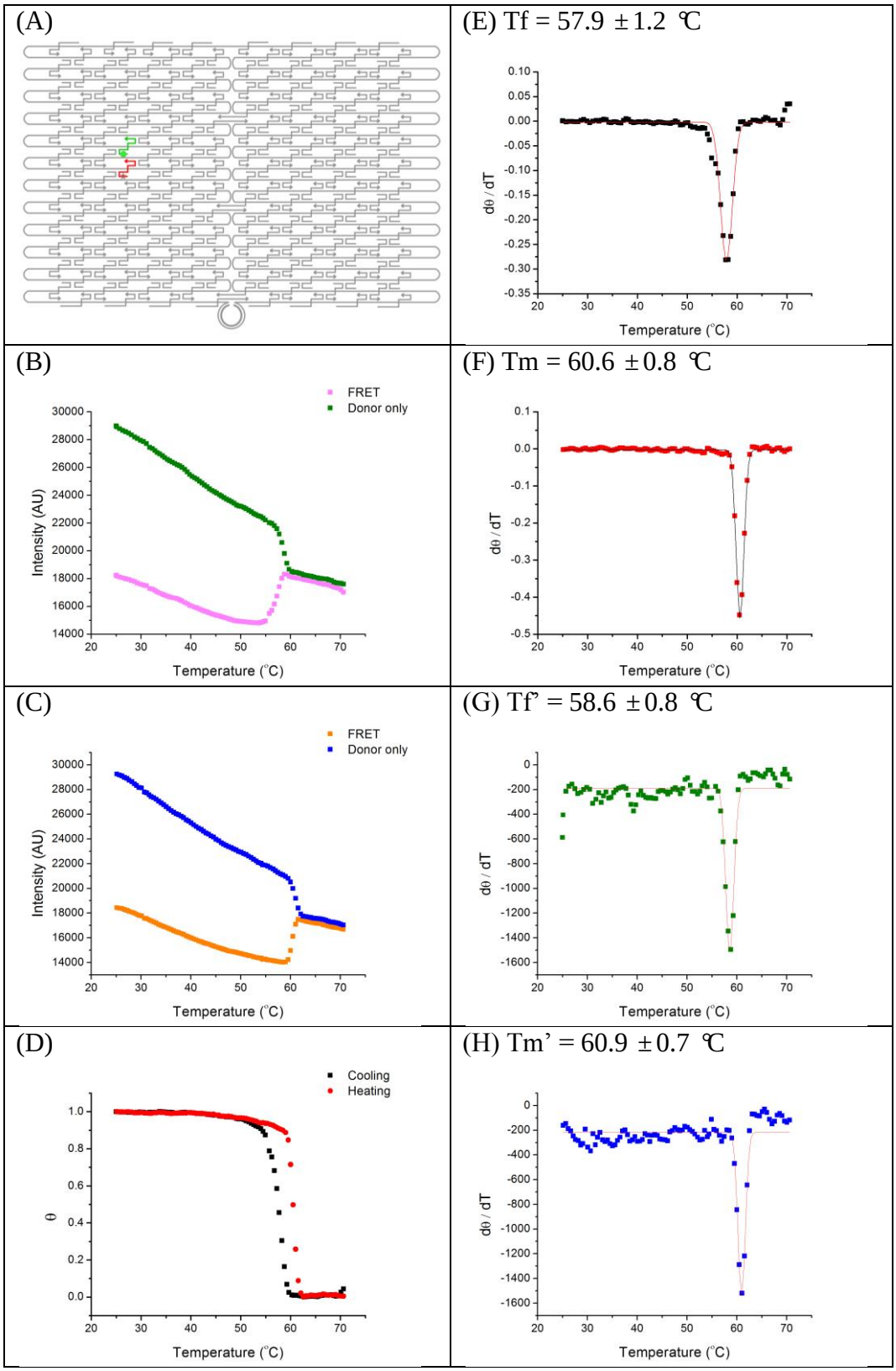

Figure S2.30. Rectangular structure - position 3 (edge staples omitted)

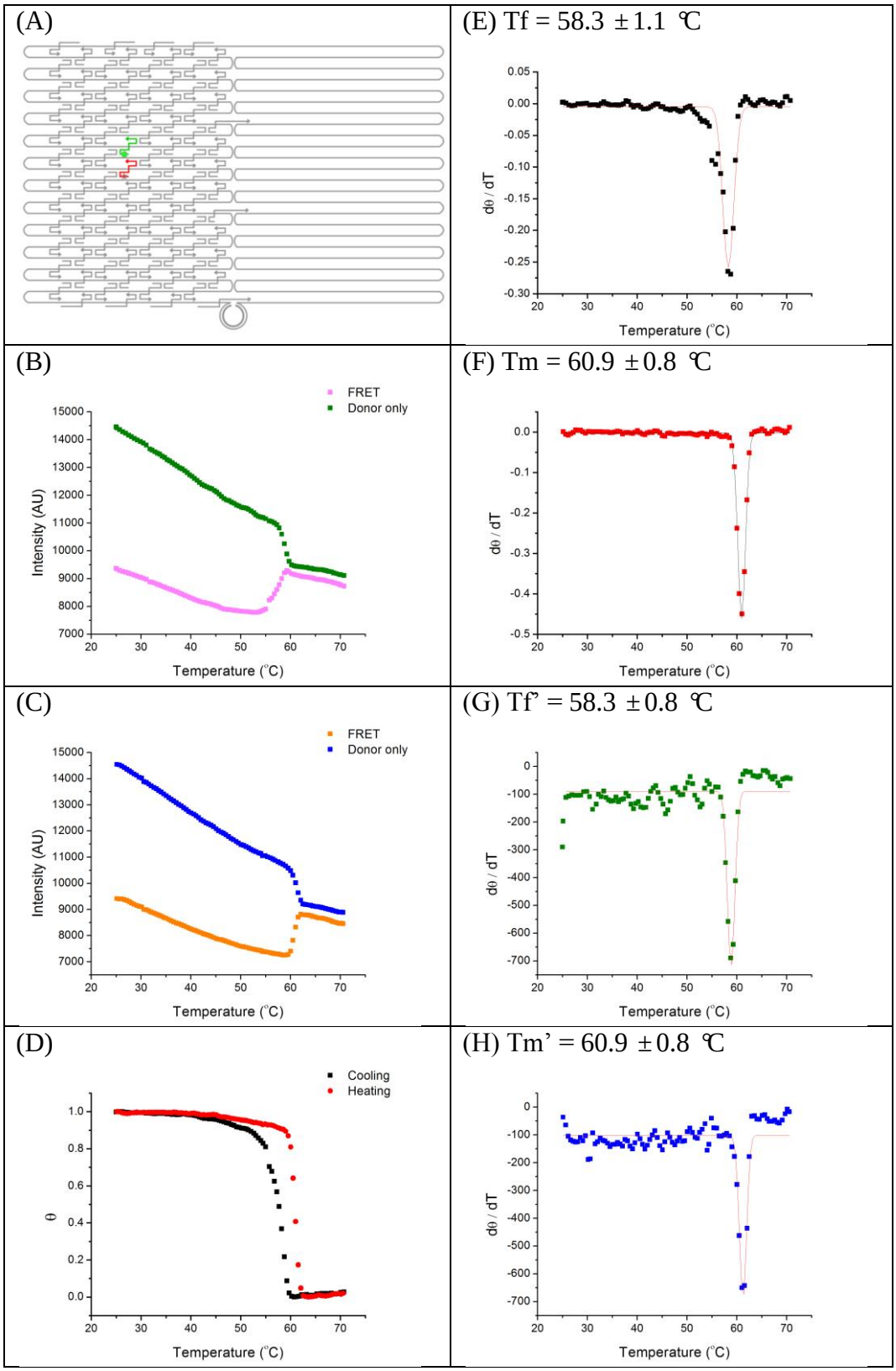

Figure S2.31. Half origami structure - position 3 (edge staples omitted)

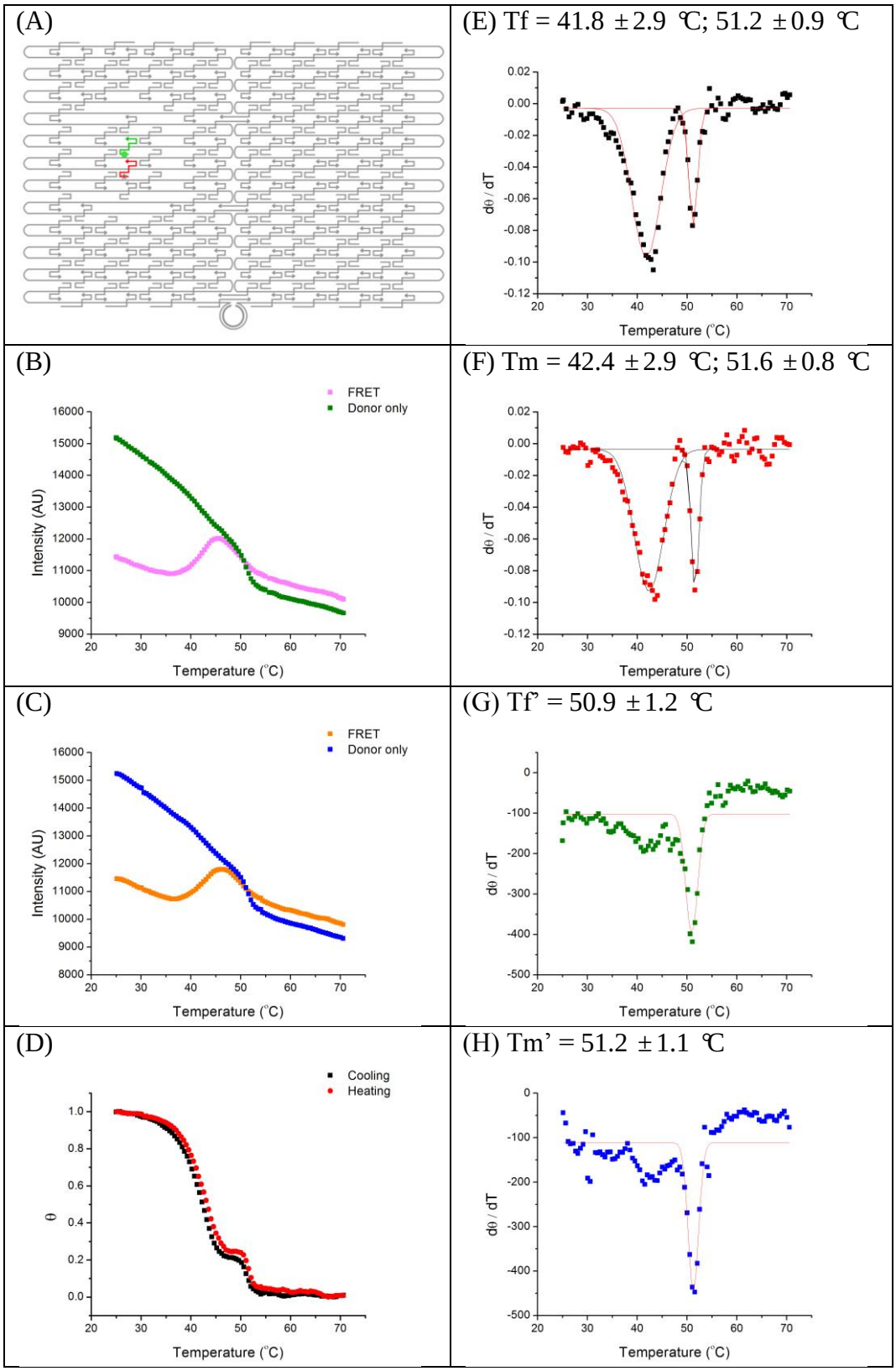

Figure S2.32. Ring-hole structure - position 3 (edge staples omitted)

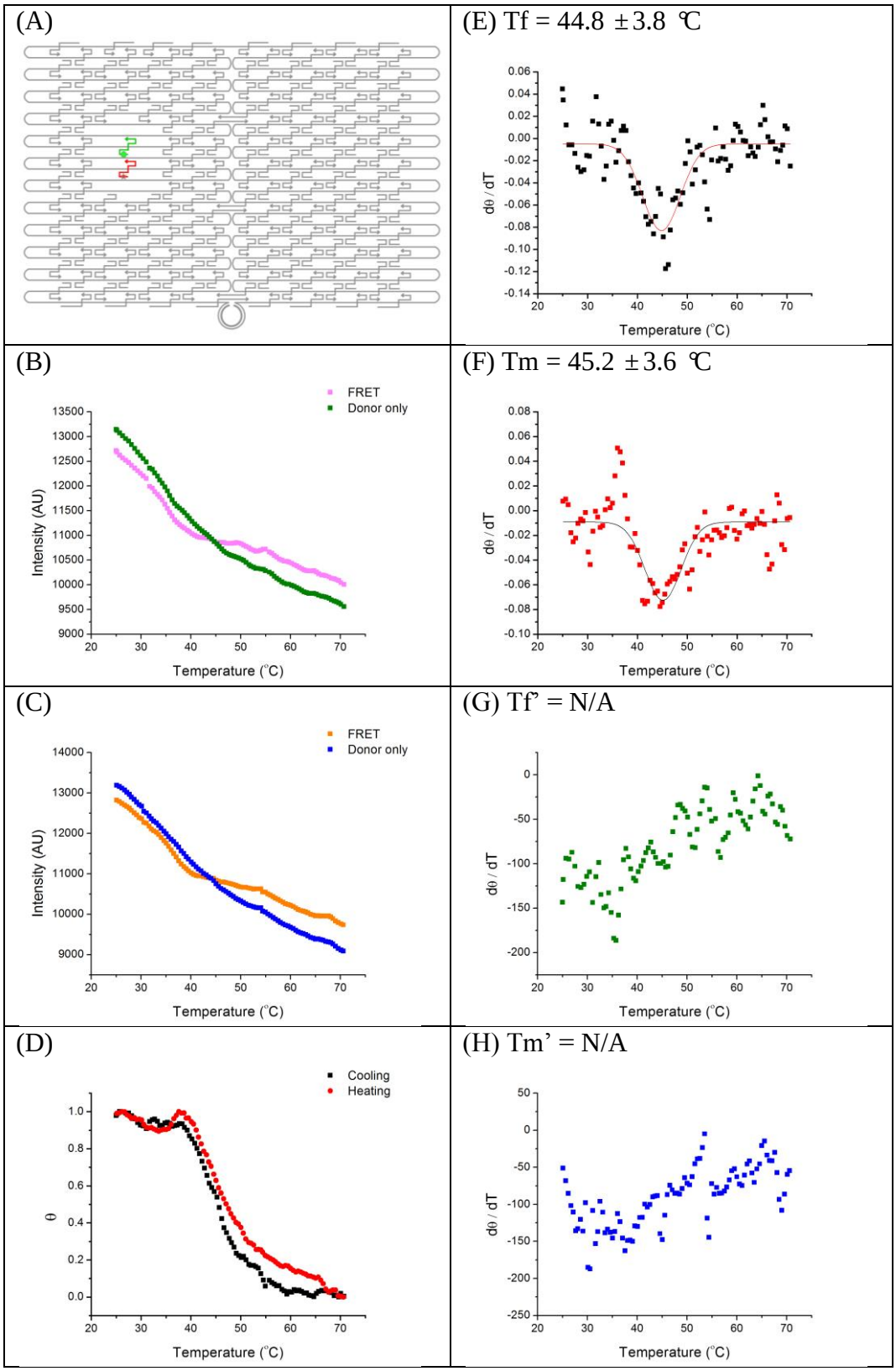

Figure S2.33. Small-hole structure - position 3 (edge staples omitted)

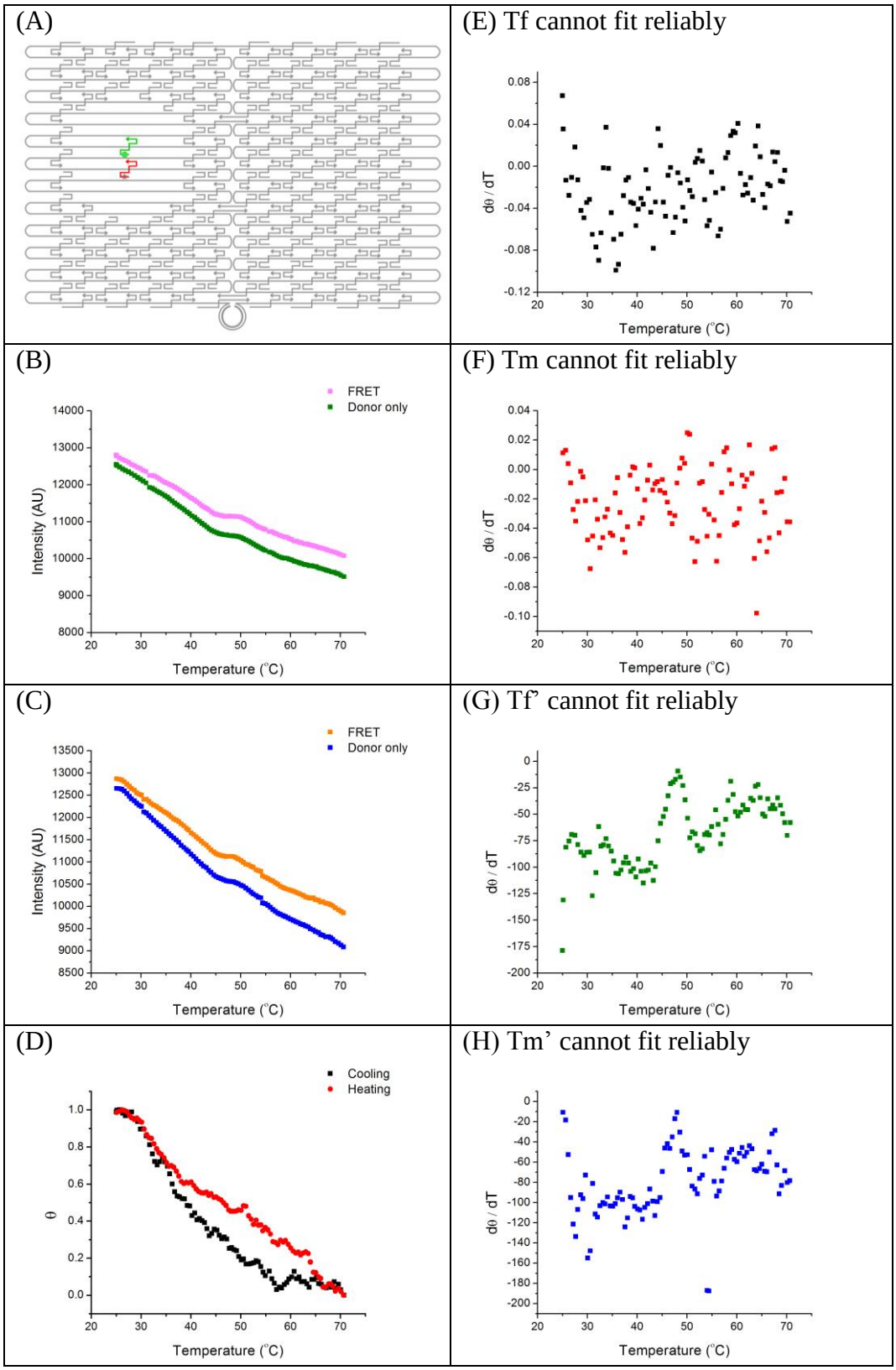

Figure S2.34. Big-hole structure - position 3 (edge staples omitted)

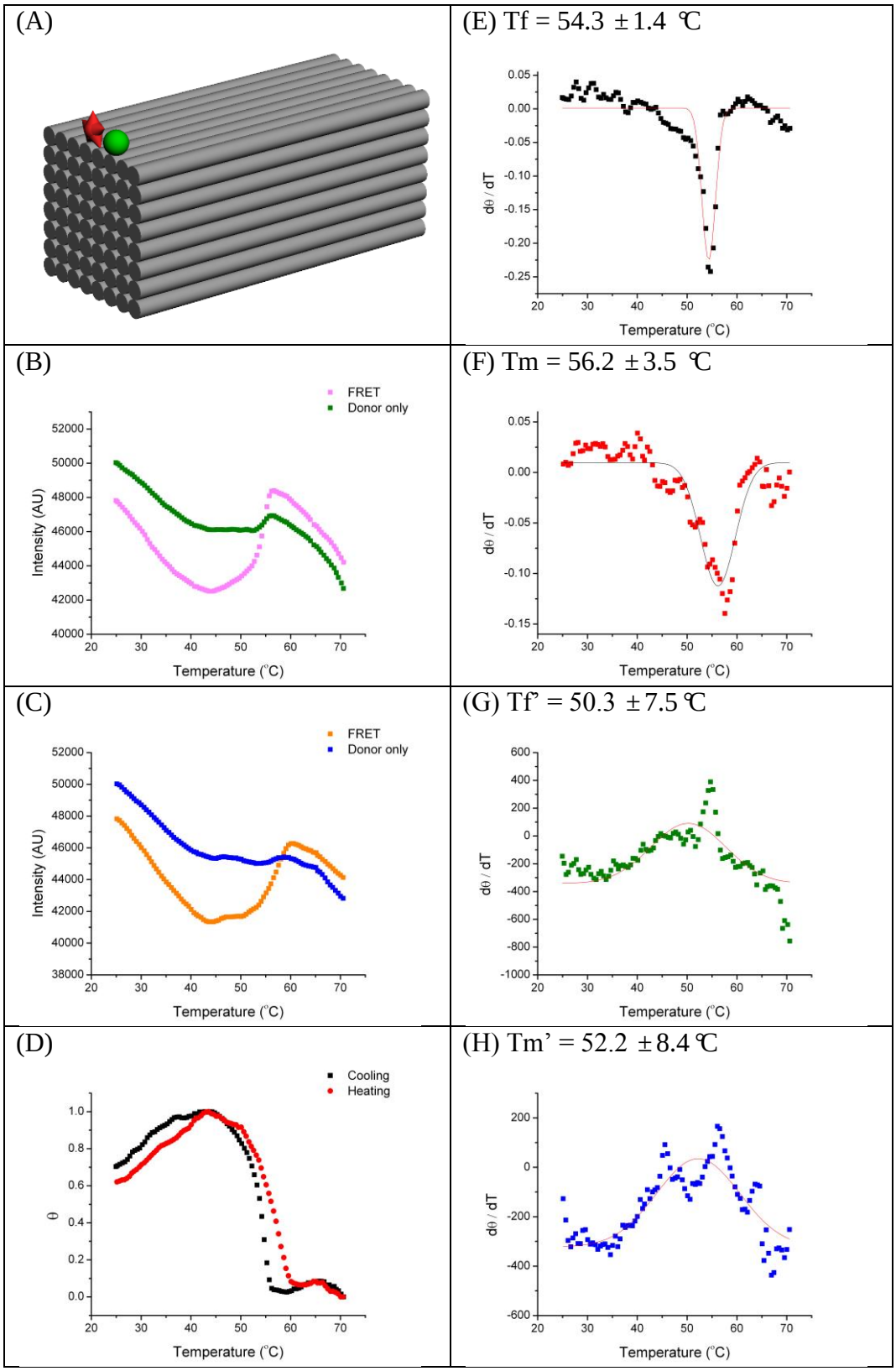

Figure S2.35. Cuboid structure – position 1

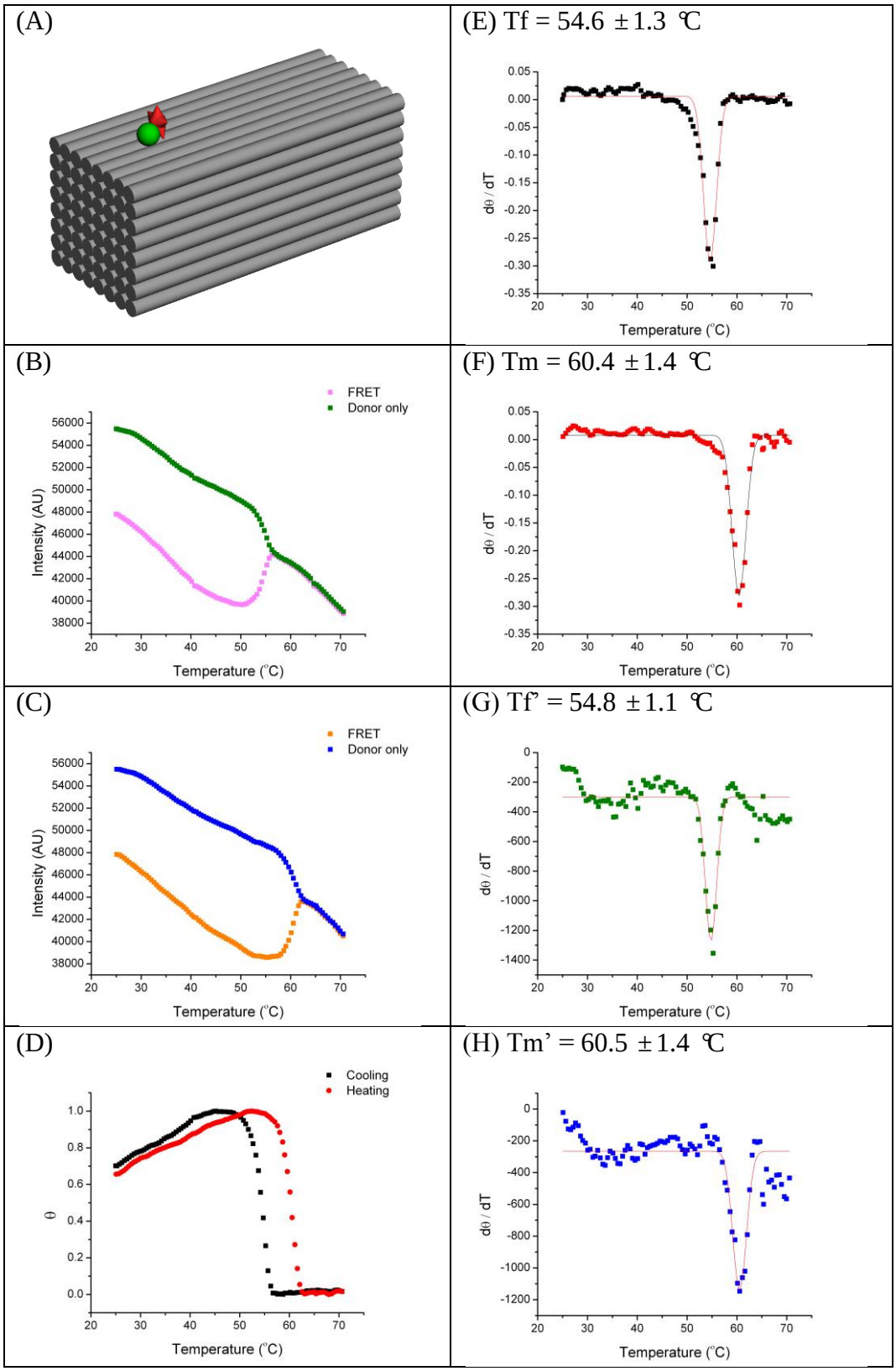

Figure S2.36. Cuboid structure – position 2

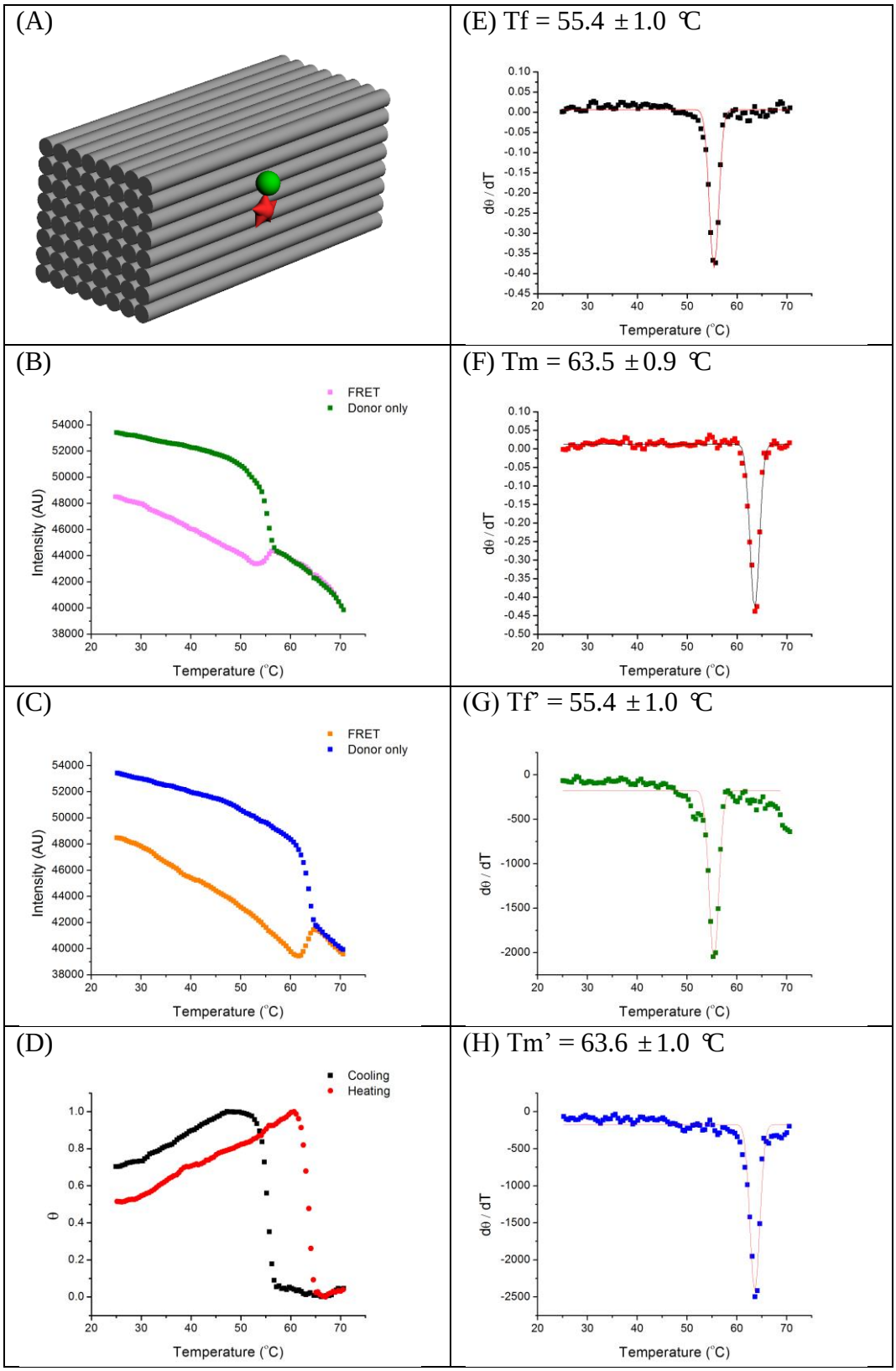

Figure S2.37. Cuboid structure – position 3

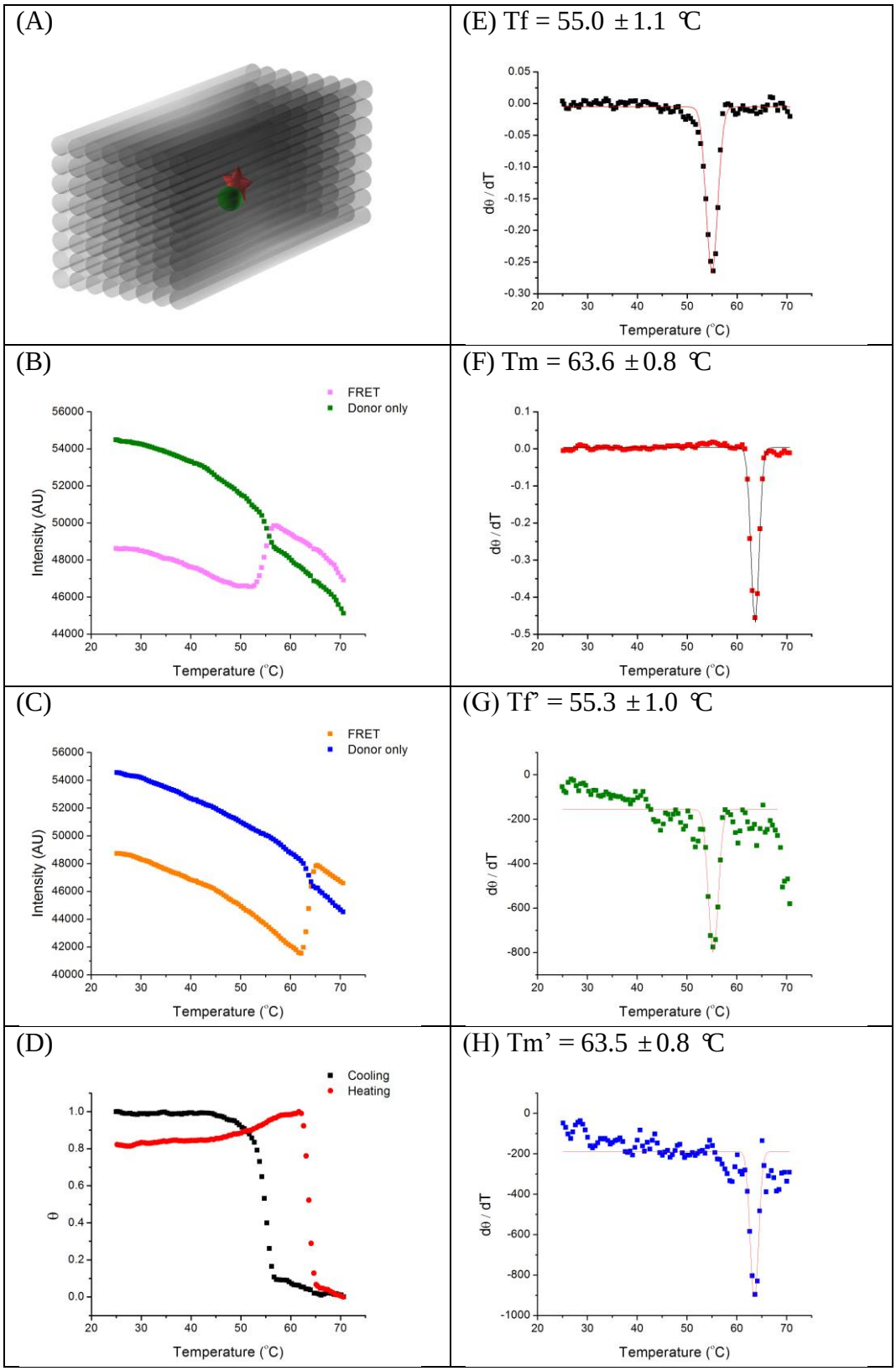

Figure S2.38. Cuboid structure – position 4

APPENDIX B

SUPPLEMENTAL INFORMATION FOR CHAPTER 3

(INTEGRATION, STABILIZATION AND SEPARATION OF DNA NANOSTRUCTURES FROM CELLS/CELL LYSATE)

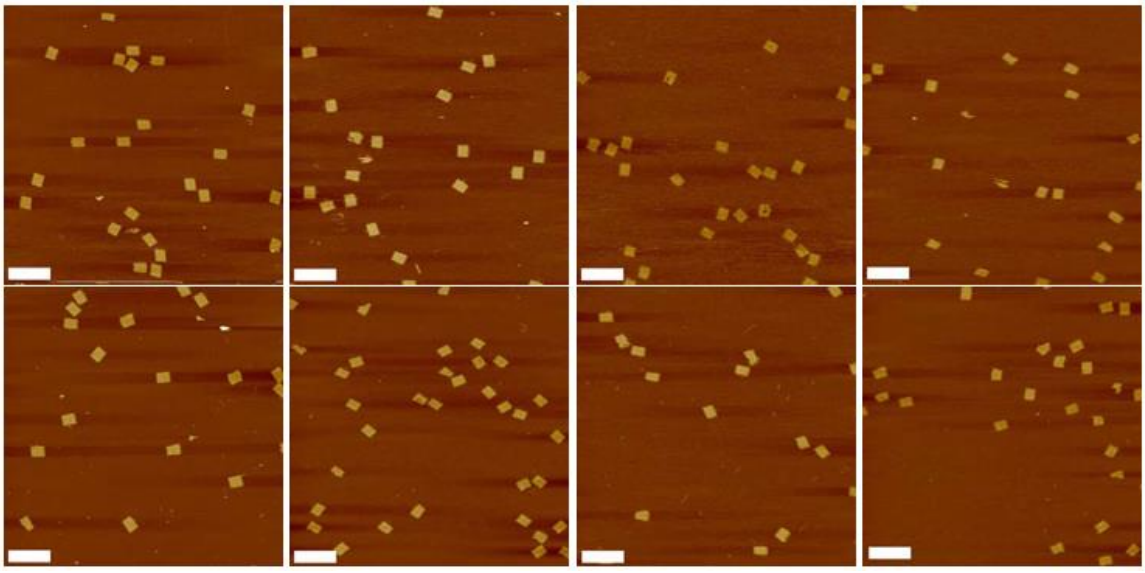

Figure S3.1. Additional AFM images of rectangular origami extracted from gels of Figure 2a. The top row is origami-cell lysate mixture incubated at 4 ℃ and bottom row is incubation at room temperature. Left to right: 5000 lysed cells incubated with origami for 12 h, 10000 lysed cells incubated with origami for 12 h, 5000 lysed cells incubated with origami for 1 h and 10000 lysed cells incubated with origami for 1 h. Scale bar= 300 nm.

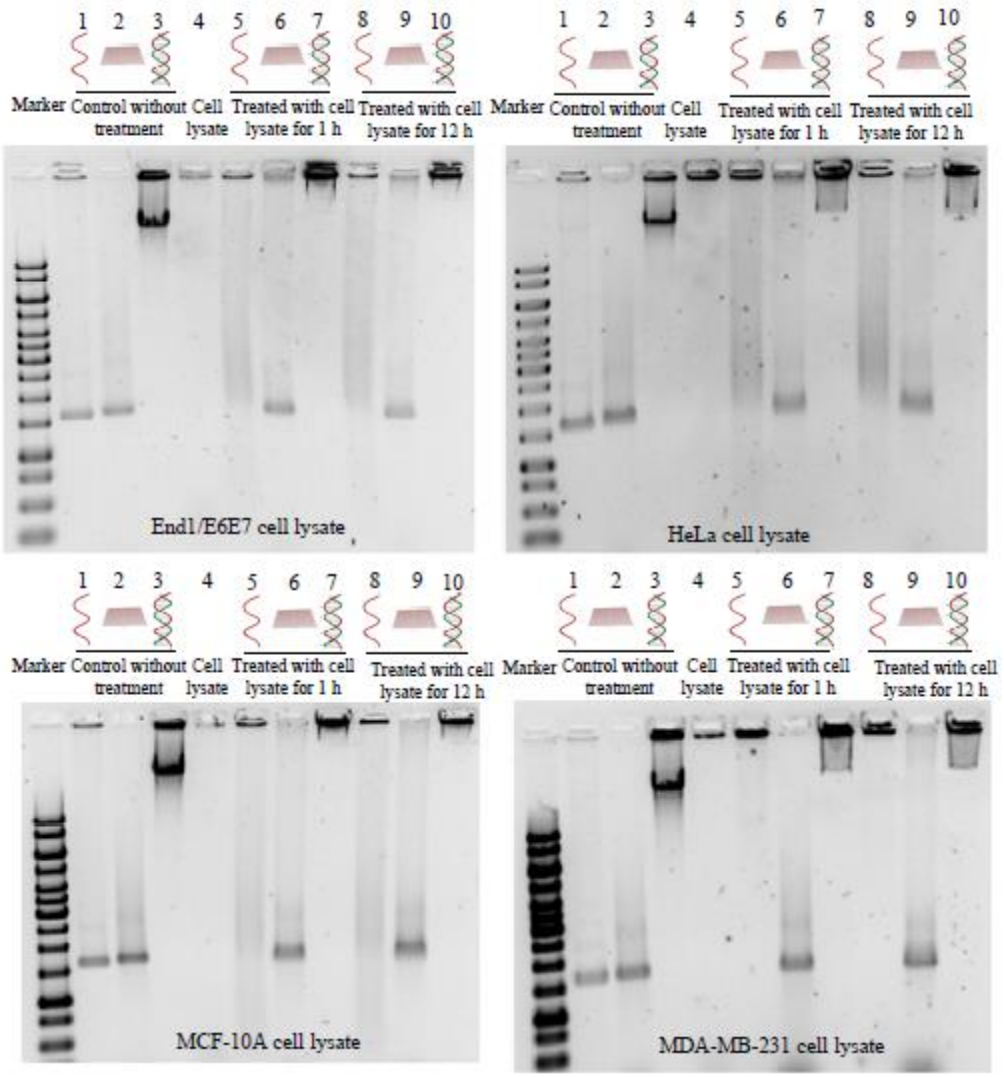

Figure S3.2. Eeffects of cell line on the stability of M13, rectangular origami, viral ss DNA and λ DNA as determined by agarose gel electrophoresis Leftmost lane: 1 kbp DNA marker; Lane 1: 10 nM M13 ssDNA; Lane 2: 10 nM origami; Lane 3: 100 nM λ DNA; Lane 4: cell lysate; Lane 5-7: M13, origami and λ DNA incubated with cell lysate for 1 h at 25 ℃; Lane 8-10: M13, origami and λ DNA incubated with cell lysate for 12 h at 25 ℃.

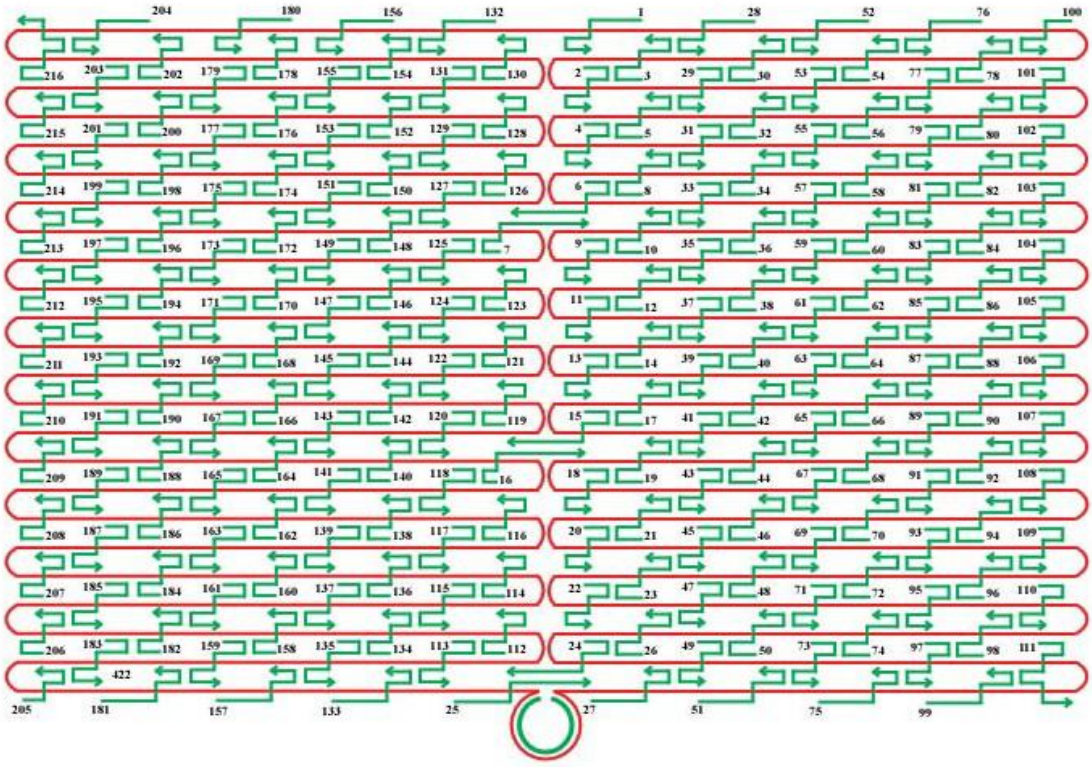

Figure S3.3. Schematic rectangular DNA origami with staple strands numbered. Single stranded, M13 viral DNA is shown in red, and staple strands are shown in green.

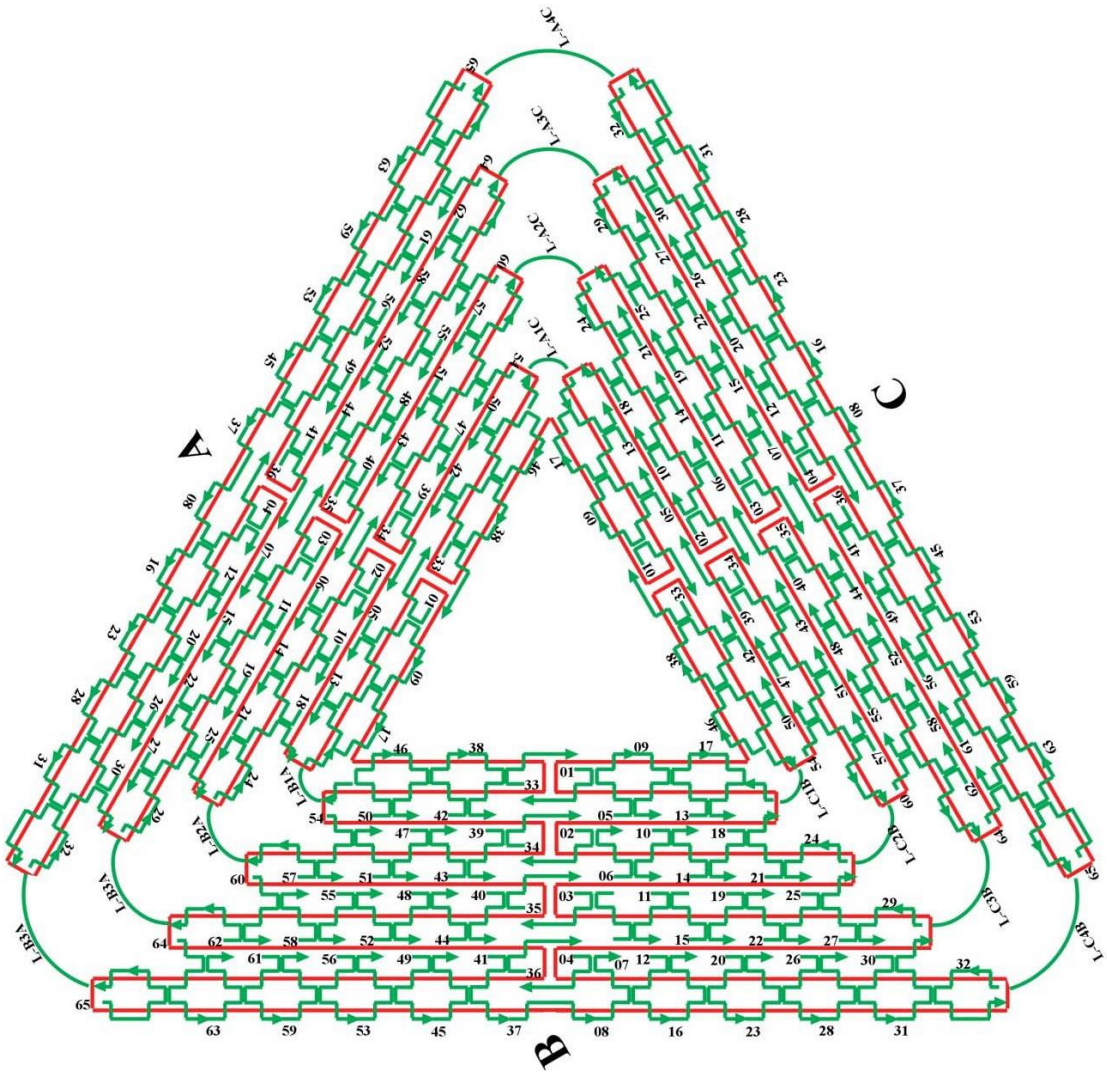

Figure S3.4. Schematic 2D triangular DNA origami with staple strands numbered. Single stranded, M13 viral DNA is shown in red, and staple strands are shown in green. The complex consists of three major domains which are labeled A, B and C.

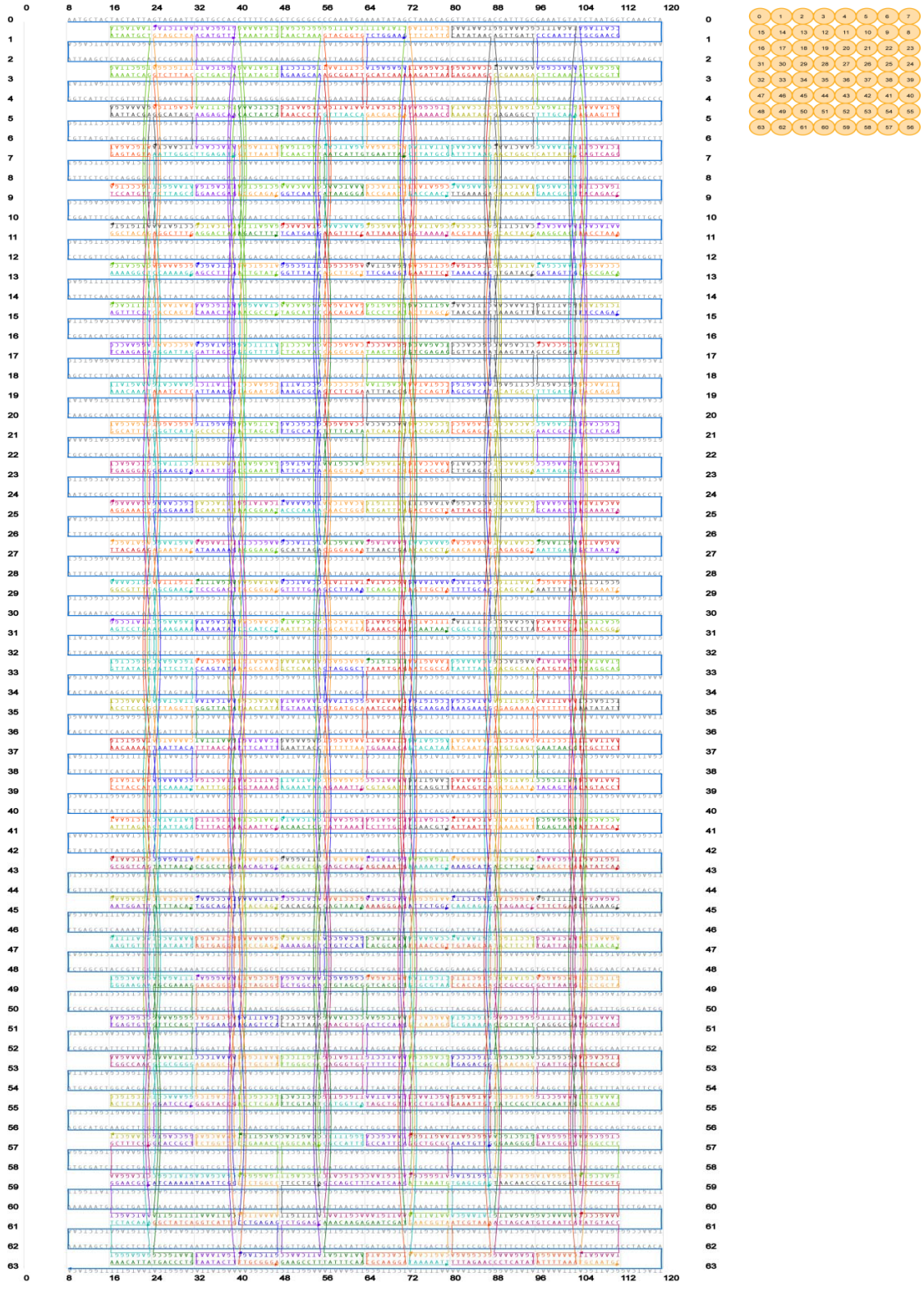

Figure S3.5. Schematic design of 8-layer 3D origami.

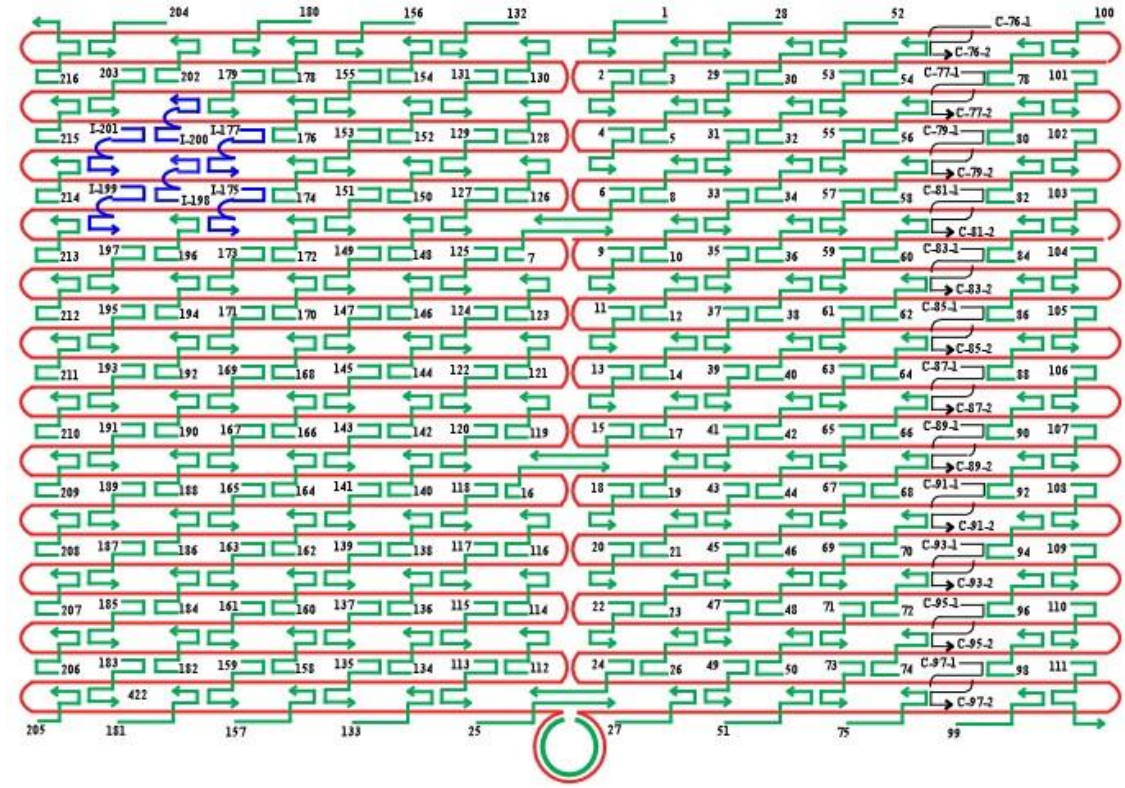
C-76-1
C-76-2
C-77-1
C-77-2
C-79-1
C-79-2
C-81-1
C-81-2
C-83-1
C-83-2
C-85-1
C-85-2
C-87-1
C-87-2
C-89-1
C-89-2
C-91-1
C-91-2
C-93-1
C-93-2
C-95-1
C-95-2
C-97-1
C-97-2
I-201
I-200
I-177
I-199
I-198
I-175
422

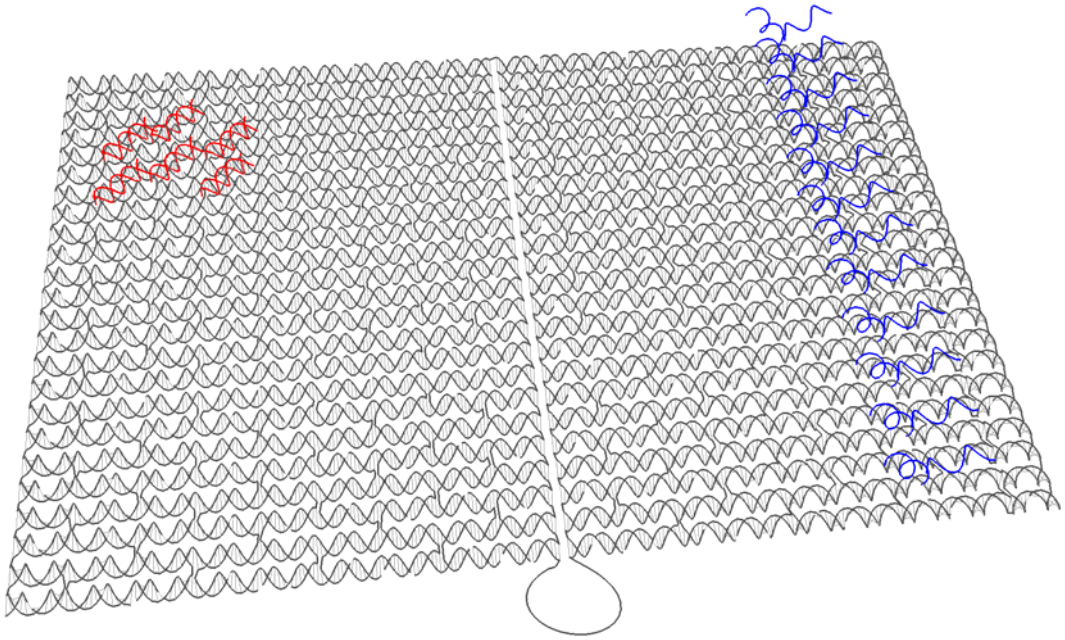

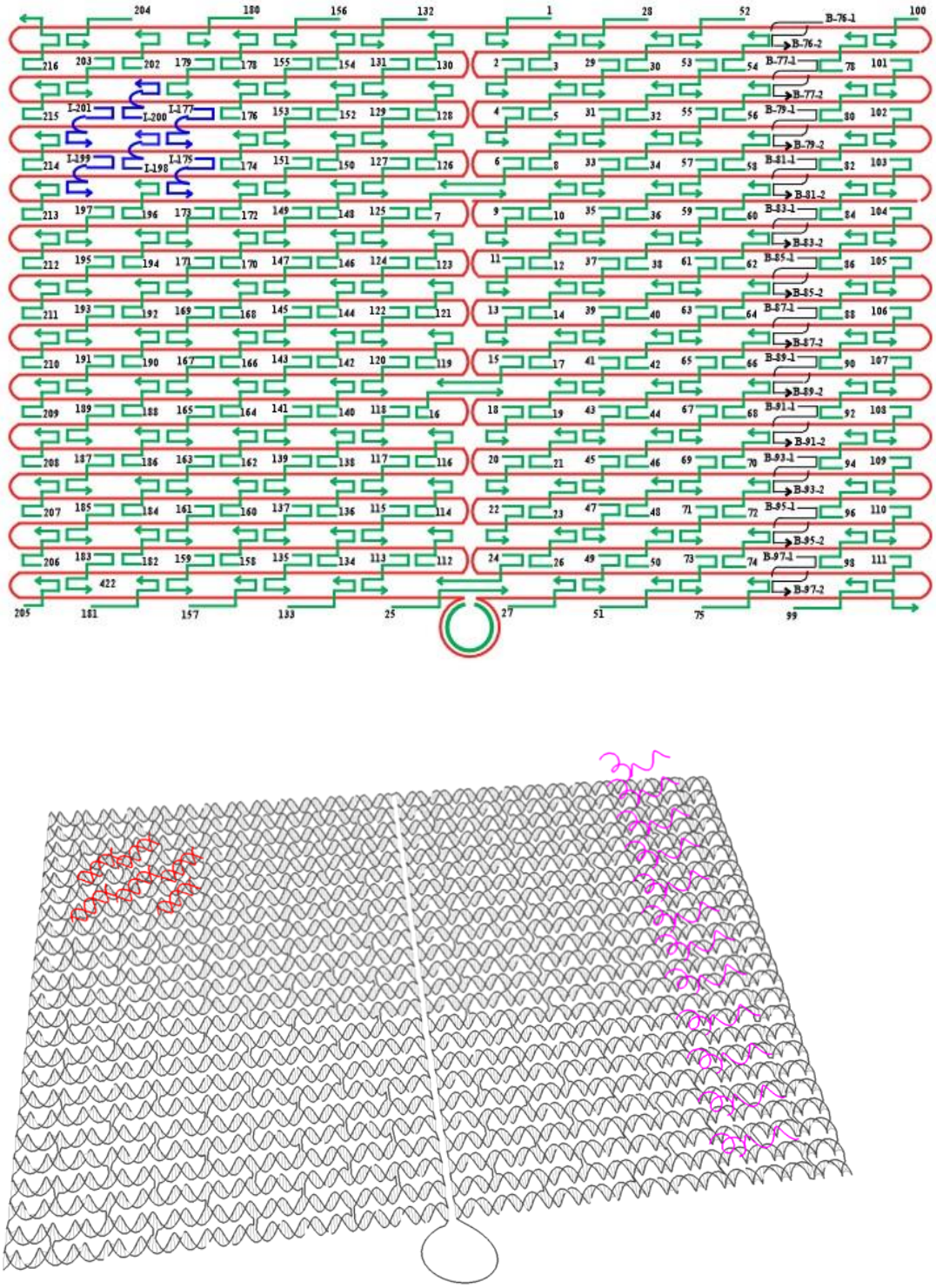

Figure S3.6. Schematic layout of the origami/probes showing the positions of Index (initiate with 'I'), Control probes (initiate with 'C'), and β-actin probes (initiate with 'B'). The 3D structures of the origami/probes are also shown below each design.

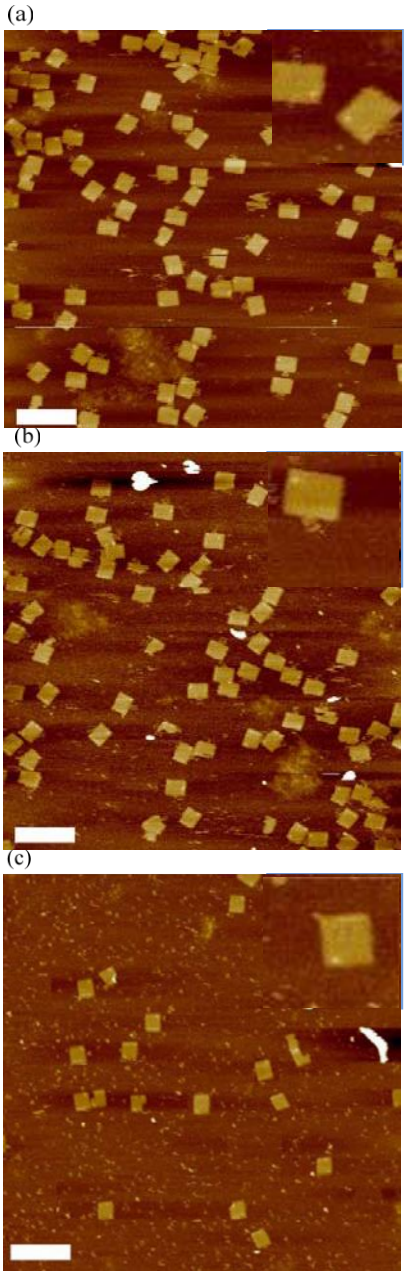

Figure S3.7. AFM images of origami bearing control probe reacted with (a) Synthetic RNA, (b) Fragmentized total cellular RNA, and (c) total cellular RNA. Scale bar= 300 nm. (image insets are 250 nm by 250 nm)

Staple strand sequence

Table S3.1. Staple sequences for 2D rectangular origami

Name	Sequence
1	CAAGCCCAATAGGAAC CCATGTACAAACAGTT
2	AATGCCCCGTAACAGT GCCCGTATCTCCCTCA
3	TGCCTTGACTGCCTAT TTCGGAACAGGGATAG
4	GAGCCGCCCCACCACC GGAACCGCGACGGAAA
5	AACCAGAGACCCTCAG AACCGCCAGGGGTCAG
6	TTATTCATAGGGAAGG TAAATATT CATTCAGT
7	CATAACCCGAGGCATA GTAAGAGC TTTTTAAG
8	ATTGAGGGTAAAGGTG AATTATCAATCACCGG
9	AAAAGTAATATCTTAC CGAAGCCCTTCCAGAG
10	GCAATAGCGCAGATAG CCGAACAATTCAACCG
11	CCTAATTTACGCTAAC GAGCGTCTAATCAATA
12	TCTTACCAGCCAGTTA CAAAATAAATGAAATA
13	ATCGGCTGCGAGCATG TAGAAACCTATCATAT
14	CTAATTTATCTTTCCT TATCATTCATCCTGAA
15	GCGTTATAGAAAAAGC CTGTTTAG AAGGCCGG
16	GCTCATTTTCGCATTA AATTTTTG AGCTTAGA
17	AATTACTACAAATTCT TACCAGTAATCCCATC
18	TTAAGACGTTGAAAAC ATAGCGATAACAGTAC
19	TAGAATCCCTGAGAAG AGTCAATAGGAATCAT
20	CTTTTACACAGATGAA TATACAGTAAACAATT
21	TTTAACGTTCGGGAGA AACAATAATTTTCCCT
22	CGACAACTAAGTATTA GACTTTACAATACCGA
23	GGATTTAGCGTATTAA ATCCTTTGTTTTCAGG
24	ACGAACCAAAACATCG CCATTAAA TGGTGGTT
25	GAACGTGGCGAGAAAG GAAGGGAA CAAACTAT
26	TAGCCCTACCAGCAGA AGATAAAAACATTTGA
27	CGGCCTTGCTGGTAAT ATCCAGAACGAACTGA
28	CTCAGAGCCACCACCC TCATTTTCCTATTATT
29	CTGAAACAGGTAATAA GTTTTAACCCCTCAGA
30	AGTGTACTTGAAAGTA TTAAGAGGCCGCCACC
31	GCCACCACTCTTTTCA TAATCAAACCGTCACC
32	GTTTGCCACCTCAGAG CCGCCACCGATACAGG
33	GACTTGAGAGACAAAA GGGCGACAAGTTACCA
34	AGCGCCAACCATTTGG GAATTAGATTATTAGC
35	GAAGGAAAATAAGAGC AAGAAACAACAGCCAT
36	GCCCAATACCGAGGAA ACGCAATAGGTTTACC
37	ATTATTTAACCCAGCT ACAATTTTCAAGAACG
38	TATTTTGCTCCCAATC CAAATAAGTGAGTTAA
39	GGTATTAAGAACAAGA AAAATAATTAAAGCCA
40	TAAGTCCTACCAAGTA CCGCACTCTTAGTTGC

41	ACGCTCAAAATAAGAA TAAACACCGTGAATTT
42	AGGCGTTACAGTAGGG CTTAATTGACAATAGA
43	ATCAAAATCGTCGCTA TTAATTAACGGATTCG
44	CTGTAAATCATAGGTC TGAGAGACGATAAATA
45	CCTGATTGAAAGAAAT TGCGTAGACCCGAACG
46	ACAGAAATCTTTGAAT ACCAAGTTCCTTGCTT
47	TTATTAATGCCGTCAA TAGATAATCAGAGGTG
48	AGATTAGATTTAAAAG TTTGAGTACACGTAAA
49	AGGCGGTCATTAGTCT TTAATGCGCAATATTA
50	GAATGGCTAGTATTAA CACCGCCTCAACTAAT
51	CCGCCAGCCATTGCAA CAGGAAAAATATTTTT
52	CCCTCAGAACCGCCAC CCTCAGAACTGAGACT
53	CCTCAAGAATACATGG CTTTTGATAGAACCAC
54	TAAGCGTCGAAGGATT AGGATTAGTACCGCCA
55	CACCAGAGTTCGGTCA TAGCCCCCGCCAGCAA
56	TCGGCATTCCGCCGCC AGCATTGACGTTCCAG
57	AATCACCAAATAGAAA ATTCATATATAACGGA
58	TCACAATCGTAGCACC ATTACCATCGTTTTCA
59	ATACCCAAGATAACCC ACAAGAATAAACGATT
60	ATCAGAGAAAGAACTG GCATGATTTTATTTTG
61	TTTTGTTTAAGCCTTA AATCAAGAATCGAGAA
62	AGGTTTTGAACGTCAA AAATGAAAGCGCTAAT
63	CAAGCAAGACGCGCCT GTTTATCAAGAATCGC
64	AATGCAGACCGTTTTT ATTTTCATCTTGCGGG
65	CATATTTAGAAATACC GACCGTGTTACCTTTT
66	AATGGTTTACAACGCC AACATGTAGTTCAGCT
67	TAACCTCCATATGTGA GTGAATAAACAAAATC
68	AAATCAATGGCTTAGG TTGGGTTACTAAATTT
69	GCGCAGAGATATCAAA ATTATTTGACATTATC
70	AACCTACCGCGAATTA TTCATTTCCAGTACAT
71	ATTTTGCGTCTTTAGG AGCACTAAGCAACAGT
72	CTAAAATAGAACAAAG AAACCACCAGGGTTAG
73	GCCACGCTATACGTGG CACAGACAACGCTCAT
74	GCGTAAGAGAGAGCCA GCAGCAAAAAGGTTAT
75	GGAAATACCTACATTT TGACGCTCACCTGAAA
76	TATCACCGTACTCAGG AGGTTTAGCGGGGTTT
77	TGCTCAGTCAGTCTCT GAATTTACCAGGAGGT
78	GGAAAGCGACCAGGCG GATAAGTGAATAGGTG
79	TGAGGCAGGCGTCAGA CTGTAGCGTAGCAAGG
80	TGCCTTTAGTCAGACG ATTGGCCTGCCAGAAT
81	CCGGAAACACACCACG GAATAAGTAAGACTCC
82	ACGCAAAGGTCACCAA TGAAACCAATCAAGTT
83	TTATTACGGTCAGAGG GTAATTGAATAGCAGC
84	TGAACAAACAGTATGT TAGCAAACTAAAAGAA
85	CTTTACAGTTAGCGAA CCTCCCGACGTAGGAA

86	GAGGCGTTAGAGAATA ACATAAAAGAACACCC
87	TCATTACCCGACAATA AACAACATATTTAGGC
88	CCAGACGAGCGCCCAA TAGCAAGCAAGAACGC
89	AGAGGCATAATTTCAT CTTCTGACTATAACTA
90	TTTTAGTTTTTCGAGC CAGTAATAAATTCTGT
91	TATGTAAACCTTTTTT AATGGAAAAATTACCT
92	TTGAATTATGCTGATG CAAATCCACAAATATA
93	GAGCAAAAACTTCTGA ATAATGGAAGAAGGAG
94	TGGATTATGAAGATGA TGAAACAAAATTTCAT
95	CGGAATTATTGAAAGG AATTGAGGTGAAAAAT
96	ATCAACAGTCATCATA TTCCTGATTGATTGTT
97	CTAAAGCAAGATAGAA CCCTTCTGAATCGTCT
98	GCCAACAGTCACCTTG CTGAACCTGTTGGCAA
99	GAAATGGATTATTTAC ATTGGCAGACATTCTG
100	TTTT TATAAGTA TAGCCCGGCCGTCGAG
101	AGGGTTGA TTTT ATAAATCC TCATTAAATGATATTC
102	ACAAACAA TTTT AATCAGTA GCGACAGATCGATAGC
103	AGCACCGT TTTT TAAAGGTG GCAACATAGTAGAAAA
104	TACATACA TTTT GACGGGAG AATTAACTACAGGGAA
105	GCGCATTA TTTT GCTTATCC GGTATTCTAAATCAGA
106	TATAGAAG TTTT CGACAAAA GGTAAAGTAGAGAATA
107	TAAAGTAC TTTT CGCGAGAA AACTTTTTATCGCAAG
108	ACAAAGAA TTTT ATTAATTA CATTTAACACATCAAG
109	AAAACAAA TTTT TTCATCAA TATAATCCTATCAGAT
110	GATGGCAA TTTT AATCAATA TCTGGTCACAAATATC
111	AAACCCTC TTTT ACCAGTAA TAAAAGGGATTCACCA GTCACACG TTTT
112	CCGAAATCCGAAAATC CTGTTTGAAGCCGGAA
113	CCAGCAGGGGCAAAATCCCTTATAAAGCCGGC
114	GCATAAAGTTCCACAC AACATACGAAGCGCCA
115	GCTCACAATGTAAAGCCTGGGGTGGGTTTGCC
116	TTCGCCATTGCCGGAA ACCAGGCATTAAATCA
117	GCTTCTGGTCAGGCTGCGCAACTGTGTTATCC
118	GTTAAAATTTTAACCAATAGGAACCCGGCACC
119	AGACAGTCATTCAAAA GGGTGAGAAGCTATAT
120	AGGTAAAGAAATCACCATCAATATAATATTTT
121	TTTCATTTGGTCAATA ACCTGTTTATATCGCG
122	TCGCAAATGGGGCGCGAGCTGAAATAATGTGT
123	TTTTAATTGCCCGAAA GACTTCAAAACACTAT
124	AAGAGGAACGAGCTTCAAAGCGAAGATACATT
125	GGAATTACTCGTTTACCAGACGACAAAAGATT
126	GAATAAGGACGTAACA AAGCTGCTCTAAAACA
127	CCAAATCACTTGCCCTGACGAGAACGCCAAAA
128	CTCATCTTGAGGCAAA AGAATACAGTGAATTT
129	AAACGAAATGACCCCCAGCGATTATTCATTAC

130	CTTAAACATCAGCTTG CTTTCGAGCGTAACAC
131	TCGGTTTAGCTTGATACCGATAGTCCAACCTA
132	TGAGTTTCGTCACCAGTACAAACTTAATTGTA
133	CCCCGATTTAGAGCTTGACGGGGAAATCAAAA
134	GAATAGCCGCAAGCGGTCCACGCTCCTAATGA
135	GAGTTGCACGAGATAGGGTTGAGTAAGGGAGC
136	GTGAGCTAGTTTCCTGTGTGAAATTTGGGAAG
137	TCATAGCTACTCACATTAATTGCGCCCTGAGA
138	GGCGATCGCACTCCAGCCAGCTTTGCCATCAA
139	GAAGATCGGTGCGGGCCTCTTCGCAATCATGG
140	AAATAATTTTAAATTGTAAACGTTGATATTCA
141	GCAAATATCGCGTCTGGCCTTCCTGGCCTCAG
142	ACCGTTCTAAATGCAATGCCTGAGAGGTGGCA
143	TATATTTTAGCTGATAAATTAATGTTGTATAA
144	TCAATTCTTTTAGTTTGACCATTACCAGACCG
145	CGAGTAGAACTAATAGTAGTAGCAAACCCTCA
146	GAAGCAAAAAAGCGGATTGCATCAGATAAAAA
147	GCTTCTGGTCAGGCTGCGCAACTGTGTTATCC
148	CCAAAATATAATGCAGATACATAAACACCAGA
149	CATTCAACGCGAGAGGCTTTTGCATATTATAG
150	ACGAGTAGTGACAAGAACCGGATATACCAAGC
151	AGTAATCTTAAATTGGGCTTGAGAGAATACCA
152	GCGAAACATGCCACTACGAAGGCATGCGCCGA
153	ATACGTAAAAGTACAACGGAGATTTCATCAAG
154	CAATGACACTCCAAAAGGAGCCTTACAACGCC
155	AAAAAAGGACAACCATCGCCCACGCGGGTAAA
156	TGTAGCATTCCACAGACAGCCCTCATCTCCAA
157	GTAAAGCACTAAATCGGAACCCTAGTTGTTCC
158	AGTTTGGAGCCCTTCACCGCCTGGTTGCGCTC
159	AGCTGATTACAAGAGTCCACTATTGAGGTGCC
160	ACTGCCCGCCGAGCTCGAATTCGTTATTACGC
161	CCCGGGTACTTTCCAGTCGGGAAACGGGCAAC
162	CAGCTGGCGGACGACGACAGTATCGTAGCCAG
163	GTTTGAGGGAAAGGGGGATGTGCTAGAGGATC
164	CTTTCATCCCCAAAAACAGGAAGACCGGAGAG
165	AGAAAAGCAACATTAAATGTGAGCATCTGCCA
166	GGTAGCTAGGATAAAAATTTTTAGTTAACATC
167	CAACGCAATTTTTGAGAGATCTACTGATAATC
168	CAATAAATACAGTTGATTCCCAATTTAGAGAG
169	TCCATATACATACAGGCAAGGCAACTTTATTT
170	TACCTTTAAGGTCTTTACCCTGACAAAGAAGT
171	CAAAAATCATTGCTCCTTTTGATAAGTTTCAT
172	TTTGCCAGATCAGTTGAGATTTAGTGGTTTAA
173	AAAGATTCAGGGGGTAATAGTAAACCATAAAT
174	TTTCAACTATAGGCTGGCTGACCTTGTATCAT

175	CCAGGCGCTTAATCATTGTGAATTACAGGTAG
176	CGCCTGATGGAAGTTTCCATTAAACATAACCG
177	TTTCATGAAAATTGTGTCGAAATCTGTACAGA
178	ATATATTCTTTTTTCACGTTGAAAATAGTTAG
179	AATAATAAGGTCGCTGAGGCTTGCAAAGACTT
180	CGTAACGATCTAAAGTTTTGTCGTGAATTGCG
181	ACCCAAATCAAGTTTTTTGGGGTCAAAGAACG
182	TGGACTCCCTTTTCACCAGTGAGACCTGTCGT
183	TGGTTTTTAACGTCAAAGGGCGAAGAACCATC
184	GCCAGCTGCCTGCAGGTCGACTCTGCAAGGCG
185	CTTGCATGCATTAATGAATCGGCCCGCCAGGG
186	ATTAAGTTCGCATCGTAACCGTGCGAGTAACA
187	TAGATGGGGGGTAACGCCAGGGTTGTGCCAAG
188	ACCCGTCGTCATATGTACCCCGGTAAAGGCTA
189	CATGTCAAGATTCTCCGTGGGAACCGTTGGTG
190	TCAGGTCACTTTTGCGGGAGAAGCAGAATTAG
191	CTGTAATATTGCCTGAGAGTCTGGAAAACTAG
192	CAAAATTAAAGTACGGTGTCTGGAAGAGGTCA
193	TGCAACTAAGCAATAAAGCCTCAGTTATGACC
194	TTTTTGCGCAGAAAACGAGAATGAATGTTTAG
195	AAACAGTTGATGGCTTAGAGCTTATTTAAATA
196	ACTGGATAACGGAACAACATTATTACCTTATG
197	ACGAACTAGCGTCCAATACTGCGGAATGCTTT
198	CGATTTTAGAGGACAGATGAACGGCGCGACCT
199	CTTTGAAAAGAACTGGCTCATTATTTAATAAA
200	GCTCCATGAGAGGCTTTGAGGACTAGGGAGTT
201	ACGGCTACTTACTTAGCCGGAACGCTGACCAA
202	AAAGGCCGAAAGGAACAACTAAAGCTTTCCAG
203	GAGAATAGCTTTTGCGGGATCGTCGGGTAGCA
204	ACGTTAGTAAATGAATTTTCTGTAAGCGGAGT
205	TTTTCGATGGCCCACTACGTAAACCGTC
206	TATCAGGGTTTTCGGTTTGCGTATTGGGAACGCGCG
207	GGGAGAGGTTTTTGTAAAACGACGGCCATTCCCAGT
208	CACGACGTTTTTGTAATGGGATAGGTCAAAACGGCG
209	GATTGACCTTTTGATGAACGGTAATCGTAGCAAACA
210	AGAGAATCTTTTGGTTGTACCAAAAACAAGCATAAA
211	AGAGAATCTTTTGGTTGTACCAAAAACAAGCATAAA
212	ATATAATGTTTTCATTGAATCCCCCTCAAATCGTCA
213	TAAATATTTTTTGGAAGAAAAATCTACGACCAGTCA
214	GGACGTTGTTTTTCATAAGGGAACCGAAAGGCGCAG
215	ACGGTCAATTTTGACAGCATCGGAACGAACCCTCAG
216	CAGCGAAAATTTTACTTTCAACAGTTTCTGGGATTTTGCTA AACTTTT
Loop1	AACATCACTTGCCTGAGTAGAAGAACT
Loop2	TGTAGCAATACTTCTTTGATTAGTAAT

Loop3	AGTCTGTCCATCACGCAAATTAACCGT
Loop4	ATAATCAGTGAGGCCACCGAGTAAAAG
Loop5	ACGCCAGAATCCTGAGAAGTGTTTTT
Loop6	TTAAAGGGATTTTAGACAGGAACGGT
Loop7	AGAGCGGGAGCTAAACAGGAGGCCGA
Loop8	TATAACGTGCTTTCCTCGTTAGAATC
Loop9	GTACTATGGTTGCTTTGACGAGCACG
Loop10	GCGCTTAATGCGCCGCTACAGGGCGC

Table S3.2. Staple sequences for 2D triangular origami

Name	Sequence
A01	CGGGGTTTCCTCAAGAGAAGGATTTTGAATTA
A02	AGCGTCATGTCTCTGAATTTACCGACTACCTT
A03	TTCATAATCCCCTTATTAGCGTTTTTCTTACC
A04	ATGGTTTATGTCACAATCAATAGATATTAAAC
A05	TTTGATGATTAAGAGGCTGAGACTTGCTCAGTACCAGGCG
A06	CCGGAACCCAGAATGGAAAGCGCAACATGGCT
A07	AAAGACAACATTTTCGGTCATAGCCAAAATCA
A08	GACGGGAGAATTAACTCGGAATAAGTTTATTTCCAGCGCC
A09	GATAAGTGCCGTCGAGCTGAAACATGAAAGTATACAGGAG
A10	TGTACTGGAAATCCTCATTAAAGCAGAGCCAC
A11	CACCGGAAAGCGCGTTTTCATCGGAAGGGCGA
A12	CATTCAACAAACGCAAAGACACCAGAACACCCTGAACAAA
A13	TTTAACGGTTCGGAACCTATTATTAGGGTTGATATAAGTA
A14	CTCAGAGCATATTCACAAACAAATTAATAAGT
A15	GGAGGGAATTTAGCGTCAGACTGTCCGCCTCC
A16	GTCAGAGGGTAATTGATGGCAACATATAAAAGCGATTGAG
A17	TAGCCCGGAATAGGTGAATGCCCCCTGCCTATGGTCAGTG
A18	CCTTGAGTCAGACGATTGGCCTTGCGCCACCC
A19	TCAGAACCCAGAATCAAGTTTGCCGGTAAATA
A20	TTGACGGAAATACATACATAAAGGGCGCTAATATCAGAGA
A21	CAGAGCCAGGAGGTTGAGGCAGGTAACAGTGCCCG
A22	ATTAAAGGCCGTAATCAGTAGCGAGCCACCCT
A23	GATAACCCACAAGAATGTTAGCAAACGTAGAAAATTATTC
A24	GCCGCCAGCATTGACACCACCCTC
A25	AGAGCCGCACCATCGATAGCAGCATGAATTAT
A26	CACCGTCACCTTATTACGCAGTATTGAGTTAAGCCCAATA
A27	AGCCATTTAAACGTCACCAATGAACACCAGAACCA
A28	ATAAGAGCAAGAAACATGGCATGATTAAGACTCCGACTTG
A29	CCATTAGCAAGGCCGGGGGAATTA
A30	GAGCCAGCGAATACCCAAAAGAACATGAAATAGCAATAGC
A31	TATCTTACCGAAGCCCAAACGCAATAATAACGAAAATCACCAG
A32	CAGAAGGAAACCGAGGTTTTTAAGAAAAGTAAGCAGATAGCCG
A33	CCTTTTTTCATTTAACAATTTCATAGGATTAG
A34	TTTAACCTATCATAGGTCTGAGAGTTCCAGTA
A35	AGTATAAAATATGCGTTATACAAAGCCATCTT
A36	CAAGTACCTCATTCCAAGAACGGGAAATTCAT
A37	AGAGAATAACATAAAAACAGGGAAGCGCATTA
A38	AAAACAAAATTAATTAAATGGAAACAGTACATTAGTGAAT
A39	TTATCAAACCGGCTTAGGTTGGGTAAGCCTGT
A40	TTAGTATCGCCAACGCTCAACAGTCGGCTGTC
A41	TTTCCTTAGCACTCATCGAGAACAATAGCAGCCTTTACAG
A42	AGAGTCAAAAATCAATATATGTGATGAAACAAACATCAAG

A43	ACTAGAAATATATAACTATATGTACGCTGAGA
A44	TCAATAATAGGGCTTAATTGAGAATCATAATT
A45	AACGTCAAAAATGAAAAGCAAGCCGTTTTTATGAAACCAA
A46	GAGCAAAAGAAGATGAGTGAATAACCTTGCTTATAGCTTA
A47	GATTAAGAAATGCTGATGCAAATCAGAATAAA
A48	CACCGGAATCGCCATATTTAACAAAATTTACG
A49	AGCATGTATTTCATCGTAGGAATCAAACGATTTTTTGTTT
A50	ACATAGCGCTGTAAATCGTCGCTATTCATTTCAATTACCT
A51	GTTAAATACAATCGCAAGACAAAGCCTTGAAA
A52	CCCATCCTCGCCAACATGTAATTTAATAAGGC
A53	TCCCAATCCAAATAAGATTACCGCGCCCAATAAATAATAT
A54	TCCCTTAGAATAACGCGAGAAAACTTTTACCGACC
A55	GTGTGATAAGGCAGAGGCATTTTCAGTCCTGA
A56	ACAAGAAAGCAAGCAAATCAGATAACAGCCATATTATTTA
A57	GTTTGAAATTCAAATATATTTTAG
A58	AATAGATAGAGCCAGTAATAAGAGATTTAATG
A59	GCCAGTTACAAAATAATAGAAGGCTTATCCGGTTATCAAC
A60	TTCTGACCTAAAATATAAAGTACCGACTGCAGAAC
A61	GCGCCTGTTATTCTAAGAACGCGATTCCAGAGCCTAATTT
A62	TCAGCTAAAAAAGGTAAAGTAATT
A63	ACGCTAACGAGCGTCTGGCGTTTTAGCGAACCCAACATGT
A64	ACGACAATAAATCCCGACTTGCGGGAGATCCTGAATCTTACCA
A65	TGCTATTTTGCACCCAGCTACAATTTTGTTTTGAAGCCTTAAA
B01	TCATATGTGTAATCGTAAAACTAGTCATTTTC
B02	GTGAGAAAATGTGTAGGTAAAGATACAACTTT
B03	GGCATCAAATTTGGGGCGCGAGCTAGTTAAAG
B04	TTCGAGCTAAGACTTCAAATATCGGGAACGAG
B05	ACAGTCAAAGAGAATCGATGAACGACCCCGGTTGATAATC
B06	ATAGTAGTATGCAATGCCTGAGTAGGCCGGAG
B07	AACCAGACGTTTAGCTATATTTTCTTCTACTA
B08	GAATACCACATTCAACTTAAGAGGAAGCCCGATCAAAGCG
B09	AGAAAAGCCCCAAAAAGAGTCTGGAGCAAACAATCACCAT
B10	CAATATGACCCTCATATATTTTAAAGCATTAA
B11	CATCCAATAAATGGTCAATAACCTCGGAAGCA
B12	AACTCCAAGATTGCATCAAAAAGATAATGCAGATACATAA
B13	CGTTCTAGTCAGGTCATTGCCTGACAGGAAGATTGTATAA
B14	CAGGCAAGATAAAAATTTTTAGAATATTCAAC
B15	GATTAGAGATTAGATACATTTCGCAAATCATA
B16	CGCCAAAAGGAATTACAGTCAGAAGCAAAGCGCAGGTCAG
B17	GCAAATATTTAAATTGAGATCTACAAAGGCTACTGATAAA
B18	TTAATGCCTTATTTCAACGCAAGGGCAAAGAA
B19	TTAGCAAATAGATTTAGTTTGACCAGTACCTT
B20	TAATTGCTTTACCCTGACTATTATGAGGCATAGTAAGAGC
B21	ATAAAGCCTTTGCGGGAGAAGCCTGGAGAGGGTAG
B22	TAAGAGGTCAATTCTGCGAACGAGATTAAGCA

B23	AACACTATCATAACCCATCAAAAATCAGGTCTCCTTTTGA
B24	ATGACCCTGTAATACTTCAGAGCA
B25	TAAAGCTATATAACAGTTGATTCCCATTTTTG
B26	CGGATGGCACGAGAATGACCATAATCGTTTACCAGACGAC
B27	TAATTGCTTGGAAGTTTCATTCCAAATCGGTTGTA
B28	GATAAAAACCAAAATATTAAACAGTTCAGAAATTAGAGCT
B29	ACTAAAGTACGGTGTCGAATATAA
B30	TGCTGTAGATCCCCCTCAAATGCTGCGAGAGGCTTTTGCA
B31	AAAGAAGTTTTGCCAGCATAAATATTCATTGACTCAACATGTT
B32	AATACTGCGGAATCGTAGGGGGTAATAGTAAAATGTTTAGACT
B33	AGGGATAGCTCAGAGCCACCACCCCATGTCAA
B34	CAACAGTTTATGGGATTTTGCTAATCAAAAGG
B35	GCCGCTTTGCTGAGGCTTGCAGGGGAAAAGGT
B36	GCGCAGACTCCATGTTACTTAGCCCGTTTTAA
B37	ACAGGTAGAAAGATTCATCAGTTGAGATTTAG
B38	CCTCAGAACCGCCACCCAAGCCCAATAGGAACGTAAATGA
B39	ATTTTCTGTCAGCGGAGTGAGAATACCGATAT
B40	ATTCGGTCTGCGGGATCGTCACCCGAAATCCG
B41	CGACCTGCGGTCAATCATAAGGGAACGGAACAACATTATT
B42	AGACGTTACCATGTACCGTAACACCCCTCAGAACCGCCAC
B43	CACGCATAAGAAAGGAACAACTAAGTCTTTCC
B44	ATTGTGTCTCAGCAGCGAAAGACACCATCGCC
B45	TTAATAAAACGAACTAACCGAACTGACCAACTCCTGATAA
B46	AGGTTTAGTACCGCCATGAGTTTCGTCACCAGGATCTAAA
B47	GTTTTGTCAGGAATTGCGAATAATCCGACAAT
B48	GACAACAAGCATCGGAACGAGGGTGAGATTTG
B49	TATCATCGTTGAAAGAGGACAGATGGAAGAAAAATCTACG
B50	AGCGTAACTACAAACTACAACGCCTATCACCGTACTCAGG
B51	TAGTTGCGAATTTTTTCACGTTGATCATAGTT
B52	GTACAACGAGCAACGGCTACAGAGGATACCGA
B53	ACCAGTCAGGACGTTGGAACGGTGTACAGACCGAAACAAA
B54	ACAGACAGCCCAAATCTCCAAAAAAAAATTTCTTA
B55	AACAGCTTGCTTTGAGGACTAAAGCGATTATA
B56	CCAAGCGCAGGCGCATAGGCTGGCAGAACTGGCTCATTAT
B57	CGAGGTGAGGCTCCAAAAGGAGCC
B58	ACCCCCAGACTTTTTCATGAGGAACTTGCTTT
B59	ACCTTATGCGATTTTATGACCTTCATCAAGAGCATCTTTG
B60	CGGTTTATCAGGTTTCCATTAAACGGGAATACACT
B61	AAAACACTTAATCTTGACAAGAACTTAATCATTGTGAATT
B62	GGCAAAAGTAAAATACGTAATGCC
B63	TGGTTTAATTTCAACTCGGATATTCATTACCCACGAAAGA
B64	ACCAACCTAAAAAATCAACGTAACAAATAAATTGGGCTTGAGA
B65	CCTGACGAGAAACACCAGAACGAGTAGGCTGCTCATTCAGTGA
C01	TCGGGAGATATACAGTAACAGTACAAATAATT
C02	CCTGATTAAAGGAGCGGAATTATCTCGGCCTC

C03	GCAAATCACCTCAATCAATATCTGCAGGTCGA
C04	CGACCAGTACATTGGCAGATTCACCTGATTGC
C05	TGGCAATTTTTAACGTCAGATGAAAACAATAACGGATTCG
C06	AAGGAATTACAAAGAAACCACCAGTCAGATGA
C07	GGACATTCACCTCAAATATCAAACACAGTTGA
C08	TTGACGAGCACGTATACTGAAATGGATTATTTAATAAAAG
C09	CCTGATTGCTTTGAATTGCGTAGATTTTCAGGCATCAATA
C10	TAATCCTGATTATCATTTTGCGGAGAGGAAGG
C11	TTATCTAAAGCATCACCTTGCTGATGGCCAAC
C12	AGAGATAGTTTGACGCTCAATCGTACGTGCTTTCCTCGTT
C13	GATTATACACAGAAATAAAGAAATACCAAGTTACAAAATC
C14	TAGGAGCATAAAAGTTTGAGTAACATTGTTTG
C15	TGACCTGACAAATGAAAAATCTAAAATATCTT
C16	AGAATCAGAGCGGGAGATGGAAATACCTACATAACCCTTC
C17	GCGCAGAGGCGAATTAATTATTTGCACGTAAATTCTGAAT
C18	AATGGAAGCGAACGTTATTAATTTCTAACAAC
C19	TAATAGATCGCTGAGAGCCAGCAGAAGCGTAA
C20	GAATACGTAACAGGAAAAACGCTCCTAAACAGGAGGCCGA
C21	TCAATAGATATTAAATCCTTTGCCGGTTAGAACCT
C22	CAATATTTGCCTGCAACAGTGCCATAGAGCCG
C23	TTAAAGGGATTTTAGATACCGCCAGCCATTGCGGCACAGA
C24	ACAATTCGACAACTCGTAATACAT
C25	TTGAGGATGGTCAGTATTAACACCTTGAATGG
C26	CTATTAGTATATCCAGAACAATATCAGGAACGGTACGCCA
C27	CGCGAACTAAAACAGAGGTGAGGCTTAGAAGTATT
C28	GAATCCTGAGAAGTGTATCGGCCTTGCTGGTACTTTAATG
C29	ACCACCAGCAGAAGATGATAGCCC
C30	TAAAACATTAGAAGAACTCAAACTTTTTATAATCAGTGAG
C31	GCCACCGAGTAAAAGAACATCACTTGCCTGAGCGCCATTAAAA
C32	TCTTTGATTAGTAATAGTCTGTCCATCACGCAAATTAACCGTT
C33	CGCGTCTGATAGGAACGCCATCAACTTTTACA
C34	AGGAAGATGGGGACGACGACAGTAATCATATT
C35	CTCTAGAGCAAGCTTGCATGCCTGGTCAGTTG
C36	CCTTCACCGTGAGACGGGCAACAGCAGTCACA
C37	CGAGAAAGGAAGGGAAGCGTACTATGGTTGCT
C38	GCTCATTTTTTAACCAGCCTTCCTGTAGCCAGGCATCTGC
C39	CAGTTTGACGCACTCCAGCCAGCTAAACGACG
C40	GCCAGTGCGATCCCCGGGTACCGAGTTTTTCT
C41	TTTCACCAGCCTGGCCCTGAGAGAAAGCCGGCGAACGTGG
C42	GTAACCGTCTTTCATCAACATTAAAATTTTTGTTAAATCA
C43	ACGTTGTATTCCGGCACCGCTTCTGGCGCATC
C44	CCAGGGTGGCTCGAATTCGTAATCCAGTCACG
C45	TAGAGCTTGACGGGGAGTTGCAGCAAGCGGTCATTGGGCG
C46	GTTAAAATTCGCATTAATGTGAGCGAGTAACACACGTTGG
C47	TGTAGATGGGTGCCGGAAACCAGGAACGCCAG

C48	GGTTTTCCATGGTCATAGCTGTTTGAGAGGCG
C49	GTTTGCGTCACGCTGGTTTGCCCCAAGGGAGCCCCCGATT
C50	GGATAGGTACCCGTCGGATTCTCCTAAACGTTAATATTTT
C51	AGTTGGGTCAAAGCGCCATTCGCCCCGTAATG
C52	CGCGCGGGCCTGTGTGAAATTGTTGGCGATTA
C53	CTAAATCGGAACCCTAAGCAGGCGAAAATCCTTCGGCCAA
C54	CGGCGGATTGAATTCAGGCTGCGCAACGGGGGATG
C55	TGCTGCAAATCCGCTCACAATTCCCAGCTGCA
C56	TTAATGAAGTTTGATGGTGGTTCCGAGGTGCCGTAAAGCA
C57	TGGCGAAATGTTGGGAAGGGCGAT
C58	TGTCGTGCACACAACATACGAGCCACGCCAGC
C59	CAAGTTTTTTGGGGTCGAAATCGGCAAAATCCGGGAAACC
C60	TCTTCGCTATTGGAAGCATAAAGTGTATGCCCGCT
C61	TTCCAGTCCTTATAAATCAAAAGAGAACCATCACCCAAAT
C62	GCGCTCACAAGCCTGGGGTGCCTA
C63	CGATGGCCCACTACGTATAGCCCGAGATAGGGATTGCGTT
C64	AACTCACATTATTGAGTGTTGTTCCAGAAACCGTCTATCAGGG
C65	ACGTGGACTCCAACGTCAAAGGGCGAATTTGGAACAAGAGTCC
L-A1C	TTAATTAATTTTTTACCATATCAAA
L-A2C	TTAATTTCATCTTAGACTTTACAA
L-A3C	CTGTCCAGACGTATACCGAACGA
L-A4C	TCAAGATTAGTGTAGCAATACT
L-B1A	TGTAGCATTCCTTTTATAAACAGTT
L-B2A	TTTAATTGTATTTCCACCAGAGCC
L-B3A	ACTACGAAGGCTTAGCACCATTA
L-B4A	ATAAGGCTTGCAACAAAGTTAC
L-C1B	GTGGGAACAAATTTCTATTTTTGAG
L-C2B	CGGTGCGGGCCTTCCAAAAACATT
L-C3B	ATGAGTGAGCTTTTAAATATGCA
L-C4B	ACTATTAAAGAGGATAGCGTCC

Table S3.3. Staple sequences for 3D cuboid origami

Name	Sequence
1	TAATAGTAATAATGCTTTTTCACG
2	TGGCTTAGAAAATCAGCAGCATCG
3	GAAAACGAAATTACGAATTGTGTC
4	ATGCAGATGAGTAGTATGCCCTGA
5	AGTTTCGTAGGAACCCTCAAGAGATTATCCGG
6	AAAAGGCTAAAGTATTAAACAAATCGTCAAAA
7	GGCTACAGCAGACGATGGCATTTTAGATAGCC
8	TCCATGTTGTCAGACTTGAGGGAGACAAAAGG
9	AGTCCTGAGCGCCTGTGTTATACAACATTTTG
10	GGCGTTTTAAAAGCCTACCTCCGGAGCAGAAG
11	TTACAGAGTAGGTCTGAACAAAATCGTCAATA
12	AGGAAACCAGATGATGCCTACCATTTCTGAAT
13	AAGTGTTTGGAACGGTGGGAAGAAGAGAGGGTTCTACAAA
14	AATGGATTCCGGCGAATGAGTGTTAATCAGCTGGAACGCC
15	GCGGTCAGCAAAAGAACGGCCAACCTCAGGAAGCTTTCCG
16	ATTTAGAAGTCGTGCCACTCTAGACCAAGCTTGCATGCCT
17	AGCCCAATCACCAGTATAATAATTGTAGCTCATTTGCGGA
18	GCGAAAGAGTCTTTACACAGTTCA
19	CCTGATAAGGCATAGTTTCAACTA
20	AAGTAAGCCGGTCATACCTTTAGCACTTAGCCATAAGGCTAATTGGG CTTGAGATG
21	TGCAGAACACAAGAAATAGAAGGCAGGATTAGGAAACATGCCAAA
22	AGG
23	TTGTTTAAAAATCCTCAGGCAGGTAGGCTTTG
24	ATTAGAGCTAATTACAGCAAAAGAGAGGAAACCGCCAAAGGGAAG
25	GTA
26	TTTAGACATTATAATCAAATACCTAATTCTTATTACTAGAAGCGAAC C
27	GAACCACCCTTAGGTTCAAAATCAAGAATAAC
28	CGACGACAGTATCGGCGCGCGGGGGGAAACCTGTATTAGAGATTAT
29	ACATCAAAAT
30	TGACCCTGTAATGCCGAGCGAAAGGGGGAAAGATTTACAT CATTAAATTTTTGTTAGTTCCAGTTTATAAATTATTAACA
31	GCACCGCTGGCCAGTGGGATCCCC
32	TCCCGACTATTATTCTGATTAGCGATTGCGAACAAACTACGTGGCAT
33	CAATTCTAC
34	AGCCTTTAAGGTCATTACATGTTT
35	AGGACTAATGCTTTAACCTGACTA
36	AATATTGATTCAGTGAGGAACGAGATACCACAAAGAGCAA
37	TGGCAGATAATCATAACCAGTATAATCAGATAAATAATATGGATAG CA
38	ATAAAAACGGAGGTTGATTAAAGCCCTCAGCA

39	TATTTGCATTTACCAGGCAATAATCAAGTTTGGCCCCCTTTATCATC
40	G
41	GGCTATCAGGTCATTGAGCTTGACGAGCGGGCGCTCATGGAGTGAG
42	GCTCAGCTAA
43	CCGCCTGCGAATTTATGGGTTATAACGATTTT
44	GGGTACCGATTGTTTGCTTTACAATTACCTGATTTAACAATTTAAGA
45	A
46	TGATAAATTAATACTTAAAGGGAT
47	ATCAAAAATAATTCGCAAAATCCCTTGGAACATACCGAAC
48	AAAACGACTCTGGTGCTCCAGTCGAGAGGCGGACTAATAG
49	TAAATATGCTGAAAAGAACGCCTG
50	TTATAGTCTTGATAAGATTGTATC
51	CACTATCACCCTCAAAAGACTTTT
52	GTTTAATTATTTAGGAGCGCAGAC
53	CTAAAGGAGGGTTTTGATTTTCAGCCCATCCT
54	ATCGTCACCAGAATGGCGGAACCTTGCGGGAG
55	GAGATTTGATTAGCGTCATTGACAAGGGAAGC
56	GCTGCTCACGGAAATTGACAGAATAACGGAAT
57	GCAAGCAAAAGCCAACCAACATGTCACCGAGT
58	AATAAGAATAACTATAAACACCGGTCACCAGT
59	AAGCCCTTTTTCATTTTCAATAGTAACAGTGC
60	TCATATGGCGTAAAACCATTTCAAACAATTCG
61	GGAAAAACGCTAGGGCGGCCGATTTTGCGGGAGAAGCCTT
62	ATTAAAAAAGAGTCCACGATTTAGCCTGAGAGGTTCTAGC
63	CACTAACATTTGCGTAAAATCGGCGTCTGGCCAAAATTCG
64	TAATCCTGAGCTCGAAGCCCGCTTCGGAAACCTGAGGGGA
65	GGCGCGAGCAACTAAAAGGAACAA
66	TGCTCCTTAGAAGCAATTTGCGGG
67	TTGAATCCTAACCCTCGTACAACG
68	CAGTTGAGTCAACTTTGTAACAAA
69	TAGCATTCCCACCCTCCTCAGTACGCCCAATA
70	GGTTTATCGCCTATTTAAAGCGCACCAATCCA
71	TCATGAGGGCCGCCAGTTGCCATCTCTTACCG
72	GGTCAATCTCAGTAGCATTCATTATAGAAAAT
73	AATTTACGACAATAAAGCTCAACATTGCAACA
74	GTTTTGAATAAGAATATGTAAATGACATCGCC
75	GCATTAGAGAGAAGAGGAATTACCTTTAGGAG
76	ACCCAAAAGAATTATTAGAAATAACATCAATA
77	AAAAGAGTAAACAGGAGCTGGCAAATTCAACCTCTGGAGC
78	CACACGACGGAGCCCCCTATTAAAATTTTGTTTTCCTGTA CACGCTGATGGTTCCGTTGGGCGCTGCCAGTTAGGCAAAG
79	ACAACTCGCGCTCACTTTCGTAATCCAGTCACGACGTTGT
80	CAGAGCCACACAGACAGAATAGAAGTACGGTGCCTTTAAT
81	AGGCCGCTAGCGGATTAATATTCA
82	GAAACAAAGTTTACCAAGATTCAT

83	AATAGCTATTTTCATACACCGTAAATAAGGGAAAATCAACAATCATT
84	GTGAATTAC
	AGACGACGAGCATGTAATTACCGCCAGGCGGATGCCCCCTAGCTTG
85	CT
86	TATTTATCGTCTCTGACCAGAGCCAAGTTTCC
87	AAAATATCTTTTTTAAGCAGAGGCGAACTGGCACAATCAAAAGGTG
88	AA
	CGGGAGCTCTGTCCATGCCAGCCAGTAGGGCTGCGTTAAAGCCTTA
89	AA
90	GCCCTAAACTGATGCAAAGACGCTCGGGAGAA
91	ATCGTAACCGTGCATCCAGGGTGGTTGCGTTGTATTAAATTGGCAAT
92	TAGAAATTG
93	TATTTCAAAATATGATGTGTAGCGCCCTAAAGCAGTAATA
94	AATTGTAAACGTTAATGAACGTGGTTTGATGGGAGCCAGC
95	CGCCATTCGGGTTTTCCATGGTCA
	TCAAGATTACAGTTAATAAGTGCCCGGAGTGAGCCCTCATCTATATT
96	TTCATTTGG
97	TTCGAGGTAGAGAGTATCTGGAAG
98	ATTAAACGTCGTCATAGCATCAAA
99	TTATCACCCATTACCCACCGAACTAGGTAGAAGACGACGA
100	AAAGGGACTAAATAAGTAATTGAGTAGGAATCGAAACCAAGCCACC
101	CT
102	TTAACTGAAACCACCAATTTACCGGGAGTTAA
103	CGTAGATTATTTTGTCATGATTAAGATAGCAGATCAAAATCCAAGCG
104	C
105	AAACAAGAGAATCGATAATCGGAAGTCACGCTATATTACCCACGCA
106	AATTCTGTCC
107	AGCAAATGCTTAGATTAATCCAATAGCCATAT
108	TAGCTGTTTCAGATGACCTTTGCCAAAATCGCTGGAAACAGAAATA
109	GC
110	TCACCATCCGCAAGGAAATCAGAG
111	GCCAGCTTTCATCAACAAATCCTGACTCCAACAACTGATA
112	TAACGCCAGCCATTCACACATTAATTTTTCTTGGTTATCT
113	TTTCATTCCTGTTTAGAGTTAGCG
114	AAGATTAATCAGGATTGAATTTCT
115	TAAAAACCCTGCGGAAGGTAAAAT
116	CTTATGCGATTATTACGACCAACT
117	AGTTTCAGGTCGAGAGTCAGAACCTCAATAAT
118	GCTTGCAGTTCCAGTACCGTATAAAGTTGCTA
119	CGATTATACACCGGAAGCCACCAGACACCCTG
120	CGGATATTGTCACCGAAAACCATCGACTCCTT
121	TTTCATCGAATCGCCATAAAGTAATTAACCGT
122	AAATAAACCGCAAGACCCGTGTGAATTCTGGC
123	GAAACAATGTACATAAAGCGATAGAAAAATCT
124	ATAAGTTTTTCAGGTTCAAGTTACCGAACGTT

125	CCAGAACAGCGCGTAACTCGTTAGTAAAAATTTTTAGAAC
126	AATGCGCGGTCAAAGGAAGCACTAGAACGGTACAGTCAAA
127	TTGAGGAATTCACCAGGCAGGCGAATTAAATGAATATTTA
128	CCTGATTATCCTGTGTAGCTAACTGGCTGCGCATGGGCGC
129	TCAATAACCATATAACCTTTCAAC
130	CCAACAGGGAGGAAGCTCGCTGAG
131	GTCCAATAAAAATAGCACCCCCAG
132	GGAACAACATTTTAAGACAAGAAC
133	TAACGATCCGCCACCCGGTTGATAGTTTTTAT
134	TAAACAGCAACAGTGCAGCGTCATCAGTTACA
135	ACGTAATGTCAGAGCCCCAGAGCCAAGAGCAA
136	TTGAAAGACACCAATGCTTGAGCCACCACGGA CGGCTGTCACAAAAGGTATTTAACGGTAATAT
137	TTTTGCACAATACCGAAAAGAACGTAGTCTTT
138	AACAAAGTGAAAACATATCAATATGAAAGGAA
139	ATTACGCATTGAATACTAACGTCAATCATATT
140	TGTAGCAAGTGCTTTCCCACCACAGCCGGAGAATCGTAAA
141	CAACAGAGGTGCCGTAGCGAAAAATATAAGCATGAGCGAG
142	AAAGCATCTTGCCCCATGAGACGGTGGTGTAGAACTGTTG ATTAATTTAATGAGTGGAAATTGTAGGCGATTAAGTTGGG
143	CTCAGAACTAAAGTTTCTAAACAAAGTTGATTAGCAAACT
144	ATATTCGGCCGAAAGATGGATAGC
145	CATCTTTGGAGAGGCTGAACTAAC
146	CCAATAATACCACCGGGGAAACGTGGACAGATTAATCTTGAACTGG CTCATTATAC
147	AAGTACCGTTTCCTTAAGCAAGCCTAAGTATACCTTGAGTTTGATAC
148	C
149	TAATTTGCACATGGCTCACCACCCCCACTACG
150	CAACAGTTATGTGAGTTGATTGCTGTATGTTAGCAAAGACATTTGGG
151	A
152	CGTATAACTACTTCTTGCCTTGCTAACGCCAATGGTTTGACCAGCTA
153	C ATGGCTATCGAGAAAAGAATCCTTCAGAGGGT
154	ATGGGATAGGTCACGTGCAACAGCGGGTGCCTTAAAAGTTGAATTA
155	TCGATGAATA
156	CCTCATATTGAGAAAGCCCGCCGCGGGTCGAGATAGAACC
157	AAAAACAGGAAGATTGCCGTCTATACGCTGGTACCTTGCT
158	GGAAGGGCGTGCTGCATATCCGCT
159	AATTTTATGGTCAGTGGCCCGGAAGGATTTTGTGTCGTCTTACATTT
160	CGCAAATGG
161	GATAGTTGAGACCGGACCCAATTC
162	AAGGCACCGTTTAGACCTTCAAAT
163	ATTAGAGCATCAAGAGGAACGGTGAATAAAACTTTGCAAA
164	CTTCTGACAAATTTAACATGTAATCGAGAACATCATTCCACCGCCAC
165	C

166	AATTGAGCCTCAGAGCTTTGATGATAACCGAT
167	TACAGTAAAAAGAAACGCAAACGTGCAAGGCCAACCGCCTAAAAC
168	ACT
169	ACTAGCATGTCAATCAGTTTTTTGGCTTAATGAACTATCGTGATTAG
170	TAGAATATA
171	GAACCTCATTCCCTTACTTTTTCACCAGAGCC
172	CACAATTCAAGGAGCGTGAGTAACGATTCGCCGAATAACCAGTTAA
173	GC
174	CAAAAGGGATTTTAAAGACGAGCA
	TAACAACCCGTCGGATAGCGGTCCCAGGGCGAATTTTTGA
	AGGGGGATGATCGGTGAAAGCCTGTGATTGCCTGGCAAAT
	TGCGAACGCCATTAGATTCCAGAC
	ATCGCGTTAGCGAACCCGCCGACA
	AGAAGTTTAGTAAAATAACCTAAA
	CAGTCAGGTCTACGTTTACAGACC
	TCTGTATGTAGGTGTAGTTTAGTAAGAACGGG
	CCCACGCATACAGGAGTTTAACGGCCTGAATC
	AATACACTCCCTCAGACCGCCACCGCTAATAT
	TGACCTTCCAGCAAAATACCATTAAGAAAATA
	GCACTCATTTAGGCAGGTAATAAGAATAACAT
	GCGTCTTTAATATATTTCTGACCTCTGAAAGC
	AAGAATTGTTGCTTCTAATTAATTAATATCAA
	AACATATACAGTACCTCAATAACGATTATCAT
	AGAACTCACGCCGCTAGTTGCTTTTGCAATGCCTGAGTAA
	CAGACAATTGGCCCACCAAATCAATATGTACCTAAAGATT
	TGGTCAGTCTTCACCGTTGCAGCATCTCCGTGAAAGCCCC
	ACCACCAGCACACAACTAAAGTGTCGGGCCTCTGACCGTA

APPENDIX C

SUPPLEMENTAL INFORMATION FOR CHAPTER 4

(USING DNA ORIGAMI TO QUANTIFY FUNCTIONAL TCRαβ REPERTOIRE WITHOUT SINGLE CELL SORTING)

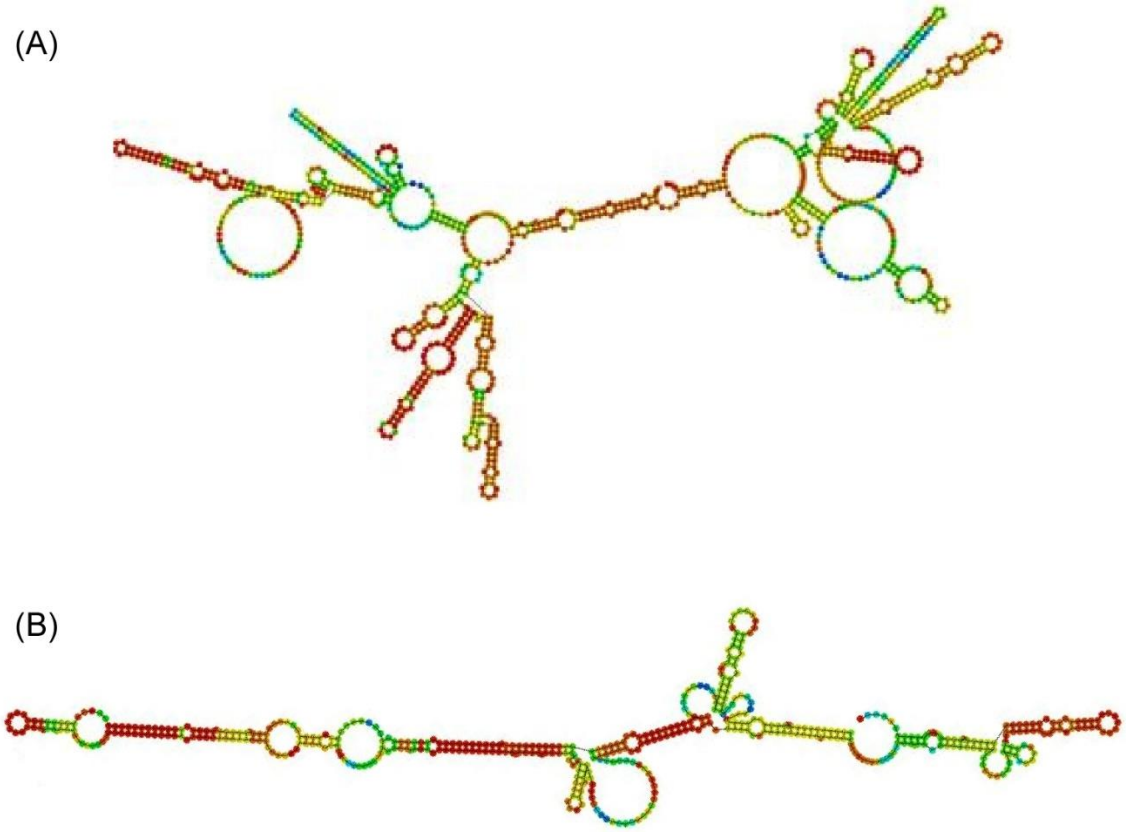

Figure S4.1 Secondary structure prediction of the C region of P14 TCRα (A) and TCRβ (B). Origami probes are designed to bind to the single stranded loop region.

Table S4.1 Staple sequences of DNA origami

Name	Sequence
1	CAAGCCCAATAGGAAC CCATGTACAAACAGTT
2	AATGCCCCGTAACAGT GCCCGTATCTCCCTCA
3	TGCCTTGACTGCCTAT TTCGGAACAGGGATAG
4	GAGCCGCCCCACCACC GGAACCGCGACGGAAA
5	AACCAGAGACCCTCAG AACCGCCAGGGGTCAG
6	TTATTCATAGGGAAGG TAAATATT CATTCAGT
7	CATAACCCGAGGCATA GTAAGAGC TTTTTAAG
8	ATTGAGGGTAAAGGTG AATTATCAATCACCGG
9	AAAAGTAATATCTTAC CGAAGCCCTTCCAGAG
10	GCAATAGCGCAGATAG CCGAACAATTCAACCG
11	CCTAATTTACGCTAAC GAGCGTCTAATCAATA
12	TCTTACCAGCCAGTTA CAAAATAAATGAAATA
13	ATCGGCTGCGAGCATG TAGAAACCTATCATAT
14	CTAATTTATCTTTCCT TATCATTCATCCTGAA
15	GCGTTATAGAAAAAGC CTGTTTAG AAGGCCGG
16	GCTCATTTTCGCATTA AATTTTTG AGCTTAGA
17	AATTACTACAAATTCT TACCAGTAATCCCATC
18	TTAAGACGTTGAAAAC ATAGCGATAACAGTAC
19	TAGAATCCCTGAGAAG AGTCAATAGGAATCAT
20	CTTTTACACAGATGAA TATACAGTAAACAATT
21	TTTAACGTTCGGGAGA AACAATAATTTTCCCT
22	CGACAACTAAGTATTA GACTTTACAATACCGA
23	GGATTTAGCGTATTAA ATCCTTTGTTTTCAGG
24	ACGAACCAAAACATCG CCATTAAA TGGTGGTT
25	GAACGTGGCGAGAAAG GAAGGGAA CAAACTAT
26	TAGCCCTACCAGCAGA AGATAAAAACATTTGA
27	CGGCCTTGCTGGTAAT ATCCAGAACGAACTGA
28	CTCAGAGCCACCACCC TCATTTTCCTATTATT
29	CTGAAACAGGTAATAA GTTTTAACCCCTCAGA
30	AGTGTACTTGAAAGTA TTAAGAGGCCGCCACC
31	GCCACCACTCTTTTCA TAATCAAACCGTCACC
32	GTTTGCCACCTCAGAG CCGCCACCGATACAGG
33	GACTTGAGAGACAAAA GGGCGACAAGTTACCA
34	AGCGCCAACCATTTGG GAATTAGATTATTAGC
35	GAAGGAAAATAAGAGC AAGAAACAACAGCCAT
36	GCCCAATACCGAGGAA ACGCAATAGGTTTACC
37	ATTATTTAACCCAGCT ACAATTTTCAAGAACG
38	TATTTTGCTCCCAATC CAAATAAGTGAGTTAA
39	GGTATTAAGAACAAGA AAAATAATTAAAGCCA
40	TAAGTCCTACCAAGTA CCGCACTCTTAGTTGC
41	ACGCTCAAAATAAGAA TAAACACCGTGAATTT
42	AGGCGTTACAGTAGGG CTTAATTGACAATAGA
43	ATCAAAATCGTCGCTA TTAATTAACGGATTCG

44	CTGTAAATCATAGGTC TGAGAGACGATAAATA
45	CCTGATTGAAAGAAAT TGCGTAGACCCGAACG
46	ACAGAAATCTTTGAAT ACCAAGTTCCTTGCTT
47	TTATTAATGCCGTCAA TAGATAATCAGAGGTG
48	AGATTAGATTTAAAAG TTTGAGTACACGTAAA
49	AGGCGGTCATTAGTCT TTAATGCGCAATATTA
50	GAATGGCTAGTATTAA CACCGCCTCAACTAAT
51	CCGCCAGCCATTGCAA CAGGAAAAATATTTTT
52	CCCTCAGAACCGCCAC CCTCAGAACTGAGACT
53	CCTCAAGAATACATGG CTTTTGATAGAACCAC
54	TAAGCGTCGAAGGATT AGGATTAGTACCGCCA
55	CACCAGAGTTCGGTCA TAGCCCCCGCCAGCAA
56	TCGGCATTCCGCCGCC AGCATTGACGTTCCAG
57	AATCACCAAATAGAAA ATTCATATATAACGGA
58	TCACAATCGTAGCACC ATTACCATCGTTTTCA
59	ATACCCAAGATAACCC ACAAGAATAAACGATT
60	ATCAGAGAAAGAACTG GCATGATTTTATTTTG
61	TTTTGTTTAAGCCTTA AATCAAGAATCGAGAA
62	AGGTTTTGAACGTCAA AAATGAAAGCGCTAAT
63	CAAGCAAGACGCGCCT GTTTATCAAGAATCGC
64	AATGCAGACCGTTTTT ATTTTCATCTTGCGGG
65	CATATTTAGAAATACC GACCGTGTTACCTTTT
66	AATGGTTTACAACGCC AACATGTAGTTCAGCT
67	TAACCTCCATATGTGA GTGAATAAACAAAATC
68	AAATCAATGGCTTAGG TTGGGTTACTAAATTT
69	GCGCAGAGATATCAAA ATTATTTGACATTATC
70	AACCTACCGCGAATTA TTCATTTCCAGTACAT
71	ATTTTGCGTCTTTAGG AGCACTAAGCAACAGT
72	CTAAAATAGAACAAAG AAACCACCAGGGTTAG
73	GCCACGCTATACGTGG CACAGACAACGCTCAT
74	GCGTAAGAGAGAGCCA GCAGCAAAAAGGTTAT
75	GGAAATACCTACATTT TGACGCTCACCTGAAA
76	TATCACCGTACTCAGG AGGTTTAGCGGGGTTT
77	TGCTCAGTCAGTCTCT GAATTTACCAGGAGGT
78	GGAAAGCGACCAGGCG GATAAGTGAATAGGTG
79	TGAGGCAGGCGTCAGA CTGTAGCGTAGCAAGG
80	TGCCTTTAGTCAGACG ATTGGCCTGCCAGAAT
81	CCGGAAACACACCACG GAATAAGTAAGACTCC
82	ACGCAAAGGTCACCAA TGAAACCAATCAAGTT
83	TTATTACGGTCAGAGG GTAATTGAATAGCAGC
84	TGAACAAACAGTATGT TAGCAAACTAAAAGAA
85	CTTTACAGTTAGCGAA CCTCCCGACGTAGGAA
86	GAGGCGTTAGAGAATA ACATAAAAGAACACCC
87	TCATTACCCGACAATA AACAACATATTTAGGC
88	CCAGACGAGCGCCCAA TAGCAAGCAAGAACGC

89	AGAGGCATAATTTCAT CTTCTGACTATAACTA
90	TTTTAGTTTTTCGAGC CAGTAATAAATTCTGT
91	TATGTAAACCTTTTTT AATGGAAAAATTACCT
92	TTGAATTATGCTGATG CAAATCCACAAATATA
93	GAGCAAAAACTTCTGA ATAATGGAAGAAGGAG
94	TGGATTATGAAGATGA TGAAACAAAATTTCAT
95	CGGAATTATTGAAAGG AATTGAGGTGAAAAAT
96	ATCAACAGTCATCATA TTCCTGATTGATTGTT
97	CTAAAGCAAGATAGAA CCCTTCTGAATCGTCT
98	GCCAACAGTCACCTTG CTGAACCTGTTGGCAA
99	GAAATGGATTATTTAC ATTGGCAGACATTCTG
100	TTTT TATAAGTA TAGCCCGGCCGTCGAG
101	AGGGTTGA TTTT ATAAATCC TCATTAAATGATATTC
102	ACAAACAA TTTT AATCAGTA GCGACAGATCGATAGC
103	AGCACCGT TTTT TAAAGGTG GCAACATAGTAGAAAA
104	TACATACA TTTT GACGGGAG AATTAACTACAGGGAA
105	GCGCATTA TTTT GCTTATCC GGTATTCTAAATCAGA
106	TATAGAAG TTTT CGACAAAA GGTAAAGTAGAGAATA
107	TAAAGTAC TTTT CGCGAGAA AACTTTTTATCGCAAG
108	ACAAAGAA TTTT ATTAATTA CATTTAACACATCAAG
109	AAAACAAA TTTT TTCATCAA TATAATCCTATCAGAT
110	GATGGCAA TTTT AATCAATA TCTGGTCACAAATATC
	AAACCCTC TTTT ACCAGTAA TAAAAGGGATTCACCA
111	GTCACACG TTTT
112	CCGAAATCCGAAAATC CTGTTTGAAGCCGGAA
113	CCAGCAGGGGCAAAATCCCTTATAAAGCCGGC
114	GCATAAAGTTCCACAC AACATACGAAGCGCCA
115	GCTCACAATGTAAAGCCTGGGGTGGGTTTGCC
116	TTCGCCATTGCCGGAA ACCAGGCATTAAATCA
117	GCTTCTGGTCAGGCTGCGCAACTGTGTTATCC
118	GTTAAAATTTTAACCAATAGGAACCCGGCACC
119	AGACAGTCATTCAAAA GGGTGAGAAGCTATAT
120	AGGTAAAGAAATCACCATCAATATAATATTTT
121	TTTCATTTGGTCAATA ACCTGTTTATATCGCG
122	TCGCAAATGGGGCGCGAGCTGAAATAATGTGT
123	TTTTAATTGCCCGAAA GACTTCAAAACACTAT
124	AAGAGGAACGAGCTTCAAAGCGAAGATACATT
125	GGAATTACTCGTTTACCAGACGACAAAAGATT
126	GAATAAGGACGTAACA AAGCTGCTCTAAAACA
127	CCAAATCACTTGCCCTGACGAGAACGCCAAAA
128	CTCATCTTGAGGCAAA AGAATACAGTGAATTT
129	AAACGAAATGACCCCCAGCGATTATTCATTAC
130	CTTAAACATCAGCTTG CTTTCGAGCGTAACAC
131	TCGGTTTAGCTTGATACCGATAGTCCAACCTA
132	TGAGTTTCGTCACCAGTACAAACTTAATTGTA

133	CCCCGATTTAGAGCTTGACGGGGAAATCAAAA
134	GAATAGCCGCAAGCGGTCCACGCTCCTAATGA
135	GAGTTGCACGAGATAGGGTTGAGTAAGGGAGC
136	GTGAGCTAGTTTCCTGTGTGAAATTTGGGAAG
137	TCATAGCTACTCACATTAATTGCGCCCTGAGA
138	GGCGATCGCACTCCAGCCAGCTTTGCCATCAA
139	GAAGATCGGTGCGGGCCTCTTCGCAATCATGG
140	AAATAATTTTAAATTGTAAACGTTGATATTCA
141	GCAAATATCGCGTCTGGCCTTCCTGGCCTCAG
142	ACCGTTCTAAATGCAATGCCTGAGAGGTGGCA
143	TATATTTTAGCTGATAAATTAATGTTGTATAA
144	TCAATTCTTTTAGTTTGACCATTACCAGACCG
145	CGAGTAGAACTAATAGTAGTAGCAAACCCTCA
146	GAAGCAAAAAAGCGGATTGCATCAGATAAAAA
147	TCAGAAGCCTCCAACAGGTCAGGATCTGCGAA
148	CCAAAATATAATGCAGATACATAAACACCAGA
149	CATTCAACGCGAGAGGCTTTTGCATATTATAG
150	ACGAGTAGTGACAAGAACCGGATATACCAAGC
151	AGTAATCTTAAATTGGGCTTGAGAGAATACCA
152	GCGAAACATGCCACTACGAAGGCATGCGCCGA
153	ATACGTAAAAGTACAACGGAGATTTCATCAAG
154	CAATGACACTCCAAAAGGAGCCTTACAACGCC
155	AAAAAAGGACAACCATCGCCCACGCGGGTAAA
156	TGTAGCATTCCACAGACAGCCCTCATCTCCAA
157	GTAAAGCACTAAATCGGAACCCTAGTTGTTCC
158	AGTTTGGAGCCCTTCACCGCCTGGTTGCGCTC
159	AGCTGATTACAAGAGTCCACTATTGAGGTGCC
160	ACTGCCCGCCGAGCTCGAATTCGTTATTACGC
161	CCCGGGTACTTTCCAGTCGGGAAACGGGCAAC
162	CAGCTGGCGGACGACGACAGTATCGTAGCCAG
163	GTTTGAGGGAAAGGGGGATGTGCTAGAGGATC
164	CTTTCATCCCCAAAAACAGGAAGACCGGAGAG
165	AGAAAAGCAACATTAAATGTGAGCATCTGCCA
166	GGTAGCTAGGATAAAAATTTTTAGTTAACATC
167	CAACGCAATTTTTGAGAGATCTACTGATAATC
168	CAATAAATACAGTTGATTCCCAATTTAGAGAG
169	TCCATATACATACAGGCAAGGCAACTTTATTT
170	TACCTTTAAGGTCTTTACCCTGACAAAGAAGT
171	CAAAAATCATTGCTCCTTTTGATAAGTTTCAT
172	TTTGCCAGATCAGTTGAGATTTAGTGGTTTAA
173	AAAGATTCAGGGGGTAATAGTAAACCATAAAT
174	TTTCAACTATAGGCTGGCTGACCTTGTATCAT
175	CCAGGCGCTTAATCATTGTGAATTACAGGTAG
176	CGCCTGATGGAAGTTTCCATTAAACATAACCG
177	TTTCATGAAAATTGTGTCGAAATCTGTACAGA

178	ATATATTCTTTTTTCACGTTGAAAATAGTTAG
179	AATAATAAGGTCGCTGAGGCTTGCAAAGACTT
180	CGTAACGATCTAAAGTTTTGTCGTGAATTGCG
181	ACCCAAATCAAGTTTTTTGGGGTCAAAGAACG
182	TGGACTCCCTTTTCACCAGTGAGACCTGTCGT
183	TGGTTTTTAACGTCAAAGGGCGAAGAACCATC
184	GCCAGCTGCCTGCAGGTCGACTCTGCAAGGCG
185	CTTGCATGCATTAATGAATCGGCCCGCCAGGG
186	ATTAAGTTCGCATCGTAACCGTGCGAGTAACA
187	TAGATGGGGGGTAACGCCAGGGTTGTGCCAAG
188	ACCCGTCGTCATATGTACCCCGGTAAAGGCTA
189	CATGTCAAGATTCTCCGTGGGAACCGTTGGTG
190	TCAGGTCACTTTTGCGGGAGAAGCAGAATTAG
191	CTGTAATATTGCCTGAGAGTCTGGAAAACTAG
192	CAAAATTAAAGTACGGTGTCTGGAAGAGGTCA
193	TGCAACTAAGCAATAAAGCCTCAGTTATGACC
194	TTTTTGCGCAGAAAACGAGAATGAATGTTTAG
195	AAACAGTTGATGGCTTAGAGCTTATTTAAATA
196	ACTGGATAACGGAACAACATTATTACCTTATG
197	ACGAACTAGCGTCCAATACTGCGGAATGCTTT
198	CGATTTTAGAGGACAGATGAACGGCGCGACCT
199	CTTTGAAAAGAACTGGCTCATTATTTAATAAA
200	GCTCCATGAGAGGCTTTGAGGACTAGGGAGTT
201	ACGGCTACTTACTTAGCCGGAACGCTGACCAA
202	AAAGGCCGAAAGGAACAACTAAAGCTTTCCAG
203	GAGAATAGCTTTTGCGGGATCGTCGGGTAGCA
204	ACGTTAGTAAATGAATTTTCTGTAAGCGGAGT
205	TTTTCGATGGCCCACTACGTAAACCGTC
206	TATCAGGGTTTTCGGTTTGCGTATTGGGAACGCGCG
207	GGGAGAGGTTTTTGTAAAACGACGGCCATTCCCAGT
208	CACGACGTTTTTGTAATGGGATAGGTCAAAACGGCG
209	GATTGACCTTTTGATGAACGGTAATCGTAGCAAACA
210	AGAGAATCTTTTGGTTGTACCAAAAACAAGCATAAA
211	GCTAAATCTTTTCTGTAGCTCAACATGTATTGCTGA
212	ATATAATGTTTTCATTGAATCCCCCTCAAATCGTCA
213	TAAATATTTTTTGGAAGAAAAATCTACGACCAGTCA
214	GGACGTTGTTTTTCATAAGGGAACCGAAAGGCGCAG
215	ACGGTCAATTTTGACAGCATCGGAACGAACCCTCAG
	CAGCGAAAATTTTACTTTCAACAGTTTCTGGGATTTTGCTAAACTT
216	TT
rt-rem1	AACATCACTTGCCTGAGTAGAAGAACT
rt-rem2	TGTAGCAATACTTCTTTGATTAGTAAT
rt-rem3	AGTCTGTCCATCACGCAAATTAACCGT
rt-rem4	ATAATCAGTGAGGCCACCGAGTAAAAG
rt-rem5	ACGCCAGAATCCTGAGAAGTGTTTTT

rt-rem6	TTAAAGGGATTTTAGACAGGAACGGT
rt-rem7	AGAGCGGGAGCTAAACAGGAGGCCGA
rt-rem8	TATAACGTGCTTTCCTCGTTAGAATC
rt-rem9	GTACTATGGTTGCTTTGACGAGCACG
rt-rem10	GCGCTTAATGCGCCGCTACAGGGCGC

FRET labeled staples:
91- Fluorescein: TATGTAAACCTTT/iFluorT/TTAATGGAAAAATTACCT
89-TAMRA: AGAGGCATAATTTCATCTTCTGACTAT/i6-TAMN/AACTA

Table S4.2 P14 TCRα probes attached to the origami template
Original helpers in origami (32nt)

73	GCCACGCTATACGTGG	CACAGACAACGCTCAT
69	GCGCAGAGATATCAAA	ATTATTTGACATTATC
65	CATATTTAGAAATACC	GACCGTGTTACCTTTT
61	TTTTGTTTAAGCCTTA	AATCAAGAATCGAGAA
57	AATCACCAAATAGAAA	ATTCATATATAACGGA
53	CCTCAAGAATACATGG	CTTTTGATAGAACCAC

New helpers with probes for TCRα mRNA:

A'-73-1	GCCACGCTATACGTGG TTTGAAGATATCTTG
A'-73-2	GGTGGCGTTGGTCTC CACAGACAACGCTCAT
A'-69-1	GCGCAGAGATATCAAA TTTGAAGATATCTTG
A'-69-2	GGTGGCGTTGGTCTC ATTATTTGACATTATC
A'-65-1	CATATTTAGAAATACC TTTGAAGATATCTTG
A'-65-2	GGTGGCGTTGGTCTC GACCGTGTTACCTTTT
A'-61-1	TTTTGTTTAAGCCTTA TTTGAAGATATCTTG
A'-61-2	GGTGGCGTTGGTCTC AATCAAGAATCGAGAA
A'-57-1	AATCACCAAATAGAAA TTTGAAGATATCTTG
A'-57-2	GGTGGCGTTGGTCTC ATTCATATATAACGGA
A'-53-1	CCTCAAGAATACATGG TTTGAAGATATCTTG
A'-53-2	GGTGGCGTTGGTCTC CTTTTGATAGAACCAC

Table S4.3 P14 TCRβ probes attached to the origami template

Original helpers in origami (32nt)

182	TGGACTCCCTTTTCAC	CAGTGAGACCTGTCGT
186	ATTAAGTTCGCATCGT	AACCGTGCGAGTAACA
190	TCAGGTCACTTTTGCG	GGAGAAGCAGAATTAG
194	TTTTTGCGCAGAAAAC	GAGAATGAATGTTTAG
198	CGATTTTAGAGGACAG	ATGAACGGCGCGACCT
202	AAAGGCCGAAAGGAAC	AACTAAAGCTTTCCAG

New helpers with probes for TCRβ mRNA:

B'-182-1	TGGACTCCCTTTTCAC	GTGTGACAGGTTTGG
B'-182-2	CTGCACTGATGTTCT	CAGTGAGACCTGTCGT
B'-186-1	ATTAAGTTCGCATCGT	GTGTGACAGGTTTGG
B'-186-2	CTGCACTGATGTTCT	AACCGTGCGAGTAACA
B'-190-1	TCAGGTCACTTTTGCG	GTGTGACAGGTTTGG
B'-190-2	CTGCACTGATGTTCT	GGAGAAGCAGAATTAG
B'-194-1	TTTTTGCGCAGAAAAC	GTGTGACAGGTTTGG
B'-194-2	CTGCACTGATGTTCT	GAGAATGAATGTTTAG
B'-198-1	CGATTTTAGAGGACAG	GTGTGACAGGTTTGG
B'-198-2	CTGCACTGATGTTCT	ATGAACGGCGCGACCT
B'-202-1	AAAGGCCGAAAGGAAC	GTGTGACAGGTTTGG
B'-202-2	CTGCACTGATGTTCT	AACTAAAGCTTTCCAG

Table S4.4 P14 TCRα RT-ligation-PCR primer setting

GTCTAGGAGGAATGGACAAGATTCTGACAGCATCATTTTTACTCCTAGGCCTT
CACCTAGCTGGGGTGAATGGCCAGCAGAAGGAGAAACATGACCAGCAGCAG
GTGAGACAAAGTCCCCAATCTCTGACAGTCTGGGAAGGAGGAACCACAGTTC
TGACCTGCAGTTATGAGGACAGCACTTTTAACTACTTCCCATGGTACCAACAG
TTCCCTGGGGAAGGCCCTGCACTTCTGATATCCATACTTTCAGTGTCCGATAA
AAAGGAAGATGGACGATTCACAACCTTCTTCAATAAAAGGGAGAAAAAGCT
CTCCTTGCACATCATAGACTCTCAGCCTGGAGACTCAGCCACCTACTTCTGTG
CAGCTCTCTATGGAAATGAGAAAATAACTTTTGGGGCTGGAACCAAACTCAC
CATTAAACCCAACATCCAGAACCCAGAACCTGCTGTGTACCAGTTAAAAGAT
CCTCGGTCTCAGGACAGCACCCTCTGCCTGTTCACCGACTTTGACTCCCAAAT
CAATGTGCCGAAAACCATGGAATCTGGAACGTTCATCACTGACAAAACTGTG
CTGGACATGAAAGCTATGGATTCCAAGAGCAATGGGGCCATTGCCTGGAGCA
ACCAGACAAGCTTCACCTGCCAAGATATCTTCAAAGAGACCAACGCCACCTA
CCCCAGTTCAGACGTTCCCTGTGATGCCACGTTGACCGAGAAAAGCTTTGAA
ACAGATATGAACCTAAACTTTCAAAACCTGTCAGTTATGGGACTCCGAATCCT
CCTGCTGAAAGTAGCGGGATTTAACCTGCTCATGACGCTGAGGCTGTGGTCC
AGTTGAGGTCTGCAAGACTGACAGAGCCTGACTCCCAAGTTCCGTCCTCCTC
ACCCCTCCGCTCCCTCTTCAAGCCAAAAGGAGCCGGCTGTCTGGGGTCTGGTT
GGCCCTGATTCACAATCCCACCTGGATCTCCCAGATTTGTGAGGAAGGTTGCT
AGAGAGCTAAGCGCTGCTGCCGCACCCACTCAGCTCCCTCACTGCTGCTGAC
CATTCACAAAAAAAAAAAAACGGCAGGGGCGGGGCTTCTCCTGGATCTGAAG
ACCCCTCCCCCATGGCAGACTCCCCTATAAAATCTCTTGGAGAATGTTGTAAA
AAATATGGGTTTTTTTTTTTGGCGGGTTTACTTTTTTAAGCATCCATAAAGAA
ATGCATATTACTCTTTCATCAAGGTGTAGAAATTATCTCATTGTCTAGACCCT
CCTGCTACTGTGTGTATTGAGCCACATTGTATATTATTCTGCTGCCCATGACA
TCATTAAAGGTGATTCAGAAA

C-Region
J-Region
V-Region
Sig-Peptide

Origami biding region: CAAGATATCTTCAAAGAGACCAACGCCACC

Cα Linker annealing location: 5’ TACCAGTTAAAAGATCCTCG 3’
Cα Linker sequence: 5’ CGAGGATCTTTTAACTGGTA3’

Vα PCR linker annealing location: 5’ TTCTGTGCAGCTCTCTATGG 3’
Vα PCR linker sequence: 5’ TTCTGTGCAGCTCTCTATGG 3’

Table S4.5 P14 TCRβ RT-ligation-PCR primer setting

ATGGGCTCCAGACTCTTCTTTGTGGTTTTGATTCTCCTGTGTGCAAAACACAT
GGAGGCTGCAGTCACCCAAAGTCCAAGAAGCAAGGTGGCAGTAACAGGAGG
AAAGGTGACATTGAGCTGTCACCAGACTAATAACCATGACTATATGTACTGG
TATCGGCAGGACACGGGGCATGGGCTGAGGCTGATCCATTACTCATATGTCG
CTGACAGCACGGAGAAAGGAGATATCCCTGATGGGTACAAGGCCTCCAGAC
CAAGCCAAGAGAATTTCTCTCTCATTCTGGAGTTGGCTTCCCTTTCTCAGACA
GCTGTATATTTCTGTGCCAGCAGTGATGCCGGGGGGGCGGAACACCTTGTACTT
TGGTGCGGGCACCCGACTATCGGTGCTAGAGGATCTGAGAAATGTGACTCCA
CCCAAGGTCTCCTTGTTTGAGCCATCAAAAGCAGAGATTGCAAACAAACAAA
AGGCTACCCTCGTGTGCTTGGCCAGGGGCTTCTTCCCTGACCACGTGGAGCTG
AGCTGGTGGGTGAATGGCAAGGAGGTCCACAGTGGGGTCAGCACGGACCCTC
AGGCCTACAAGGAGAGCAATTATAGCTACTGCCTGAGCAGCCGCCTGAGGGT
CTCTGCTACCTTCTGGCACAATCCTCGCAACCACTTCCGCTGCCAAGTGCAGT
TCCATGGGCTTTCAGAGGAGGACAAGTGGCCAGAGGGCTCACCCAAACCTGT
CACACAGAACATCAGTGCAGAGGCCTGGGGCCGAGCAGACTGTGGGATTAC
CTCAGCATCCTATCAACAAGGGGTCTTGTCTGCCACCATCCTCTATGAGATCC
TGCTAGGGAAAGCCACCCTGTATGCTGTGCTTGTCAGTACACTGGTGGTGATG
GCTATGGTCAAAAGAAAGAATTCA

Sig-Peptide
V-Region
D-Region
J-Region
C-Region

Origami biding region: CCAAACCTGTCACACAGAACATCAGTGCAG

Vβ linker primer annealing location: TATTTCTGTGCCAGCAGTGAT
Vβ linker primer sequence: 5’ ATCACTGCTGGCACAGAAATA 3’

Cβ RT linker primer annealing location: TCCACCCAAGGTCTCCTTGT
Cβ RT linker primer sequence: 5’ ACAAGGAGACCTTGGGTGGA 3’

Cβ PCR linker primer annealing location: GAGGATCTGAGAAATGTGAC
Cβ PCR linker primer sequence: 5’ GTCACATTTCTCAGATCCTC 3’

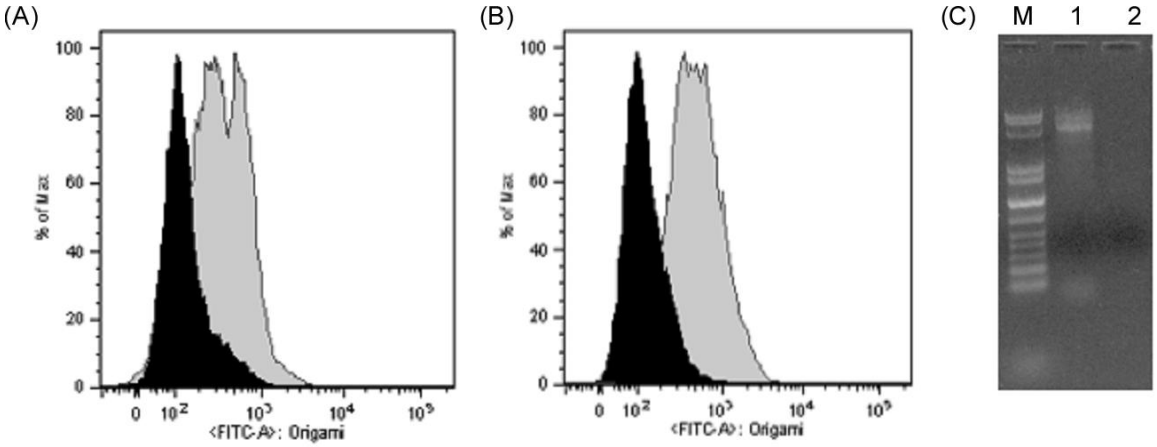

Figure S4.2 Transfection of primary lymphocytes with origami nanostructures. (A) Lymphocytes from C57Bl/6 mice were mock transfected (black) or transfected with DNA origami nanostructures (gray). (B) To ensure that origami structures were being taken by cells, rather than binding to the cell surface, cells were treated after transfection with DNase (mock=black, origami=gray). (C) DNAse digestion destroys DNA origami nanostructures (disappeared origami band in lane 2 vs positive control lane 1 on 1% agarose gel)